IMPROVING WATER QUALITY FORECASTING USING DATA ASSIMILATION

by

Hamideh Riazi

Presented to the Faculty of the Graduate School of
The University of Texas at Arlington in Partial Fulfillment
of the Requirements
for the Degree of

DOCTOR OF PHILOSOPHY

THE UNIVERSITY OF TEXAS AT ARLINGTON
December 2015

Acknowledgements

I cannot imagine coming this far without my Mom's support. She is the one who always encouraged me to move forward with my life no matter how hard the situation may be. She always advised me to be an independent and strong woman and never to depend on anyone.

I love you Dad for raising me as who I am today. He might not remember my name today or call me by my name ever again, but I am who I am today because of my wonderful parents.

I cannot thank enough my sisters, Fatemeh and Saeideh. They are my idols of kindness, support and unconditional love. They motivated me every day throughout my PhD.

Dr. Seo, thank you for giving me this opportunity to continue my education and for your support throughout my PhD program.

I am very thankful for all the support and advice from Dr. Kim and Dr. Shin through my PhD program.

I am very grateful to my friends Behzad Yazdi, Amir, Hamideh, Margarita, Josh, Cheeku, Behzad Nazari, Ray and Hossein.

This work was supported by the Water Quality Control Center of the National Institute of Environmental Research, the Republic of Korea, under the Cooperative Study Agreement between Geosystem Research Corporation, Korea, and The University of Texas at Arlington. This support is greatly appreciated.

November 20, 2015

Abstract

IMPROVING WATER QUALITY FORECASTING

USING DATA ASSIMILATION

Hamideh Riazi, PhD

The University of Texas at Arlington, 2015

Supervising Professor: Dong-Jun (DJ) Seo

Population growth increases agricultural, industrial and human activities which threaten the quality of water resources, especially water supply sources such as lakes and reservoirs. In potentially high-impact situations such as algal blooms, active measures such as controlled release from reservoirs may be necessary. To minimize release while meeting the water quality requirements, accurate short-range water quality forecast is necessary. Because watershed water quality models have a large number of state variables most of which are never observed, their initial conditions (IC) are subject to large uncertainties which may propagate into large forecast errors. In this research, a data assimilation (DA) algorithm is developed and evaluated which updates the ICs of the watershed water quality model, the Hydrologic Simulation Program – Fortran (HSPF), based on real-time observations of water quality and streamflow. The water quality observations include streamflow, water temperature (TW), ammonium (NH_4), nitrate (NO_3), phosphate (PO_4), chlorophyll-a (CHL-a), total nitrate (TN), total phosphate (TP), total organic carbon (TOC), biochemical oxygen demand (BOD), and dissolved oxygen (DO). The DA technique used is maximum likelihood ensemble filter (MLEF) which combines the strengths of variational assimilation (VAR) and ensemble Kalman filter (EnKF). In this work, the resulting DA algorithm is developed into a plugin module,

referred to as MLEF-HSPF, for the Water Quality Forecast System at the National Institute of Environmental Research (WQFS-NIER). To evaluate the MLEF-HSPF module, hindcast experiments were designed and carried out for a large number of catchments in the four major river basins in the Republic of Korea. To compare the performance of HSPF and DA with a purely data-driven approach, time series modeling was carried out for simulation and prediction for selected catchments. The results show that MLEF-HSPF consistently improves analysis and prediction of most of the water quality variables and streamflow over the DA-less results, but that the improvement varies significantly from catchment to catchment and from variable to variable. Comparisons with time series modeling and prediction show that the incremental value of water quality modeling and prediction using HSPF and DA is rather uneven; it varies significantly across catchments and variables. The findings suggest that there exists large room for improvement in HSPF modeling, including model physics and calibration. Also described toward that end are the factors limiting the performance of DA and the areas of improvement in the end-to-end forecast process to improve watershed water quality modeling and the performance of DA.

Keywords: Watershed water quality forecasting, HSPF, Data assimilation, Maximum likelihood ensemble filter

Table of Contents

List of Illustrations

List of Tables

Chapter 1

Introduction

The quality of inland water is of great importance to water supply, agriculture, the ecosystem and recreation. For proactive and timely protection and management of water quality, the decision makers need skillful predictive water quality information. When bacterial contamination or harmful algal blooms occur rapidly, the time window for action is very limited (Twigt et al. 2011). In aquaculture, decision makers need to take immediate action to avert disasters such as fish mortality which may occur from a single water pollution event (Bode and Nusch 1999). Whereas in-situ analysis only allows monitoring of the current state of water quality, forecasting provides an added ability to predict water quality states and to assess the potential consequences of possible actions, thereby allowing proactive decision making. Despite the clear needs and potential benefits, however, real-time water quality forecasting is not practiced very widely for multiple reasons. The first is that it involves a wide range of scientific, engineering and technological capabilities which, collectively, may require a large investment. The second is that, in the U.S. and elsewhere, the primary purpose of water quality modeling has been to meet regulatory requirements rather than to support real-time forecasting. As such, there are significant gaps in modeling and supporting tools for forecasting applications. The third is that the biophysiochemical processes involved in water quality forecasting are complex, operate over a wide range of space-time scales and are often highly variable in space and time. The recently-initiated real-time water quality forecasting operation at the Water Quality Control Center of the National Institute of Environmental Research (NIER) hence provides a golden opportunity to advance understanding, assess value and ascertain the limits of real-time water quality forecasting, and to develop new methodologies and tools and identify directions for improvement.

1.1. Statement of Problem

Plankton algae population in a water system is generally beneficial to fish and aquatic life. In some cases, however, these microscopic cells increase in abundance leading to negative impacts on aquaculture, fisheries and human health. Harmful Algal Blooms (HAB) in major rivers and lakes are a large environmental issue in the Republic of Korea and elsewhere. HABs cover a heterogeneous set of events that share two characteristics; they are caused by microalgae and have a negative impact on human activities (Zingone and Enevoldsen 2000). As explained by Coad et al. (2014), algal bloom management programs offer environmental managers limited capacity to adequately monitor and respond to algal blooms due to the cost of field monitoring, insufficient staff availability and resources, field safety issues, large sampling intervals, and lack of means for reporting and public notification. The diverse impact of algal blooms requires management strategies that mitigate threats to the economy and to human health (Zingone and Enevoldsen 2000). One of the most active measures for responding to major HABs is controlled release of impounded water from the reservoirs. For such measures to be cost-effective, however, accurate short-range forecasts of both water quantity and quality are necessary so that the water quality requirements may be met while minimizing the release.

There are multiple sources of uncertainty in water quality forecasting: uncertain observations, model states, model parameters, model structures, future input forcings and anthropogenic control and alternations of water quantity and quality (Beck 1987, Seo et al. 2010, see Figure 1-1):

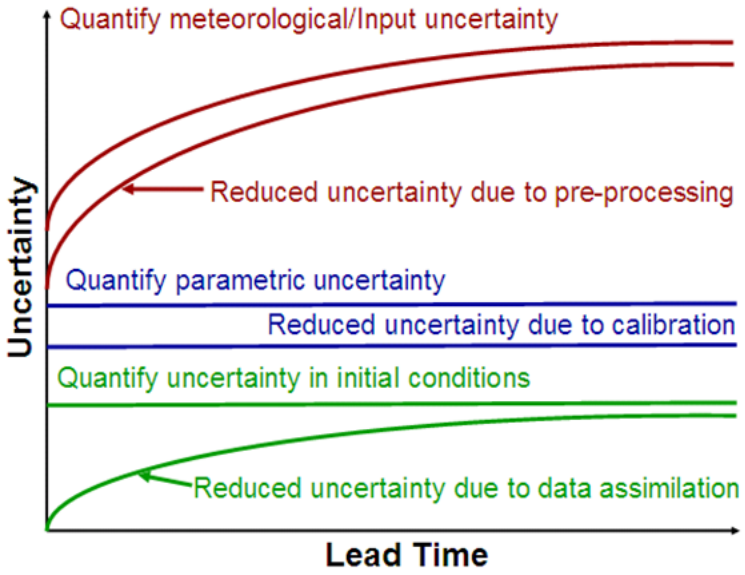

Figure 1-1 Sources of uncertainty in water quality forecasting (from Seo et al. 2010).

A number of studies have shown that the largest errors in water quality prediction occur when the state variables change rapidly due to increased biochemical activities (see, e.g., Beck 1987 and references therein). Through calibration and pre-processing, one may be able to reduce the uncertainties associated with model parameters, observations and inputs to a varying extent (see Figure 1-1). Calibration, however, is a time-consuming effort and may not be undertaken routinely. Because many model states in water quality models are never observed (see Table 1-1) and the models are never perfect, it is very likely that the initial conditions (IC) of the models are highly uncertain. To keep the model states in line with the unfolding reality as reflected in the real-time observations of water quality and hydrologic variables, it is necessary in operational forecasting to employ some form of real-time state updating. Data assimilation (DA) is an objective way to optimally estimate the model states by jointly utilizing the actual observations available in real time and the model-predicted observations that can be compared to the real observations for inference on the adjustment necessary to the

model states. DA has gained great popularity and importance recently in oceanography, atmospheric sciences and hydrology (e.g. Evensen 1994, Houtekamer and Mitchell 1998, Whitaker and Hamill 2002, Zupanski 2005, Seo et al. 2003). The positive impact of reducing uncertainties in the model ICs on improving forecast accuracy has been amply demonstrated in oceanography, weather forecasting and hydrology (Han et al. 2012, Carrassi et al. 2009, Komma et al. 2008, Kim et al. 2014, Rafieeinasab et al. 2014). The World Meteorological Organization (WMO), for example, identifies DA as an essential technique for accurate flood forecasting (WMO, 1992).

To provide the reservoir managers with accurate predictive water quality information, the Water Quality Control Center of NIER in the Republic of Korea produces real-time water quality forecasts for the four major rivers in Korea (see Figure 1-2). For watershed water quality forecasting, NIER uses the Hydrological Simulation Program-Fortran (HSPF, Bicknell et al. 2001). For river water quality forecasting, the Environmental Fluid Dynamics Code (EFDC, Hamrick 2007) is used (see Figure 1-3). The HSPF model is one way-coupled with EFDC such that the former provides the latter with the boundary conditions (BC) along the major tributaries and main stems of the river systems. For real-time operation of these models, NIER uses the Water Quality Forecast System (WQFS)-NIER, developed jointly by Deltares and NIER, based on the Delft-Flood Early Warning System (FEWS) (Werner et al. 2004). Figure 1-3 shows the schematic of the daily water quality forecast operation at NIER.

The watershed water quality model used, HSPF, is a continuous semi-distributed model for simulation of hydrologic and water quality processes on pervious and impervious land surfaces and in streams as well as in well-mixed impoundments (Bicknell et al. 2001). A successor to the Stanford model developed in the 1960s for continuous simulation of hydrologic processes (Crawford and Burges 2004), HSPF was developed to

determine non-point loads and total maximum daily loads (TMDL), and has many state variables (see Table 1-1). Because only a small subset of the model states is actually observed (see Table 1-1), it is very likely that the model ICs have large uncertainties. Given that the HSPF results are used as the BCs of the EFDC model, one may expect that improving the accuracy of the ICs of the watershed water quality model will not only improve the accuracy of the river water quality forecasts by providing more accurate BCs for the hydrodynamical model but also increase the lead time by leveraging the hydrologic memory in the upstream catchments which is significantly longer than the hydraulic memory in the river systems. Toward that end, this research aims at obtaining more accurate ICs for HSPF by objectively updating the model states via advanced DA. Because of the semi-distributed nature of the HSPF model, the number of model states to be updated by DA is very large. State updating for such a system is a high-dimensional inverse problem for which manual updating is effectively infeasible and automatic DA is the only practical solution.

Figure 1-2 An example of real-time water quality forecast for the four major rivers in Korea produced by the Water Quality Control Center of the National Institute of Environmental Research. Real Time Water Quality Index (RTWQI) provides information on the water quality of rivers in Korea (adapted from NIER 2014).

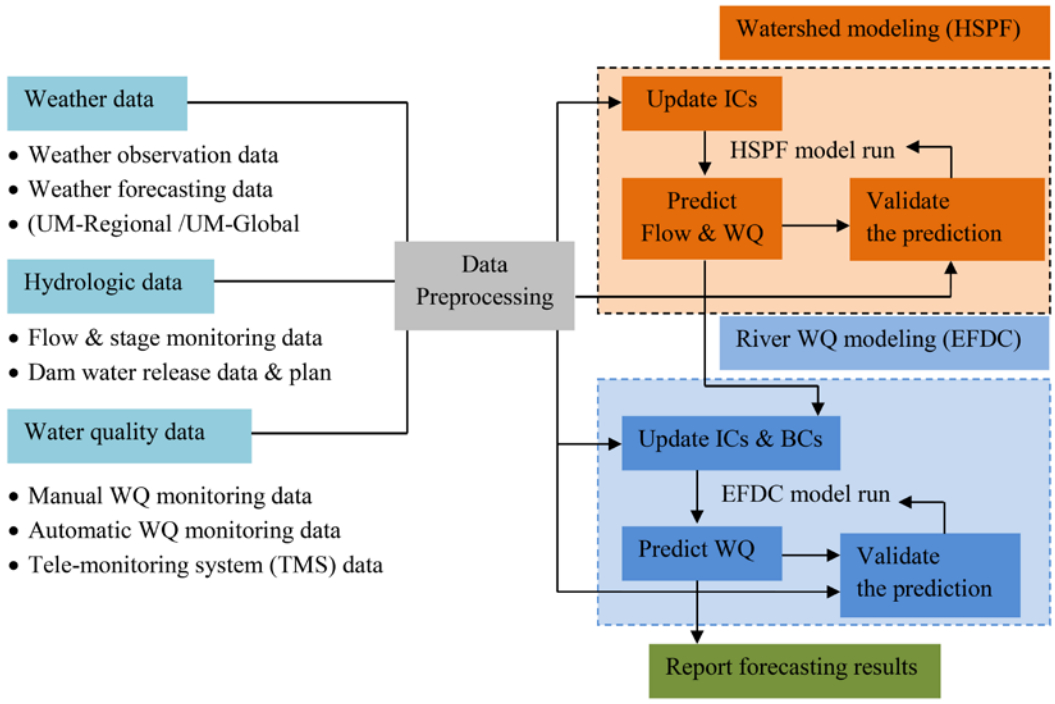

Figure 1-3 Schematic of the water quality forecast process using WQFS-NIER (from Shin 2013).

Table 1-1 HSPF state variables.

Module	Variable name	Observation data	Definition
PERLND (for pervious land)	CEPS	No	interception storage
	SURS	No	surface (overland flow) storage
	UZS	No	upper zone storage
	IFWS	No	interflow storage
	LZS	No	lower zone storage
	AGWS	No	active groundwater storage
	GWVS	No	index to groundwater slope
	SQO-NH_4	No	storage of NH_4 on the surface
	SQO-NO_3	No	storage of NO_3 on the surface
	SQO-PO_4	No	storage of PO_4 on the surface
	SQO-BOD	No	storage of biochemical oxygen demand (BOD) on the surface
IMPLND (for impervious land)	RETS	No	retention storage
	SURS	No	surface (overland flow) storage
	SQO-NH_4	No	storage of NH_4 on the impervious surface
	SQO-NO_3	No	storage of NO_3 on the impervious surface
	SQO-PO_4	No	storage of PO_4 on the impervious surface
	SQO-BOD	No	storage of biochemical oxygen demand on the impervious surface
RCHRES (for in-stream process)	VOL	No	volume of water in the RCHRES at end of interval
	TW	Yes	water temperature
	DOX	Yes	dissolved oxygen concentration
	BOD	Yes	biochemical oxygen demand concentration
	NO_3	Yes	dissolved concentration of NO_3
	TAM	Yes	dissolved concentration of TAM (incl. NH_3, NH_4)
	PO_4	Yes	dissolved concentration of PO_4
	PHYTO	No	phytoplankton concentration
	ORP	No	organic refractory phosphorus
	ORN	No	organic refractory nitrogen
	ORC	No	organic refractory carbon

1.2. Objectives

This research develops, implements and evaluates a plugin DA module for the watershed water quality model, HSPF, in the open architecture forecast system, WQFS-NIER, for real-time short-range (a few to several days ahead) water quality forecasting for the four major rivers in the Republic of Korea. HSPF is one of the most widely used watershed water quality model in the world and FEWS is widely used for operational hydrologic forecasting around the world (Singh et al. 2005, Shirinian-Orlando 2007, Verwey et al. 2006, Twigt et al. 2011). This research has the following specific objectives:

- **Improve water quality forecasting of major rivers by improving the ICs of watershed water quality model via advanced DA.** The predictability of water quality in a watershed is limited by the residence time of water in various storages as well as the reaction time of the biophysiochemical processes involved. Given the generally longer residence time in the runoff generating areas of the watershed compared to that in the rivers, one may expect that improving the accuracy of the ICs for HSPF will increase the accuracy and lead-time of the water quality forecasts for the river systems.
- **Advance understanding of the limits of state-of-the-art water quality modeling and DA, and identify and assess the limiting factors.** For DA to be effective, the model has to be representative of the reality. If the model cannot simulate the biophysiochemical processes that occur in the catchment, one may not expect DA to add significant skill. As such, understanding the performance and limitations of the model is critical to assessing and improving the performance and potency of DA.
- **Assess predictability of water quality variables by data-driven modeling and comparatively evaluate HSPF and DA**. A potentially less expensive alternative to using HSPF and DA is to use time series modeling and forecasting. Such data-driven

modeling results would provide reference against which the HSPF modeling and DA results may be judged. Also, model identification and parameter estimation would indicate and reflect statistical structure and predictability of the water quality variables and help advance understanding of the different processes at work in different catchments.

For Objective 2, different aspects of model performance, such as whether HSPF is able to capture the variability of water quality variables, is examined in evaluating the quality of the base (i.e., DA-less) model simulations. All DA techniques have their own limitations and strengths depending on the problem. Aspects such as the linear-vs.-nonlinear model dynamics, structure of the observation equations, structure of the model errors, structure of the observation errors, and the degrees of freedom of the inverse problem should be called into consideration for effective application of DA. Since the relationships between the observations and the model states may be highly nonlinear (e.g., streamflow observations and model soil moisture states), the DA technique should be able to handle nonlinear observation equations as well as nonlinear model dynamic. For Objective 3, auto regressive integrated moving average (ARIMA) time series model is used to simulate and forecast water quality variables in multiple catchments. The ARIMA model prediction results are then compared with the DA-aided predictions to assess the value of HSPF modeling and DA. The specific questions to be addressed by this research include:

- How much improvement does DA bring to watershed water quality forecasting?
- What are the limiting factors for DA in watershed water quality forecasting?
- What is the potential of DA in watershed water quality forecasting?
- How skillful is HSPF?
- How does the goodness of HSPF impact performance of DA?

- How predictable are the water quality variables? How does the predictability vary from catchment to catchment? What are the factors contributing to the variations?
- How does the predictability relate to the performance of DA?

The new contributions of this research are as follows:

- Assessment of the value and potential of DA in watershed water quality forecasting using HSPF,
- Advanced understanding of the sensitivity of DA performance to ensemble size, size of the assimilation window, magnitude and structure of model errors, and magnitude and structure of observation errors,
- Advanced understanding and solution of under-determined inverse problems in watershed water quality modeling and prediction using HSPF,
- Identification of limitations of and constraints for DA for real-time watershed water quality forecasting using HSPF, and
- Advanced understanding and assessment of predictability of water quality variables using time series modeling and comparison with HSPF modeling and DA.

Chapter 2

Literature review

As argued in Chapter 1, an effective way to improve the accuracy of water quality predictions is to reduce uncertainties in the ICs of the water quality models by updating the model states based on real-time observations of water quality and streamflow. DA is an objective way to optimally estimate the model states by jointly utilizing the actual observations available in real time and the model-simulated observations. The state space of a dynamic system modeled may be described as:

$$x_{t+1} = M(x_t, \theta, u_{t+1}) + w_{t+1} \quad (2\text{-}1)$$

where x_t and x_{t+1} denote the state vectors at times t and t+1, respectively, $M(\,)$ denotes the nonlinear model, θ denotes the model parameter vector, u_{t+1},denotes the input vector at time t+1 and w_{t+1} denotes the model error vector at time t+1. Model error accounts for the uncertainties in the model dynamics, i.e., $M(\,)$ in Eq.(2-1). In this work, all HSPF variables that represent the model states are considered as the state variables. In state-space representation, the model states are related to the observations via the observation equation as follows:

$$z_{t+1} = H(x_{t+1}, \theta) + \varepsilon_{t+1} \quad (2\text{-}2)$$

where z_{t+1} denotes the observation vector at time t+1, H denotes the observation operator and ε_{t+1} denotes the observation error at time t+1. In this work, $M(\,)$ in Eq. (2-1) represents the HSPF model, and $H(\,)$ in Eq. (2-2) represents the nonlinear relationship between the model states and the model-simulated observations.

Various DA techniques have been used in water quality forecasting since the 1970s to improve forecast accuracy by reducing uncertainties in the ICs or parameters (Beck and Young 1976). Canale et al. (1980) used DA to improve prediction of PO_4 concentration. The most popular choice for the DA technique in water quality forecasting

has been Kalman filter (KF) and its variants owing to the algorithmic simplicity and ease of implementation. Below, a general overview of different DA techniques and their applications in different areas of water quality modeling and prediction are given.

2.1. Kalman filter (KF)

Kalman Filter (Kalman 1960) is a sequential filtering method; the model is integrated forward in time and, whenever measurements are available, they are used to reinitialize the model before the integration continues (Evensen 2003). The main assumptions for optimality for KF are that both the model and observation operators are linear and the model and observation errors are Gaussian. Algorithmically, KF consists of a forecast step and an update step. The model states are first propagated forward in time from the initial states. When a set of observations becomes available, the model states are updated (analysis step). In the following step, the updated model states are integrated forward over the forecast horizon to produce forecast (forecast step).

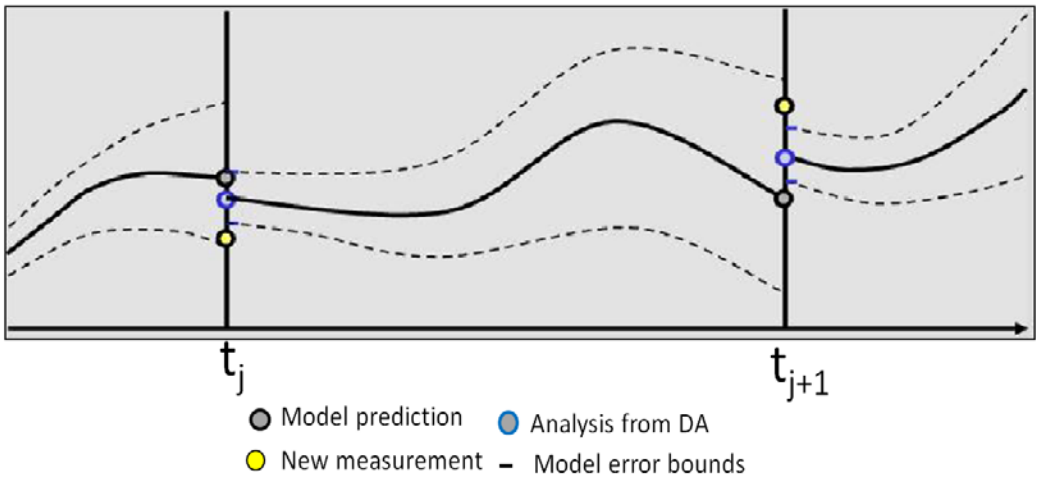

Figure 2-1 Schematic illustration of Kalman filter (Kim et al. 2013).

In the forecast step, the condition mean and covariance of the current states are integrated forward over the forecast horizon (see Eqs. (2-3) and (2-4)). In the update

step, the model states are updated by optimally weighing the actual observations and model-simulated observations (see Eqs. (2-5), (2-6) and (2-7)):

$$x_t^f = Mx_{t-1}^a + w_t \quad (2\text{-}3)$$

$$P_t^f = MP_{t-1}^a M^T + Q_t \quad (2\text{-}4)$$

$$x_t^a = x_t^f + K_t(z_t - Hx_t^f) \quad (2\text{-}5)$$

$$P_t^a = P_t^f - K_t H P_t^f \quad (2\text{-}7)$$

In Eq.(2-5), the Kalman gain, K_t, is given by:

$$K_t = P_t^f H^T \left(HP_t^f H^T + R_t\right)^{-1} \quad (2\text{-}6)$$

where P_t^a, P_t^f and R_t denote the error covariance matrices of analysis, forecast and observation, respectively. M and H denote the linear model and observation operators, respectively. In the above, T stands for transpose, z_t denotes the observation vector and Q_t denotes the model error covariance matrix.

Note that the magnitude of the Kalman gain depends on the relative magnitude of the state (P) and observation (R) error covariance (see Eq. (2-6)). Therefore, if the magnitude of R or P is large, the Kalman gain will be small, and the correction of the forecast vector will be small.

Guo et al. (2003) developed a stochastic water quality forecasting system based on KF to predict dissolved oxygen (DO) and biochemical oxygen (BOD) demand levels in the Yiluo River in northern China. They suggested that the forecast results could be used for regional water quality management. Schilling and Martens (1986) used KF to predict DO concentration in the Leine River south of Hannover in West Germany. KF was used to estimate biogeochemical rates or model state variables (McNair et al. 2013, Batt and Carpenter 2012).

The KF method has proven effective and efficient for linear problems but works poorly for nonlinear systems (Evensen 1992, Miller et al. 1994, Kang and Lansey 2009). Therefore, variants of the KF algorithm have been developed to cope with nonlinearities.

2.2. Extended Kalman filter (EKF)

Extended Kalman filter (Jazwinski 1970) was developed to handle nonlinear model operators and to approximate nonlinear observation operators with a tangent linear operator (Jacobian). Therefore, EKF yields an approximation of the optimal estimate if the model dynamics and/or the observation equation is nonlinear. EKF uses linearized forms of the model and observation operators, M and H, respectively, and utilizes the KF solution described in the previous subsection (see Eq. (2-3) through (2-7)).

EKF was the DA technique of choice in the 1970s and 1980s (Beck 1987, Beck and Young 1976, Cosby et al. 1984). It was used to forecast algal bloom (Mao et al. 2009) and to update the parameters of a DO-chlorophyll (CHL-a) model (Pastres et al. 2003). EKF was used to estimate the optimal parameters and to assess the structure of a simple model, which is capable of simulating NO_3 (Sloan et al. 1994). Whitehead and Hornberger (1984) used an algal model and performed sensitivity analysis to identify the key parameters controlling the highly nonlinear algal behavior. They then used EKF to estimate the parameters. Ennola et al. (1998) applied EKF for modeling zooplankton population dynamics. Voutilainen et al. (2007) used a reduced-order iterative EKF to estimate lake water constituents. They suggested that the practical use of EKF in high dimensional problems is computationally expensive, and that a dimension reduction technique may be necessary to reduce the computational burden of filtering.

2.3. Ensemble Kalman filter (EnKF)

For strongly nonlinear systems, EKF may produce instabilities or even diverge (Hoteit et al. 2005, Evensen 1992). In addition, unbounded error growth may occur in

EKF due to an oversimplified closure in error covariance modeling (Evensen 1994). EnKF is a non-linear ensemble-based filtering technique introduced by Evensen (1994) to overcome limitations associated with EKF for cases of strong nonlinear dynamics and large state spaces (Burgers et al. 1998, Evensen 2003, 2009). Unlike EKF, EnKF does not require linearization of the model or the observation operator. If the observation equation is linear, EnKF is optimal in the second-order sense (Kalman 1960, RafieeiNasab et al. 2014).

EnKF is a sequential Monte-Carlo assimilation technique in which an ensemble of model states perturbed by adding noise to a best-guess estimate is propagated forward in time to predict the states as an ensemble valid at future time steps (see Eq. (2-8) and Figure 2-2) in which the ensemble represents the probability distribution of the states:

$$X_t = [x_t^1, x_t^2, \dots, x_t^{N-1}, x_t^N] \xrightarrow{one-step\ forward\ integration} X_{t+1} = [x_{t+1}^1, x_{t+1}^2, \dots, x_{t+1}^{N-1}, x_{t+1}^N] \quad (2\text{-}8)$$

where x_t^i denotes the prior estimate of the model state at time t represented by the i-th ensemble member, and N denotes the number of ensemble members. In EnKF, Eqs. (2-5) and (2-6) are applied to each ensemble member. Since the true state is not known, in practice the forecast error variance is prescribed by the error covariance around the ensemble mean, $\bar{x}_t^f$, as defined in Eq. (2-9) (Burgers et al. 1998, Liu and Gupta 2007):

$$P_t^f = \overline{(x_t^f - \bar{x}_t^f)(x_t^f - \bar{x}_t^f)^T} \quad (2\text{-}9)$$

EnKF uses an ensemble of observations at each analysis time in which perturbations may be added to represent observational uncertainty. This step is very important to maintain variance in the updated ensemble but at the same time does not affect the prediction of the ensemble mean (Burgers et al. 1998).

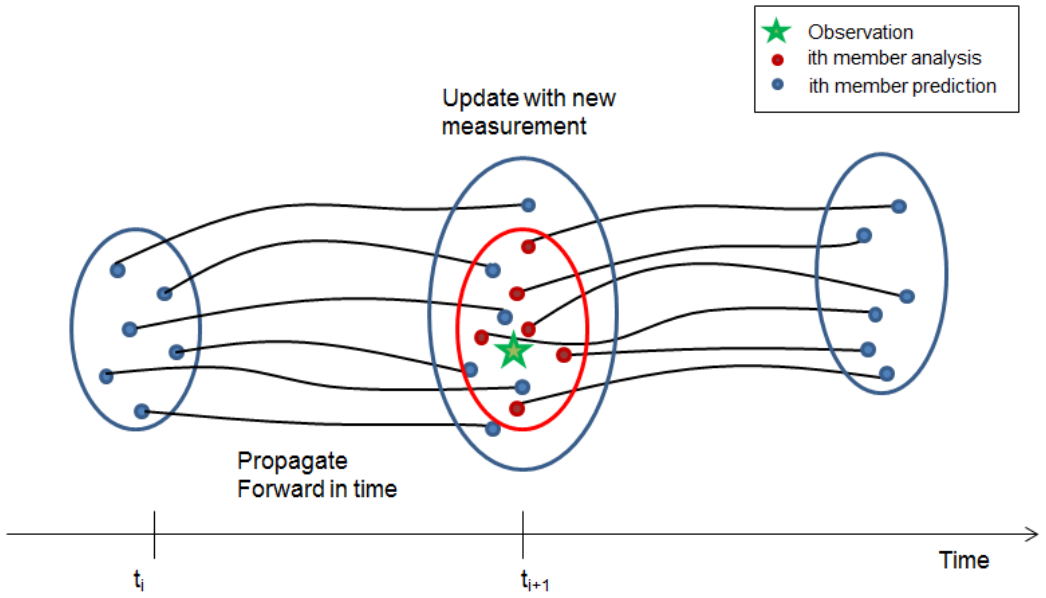

Figure 2-2 Schematic illustration of ensemble Kalman filter.

EnKF has been applied widely in climatology, meteorology and oceanography as well as hydrologic and water quality forecasting (Eknes and Evensen 2002, Moradkhani et al. 2005b, Neal et al. 2007, Vrugt and Robinson 2007, Clark et al. 2008, Xie and Zhang 2010, Xue et al. 2012, Huang et al. 2013, Kim et al. 2014). Huang et al. (2013) used EnKF to assimilate measured CHL-a into a spatial hydrodynamic-phytoplankton model to predict the short-term changes in the CHL-a concentration as a measure of the phytoplankton biomass in Lake Taihu in China. They found that good ICs for CHL-a are critical to good predictions of phytoplankton biomass. Kim et al. (2014) used EnKF to improve prediction of algal bloom and to evaluate its applicability in Han River in the Republic of Korea. They suggested a DA framework composed of 1) two models linked together to simulate the watershed and the river channels and 2) error models at the interface of the two models to reflect the uncertainty of the watershed simulation. The authors found that the use of EnKF improves river water quality predictions, and that, if the state variables of the watershed water quality model are not updated, the effect of DA

vanishes very quickly when the flow velocities are high. EnKF gained popularity owing to algorithmic simplicity and relative ease of implementation (e.g., no adjoint code is necessary) (Evensen 2003, Hotiet et al. 2005). As argued by Madsen and Skotner (2005), however, the computational cost may still be too high in operational systems; the ensemble size necessary to obtain a reliable representation of the covariance structures is typically on the order of 100.

2.4. Particle filter (PF)

PF (Arulampalam et al. 2002, Weerts and El Serafy 2006) uses Monte Carlo sampling to estimate the system state directly via Bayes theorem thereby avoiding the linearity assumption typical of the KF family of filters. The advantage of PF over KF is that the state-space model does not assume linearity or normality (see Figure 2-3). Early applications of PF were based on Sequential Importance Sampling (SIS) to represent the posterior density function by a set of random samples with associated weights (see e.g. Weerts and El Serafy 2006). With a large number of particles, this Monte Carlo characterization becomes equivalent to the posterior pdf (Arulampalam et al. 2002) which is approximated by:

$$p(x_k|z_{1:k}) \approx \sum_{i=1}^{N} w_k^i \delta(x_k - x_k^i) \quad (2\text{-}10)$$

where N denotes the number of the particles, $\delta(\,)$ denotes the Dirac delta function, w_k^i denotes the weights and x_k denotes the posterior state. In practice, samples are drawn from a known distribution, in lieu of the posterior density function (Weerts and El Serafy 2006), referred to as the importance density (DeChant and Moradkhani 2012, Weerts and El Serafy 2006), $q(x_n|z_n)$. The weights are given by (Arulampalam et al. 2002):

$$w_k^{i(*)} \propto w_{k-1}^{i(*)} \frac{p\left(z_k|x_k^i\right)p\left(x_k^i|x_{k-1}^i\right)}{q\left(x_k^i|x_{k-1}^i,z_k\right)} = \frac{p\left(x_k^i|z_{1:k}\right)}{q\left(x_k^i|z_{1:k}\right)} \quad i = 1,\ldots,n \quad (2\text{-}11)$$

Therefore, it is possible to sequentially update the importance weights given an appropriate choice of the importance density $q\left(x_k^i \middle| x_{k-1}^i, z_k\right)$.

A common problem with PF is filter degeneracy in which the weights of all particles collapse into one. This degeneracy implies that a large computational effort is necessary to update the particles that are not contributing to the inference of the posterior distribution (Arulampalam et al. 2002). To refine the weights, Sequential Importance Resampling (RIS) was proposed by Gordon et al. (1993). By resampling the weights and moving the particles, the degeneracy problem is addressed to an extent but at the expense of increased computational burden (Pham 2001). PF can be applied to non-Gaussian models and, in its basic form, it is very easy to implement. Applications of KF appear much more often than those of PF in the literature for water quality forecasting due to the KF's longer history and to the fact that, for high-dimensional problems, PF may be computationally too expensive to be operationally viable.

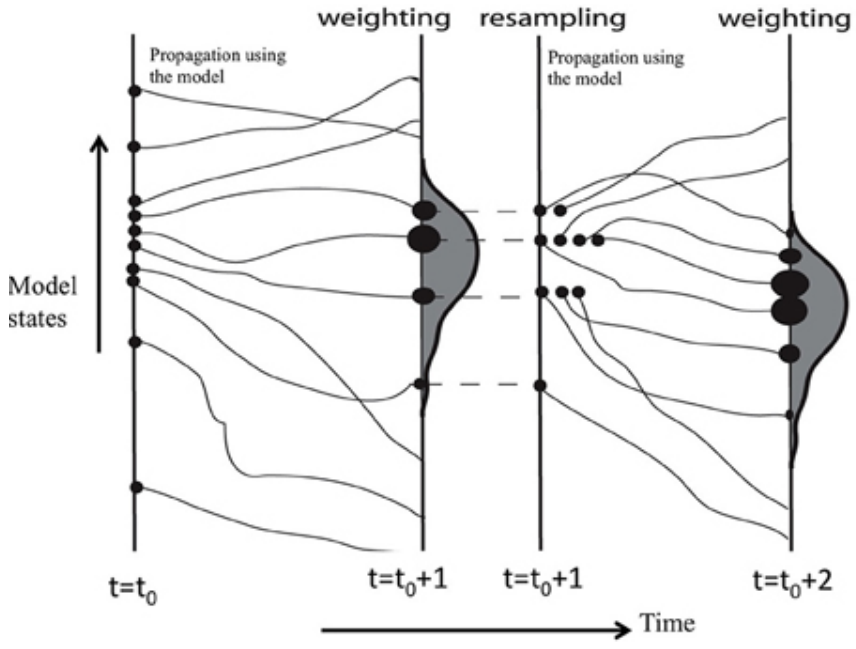

Figure 2-3 Schematic illustration of particle filtering (from Guiot et al. 2014).

PF has been applied in climatology, meteorology and hydrology (Pham 2001, Moradkhani et al. 2005a, Weerts and El Serafy 2006, Van Leeuwen 2009, DeChant and Moradkhani 2011a, Guingla et al. 2013, Yan et al. 2015). Leisenring and Moradkhani (2012) used PF for prediction of suspended sediment load. Nagarajan et al. (2011) used PF to improve root-zone soil moisture estimates by assimilating synthetic and field observations of soil moisture under dynamic vegetation. PF was used to assimilate water stage records into hydraulic models (Matgen et al. 2010, Giustarini et al. 2011).

2.5. Variational Assimilation (VAR)

Unlike the KF and PF family of filters which assimilate observations sequentially, VAR assimilates observations in batches (Figure 2-4) to update the model ICs (Drecourt 2004). As such, variational methods are smoothers (Liu and Gupta 2007). The principle behind this type of DA is to minimize the cost function *J( )* (see Eq.(2-12)) that weights the departure of the updated states from the background states (the first term in Eq.(2-12)) and that of the model-simulated observations (based on the updated model states) from the actual observations over the time interval or the assimilation window (the second term in Eq.(2-12)) (Ide et al. 1997):

$$J(x) = (x - x_b)^T P^{-1}(x - x_b) + \sum_{i=0}^{n}(z_i - H_i(x_i))^T R_i^{-1}(z_i - H_i(x_i)) \quad (2\text{-}12)$$

where x_b denotes the background state. VAR minimizes *J( )* for x in Eq. (2-12) to obtain the best estimate of the model states (Li and Navon 2001). An important aspect of VAR is that, for gradient-based minimization, adjoint code is required which may not be very easy to generate, depending on the structure of the computer program of the model (i.e., the forward code) and the way and the language in which it is written.

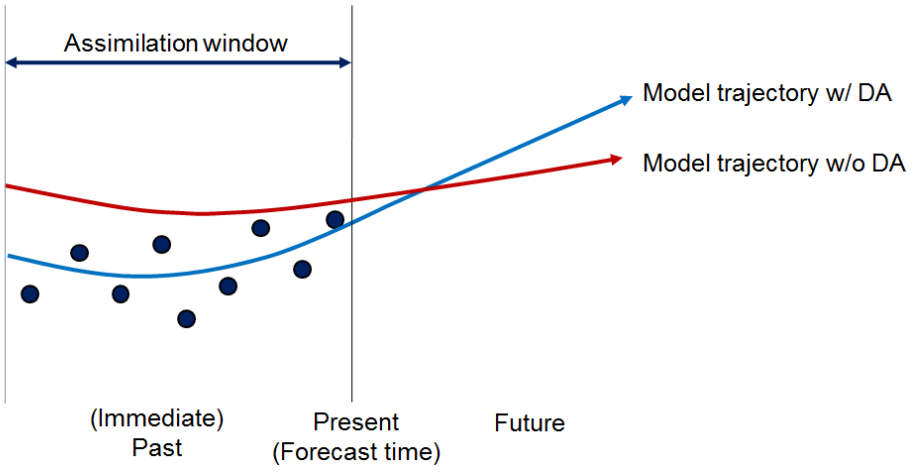

Figure 2-4 Schematic illustration of variational data assimilation.

Limited applications of VAR are found in water quality forecasting. Xie (2012) and Sebens et al. (2013) used a VAR approach to simulate water column temperature in a eutrophic reservoir in central Indiana. They addressed improving the model performance by combining water temperature from multi-spectral remote sensing analysis and in-situ measurements. VAR is widely used in hydrologic and weather forecasting (Li and Navon 2001, Seo et al. 2003, 2009, Lee et al. 2012). Reichle et al. (2001) used VAR for large-scale soil moisture assimilation. Seo et al (2003) used VAR for hydrologic operational forecasting. Seo et al. (2003) and Lee et al. (2012) found that VAR improves streamflow forecast accuracy. Seo et al. (2009) used VAR to assimilate discharge observations into the Sacramento Soil Moisture Accounting (SAC-SMA) model (Burnash et al. 1973) for a large number of watersheds in Texas. Lee et al. (2012) found that automatic state updating of the gridded SAC-SMA and kinematic-wave routing model states via 4-dimensional VAR (4DVAR) provided significant improvement in streamflow predictions. Ragnoli et al. (2012) proposed a variational method to assimilate ocean surface current measurements into a numerical ocean model based on data from High Frequency Radar (HFR).

Whereas KF provides error covariance estimates for prediction, VAR in itself does not (Liu and Gupta 2007). Also, in cases where observations arrive continuously in time, the sequential methods may be more suitable for real-time DA (Liu and Gupta 2007). EKF relies on tangent linear model and assumes linear observation operators to approximate the state and observation equations. VAR, on the other hand, does not assume linear model dynamics or linear observation equations but relies on tangent linear model for adjoint-based gradient evaluation. EnKF does not assume linear model dynamics but assumes linear observation equations. PF, on the other hand, does not assume linear model dynamics or linear observation equations.

2.6. Maximum likelihood ensemble filter (MLEF)

Maximum likelihood ensemble filter (MLEF, Zupanski 2005) combines the strengths of VAR (Jazwinski 1970, Li and Navon 2001, Seo et al. 2003, 2009, Lee et al. 2011, 2012) and EnKF (Evensen 1994). MLEF may be viewed as an ensemble extension of VAR or iterative EnKF (Lorentzen and Naevdal 2011). The minimization of the cost function in MLEF is performed in an ensemble-spanned subspace while, in VAR (see Eq. (2-12)), the full model space is used. Unlike VAR, however, MLEF does not require adjoint code for gradient evaluation. Unlike EnKF, MLEF does not assume that the observation equation is linear. For more detail regarding the mathematical framework of the MLEF, see Subsection 4.3.13.1.

MLEF was used to assimilate precipitation-affected microwave radiances into the Weather Research and Forecasting (WRF) model (Zhang et al. 2013); the results show that MLEF improves the quality of precipitation analysis in terms of spatial distribution and intensity in accumulated surface rainfall as verified by independent ground-based precipitation observations. Zupanski et al (2011) used WRF and MLEF to examine the potential impact of assimilating observations from the future Geostationary Operational

Environmental Satellite - Generation R (GOES-R Advanced Baseline Imager (ABI)) on improving the knowledge about model-simulated clouds. The DA and short-term forecast results over multiple assimilation cycles have clearly indicated improvements due to assimilation of the GOES-R ABI radiance observations compared to the DA-less. Zupanski et al. (2007) used MLEF to estimate and reduce biases in the CO_2 photosynthesis and respiration fluxes. For evaluation, they compared the MLEF results with KF results. Since the problem was linear, the KF solution was considered optimal. Their results indicates that MLEF had a stable performance over a wide range of ensemble sizes, and converged smoothly to the KF solution as the ensemble size approached the size of the control variable. Rafieeinasab et al. (2014) compared MLEF and EnKF for real time assimilation of streamflow data into an operational hydrologic model. Their results indicate that MLEF outperformed EnKF under varying conditions of observation and model errors, and ensemble size, and that MLEF performed well with an ensemble size as small as 5 whereas EnKF required a much larger ensemble size to perform closely to MLEF.

Due to the complex nonlinear nature of the biophysiochemical processes that occur in water bodies, water quality prediction is very uncertain and generally has smaller predictive skills for most water quality variables than flood prediction. Capturing nonlinear dynamics is hence important in reducing forecasting errors via DA in water quality forecasting (Jian and Yu 1998). One may then expect that DA for operational water quality forecasting has to be able to handle both nonlinear model dynamics and nonlinear observation operators. Based on the above considerations, MLEF was selected as the DA methodology of choice in this research, and a prototype DA algorithm for HSPF and the supporting modules for initialization have been developed, tested and evaluated, as describe in the chapters to follows.

Chapter 3

Methodology

Based on the experience in Seo et al. (2003, 2009) and Lee et al. (2011, 2012), a fixed-lag smoother formulation (Schweppe 1973, Li and Navon 2001) is used for MLEF-HSPF, which is described below (see Figure 3-1). In each assimilation cycle, all observations within the assimilation window are assimilated to update the model ICs valid at the beginning of the assimilation window and the multiplicative adjustment factors to mean areal precipitation (MAP) and mean areal potential evapotranspiration (MAPE) valid over the window. Because large errors may exist in the estimates of MAP and MAPE, two control variables representing the multiplicative adjustment factors, or biases, for MAP and MAPE were added to the control vector. It is well known that forcing errors greatly impact the accuracy of ICs of both hydrologic and water quality variables. Following Seo et al. (2003, 2009) and Lee et al. (2011, 2012), the biases are assumed to be spatially constant over the subcatchment of interest and temporally constant within the assimilation window. To implement the multiplicative adjustment factors to MAP and MAPE, segment-specific precipitation and PE within the subcatchment were weight-averaged according to the size of the area to derive MAP over the entire subcatchment. The adjustment factors inflate or deflate MAP and MAPE while keeping the spatial pattern of MAP and MAPE among the segments as originally prescribed. While the choice of spatiotemporally constant bias may seem overly simplistic, experience with hydrologic models indicate that the gain from a more complex approach such as spatiotemporally-varying bias is rather small.

The ICs and the adjustment factors form the control vector for the DA algorithm. The assimilation window, or the time scale of the fixed lag, is a few to several days long for headwater basins in reflection of the response time of the basins in the study area

(Seo et al. 2012). Because the sampling frequency of water quality observations is only about once a week, an assimilation window of 7 days was chosen to increase the frequency of DA. For prediction, HSPF is run over the assimilation window using the updated ICs valid at the beginning of the assimilation window and the adjustment factors valid over the assimilation window to produce the updated model states valid at the prediction time, which are then used to forward-integrate the model 3 to 7 days into the future. For the next assimilation cycle, HSPF is forward-integrated from the beginning of the current assimilation window to that of the next window to produce the updated model ICs valid at the beginning of the next assimilation cycle.

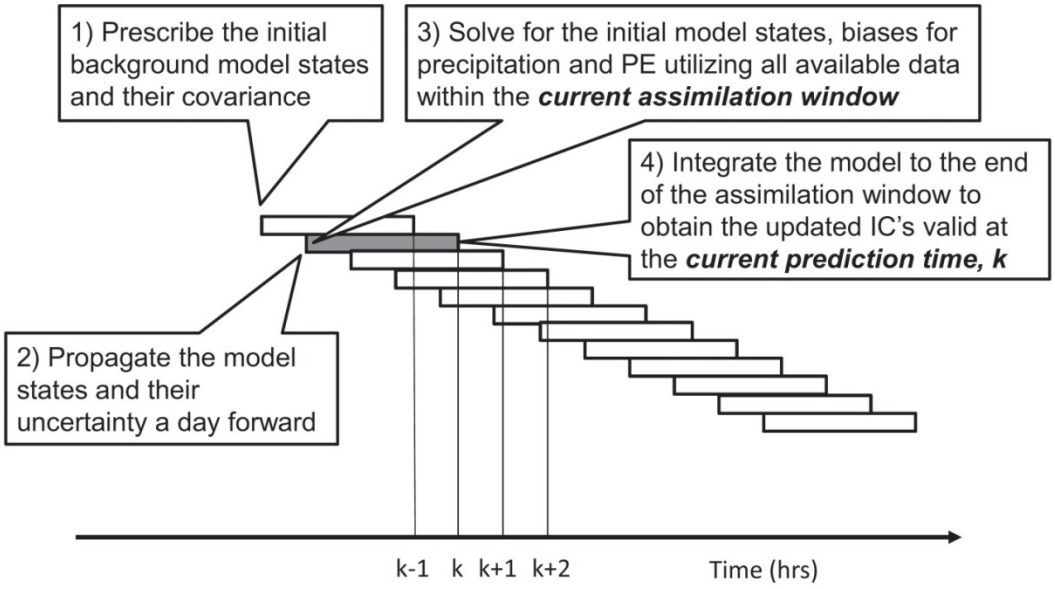

Figure 3-1 Schematic of the DA cycle based on the fixed-lag smoother formulation.

3.1. Maximum likelihood ensemble filter (MLEF)

Algorithmically, the sequential assimilation process using the fixed lag smoother consists of the following steps (see also Figure 3-2 for flowchart). DA is initiated when there exist observations valid at any time within the current assimilation window. For

notational brevity, the index for the current time step k is omitted. It is hence to be understood that all time-dependent variables are associated with the time step of k unless indicated otherwise. In Step 1, the square root of the (SxS) forecast error covariance, P_f , where S denotes the number of ensemble members and k-1 denotes the previous time step, is specified by:

$$P_f^{1/2} = (b_1 b_2 \dots b_s) \tag{4-1}$$

where

$$b_i = \tilde{M}\tilde{p}_i \approx M(x_{k-1} + \tilde{p}_i) - M(x_{k-1}) \tag{4-2}$$

In the above, i denotes the i-th ensemble member, b_i denotes the (Nx1) i-th ensemble member of the (NxS) matrix where N denotes the number of control variables, $M()$ denotes the (Nx1) one-step forward-integrated control vector of the model states and adjustment factors, $\tilde{M}$ denotes the (NxN) Jacobian of the model with respect to the control vector transitioning from time step k-1 to time step k, and $\tilde{p}_i$denotes the i-th (1xN) vector in the (NxS) square root of the analysis error covariance, $P_a^{1/2}$, from the previous assimilation cycle (see Eq.(4-11)) defined as:

$$P_a^{1/2} = (\tilde{p}_1 \tilde{p}_2 \dots \tilde{p}_s) \tag{4-3}$$

where

$$\tilde{p}_i = \left(p_{1,i}\ p_{2,i} \dots\ p_{N,i}\right)^T; i = 1,2, \dots, s \tag{4-4}$$

The entry, $p_{\mathrm{j},i}$, in Eq.(4-4) denotes the ensemble perturbation for the j-th control variable in the i-th ensemble member. With the above definitions, it should be clear that b_i in Eq.(4-2) represents the perturbations in the i-th ensemble member of the control vector valid at time step k around the corresponding control, or the maximum likelihood, solution. In the very beginning of DA when there is no analysis error covariance available, the perturbations, b_i, are generated by sampling from lognormal distributions (see

section 4.3.2). In Step 2, MLEF-HSPF performs the following weakly-constrained minimization in ensemble subspace, the solution of which represents the maximum likelihood estimate of the control variables:

Minimize

$$J(x) = \frac{1}{2}(x - x_b)^T P_f^{-1}(x - x_b) + \frac{1}{2}(y - H(x))^T R^{-1}(y - H(x)) \quad (4\text{-}5)$$

subject to

$$x = M(x_{k-1}) + w_{k-1} \quad (4\text{-}6a)$$

$$x_{lower} \leq x_k \leq x_{upper} \quad (4\text{-}6b)$$

where x denotes the (Nx1) control vector, x_{lower} and x_{upper} denote the (Nx1) lower and upper bounds of the control vector, respectively, x_b denotes the (Nx1) a priori, or background, states of the control vector, y denotes the (Mx1) observation vector, $H()$ denotes the nonlinear observation operator, R denotes the (MxM) observation error covariance matrix and w_{k-1} denotes the (Nx1) dynamical model error vector at time step k-1. The observation equation associated with the above cost function is given by:

$$y = H(x) + v \quad (4\text{-}7)$$

where v denotes the (Mx1) observation error vector at time step k. MLEF solves the nonlinear constrained minimization problem of Eqs.(4-5) and (4-6) in ensemble subspace via the following variable transformation which also serves as a perfect preconditioner (Zupanski, 2005):

$$x - x_b = P_f^{1/2}(I + C)^{-T/2}\zeta \quad (4\text{-}8)$$

In the above, I denotes the (SxS) identity matrix, ζ denotes the (Sx1) control vector in ensemble subspace and C denotes the (SxS) information matrix (see Zupanski 2005 for definition) whose ij-th entry is given by $z_i^T z_j$ where the (Mx1) vector $z_i, i = 1, \ldots, s,$ is defined and approximated via finite differencing by:

$$Z_i = (R^{-1/2}\tilde{H}P_f^{1/2})_i = R^{-1/2}\tilde{H}b_i \approx R^{-1/2}H(x+b_i) - R^{-1/2}H(x) \quad (4\text{-}9)$$

In the above, $\tilde{H}$ denotes the (MxS) Jacobian of the observation function, $H()$, with respect to the control variables. The gradient of the cost function with respect to the control vector in ensemble subspace is given by (Zupanski 2005):

$$g_\zeta = (I+C)^{-1}\zeta - (I+C)^{-\frac{1}{2}}\left(R^{-1/2}\tilde{H}P_f^{1/2}\right)^T R^{-1/2}\left\{y - H\left[x_b + P_f^{1/2}(I+C)^{-\frac{T}{2}}\zeta\right]\right\} \quad (4\text{-}10)$$

In Step 3, the control solution in ensemble subspace, ζ, is back-transformed to that in the physical space, x_{opt}, via Eq.(4-8). In Step 4, the square root analysis covariance matrix of the model state, $P_a^{1/2}$, is specified by Eq.(4-11) which is then used as ensemble perturbations for the next analysis cycle according to Eqs. (4-3) and (4-4):

$$P_a^{1/2} = P_f^{1/2}[I + C(x_{opt})]^{-T/2} \quad (4\text{-}11)$$

Finally, in Step 5, MLEF-HSPF makes the last call to HSPF to generate the DA-aided forecasts using the updated ICs. In evaluating $[I + C(x_{opt})]^{-T/2}$, MLEF-HSPF performs eigenvalue decomposition using the LAPACK algorithm, dspev (Linear Algebra Package, http://www.netlib.org/lapack). Noting that $[I + C(x_{opt})]^{-T/2}$ is a scaling and rotation operation on the ensemble subspace solution, the eigenvalue spectrum reflects the information content present in the ensemble members (see Subsection 6.3 for an example). Because MLEF is a reduced-rank filter, MLEF-HSPF may be rank-deficient in some assimilation cycles. The eigenvalue analysis helps assess possible rank deficiency. For minimization, MLEF-HSPF uses the Fletcher-Reeves-Polak-Ribiere algorithm of FRPRMN in Numerical Recipes (Press et al. 1986), a nonlinear conjugate gradient method.

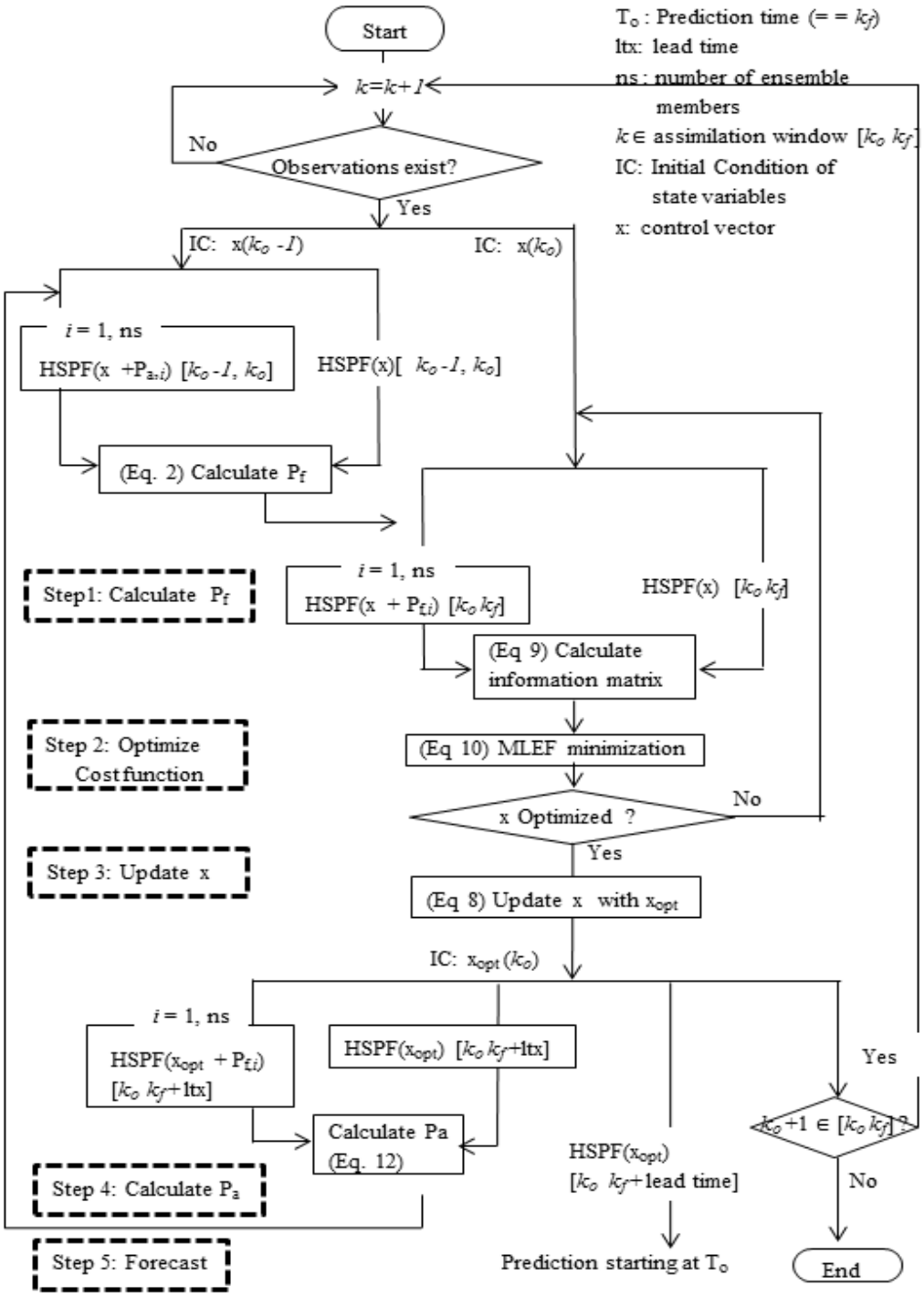

Figure 3-2 Flowchart of the MLEF-HSPF algorithm.

3.2. Initial perturbations of ICs

In the first step of the MLEF-HSPF algorithm, lognormal distribution is assumed for the control variables, in which the mean is given by the current state of the control variables and standard deviation given by the user-specified fraction of the current state. A number of state variables in the HSPF are collinear (e.g., PO_4 and CHL-a in the reaches). As such, it is necessary to account for interdependences among the state variables in the initial perturbations. It is well known (references here), however, that, even if the dependence structure among the initial states may not be realistic, the MLEF-updated ICs develop a realistic structure after a number of assimilation cycles.

3.3. Accounting of model errors

The original formulation of MLEF (Zupanski 2005) assumes a perfect dynamical model. MLEF has been used since to estimate and correct systematic model errors or biases (Zupanski and Zupanski 2006) but without accounting for random errors. Two approaches, direct perturbation and state augmentation were considered in this work to account for model errors as described below

3.3.1 *Direct perturbation approach*

In this approach, the residual model error $w_k^{p_i} - w_{k-1}^{c}$ is added to Eq.(4-2) where $w_k^{p_i}$ and w_{k-1}^{c} denote the dynamical model errors associated with the i-th perturbation and control runs, respectively. Because $w_k^{p_i} - w_{k-1}^{c}$ is a first order difference, model errors of the same direction cancel out and one may expect its magnitude to be smaller than that of w_{k-1} in Eq.(4-6a). In this work, $w_k^{p_i} - w_{k-1}^{c}$ was modeled as a fraction of the upper bound of the individual state variables based on the experience of applying MLEF

to hydrologic models for streamflow prediction (Rafieeinasab et al. 2014). The setting for the fraction was chosen based on sensitivity analysis (see Chapter 4).

3.3.2 *State augmentation approach*

In this approach, random errors in the dynamical model are explicitly accounted for by augmenting the square root forecast covariance matrix as follows:

$$P_f^{1/2} = [\{\tilde{M}P_{a,k-1}\}^{\frac{1}{2}} Q_{k-1}^{\frac{1}{2}}]^T \tag{4-12}$$

where Q_{k-1} denotes the (NxN) covariance matrix of the random error at time step k-1. Note that, by post-multiplying $(P_f^{1/2})^T$ to both sides of Eq.(4-12), one has $P_f = \tilde{M}P_{a,k-1}\tilde{M}^T + Q_{k-1}$, which is equivalent to the second-order moment propagation equation in KF. The above state augmentation, however, increases the dimensionality of the ensemble subspace by the size of the control vector, N, if the random errors are assumed to be mutually independent:

$$\begin{aligned} Q_{k-1} &= Q_{k-1}^{1/2} Q_{k-1}^{T/2} \\ &= \begin{bmatrix} w_{1,k-1} & \cdot & \cdot & 0 \\ \cdot & \cdot & \cdot & \cdot \\ \cdot & \cdot & \cdot & \cdot \\ 0 & \cdot & \cdot & w_{nnp2,k-1} \end{bmatrix} \begin{bmatrix} w_{1,k-1} & \cdot & \cdot & 0 \\ \cdot & \cdot & \cdot & \cdot \\ \cdot & \cdot & \cdot & \cdot \\ 0 & \cdot & \cdot & w_{nnp2,k-1} \end{bmatrix}^T \\ &= \begin{bmatrix} w_{1,k-1}^2 & \cdot & \cdot & 0 \\ \cdot & \cdot & \cdot & \cdot \\ \cdot & \cdot & \cdot & \cdot \\ 0 & \cdot & \cdot & w_{nnp2,k-1}^2 \end{bmatrix} \end{aligned} \tag{4-13}$$

In the above, nnp2 denotes the dimensionality of the control vector, nn+2, where nn denotes the total number of active HSPF state variables and the two additional entries representing the multiplicative adjustment factors for MAP and MAPE. Because the total

number of active HSPF state variables (i.e. nn) is very large, the increased computational burden associated with this approach can also be very large. For this reason, it is assumed in this work that the random errors are perfectly correlated among all control variables in which case the dimensionality is increased only by one:

$$
\begin{aligned}
Q_{k-1} &= Q_{k-1}^{1/2} Q_{k-1}^{T/2} \\
&= \begin{bmatrix} w_{1,k-1} \\ . \\ . \\ w_{nnp2,k-1} \end{bmatrix} [w_{1,k-1} \quad . \quad . \quad w_{nnp2,k-1}] \\
&= \begin{bmatrix} w_{1,k-1}^2 & . & . & w_1(k-1)w_{nnp2,k-1} \\ . & . & . & . \\ . & . & . & . \\ w_{nnp2,k-1}w_{1,k-1} & . & . & w_{nnp2,k-1}^2 \end{bmatrix}
\end{aligned}
\tag{4-14}
$$

To assess comparative performance between the direct perturbation and state augmentation approaches and between the independence and dependence assumptions for the state augmentation approach, a set of twin experiments were carried out, which are described in Subsection 4.6.

3.4. Observational error variance

Ideally, the observational error should be modeled heteroscedastically. Since the truth is not generally not known, however, such modeling is a tall order. In this work, all observational errors are modeled as homoscedastic for simplicity and parsimony and prescribed based on sensitivity analysis (see Appendix A) for each observed water quality variable (see Table 4-2). Experience also suggests that heteroscedastic modeling is rather tricky and requires uncertainty information which is usually not available in the real world (Rafieeinasab et al. 2014).

3.5. Bias correction

DA as formulated above addresses uncertainties in the ICs and observed BCs of MAP and MAPE only. If significant parametric or structural errors exist in the model, DA is likely to adjust the model ICs for the wrong reasons to compensate for any systematic biases resulting from other sources of error. Ideally, issues such as model bias, scale-dependent variability and limited dynamic range should be addressed by improving model physics and calibration before DA. Such an effort, however, is expected to occur over time and hence is beyond the scope of this research. As an alternative, MLEF-HSPF employs a bias correction procedure to account for systematic errors so that the DA solution may be found within the dynamic range of the model. To correct conditional biases in model simulations particularly in the right tail end of their distributions, MLEF-HSPF uses conditional bias-penalized optimal linear estimation (Seo 2013, Seo et al. 2014). The operation amounts to embedding linear transformation in the observation equation, Eq.(4-7), under the assumption that the model simulation and the verifying observation are linearly related according to:

$$Y_i = a_i X_i + b_i + \varepsilon_i \tag{4-15}$$

where X_i and Y_i denote the model-simulated and actual observations of the i-th variable, respectively, a_i and b_i denote the coefficients of the i-the variable to be determined, and ε_i denotes the zero-mean random error for the i-th variable. In conventional linear estimation or regression, the coefficients are solved for by minimizing the error variance only, $E_{Y_i^*,Y_i}[(Y_i^* - Y_i)^2]$, where $Y_i^* = a_i X_i + b_i$ and the subscripts denote the variables for which the expectation is taken. In conditional bias-penalized linear estimation, the penalty term for Type-II conditional bias is added to the objective function (Seo 2013):

$$J_i = E_{Y_i^*, Y_i}[(Y_i^* - Y_i)^2] + \alpha_i E_{Y_i}[\{E_{Y_i^*}[Y_i^* \mid Y_i] - Y_i\}^2] \quad (4\text{-}16)$$

where α_i denotes the weight given to the conditional bias penalty term for the i-th variable. Using the Bayesian optimal linear estimator (Schweppe 1973) for $E_{Y_i^*}[Y_i^* \mid Y_i]$, it can be easily shown that the solution for the above minimization is given by (Seo 2013):

$$a_i = \frac{1+\alpha_i}{1+\alpha_i \rho_{X_i Y_i}^2} \rho_{X_i Y_i} \frac{\sigma_{Y_i}}{\sigma_{X_i}} \quad (4\text{-}17)$$

$$b_i = m_{Y_i} - a_i m_{X_i} \quad (4\text{-}18)$$

where $\rho_{X_i Y_i}$ denotes the correlation between X_i and Y_i, σ_{X_i} and σ_{Y_i} denote the standard deviation of X_i and Y_i, respectively, and m_{X_i} and m_{Y_i} denote the mean of X_i and mean of Y_i, respectively. Note that, if α_i=0 (i.e. conditional bias is not at all important), the slope a_i is reduced to the conventional optimal linear estimation solution, i.e., $a_i = \rho_{X_i Y_i} \sigma_{Y_i} / \sigma_{X_i}$. If $\alpha_i \to \infty$ (i.e. conditional bias is of sole importance), the slope a_i is reduced to $a_i = (1/\rho_{X_i Y_i}) \sigma_{Y_i} / \sigma_{X_i}$. The weight, α_i, is chosen based on sensitivity analysis and visual inspection of the fit as described in Subsection 6.2. Once the bias correction parameters are estimated for each observed variable, they are used in MLEF-HSPF in two different ways. The first is to transform the actual observations, y in Eqs. (4-5) and (4-10), into the model state space by inverting them via $Y_i^* = a_i X_i + b_i$. The second is to transform the updated model states, x_{opt} in Eq. (4-11), and the predicted states into the observation space via $Y_i^* = a_i X_i + b_i$ for DA-aided analysis and predictions, respectively.

Chapter 4

MLEF-HSPF parameters and their estimation

MLEF-HSPF employs a set of DA-specific parameters to optimize performance and to maximize flexibility. The parameters include ensemble size, assimilation window, tolerance (for terminating minimization), multiplicative scaling factors to initially perturb the ICs, magnitude of model error, and observation error variances. The selection of the optimal settings based on sensitivity analysis for each parameter is explained in Subsections 4.1 through 4.7. The sensitivity analyses were carried out only for the Kumho Catchment in the Nakdong River Basin for a two-year period (2008-2009) to compare HSPF simulation results 1) without bias correction or DA (Base), 2) with bias correction only (BC-Base) and 3) with bias correction and DA (BC-DA) under the assumption of clairvoyant future MAP and MAPE. To assess performance, root mean square error (RMSE) was calculated for Base, BC-Base and BC-DA for analysis and Day-1 through -3 predictions of biochemical oxygen demand (BOD), chlorophyll-a (CHL-a), dissolved oxygen (DO), nitrate (NO_3), phosphate (PO_4), water temperature (TW) and streamflow.

4.1. Ensemble size

A set of sensitivity analyses were performed to determine the optimum ensemble size. The ensemble sizes of 9, 15, 18 and 24 were considered (see Table 4-1) for the sensitivity analyses. Figure 4-2 through Figure 4-8 show the RMSE of Base (black bars), BC-Base (white bars) and BC-DA (green bars) for analysis and Day-1 through -3 predictions of water quality variables and streamflow. It was observed that the performance of MLEF is not very sensitive to the ensemble size and the performance is satisfactory even with an ensemble size as small as 9. Therefore, an ensemble size of 9 was chosen throughout the rest of this work.

4.2. Assimilation window

It is necessary to consider a number of factors in sizing the assimilation window. If the window is too large, the set of observations being assimilated in each cycle would be large and some of the observations may be too old and/or redundant. If the window is too small, the DA procedure would work mostly like a filter than a smoother, thereby compromising performance. In this research, the window sizing was dictated largely by the fact that the water quality observations are available only about once a week on average. It means that, in order to perform DA on a daily basis, the assimilation window has to be at least as large as 7 days. Based on the above considerations, a 7-day assimilation window was chosen in this work so that water quality observations were available for assimilation in most cycles (see Appendix A).

4.3. Tolerance for terminating minimization

The DA algorithm uses the Fletcher-Reeves-Polak-Ribiere algorithm (FRPRMN, Press et al. 1986) for minimization. A large/small value of *ftol* prescribes a large/small tolerance in the stopping criterion, expressed in terms of reduction in the cost function. Two values, 10e+1 and 10e+3, of tolerance were compared (see Table 4-1). A smaller ftol increases the number of iterations thereby increasing the computational amount while a larger ftol may not produce a near-optimal solution. Based on the RMSE results, a setting of 10e+3 was chosen (see Figure 4-2 through Figure 4-8).

4.4. Multiplicative scaling factor for initial perturbation

The multiplicative scaling factor (frac_state) for the HSPF state variables specifies the standard deviation of the perturbations to the model states. For example, if it is set to 0.1, the standard deviation of the perturbations is 10% of the magnitude of the states. Based on the sensitivity analysis (see Appendix A), it was set to 0.01.

4.5. Model error factor

The model error factor, f (frac_gen), represents a fraction of the difference between the current model states and the model states at the receding time step. Based on the sensitivity analysis (see Appendix A), the model error factor was set to 0.1 (i.e., 10% of the difference in the model states between the current and the preceding time steps). An extremely large value of f means that the model has no predictive skill and $f = 0$ implies that the model is perfect. In the former, MLEF would draw information solely from the observations within the current assimilation window whereas, in the latter, MLEF would place a large weight to the model predictions when combining with the observations.

4.6. Model error augmentation

In the state augmentation approach (iaug), the model errors may be considered either dependent or independent among all state variables. If *iaug* is set to 1, model errors are assumed independent. If *iaug* is set to 2, model errors are assumed dependent. Two sets of experiments were carried out to evaluate the performance of DA in each approach (Figure 4-1). The computational burden under the assumption of independent model error is far greater (15 days for a 1-yr run) than dependent model error (1 day for the same 1-yr run). Yet, it was found that the performance of DA under the dependence assumption is superior. The reduction in RMSE for prediction is 5% for TW, 10% for BOD, DO, NO_3, and PO_4, and 15% for streamflow and CHL-a over the results based on the independence assumption.

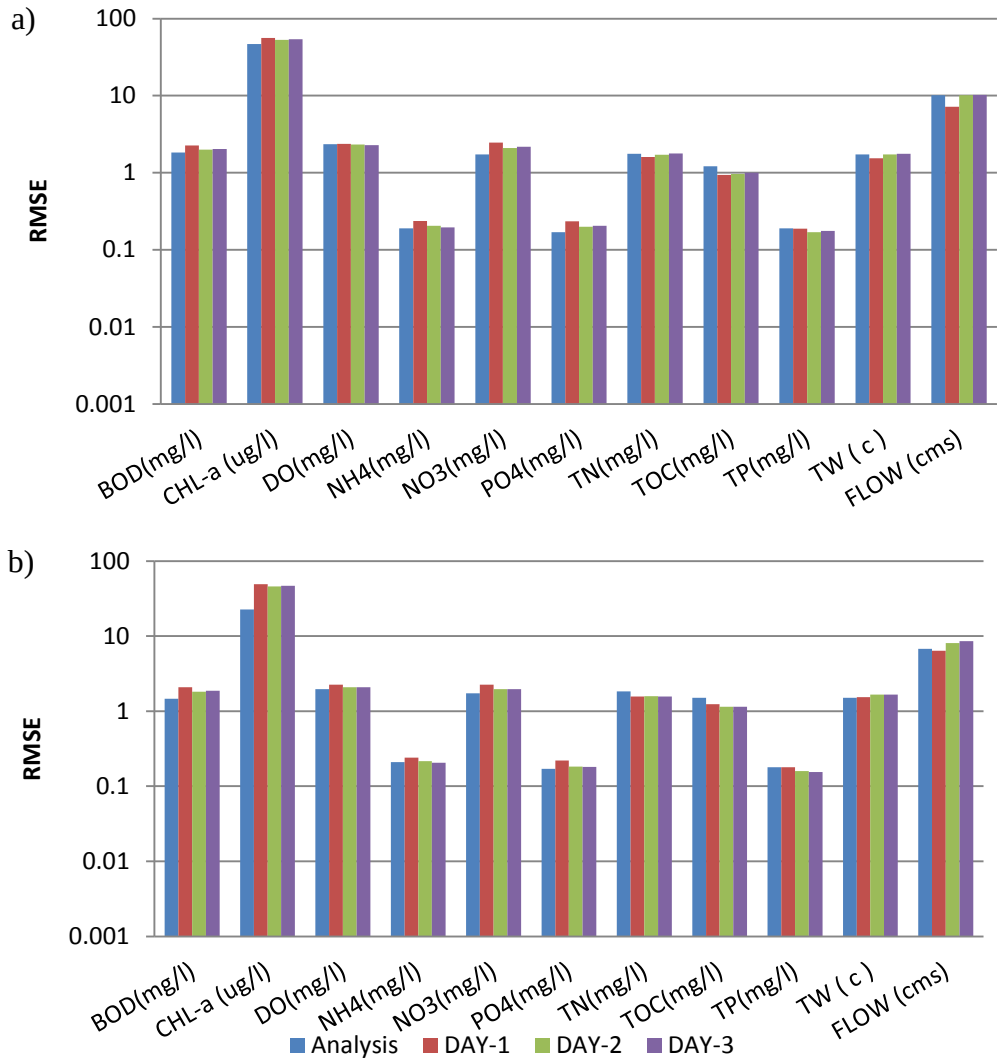

Figure 4-1 RMSE for DA performance using the state augmentation approach (a) independence and (b) dependence assumptions.

4.7. Observational error variance

All observation errors are assumed to be independent of one another. An extremely large value for the observation error variances indicates non-informative data, in which case DA has no impact on the base (i.e. DA-less) model prediction. An extremely small value, on the other hand, indicates near-perfect observations, in which

case DA would weigh the data very heavily even if it may mean deviating greatly from the model prediction. The magnitude of the observation error variances are based on a combination of laboratory analysis (Ministry of Environment, 2011) and sensitivity analysis. The initial estimates for observation error variances were used in Run 1. Except for BOD, DA reduced analysis RMSE for all water quality variables. The observation error variance for BOD was then reduced by an order of magnitude to assess sensitivity (Run 3), which further reduced RMSE. The observation error variance for BOD was reduced again by an order of magnitude (Run 4) which, while reduced RMSE for BOD analysis, increased RMSE for analysis of other variables such as CHL-a. In Run 6, the observation error variances were reduced by two orders of magnitude compared to those for Run 5. For most water quality variables, the results for both analysis and prediction were similar to those for Run 3. As such, the observation error variances for Run 3 were selected (see Table 4-1 and Figure 4-2 through Figure 4-8). It was seen that, among all runs for the Kumho Catchment, the RMSE of BC-DA compared to Base for most of the water quality variables and streamflow was greatly reduced in Run 3. Thus, the parameter settings associated with Run 3 were identified to be the best (see Table 4-2).

Table 4-1 The MLEF-HSPF parameters settings for systematic sensitivity analysis runs for the Kumho Catchment.

Run		1	2	3	4	5	6	7	8	9	10	11	12	13	14	15	16
Ensemble size		9	9	9	9	9	9	15	9	9	18	9	18	18	24	9	9
Tolerance for terminating minimization		10^{-4}	10^{-4}	10^{-4}	10^{-4}	10^{-4}	10^{-4}	10^{-4}	10^{-2}	10^{-4}	10^{-4}	10^{-2}	10^{-4}	10^{-2}	10^{-4}	10^{-4}	10^{-4}
Model error		0.1	0.1	0.1	0.1	0.1	0.1	0.1	0.1	0.1	0.1	0.1	0.1	0.1	0.1	0.1	0.1
Multiplicative scaling factor		0.01	0.01	0.01	0.01	0.01	0.01	0.01	0.01	0.01	0.01	0.01	0.01	0.01	0.01	0.01	0.01
Observation error variance	**Daily flow**	0.1	0.1	0.1	0.1	1	0.01	0.1	0.1	0.1	0.1	0.1	0.1	0.1	0.1	0.1	0.1
	Hourly flow	0.1	0.1	0.1	0.1	1	0.01	0.1	0.1	0.1	0.1	0.1	0.1	0.1	0.1	0.1	0.1
	Dftmdl flow	1	1	1	1	10	0.1	1	1	1	1	1	1	1	1	1	1
	TW	0.1	0.1	0.1	0.1	1	0.01	0.1	0.1	1	1	1	0.1	0.1	0.1	0.1	0.1
	NH_4	0.001	0.001	0.001	0.001	0.01	0.0001	0.001	0.001	0.001	0.001	0.001	0.001	0.001	0.001	0.001	0.001
	NO_3	0.1	0.1	0.1	0.1	1	0.01	0.1	0.1	1	1	1	0.1	0.1	0.1	0.1	0.1
	PO_4	0.01	0.01	0.01	0.01	0.1	0.001	0.01	0.01	0.1	0.1	0.1	0.01	0.01	0.01	0.01	0.01
	BOD	0.1	0.01	0.01	0.001	0.1	0.001	0.01	0.01	0.01	0.01	0.01	0.01	0.01	0.01	0.01	0.01
	CHL-a	1	1	1	1	10	0.1	1	1	1	1	1	1	1	1	1	1
	DO	0.01	0.01	0.01	0.01	0.1	0.001	0.01	0.01	0.01	0.01	0.01	0.01	0.01	0.01	0.01	0.01
	Precipitation	0.1	1	0.1	0.1	1	0.01	0.1	0.1	0.1	0.1	0.1	0.1	0.1	0.1	0.1	0.1
	Evaporation	0.1	1	0.1	0.1	1	0.01	0.1	0.1	0.1	0.1	0.1	0.1	0.1	0.1	0.1	0.1
	TP	1	1	1	1	10	0.1	1	1	10	10	10	1	1	1	1	1
	TN	1	1	1	1	10	0.1	1	1	10	10	10	1	1	1	1	1
	TOC	1	1	1	1	10	0.1	1	1	10	10	10	1	1	1	1	1
Model error augmentation		2	2	2	2	2	2	2	2	2	2	2	2	2	2	1	2

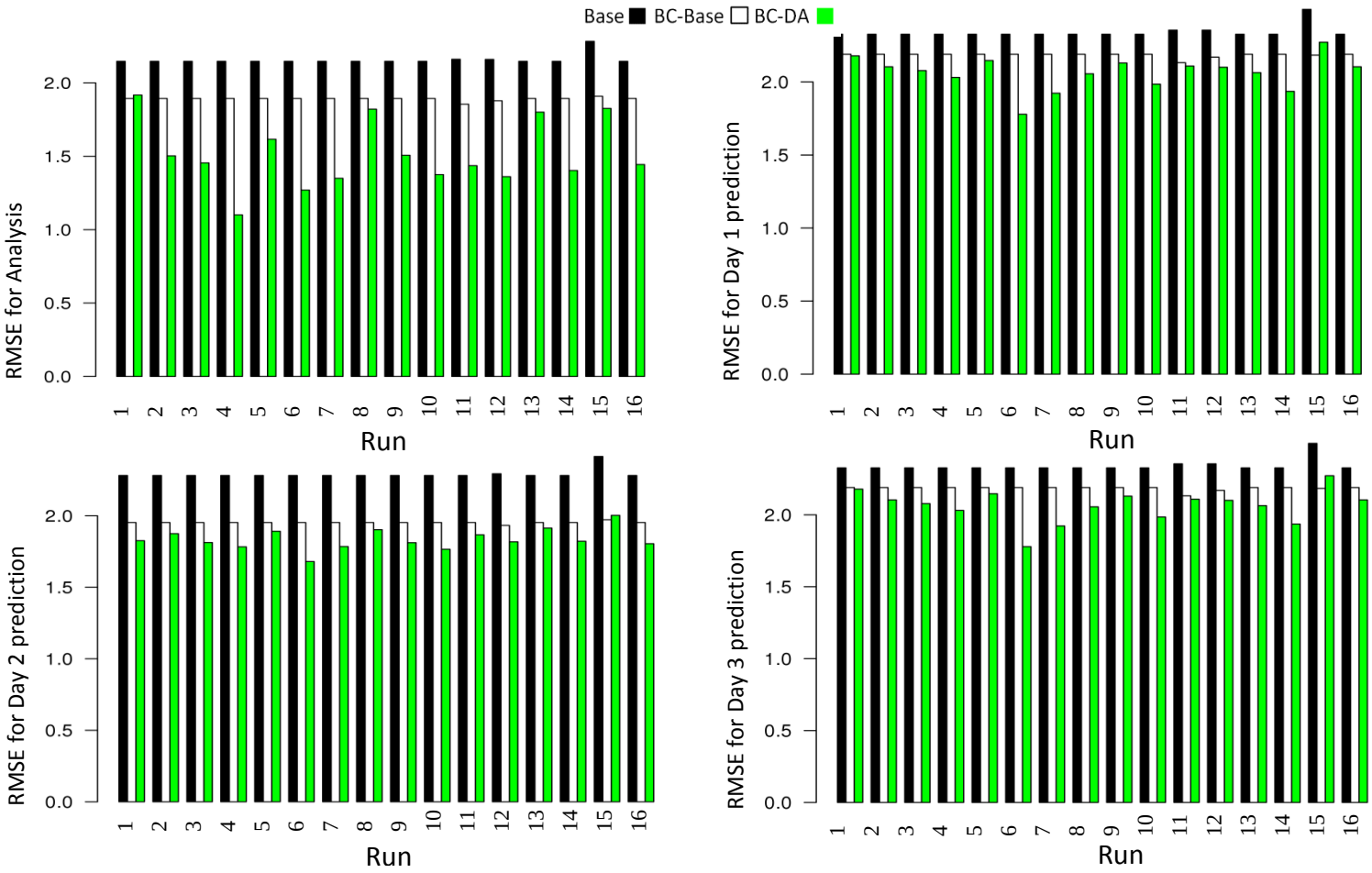

Figure 4-2 RMSE of Base, BC-Base and BC-DA for analysis and Day-1 through Day-3 prediction of BOD.

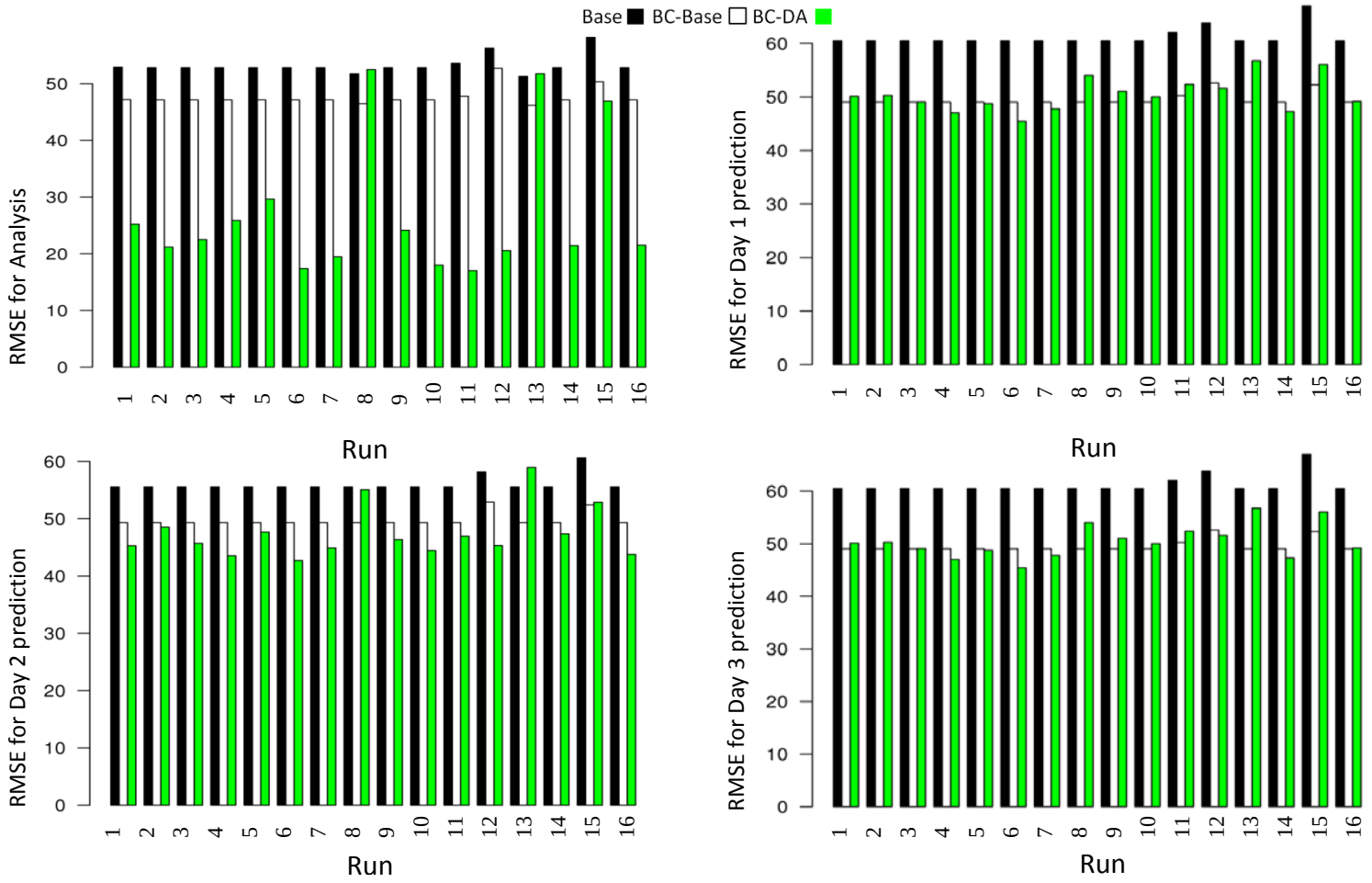

Figure 4-3 RMSE of Base, BC-Base and BC-DA for analysis and Day-1 through Day-3 prediction of CHL-a.

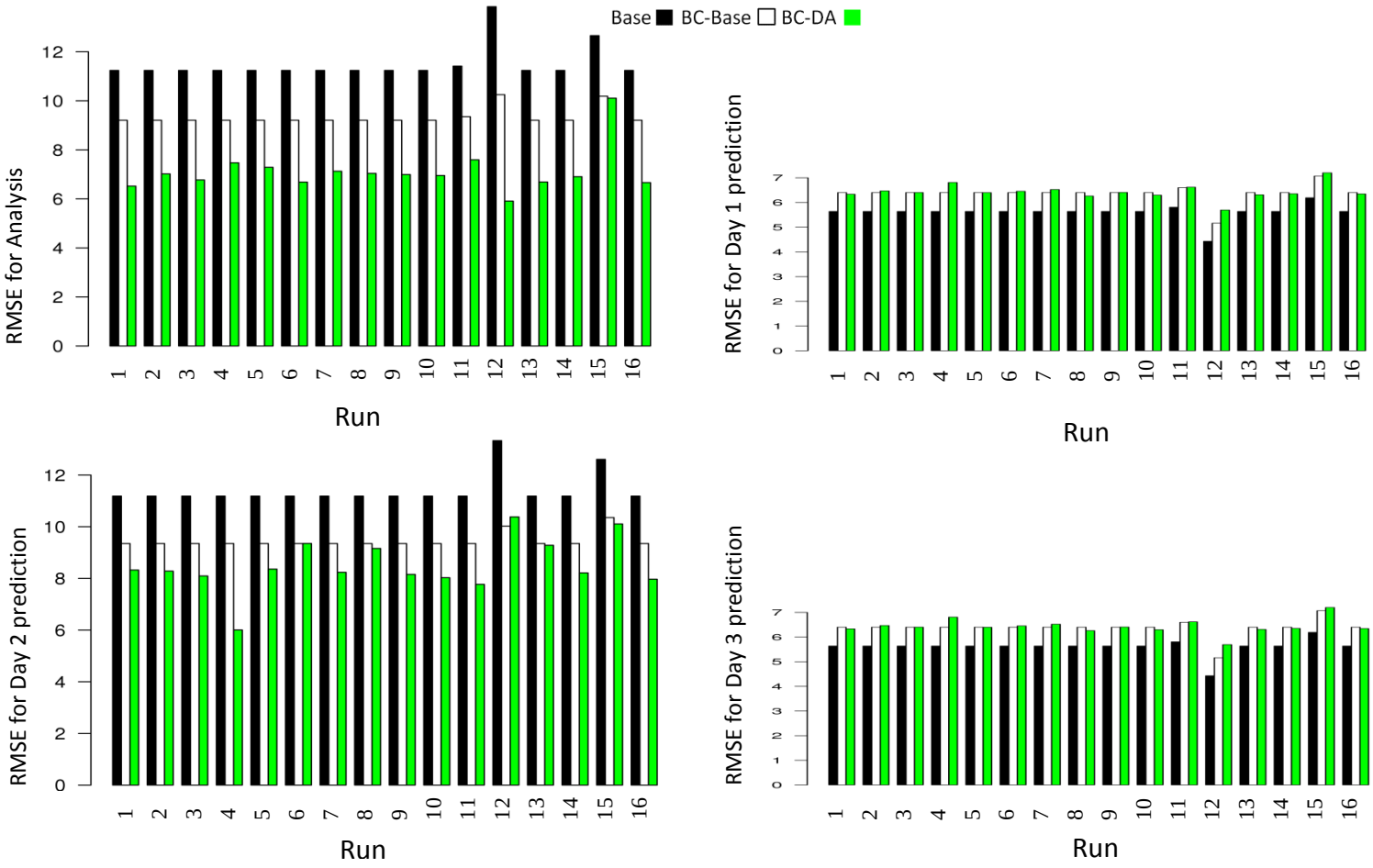

Figure 4-4 RMSE of Base, BC-Base and BC-DA for analysis and Day-1 through Day-3 prediction of Flow.

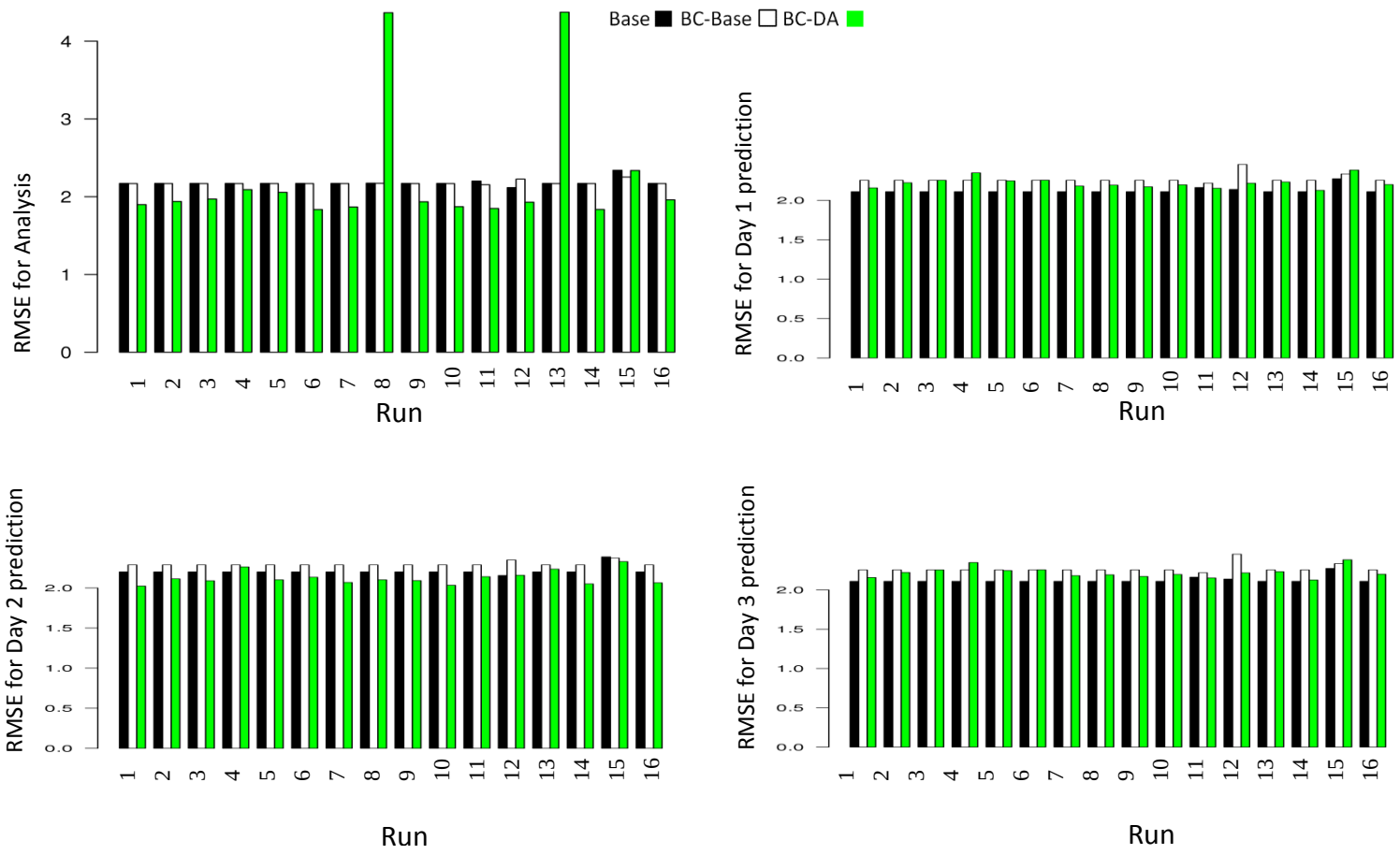

Figure 4-5 RMSE of Base, BC-Base and BC-DA for analysis and Day-1 through Day-3 prediction of DO.

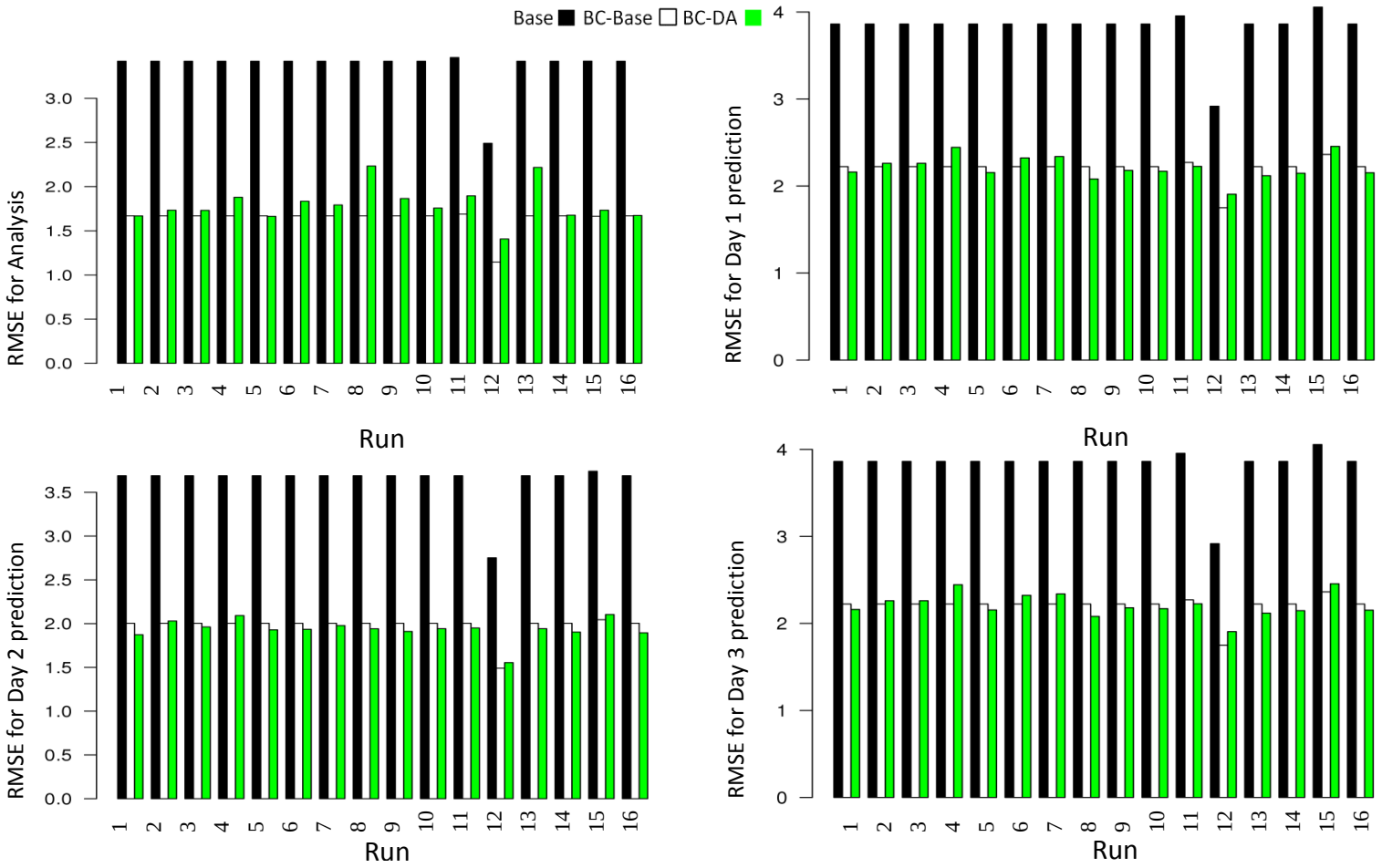

Figure 4-6 RMSE of Base, BC-Base and BC-DA for analysis and Day-1 through Day-3 prediction of NO_3.

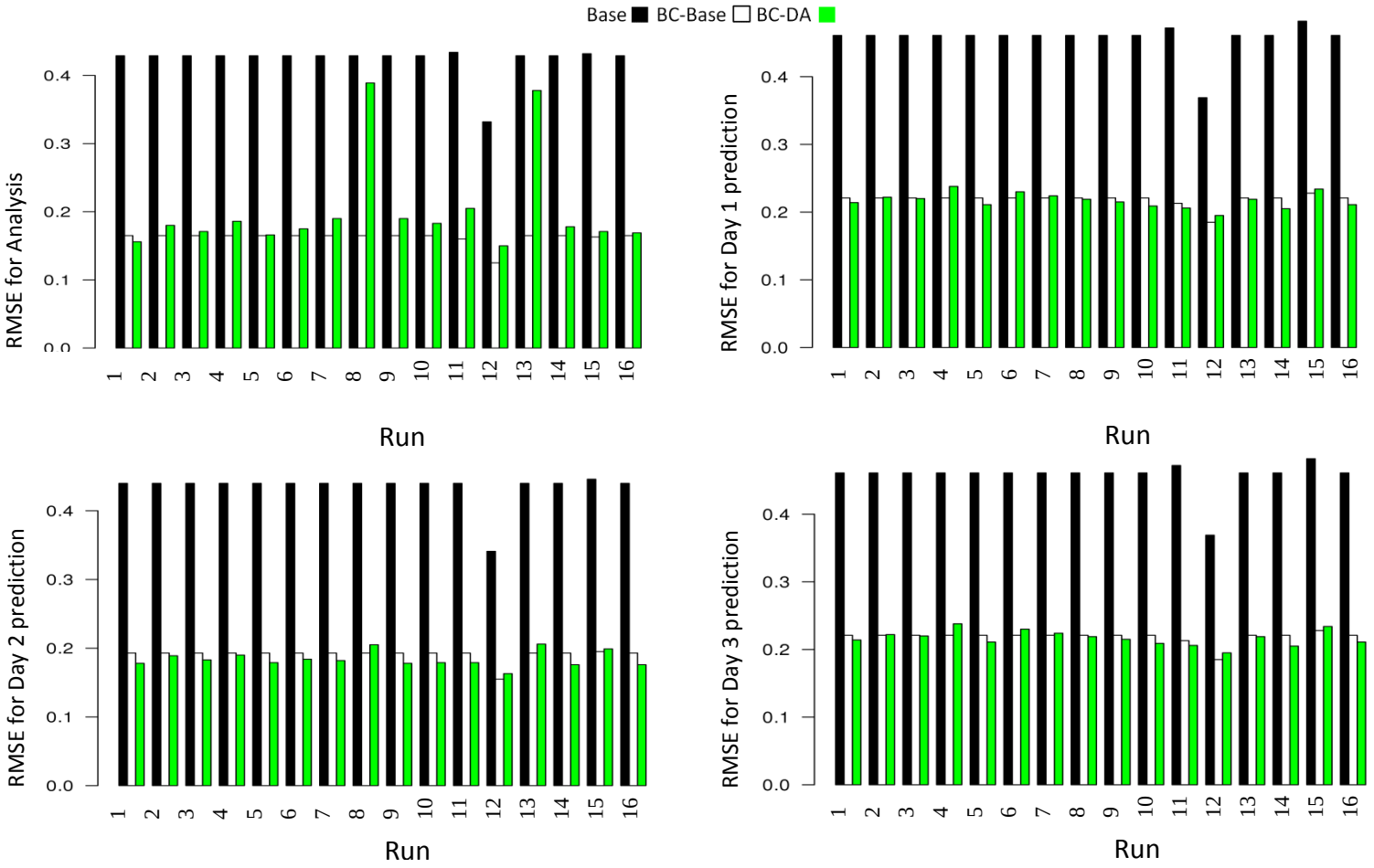

Figure 4-7 RMSE of Base, BC-Base and BC-DA for analysis and Day-1 through Day-3 prediction of PO_4.

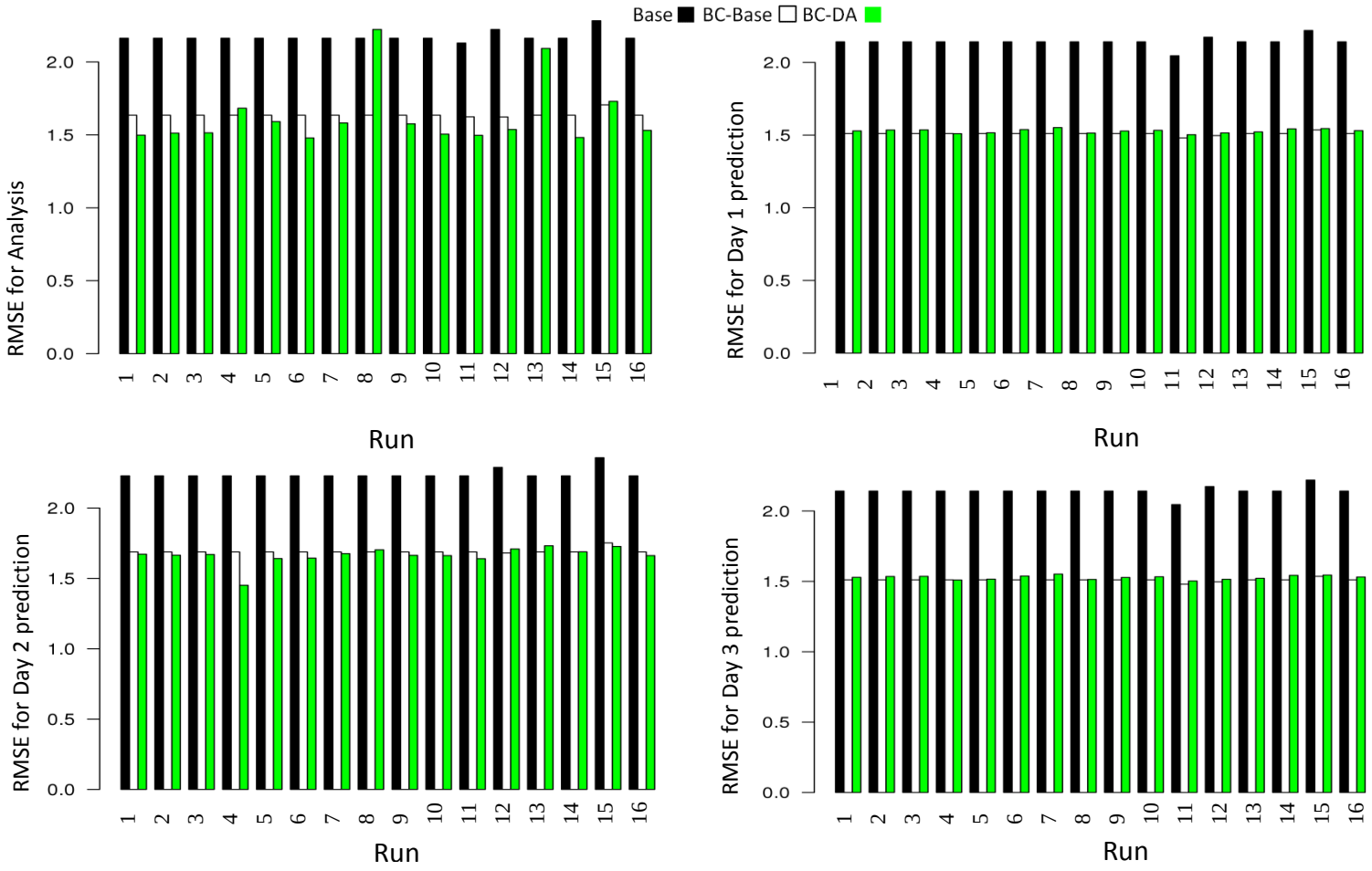

Figure 4-8 RMSE of Base, BC-Base and BC-DA for analysis and Day-1 through Day-3 prediction of TW.

Table 4-2 MLEF-HSPF parameter settings for the Kumho Catchment. Shown in the parentheses are the parameter names used in MLEF-HSPF.

<table>
<tr><td colspan="5">Description (parameter name)</td><td colspan="3">Recommended setting</td></tr>
<tr><td colspan="5">Dynamical model error in one-step transition (frac_gen)</td><td colspan="3">0.1</td></tr>
<tr><td colspan="5">Multiplicative scaling factor to the HSPF state variables for the initial perturbation (frac_state)</td><td colspan="3">0.01</td></tr>
<tr><td colspan="5">Ensemble size (ns)</td><td colspan="3">9</td></tr>
<tr><td colspan="5">Option for mean daily flow observations (idf)</td><td colspan="3">0</td></tr>
<tr><td colspan="5">Assimilation window in hrs (nwin)</td><td colspan="3">7 x 24</td></tr>
<tr><td colspan="5">Option for the use of LAPACK solver (ilapack)</td><td colspan="3">1</td></tr>
<tr><td colspan="5">Tolerance for the stoppage condition for conjugate gradient minimization (ftol)</td><td colspan="3">10.e+3</td></tr>
<tr><td rowspan="4">Control variables</td><td rowspan="3">Number of HSPF state variables to be updated (nstate)</td><td>Pervious</td><td colspan="2">Interception storage
Surface (overland flow) storage
Interflow storage
Active groundwater storage
Upper zone storage
Lower zone storage
Index to groundwater slope
BOD, NH_4, NO_3, PO_4</td><td>11</td><td rowspan="3">28</td><td rowspan="4">30</td></tr>
<tr><td>Impervious</td><td colspan="2">Retention storage
Surface (overland flow) storage
BOD, NH_4, NO_3, PO_4</td><td>6</td></tr>
<tr><td>Reach</td><td colspan="2">Volume of water in the reach
water temperature
Chlorophyll-a,
DOX,ORP,ORN,ORC
BOD, NH_4, NO_3, PO_4</td><td>11</td></tr>
<tr><td colspan="5">multiplicative adjustment factors for MAP and MAPE</td><td>2</td></tr>
<tr><td colspan="3" rowspan="14">Observation error variance</td><td colspan="3">Mean daily flow, $(cms)^2$</td><td>0.1</td></tr>
<tr><td colspan="3">Hourly flow, $(cms)^2$</td><td>0.1</td></tr>
<tr><td colspan="3">Instantaneous flow, $(cms)^2$</td><td>1.</td></tr>
<tr><td colspan="3">Water temperature (degrees $C)^2$</td><td>0.1</td></tr>
<tr><td colspan="3">NH_4, $(mg/l)^2$, RCH only</td><td>0.001</td></tr>
<tr><td colspan="3">NO_3, $(mg/l)^2$</td><td>0.1</td></tr>
<tr><td colspan="3">PO_4, $(mg/l)^2$</td><td>0.01</td></tr>
<tr><td colspan="3">BOD, $(mg/l)^2$, RCH only</td><td>0.1</td></tr>
<tr><td colspan="3">CHL-a, $(ug/l)^2$, RCH only</td><td>1.</td></tr>
<tr><td colspan="3">DO, $(mg/l)^2$, RCH only</td><td>0.01</td></tr>
<tr><td colspan="3">TP, $(mg/l)^2$, RCH only</td><td>1.</td></tr>
<tr><td colspan="3">TN, $(mg/l)^2$, RCH only</td><td>1.</td></tr>
<tr><td colspan="3">TOC, $(mg/l)^2$, RCH only</td><td>1.</td></tr>
<tr><td colspan="3">Hourly precipitation, $(mm)^2$</td><td>1.</td></tr>
<tr><td colspan="3">Hourly PE, $(mm)^2$</td><td>1.</td></tr>
</table>

Chapter 5

Evaluation

Ideally, one would like to test and evaluate MLEF-HSPF in real time environment for operational forecasting. Due to lack of real-time observations and forecast forcings, however, such testing and evaluation were not possible. Instead, a set of hindcasting experiments were designed and carried out for retrospective evaluation of MLEF-HSPF using the observed forcings of MAP and MAPE under the assumption of clairvoyant future forcings.

5.1. Study area

The four major river basins in the Republic of Korea are the Han, the Geum, the Nakdong and the Youngsan River Basins. The four river basins consist of 32 catchments ranging in size from 66 km^2 to 7200 km^2 (Table 5-1). For evaluation of MLEF-HSPF, multiple catchments were chosen based on examination of the overall quality of HSPF simulations, the number of water quality variables observed, the period of record of observations, and the observation frequency. The streamflow and water quality observations used in this research are made approximately once a week at the water quality and point-source monitoring stations. They are the instantaneous observations of streamflow, water temperature (TW), ammonium (NH_4), nitrate (NO_3), phosphate (PO_4), chlorophyll-a (CHL-a), total nitrate (TN), total phosphate (TP), total organic carbon (TOC), biochemical oxygen demand (BOD), and dissolved oxygen (DO). The observation time, typically between 10 am to 5 pm, varies from station to station and according to the sampling schedule.

The MLEF-HSPF module is capable of assimilating observations from both the outlet and interior locations within a catchment. Because HSPF has not been calibrated

for the interior locations, however, the hindcasting experiments were performed only for the most downstream (outlet) monitoring station in each catchment.

Table 5-1 Catchments in the Geum, Han, Nakdong, and Yeongsan River Basins.

River Basin	Catchment	Most downstream monitoring station ID	Area (km^2)	Number of monitoring stations
Geum	Daekyo	38	66	1
	Gap	40	649	9
	Jeongahn	34	161	1
	Miho	26	1855	15
	Yongsu	37	98	1
	Yugu	43	283	1
Han	Bokha	100	312	3
	Cheongmi	132	580	3
	Cheongpyeong	35	7182	19
	Chungjudam	185	6683	24
	Dal	164	1593	12
	Gyeongan	80	545	4
	Jojong	34	262	3
	Seom	130	1483	12
	Yanhwa	106	353	1
Nakdong	Andongdam	51	1610	8
	Banbyeon	52	1957	8
	Gam	90	1000	3
	Hoe	158	775	3
	Hwang	161	1301	9
	Kumho	135	2170	12
	Naeseong	49	1804	11
	Nam	186	3437	20
	Whi	74	1396	6
	Yeong	63	909	3
Yeongsan	Gomakwo	68	218	3
	Gwangju	34	114	2
	Hwangnyong	40	554	4
	Jisuk	46	654	6
	Manbong	65	108	2
	Pungyeongjeong	29	117	1
	Yeongsan	28	476	3

5.2. Data availability

Table 5-2 shows the availability of observations at the most downstream monitoring stations in the four major river basins in Korea. Most water quality variables

are sampled weekly (w) or monthly (m). For most monitoring stations, the period of record for the water quality observations is different from that for the streamflow observation before 2011. Since 2011, however, both the sampling interval and period of record are the same for all observations. The observations of NO_3, NH_4, PO_4, CHL-a and TOC are sampled more infrequently than other water quality observations in several catchments (see Column 9 in Table 5-2).

5.3. Study catchments

The NIER's calibration period of HSPF for all catchments is from Jan 2008 to Dec 2010. For dependent validation, the Kumho Catchment in the Nakdong River Basin is used based on the availability of observations and the quality of HSPF simulation. The Kumho River is the largest tributary of the Nakdong River and runs through Daegu, the third largest city in the Republic of Korea. As such, the Kumho River is susceptible to degradation in water quality and has a clear need for accurate water quality forecasting to avoid hazardous water quality situations. Similarly, based on the availability of the observations and the quality of the HSPF simulations, 12 catchments were selected for independent validation. The selected catchments include the Gap and Miho Catchments in the Geum River Basin, the Cheongmi, Jojong, Seom and Yanhwa Catchments in the Han River Basin, the Gam, Kumho and Nam Catchments in the Naktong River Basin and the Gomakwo, Jisuk and Uchi Catchments in the Youngsan River Basin.

The cross-correlation functions (CCF) between the observed and simulated variables were estimated for the selected catchments for a 6-year period of 2008 to 2013. Table 5-3 shows the maximum cross correlation values along with the time lags at which the maxima occur. A non-zero lag indicates a phase error (a lag of 1 corresponds to one week). Among the 12 catchments, those catchments for which the lags are close to zero for most of the variables are selected for independent validation. Therefore for

independent validation, MLEF-HSPF module has been tested and evaluated extensively for the Kumho Catchment in the Nakdong River Basin, the Jojong and Yanghwa Catchments in the Han River Basin and the Miho Catchment in the Geum River Basin (see Figure 5-1). The area pie charts in Figure 5-1 show the land use patterns in the catchment. Six different land usages are represented in each catchment: forest, agricultural land, pervious developed land, impervious land, wet land, and water. Note that the Miho Catchment has the highest percentage of urban area.

5.4. Selection of the catchments for comparison between HSPF-DA and time series modeling

Comparisons between the DA-aided predictions using HSPF and those based on time series modeling are made for the Kumho, Banbyeon, Naeseong, and Nam Catchments in the Nakdong River Basin, the Seom Catchment in the Han River Basin, and the Uchi Catchment in the Youngsan River Basin (see Figure 5-2). The available period of record for these catchments is from Jan 2008 to Dec 2013 during which all the variables were observed weekly.

Table 5-4 through Table 5-9 show the statistical measures including root mean square error (RMSE), mean square error (MSE) decomposition, correlation coefficient and Nash-Sutcliff efficiency (NSE) of all observed variables at the outlet of the selected catchments in the four major river basins in Korea. Note that, except for the Kumho and Seom Catchments, the HSPF simulations for most of the variables are generally poor.

Table 5-2 availability of observations at each monitoring station in the four major river basins.

River Basin	Catchment	Flow (m3/s)			Water quality variables			Water quality variables collected separately from the 6, 7, and 8th columns
		Start	Sample size	Sampling frequency	Start	Sample size	Sampling frequency	
Geum	Daekyo	2012	67	w	2012	75	w	TOC: 53 since 2012
	Gap	2009	183	w	2008	308	w	TOC: 296
	Jeongan	2012	128	m & w	2008	128	m & w	TOC: 29 since 2011
	Miho	2009	147	w	2008	308	w	TOC: 196 since 2008
	Yongsu	2012	64	m & w	2008	128	m & w	TOC: 51 since 2012
	Yugu	2012	74	m & w	2008	128	m & w	TOC: 51 since 2012
Han	Bokha	2011	124	w	2008	270	w	NO_3,NH_4,PO_4: 92 since 2010, CHL-a: 76 since 2011
	Cheongmi	2011	126	w	2008	269	w	CHL-a: 138 since 2008
	Cheongpyeong	2011	129	w	2008	217	w	NO_3,NH_4,PO_4,CHL-a: 94 since 2010
	Chungjudam	2011	126	w	2008	267	w	CHL-a: 72 since 2008
	Dal	2011	120	w	2008	267	w	CHL-a: 136 since 2008
	Gyeongan	2011	142	w	2008	290	w	NO_3,NH_4,PO_4,CHL-a: 96 since 2010
	Jojong	2011	122	w	2008	267	w	CHL-a: 138 since 2008
	Seom	2011	125	w	2008	302	w	--
	Yanhwa	2011	123	w	2008	269	w	CHL-a: 138 since 2008
Nakdong	Andongdam	2008	290	w	2008	290	w	TOC: 152 since 2008, m & w
	Banbyeon	2008	282	w	2008	289	w	--
	Gam	2012	63	w	2008	116	m & w	--
	Hoe	2008	237	w	2008	239	w	NO_3,NH_4,PO_4: 154, m & w, CHL-a:193 since 2008
	Hwang	2008	239	w	2008	240	w	NO_3,NH_4,PO_4: 157, m & w, CHL-a:194 since 2008
	Kumho	2008	283	w	2008	289	w	--
	Naeseong	2008	268	w	2008	289	w	--
	Nam	2008	279	w	2008	289	w	--
	Whi	2008	233	w	2008	238	w	CHL-a:193 since 2008, m & w
	Yeong	2008	237	w	2008	239	w	NO_3,NH_4,PO_4: 159, m & w, CHL-a:194 since 2008
Yeongsan	Gomakwo	2012	92	w	2008	264	w	NO_3,NH_4,PO_4,CHL-a:73 since 2008
	Gwangju	2012	74	m & w	2008	127	m & w	NO_3,NH_4,PO_4:118 since 2008, TOC: 85 since 2011
	Hwangnyong	2012	67	w	2008	299	w	--
	Jisuk	2012	71	w	2008	299	w	--
	Manbong	2012	71	w	2012	72	w	NO_3,NH_4,PO_4: 54 since 2012
	Pungyeongjeong	2012	72	m &w	2008	125	m &w	NO_3,NH_4,PO_4: 97, TOC:74 since 2011
	Uchi	2011	154	w	2008	306	w	TOC: 288

Table 5-3 Maximum CCF value along with corresponding lag value for all the variables for the selected catchments.

River Basin	Catchments	Variable	TW	FLOW	PO_4	DO	BOD	NO_3	NH_4	CHL-a	TP	TN	TOC
GEUM	Miho	CCF	0.96	0.72	0.34	0.55	0.52	0.62	0.61	0.65	0.3	0.59	-0.31
		lag	0	0	-1	0	1	0	1	0	8	0	13
	Gap	CCF	0.97	0.8	0.31	0.29	0.57	-0.23	0.52	0.49	0.75	0.52	-0.29
		lag	0	0	-14	-13	1	10	0	1	0	0	15
HAN	Jojong	CCF	0.95	0.85	0.31	0.84	0.41	0.61	-0.31	0.48	0.23	0.63	0.31
		lag	0	0	0	1	0	3	-7	0	-1	2	4
	Yanhwa	CCF	0.97	0.67	0.33	0.71	0.45	0.75	0.69	0.7	0.28	0.74	0.43
		lag	0	0	2	0	1	0	1	0	1	2	8
	Seom	CCF	0.97	0.83	0.62	0.76	0.46	-0.48	0.76	0.66	0.53	0.72	0.34
		lag	0	0	0	0	7	21	-1	0	0	-2	4
	Cheongmi	CCF	0.98	0.67	0.17	0.7	0.41	0.56	0.77	0.57	0.14	0.6	0.45
		lag	0	0	-19	0	1	2	1	0	-19	1	1
Nakdong	Gam	CCF	0.96	0.64	0.73	0.67	-0.28	0.46	0.57	0.35	0.64	0.48	-0.39
		lag	0	0	0	1	-4	0	1	1	0	0	10
	Kumho	CCF	0.97	0.92	0.88	0.74	0.54	0.72	0.49	0.49	0.86	0.76	0.39
		lag	0	0	0	0	5	0	3	0	0	0	0
	Nam	CCF	0.97	0.92	0.23	0.82	0.38	0.67	0.7	0.45	0.57	0.81	0.48
		lag	0	0	20	1	20	-1	2	0	1	1	16
Yeongsangang	Jisuk	CCF	0.97	0.82	0.29	0.86	-0.5	0.6	-0.18	0.29	0.36	0.63	0.46
		lag	0	0	19	0	-20	0	-18	1	1	3	11
	Gomakwo	CCF	0.97	0.71	0.56	0.85	0.43	0.75	-0.35	0.36	0.37	0.52	0.54
		lag	0	0	0	0	1	0	-1	-9	9	-1	4
	Uchi	CCF	0.97	0.64	-0.15	0.35	-0.28	0.62	0.27	0.49	0.29	0.57	0.34
		lag	0	0	-7	0	-11	-1	3	0	-21	2	1

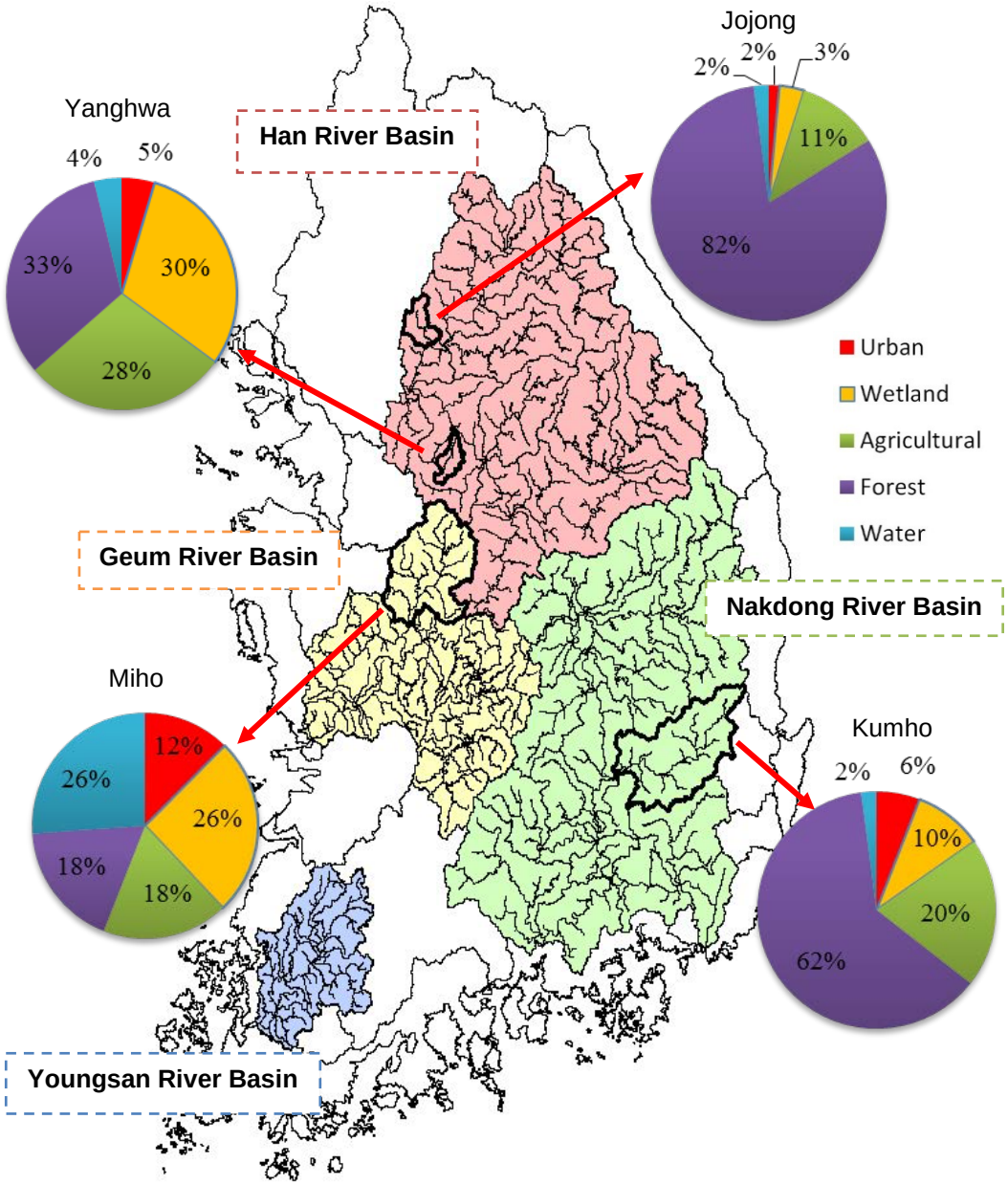

Figure 5-1 The location and land-use maps of the Kumho, Miho, Yanghwa and Jojong Catchments in the Nakdong, Geum and Han River Basins, respectively.

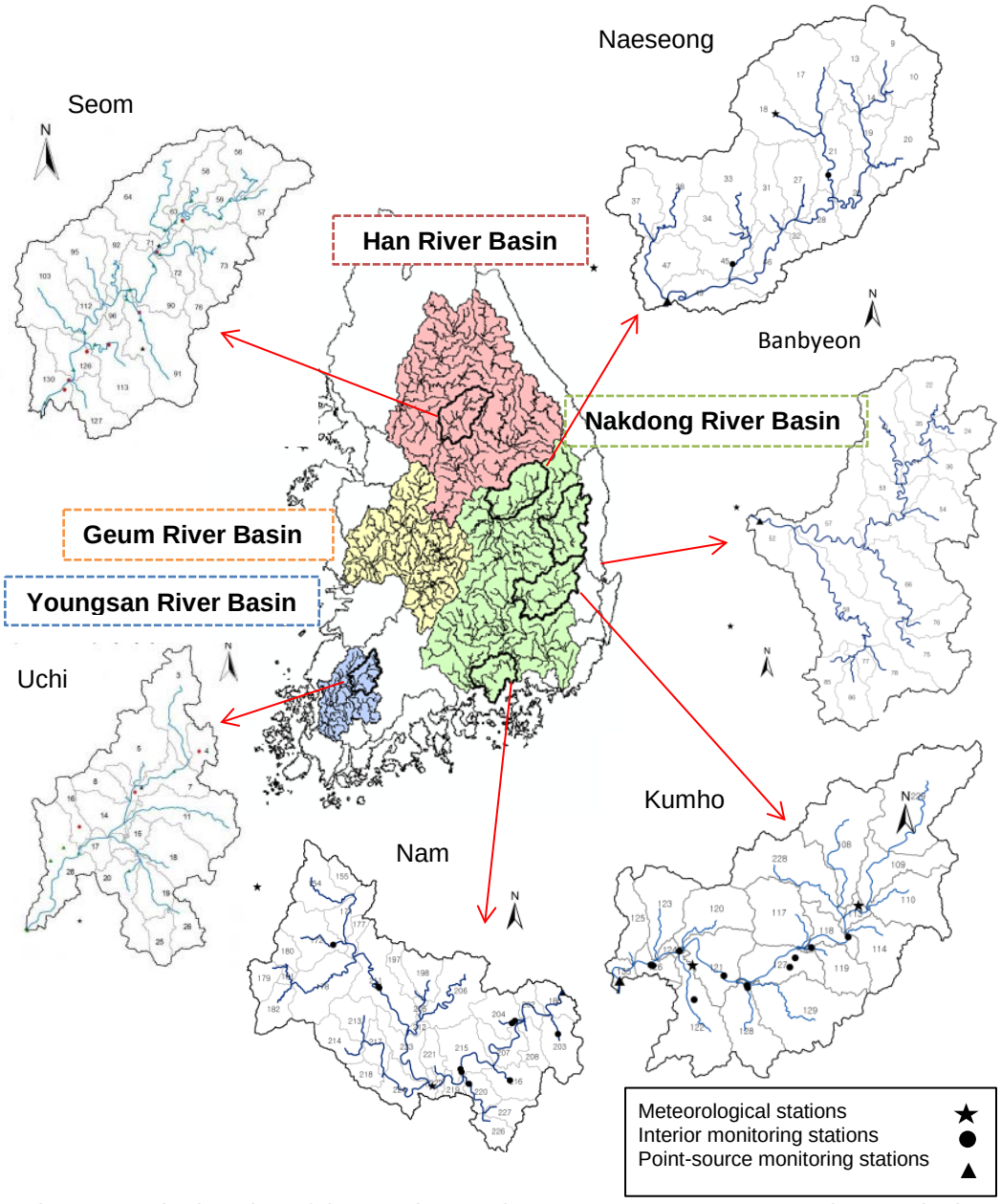

Figure 5-2 The location of the Kumho, Banbyeon, Naeseong, Nam Catchments in the Nakdong River Basin, Seom Catchment in the Han River Basin and Uchi Catchment in the Youngsan River Basin, respectively.

Table 5-4 Statistics measures for the outlet of the Seom Catchment in the Han River Basin.

Variable	sample size	NSE	Correlation	RMSE	(Bias in Mean)^2	(Bias in STD)^2	Cross term
Flow(cms)	124	0.709	0.845	37.979	1.624	42.329	1410.171
TW(C)	302	0.951	0.976	2.073	0.074	0.042	4.195
PO_4(mg/l)	302	-1.942	0.645	0.098	0.003	0.002	0.004
DO(mg/l)	302	0.492	0.773	1.660	0.493	0.061	2.209
BOD(mg/l)	302	-0.074	0.382	0.965	0.034	0.032	0.869
NO_3(mg/l)	302	-1.591	0.388	1.098	0.072	0.196	0.941
NH_4(mg/l)	302	0.481	0.699	0.477	0.000	0.065	0.163
CHLA(μg/l)	301	0.388	0.654	9.163	2.318	5.170	76.740
TP(mg/l)	302	-0.948	0.521	0.104	0.002	0.001	0.008
TN(mg/l)	302	0.049	0.671	1.172	0.000	0.134	1.244
TOC(mg/l)	293	-0.329	0.249	1.900	0.902	0.703	2.015

Table 5-5 Statistics measures for the outlet of the Nam Catchment in the Nakdong River Basin.

Variable	sample size	NSE	Correlation	RMSE	(Bias in Mean)^2	(Bias in STD)^2	Cross term
Flow(cms)	231	-5.131	0.580	331.108	485.017	65656.045	43966.189
TW(C)	241	0.914	0.974	2.561	1.997	1.065	3.516
PO_4(mg/l)	241	-2.990	0.225	0.041	0.000	0.000	0.001
DO(mg/l)	241	0.611	0.803	1.353	0.142	0.303	1.393
BOD(mg/l)	241	-1.098	0.330	2.313	0.165	0.407	4.799
NO_3(mg/l)	241	-0.120	0.668	0.995	0.150	0.078	0.765
NH_4(mg/l)	241	0.392	0.675	0.253	0.001	0.001	0.062
CHLA(μg/l)	241	0.070	0.446	40.321	116.609	164.673	1350.773
TP(mg/l)	241	-0.604	0.537	0.065	0.000	0.001	0.004
TN(mg/l)	241	0.487	0.812	1.177	0.352	0.001	1.036
TOC(mg/l)	236	-1.736	0.428	2.383	0.000	1.378	4.325

Table 5-6 Statistics measures for the outlet of the Naeseong Catchment in the Nakdong River Basin.

Variable	sample size	NSE	Correlation	RMSE	(Bias in Mean)^2	(Bias in STD)^2	Cross term
Flow(cms)	220	0.467	0.814	53.909	21.768	350.240	2547.362
TW(C)	238	0.886	0.966	3.170	4.029	0.336	5.708
PO_4(mg/l)	241	-5.583	-0.387	0.063	0.001	0.000	0.003
DO(mg/l)	241	0.640	0.867	1.511	0.678	0.252	1.359
BOD(mg/l)	241	0.104	0.384	0.781	0.029	0.246	0.338
NO_3(mg/l)	241	0.132	0.532	0.732	0.032	0.015	0.492
NH_4(mg/l)	241	-0.188	0.214	0.053	0.000	0.000	0.002
CHLA(μg/l)	241	-0.277	0.020	10.195	0.815	17.521	86.029
TP(mg/l)	241	-1.546	-0.337	0.118	0.001	0.000	0.013
TN(mg/l)	241	-0.299	0.483	0.861	0.186	0.002	0.555
TOC(mg/l)	236	-0.304	0.194	2.357	1.453	2.621	1.500

Table 5-7 Statistics measures for the outlet of the Kumho Catchment in the Nakdong River Basin.

Variable	sample size	NSE	Correlation	RMSE	(Bias in Mean)^2	(Bias in STD)^2	Cross term
Flow(cms)	236	0.807	0.918	48.326	0.025	889.487	1455.868
TW(C)	241	0.943	0.974	1.938	0.275	0.001	3.495
PO_4(mg/l)	241	-0.294	0.878	0.217	0.018	0.015	0.015
DO(mg/l)	242	0.512	0.742	1.827	0.030	1.344	1.979
BOD(mg/l)	242	-0.166	0.348	1.702	0.711	0.982	1.213
NO_3(mg/l)	241	-0.270	0.719	1.807	0.340	0.722	2.214
NH_4(mg/l)	241	0.132	0.436	0.215	0.001	0.007	0.038
CHLA(μg/l)	241	0.140	0.488	39.621	167.810	344.957	1062.881
TP(mg/l)	242	0.182	0.865	0.192	0.007	0.012	0.019
TN(mg/l)	242	0.033	0.759	1.707	0.016	0.733	2.178
TOC(mg/l)	237	-3.195	0.389	2.932	5.947	0.006	2.654

Table 5-8 Statistics measures for the outlet of the Banbyeon Catchment in the Nakdong River Basin.

Variable	sample size	NSE	Correlation	RMSE	(Bias in Mean)^2	(Bias in STD)^2	Cross term
Flow(cms)	234	0.409	0.696	43.599	0.841	1076.290	831.909
TW(C)	240	0.888	0.964	2.808	2.871	0.130	4.905
PO_4(mg/l)	241	0.121	0.369	0.008	0.000	0.000	0.000
DO(mg/l)	241	0.615	0.869	1.390	0.668	0.224	1.045
BOD(mg/l)	241	-0.376	-0.162	0.742	0.027	0.136	0.389
NO_3(mg/l)	241	-0.338	0.431	0.544	0.107	0.031	0.159
NH_4(mg/l)	241	-0.181	0.134	0.030	0.000	0.000	0.001
CHLA(μg/l)	241	-0.137	-0.110	5.673	0.963	16.854	14.493
TP(mg/l)	241	-0.019	-0.039	0.034	0.000	0.001	0.000
TN(mg/l)	241	-0.513	0.460	0.677	0.217	0.061	0.181
TOC(mg/l)	236	-1.973	-0.114	3.391	7.540	3.305	0.670

Table 5-9 Statistics measures for the outlet of the Uchi Catchment in the Yeongsan River Basin.

Variable	sample size	NSE	Correlation	RMSE	(Bias in Mean)^2	(Bias in STD)^2	Cross term
Flow(cms)	154	0.394	0.641	18.614	5.831	113.170	229.722
TW(C)	306	0.942	0.975	2.034	0.433	0.040	3.678
PO_4(mg/l)	306	-0.861	-0.068	0.033	0.000	0.000	0.001
DO(mg/l)	306	0.115	0.346	7.157	0.068	29.552	21.771
BOD(mg/l)	306	-2.409	0.121	2.720	2.324	0.175	4.916
NO_3(mg/l)	303	0.226	0.588	0.611	0.008	0.004	0.363
NH_4(mg/l)	306	-0.040	0.223	0.146	0.000	0.005	0.017
CHLA(μg/l)	306	0.193	0.492	19.189	13.754	63.289	292.320
TP(mg/l)	306	-1.571	0.039	0.065	0.001	0.000	0.003
TN(mg/l)	306	-0.340	0.470	0.791	0.142	0.000	0.485
TOC(mg/l)	288	-0.844	0.307	2.765	1.125	0.064	6.480

5.5. Performance measures

To assess the quality of the analysis and prediction results of water quality variables and streamflow, visual examination of the time series and scatter plots, and a set of statistical measures, including root mean square error (RMSE), skill score, mean square error (MSE) decomposition, correlation coefficient and Nash-Sutcliff efficiency (NSE), were used. RMSE gives the standard deviation of the error in the same unit as simulation and observation. A smaller RMSE indicates better performance:

$$RMSE = \sqrt{\frac{\sum_{i=1}^{n}(Sim_i - Obs_i)^2}{n-1}} \quad (5\text{-}1)$$

where n denotes the number of pairs of simulated and observed water quality variables or streamflow. The skill score is defined based on MSE as follows:

$$SS_{DA} = 1 - \frac{MSE_{DA}}{MSE_{Base}} \quad (5\text{-}2)$$

where MSE_{DA} denotes the MSE of the DA-aided prediction or analysis and MSE_{Base} denotes the MSE of the base, i.e., DA-less, prediction or analysis. A skill score of unity represents perfect analysis or prediction whereas a skill score of zero indicate that DA does not add any skill to the base simulation. MSE can be decomposed into three terms as follows (Murphy and Winkler 1987, Nelson et al. 2010):

$$MSE = \sum_{i=1}^{N}(f_i - o_i)^2 = (m_f - m_o)^2 + (\sigma_f - \sigma_o)^2 + 2\sigma_f\sigma_o(1-\rho) \quad (5\text{-}3)$$

where f_i and o_i denote the ith forecast and verifying observation, respectively, N denotes the number of pairs of forecast and verifying observation, m_f and m_o denote the mean of forecast and that of verifying observation, respectively, σ_f and σ_o denote the standard deviation of forecast and that of verifying observation, respectively, and ρ denotes the correlation between the forecast and the verifying observation. In the RHS of Eq.(5-3), the first and second terms measure the bias in the mean and that in the standard deviation, respectively, and the third term measures the strength of covariation

(the smaller, the stronger) between the forecast and the verifying observation (Nelson et al. 2010). The correlation coefficient is a measure of linear association between the simulated and observed variables:

$$Corr = \frac{Cov(sim,obs)}{\sigma_{sim}\sigma_{obs}} \quad (5\text{-}4)$$

where σ_{sim} and σ_{obs} denote the standard deviation of the simulated and that of the observed, respectively, and $Cov(sim, obs)$ denotes the covariance between the observed and the simulated. The Nash-Sutcliffe efficiency is a skill score that expresses the relative magnitude of the residual variance ("noise") compared to the measured data variance ("information") (Nash and Sutcliffe 1970):

$$NSE = 1 - \frac{\sum_{i=1}^{n}(sim_i - obs_i)^2}{\sum_{i=1}^{n}(obs_i - \overline{obs})^2} \quad (5\text{-}5)$$

where $\overline{obs}$ denotes the mean of the observations. The Nash-Sutcliffe efficiencies range from negative infinity to unity. An NSE equal to one corresponds to a perfect simulation. An NSE equal to zero indicates that the model simulation is no more skillful than the mean of the observations. An NSE of less than zero indicates that the observed mean is better than the model simulation.

5.6. Comparative evaluation with time series modeling

The effectiveness of DA depends not only on the quality of the model but also on the predictability of the water quality variables. If the biophysiochemical processes of interest have little memory, one may not expect DA to improve prediction significantly. Certain processes, on the other hand, may be very predictable in which case one may expect DA to do well. In this element of the research, time series modeling (Box and Jenkins 1970, Bras and Rodriguez-Iturbe 1985) is carried out for the water quality variables to better understand the statistical nature of the processes modeled and their predictability. For this purpose, auto-regressive integrated moving average (ARIMA)

model was used to simulate and predict the water quality variables. Several studies used different types of ARIMA models to simulate water quality variables and to predict the long- and short-term trends of water quality in river systems or a basins (Balasuriya et al. 1982, Montanari et al. 1997, Ragavan et al. 2006, Parmar and Bhardwaj 2014).

Arya and Zhang (2015) applied the order series method and ARIMA model for univariate simulation of DO and TW for four water quality assessment stations on the Stillaguamish River in WA. The time series model identified for each univariate water quality time series was found to be capable of predicting future values with reasonable accuracy. Therefore, they suggested that the time series modeling approach might be an effective tool for assessing water quality in river systems. Worrall and Burt (1999) applied autoregressive (AR) and autoregressive-moving average (ARMA) modeling to examine the nature of the detrended and deseasoned residual time series for NO_3 levels. In addition, they used the time series models derived from spatial variations of nitrate concentrations from three catchments in the North and South of England to predict future NO_3 levels. They concluded that ARMA modeling proved to be an effective prediction tool. Chen et al. (2015) developed an ARIMA model to predict daily CHL-a concentrations using data from Taihu Lake in China. In addition, they developed a multivariate linear regression (MVLR) model to predict daily CHL-a concentrations using the same data. They compared the prediction results of the MVLR model with the ARIMA model. They concluded that the ARIMA model had more advantages compared to the MVLR model because the ARIMA model needed only one input (CHL-a observation) variable and provided short-term predictions with acceptable accuracy. Unlike the ARMA model, the ARIMA model is able to handle non-stationarity by allowing differencing of the data series. Appendix B describes ARIMA modeling used in this work.

Chapter 6

Results and discussions

6.1. MLEF-HSPF evaluation experiments

The MLEF-HSPF module was evaluated via dependent and independent validation. Dependent validation represents evaluation of MLEF-HSPF for the period for which HSPF was calibrated by NIER. Independent validation represents evaluation of MLEF-HSPF for the period outside of the HSPF calibration period. The dependent validation was performed for the Kumho Catchment, and independent validation was performed for multiple catchments in the four river basins. Before presenting the DA results, the bias correction results are presented first below.

6.2. Bias correction

To specify α and the bias correction parameters, a and b (see Eq. (4-15), Subsection 3.5 for details), HSPF simulations of streamflow, TW, NH_4, NO_3, PO_4, CHL-a, TN, TP, TOC, BOD, and DO were compared with the observed. The bias correction parameters were then estimated based on simulations and observations from a two-year period of 2011-2012 for the Kumho Catchment. The criteria used to specify α and to estimate the bias correction parameters are as follows:

1. The coefficient a should be greater than 0.5, or the ranges of bias-corrected simulations become unrealistic and the simulations might not capture the variability of the observations.
2. The coefficient a should not be negative, or the feasible region of the model physics might be violated and the bias-corrected model simulations might become unrealistic.
3. The absolute value of the coefficient b should not be very large compared to the magnitude of observations.

4. The weight α may be selected based on visual comparison of the bias-corrected model simulations with the observed.
5. If the coefficients a and b violate the above criteria, bias correction is not be used for that variable and set a and b to unity and zero, respectively.

Figure 6-1 shows the scatter plots of CHL-a between the simulated and the observed for different values of α. As may be seen in the figure, values of α greater than 2 resulted in negative values of CHL-a whereas an α of zero was unable to capture the variability of the observed. Hence, α=1 was chosen for CHL-a. Figure 6-2 shows the scatter plots of NO_3 for different values of α. It is seen from the figure that, as α increases from zero to five, the bias correction procedure reduces systematic first-order conditional biases and captures the variability of the observations effectively. As such, α=5 was chosen for NO_3. The highlighted values in Table 6-1 represent the selected bias correction parameters for each of the water quality variables for the Kumho Catchment.

Table 6-1 The calculated bias correction parameters for different values of α.

Variable		α						Selected a&b
		0	1	2	3	4	5	
Flow	a	0.642	0.750	0.795	0.819	0.834	0.845	0.845
	b	9.046	4.559	2.708	1.698	1.061	0.624	0.624
TW	a	0.973	0.998	1.007	1.012	1.014	1.016	0.998
	b	0.544	0.131	-0.012	-0.084	-0.128	-0.157	0.131
NH_4	a	0.542	0.981	1.345	1.651	1.911	2.136	0.981
	b	0.137	0.062	-0.001	-0.053	-0.098	-0.136	0.062
NO_3	a	0.447	0.588	0.657	0.698	0.725	0.744	0.744
	b	3.037	2.275	1.901	1.679	1.532	1.428	1.428
PO_4	a	0.583	0.665	0.697	0.715	0.726	0.733	0.733
	b	0.074	0.0512	0.042	0.037	0.034	0.032	0.032
BOD	a	1.243	1.998	2.504	2.867	3.141	3.354	1.243
	b	0.062	-1.858	-3.147	-4.072	-4.769	-5.312	0.062
CHL-a	a	0.740	1.173	1.457	1.658	1.807	1.923	1.173
	b	17.219	4.432	-3.957	-9.884	-14.293	-17.702	4.432
DO	a	1.272	1.546	1.666	1.733	1.775	1.805	1.0
	b	-2.709	-5.570	-6.819	-7.519	-7.967	-8.278	0.0
TP	a	0.606	0.699	0.738	0.758	0.771	0.779	0.779
	b	0.131	0.098	0.085	0.078	0.073	0.069	0.069
TN	a	0.485	0.638	0.712	0.757	0.786	0.807	0.807
	b	3.633	2.686	2.223	1.948	1.765	1.636	1.636
TOC	a	0.368	0.633	0.833	0.989	1.114	1.217	1.216
	b	4.656	3.671	2.929	2.349	1.884	1.503	1.503

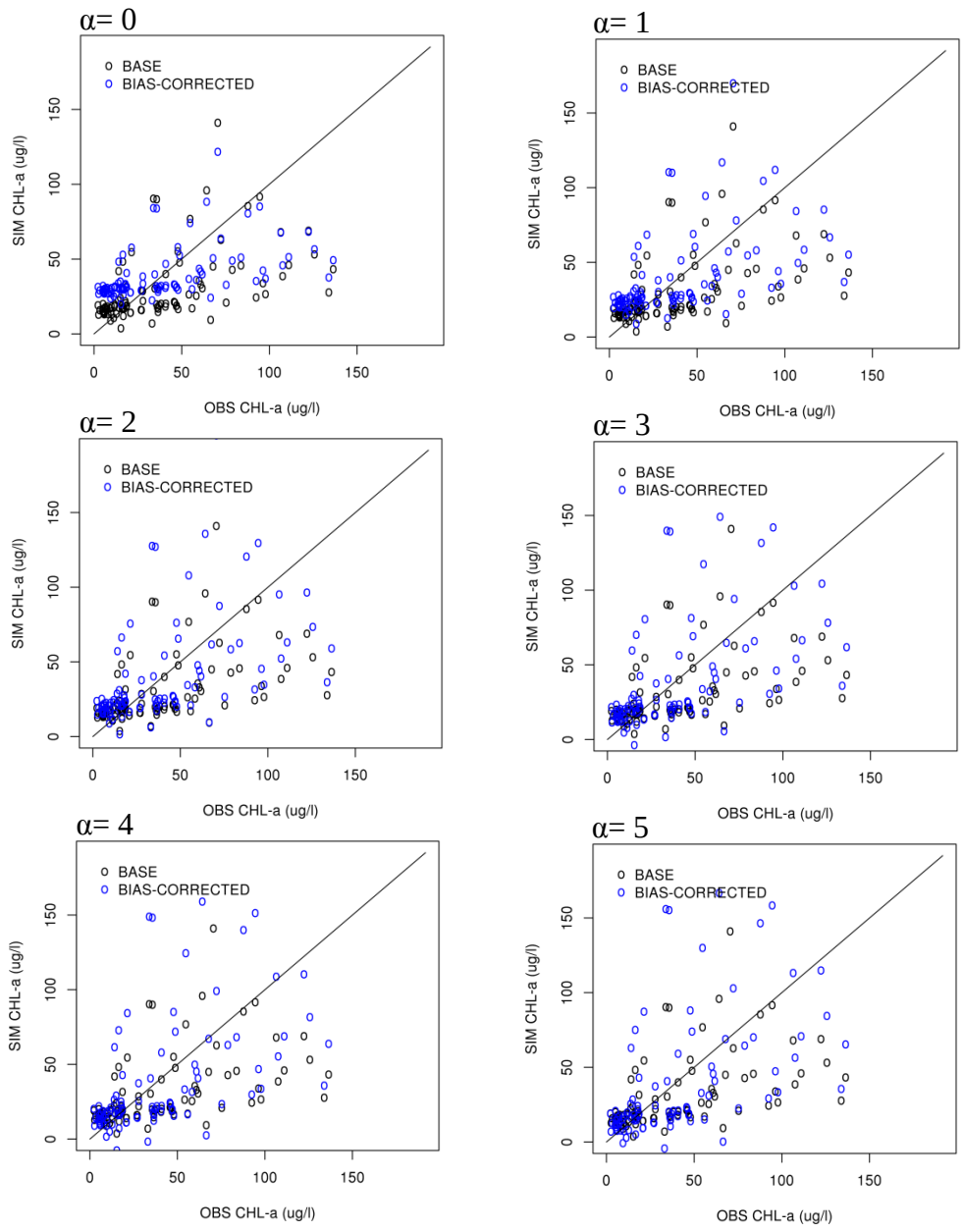

Figure 6-1 Selection of α for CHL-a for the Kumho Catchment based on available observations in 2011-2012.

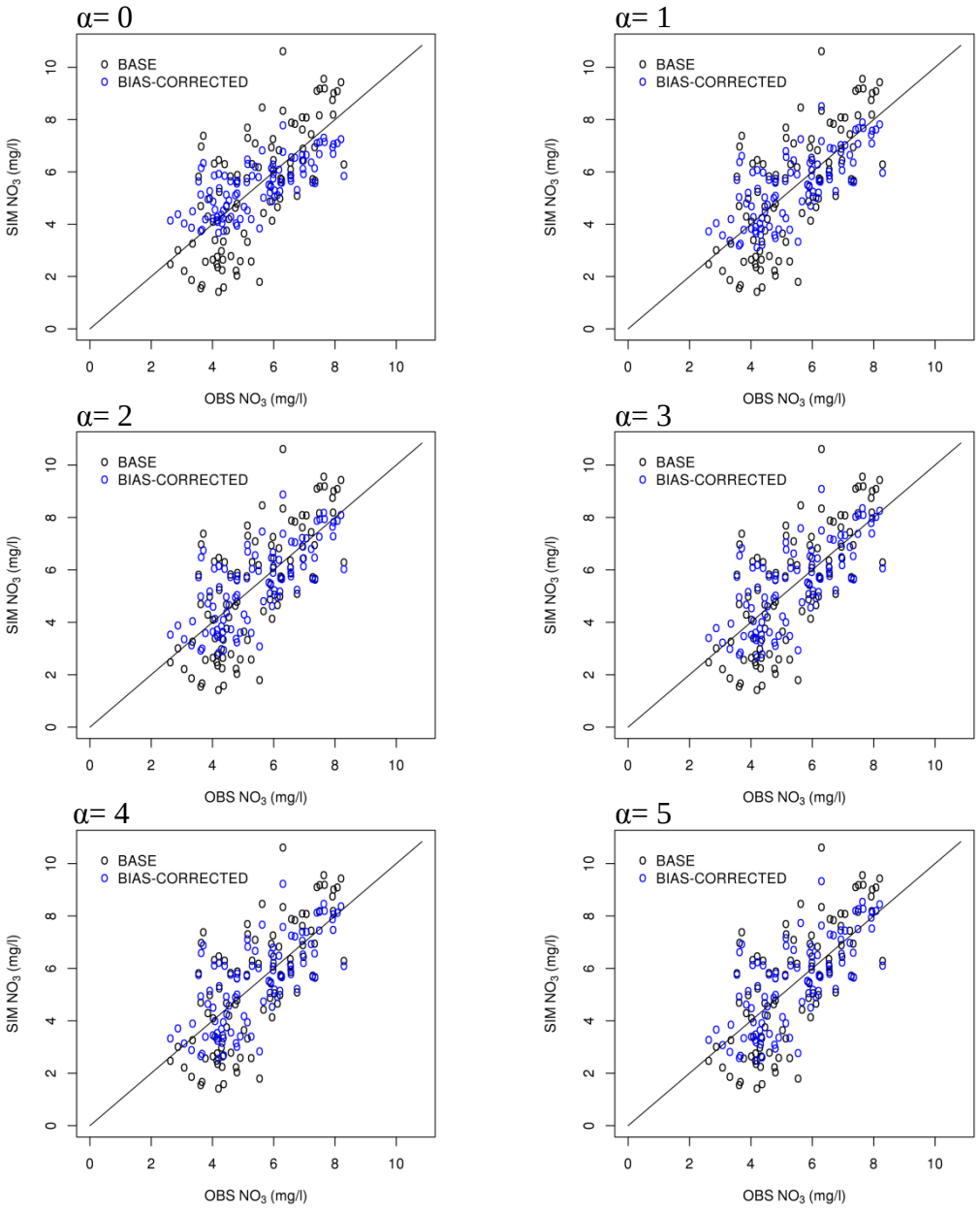

Figure 6-2 Selection of α for NO_3 for the Kumho Catchment based on available observations in 2011-2012.

6.3. Dependent validation of MLEF-HSPF

The Kumho Catchment has a drainage area of 2170.65 km^2. The observations are available weekly at the outlet location where the evaluation was made. HSPF simulates hydrologic and water quality processes for 31 model segments in the Kumho Catchment which leads to a total of 333 control variables including the multiplicative adjustment factors for MAP and MAPE.

In the hindcasting experiment, the observed variables were predicted out to three days into the future in each assimilation cycle for 2008. Based on the sensitivity analysis, an ensemble size of 9 was used. Figure 6-3 shows the time series of the BC-DA (●) vs. Base (o) and BC-Base (x) results and the verifying observation (●) for CHL-a at the catchment outlet. Note in the figure that there are multiple BC-DA results for each verifying observation. This is because DA is performed every day over an assimilation window of 7 days, resulting in as many as 7 analysis results. It is readily seen in the figure that BC-DA tracks the verifying observations much more closely than Base or BC-Base.

Figure 6-4 shows the MSE decomposition of the analysis result by Base, BC-Base and BC-DA for CHL-a. Note that BC reduces biases in the mean and standard deviation, and significantly improves the strength of covariation between the observed and simulated values. Figure 6-5 shows the RMSE of the Base (left bars), BC-Base (middle bars) and BC-DA (right bars) results for analysis and Day-1 through -3 predictions for BOD, CHL-a, DO, NO_3, TW, PO_4 and streamflow at the catchment outlet. Note that BC-DA significantly reduces RMSE compared to Base.

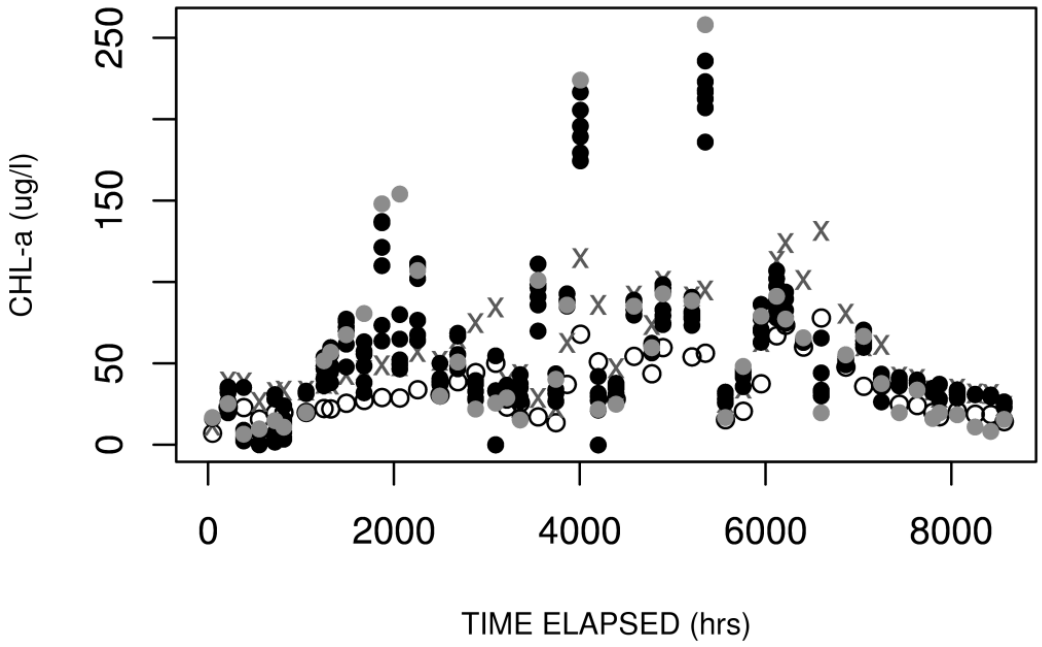

Figure 6-3 Base, BC-Base and BC-DA vs. the verifying observations of CHL-a at the outlet of the Kumho Catchment.

Figure 6-6 shows the MSE-based skill score of the analysis and Day-1 through -3 predictions. Note that DA has larger predictive skills compared to the base simulation results except for Day-1 predictions of streamflow and DO. It was found that predictions based on 7 day-old observations provide little predictive skill and hence should not be considered for assimilation. As such, a screening criterion was added to check the quality of the DA results based on assimilating 7 day-old observations and the DA solutions are accepted only if the analysis results show significant improvement.

Figure 6-7 shows the eigenvalue spectra of $\{I + C(x)\}^{-T/2}$ in Eq. (4-8) at $x = x_{opt}$ (see Eq. (4-11)) for all assimilation cycles in 2008. With 9 ensemble members and the use of state augmentation approach for dynamical model errors, the dimensionality of the above matrix is 10. Via eigenvalue decomposition, $\{I + C(x)\}^{-T/2}$

may be expressed as $V(1+\Lambda)^{-1/2}V^T$ where V and Λ denote the eigenvector and eigenvalue matrices, respectively. Figure 6-7 plots $(1+\lambda_i^2)^{-1/2}$ where λ_i^2 denotes the i-th eigenvalue. Note in Eq. (4-8) that $\{I+C(x)\}^{-T/2}$ maps the DA solution in ensemble subspace to the incremental solution in the physical space. Hence, the eigenvalues represent the principal components of the incremental solution in the orthogonal space spanned by the ensemble members. The Figure 6-7 indicates that, in most assimilation cycles, only about four ensemble members carry significant information, and that about 7 members capture all information in all assimilation cycles. The above observation supports the choice of the ensemble size of 9 used in this research and also points out the lack of realism in HSPF necessary to simulate diverse ensemble members from perturbed ICs.

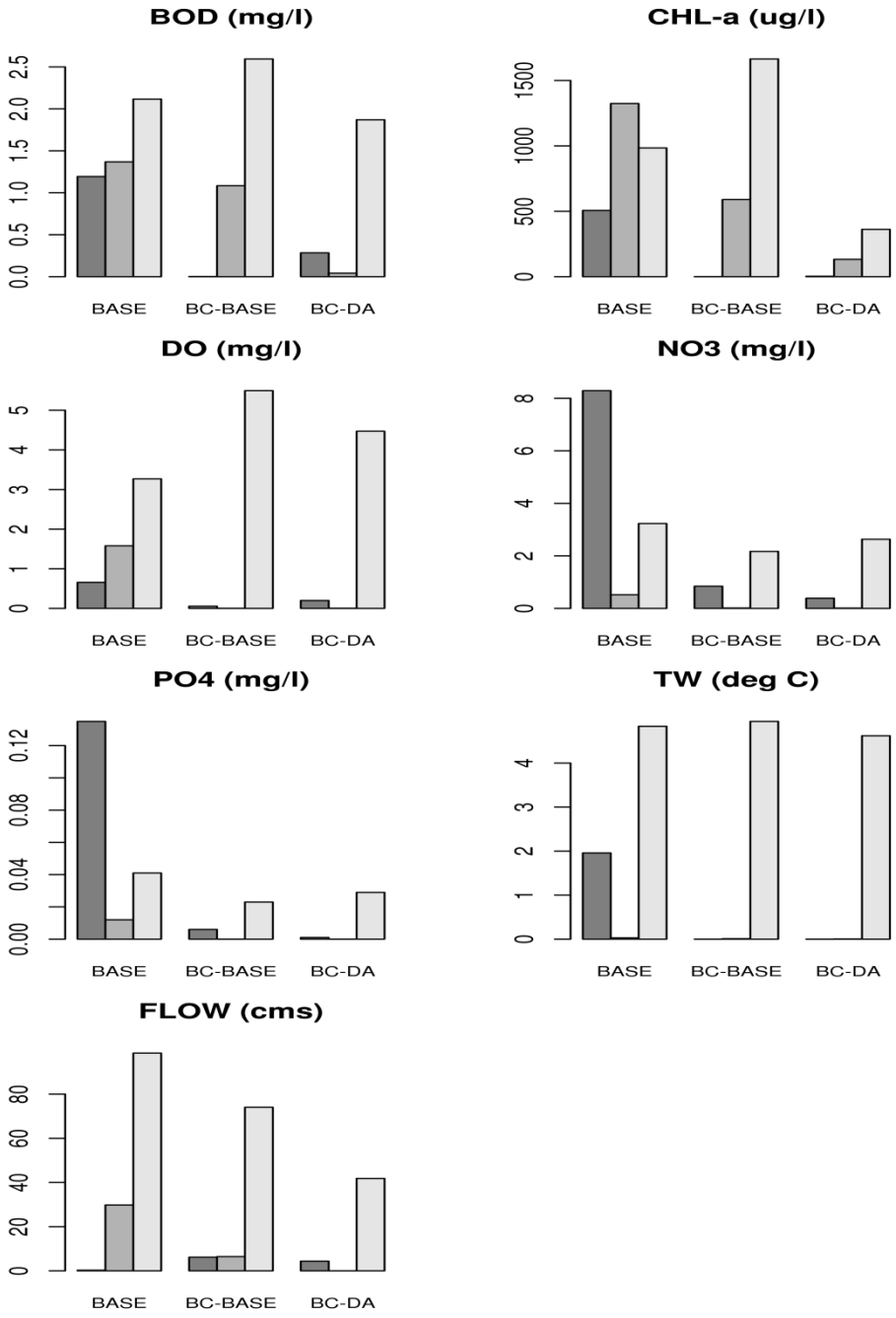

Figure 6-4 MSE decomposition into bias in mean squared (■), bias in standard deviation squared (■), and strength of covariation (the smaller, the stronger) (■) for BASE, BC-BASE and BC-DA analysis for CHL-a for 2008.

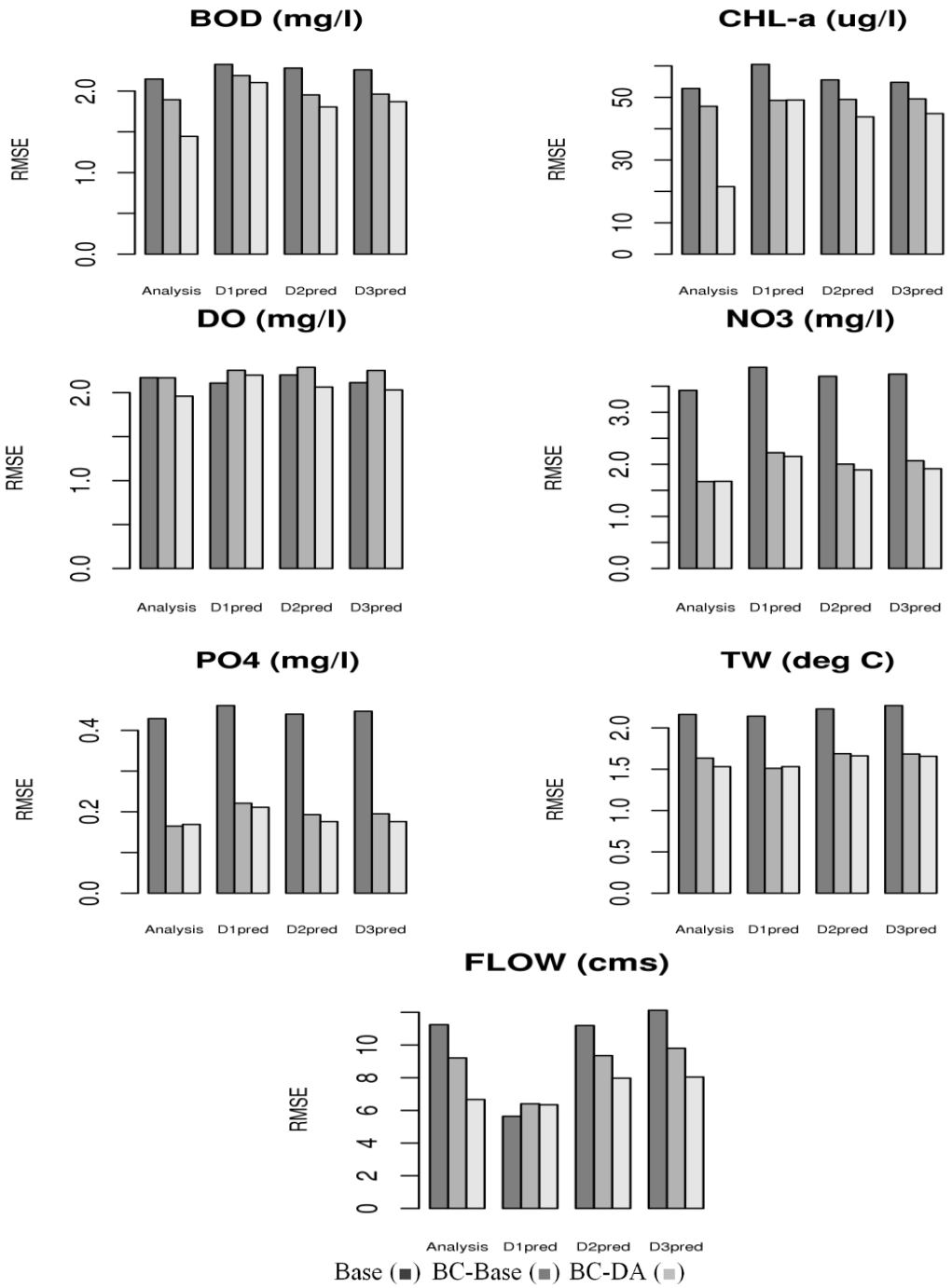

Figure 6-5 RMSE of BASE, BC-BASE and BC-DA analysis and Day-1 through -3 predictions for CHL-a for 2008.

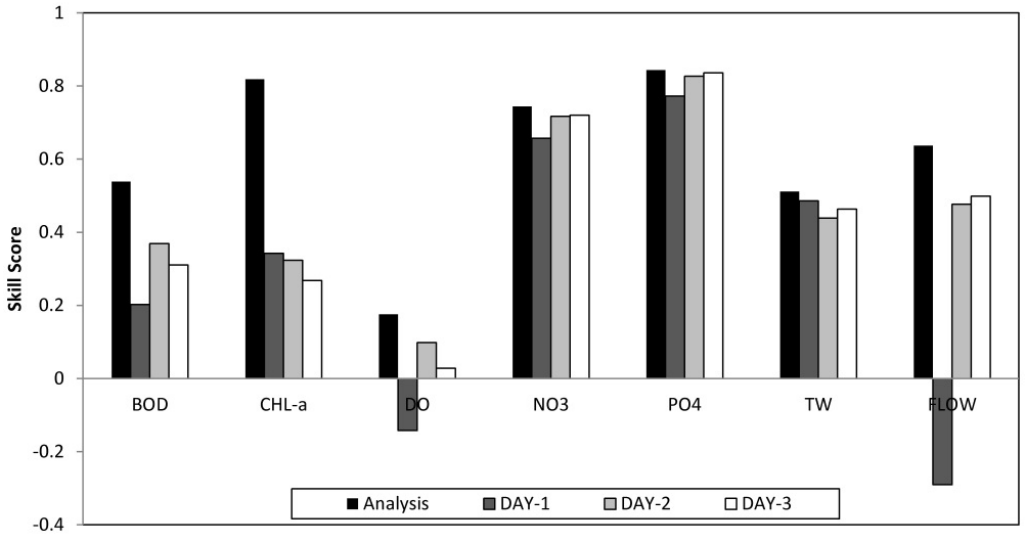

Figure 6-6 MSE skill score of BC–DA analysis and Day-1 through -3 predictions for BOD, CHL-a, DO, NO_3, PO_4, TW and flow. The reference is BASE.

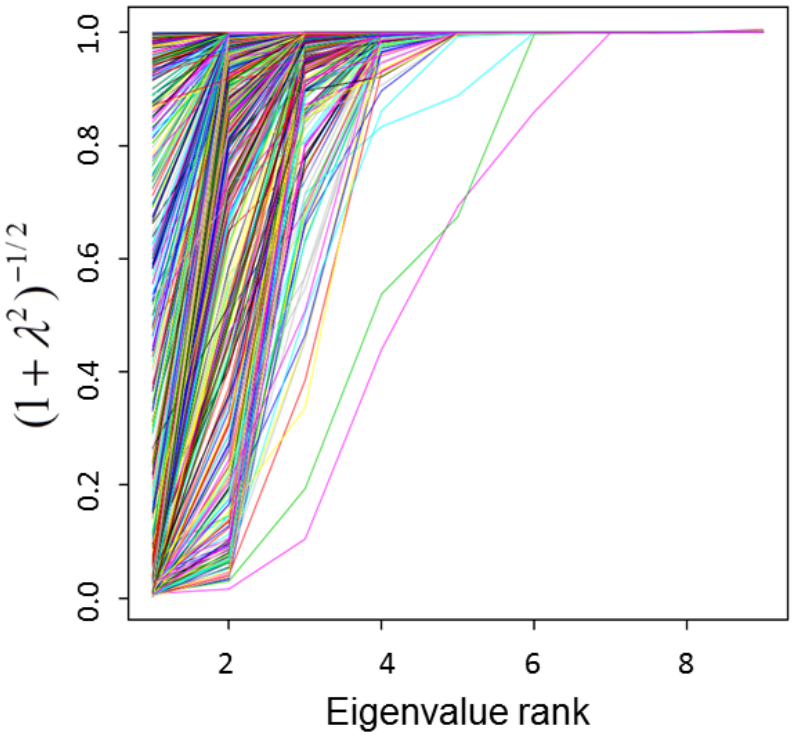

Figure 6-7 Eigenvalue spectra of $[I + C(x_{opt})]^{-1/2}$ for all assimilation cycles in 2008.

6.4. Independent validation of MLEF-HSPF

The hindcasting experiment for independent validation was performed for the Kumho Catchment in the Nakdong River Basin, the Jojong and Yanghwa Catchments in the Han River Basin and the Miho Catchment in the Geum River Basin; they comprise 31, 10, 10 and 39 model segments resulting in 331, 103, 103 and 412 control variables, respectively. Figure 6-8 shows the empirical cumulative distribution functions of streamflow and CHL-a for the period of 2008 to 2013 for Kumho and for the period of 2011 to 2013 for all others. As seen in the figure, the Kumho and Miho Catchments have much larger flow and higher concentration of CHL-a than Jojong and Yanghwa. As it was shown in Figure 5-1, the Kumho and Miho Catchments have larger fraction of urban areas and are more prone to water quality contaminations.

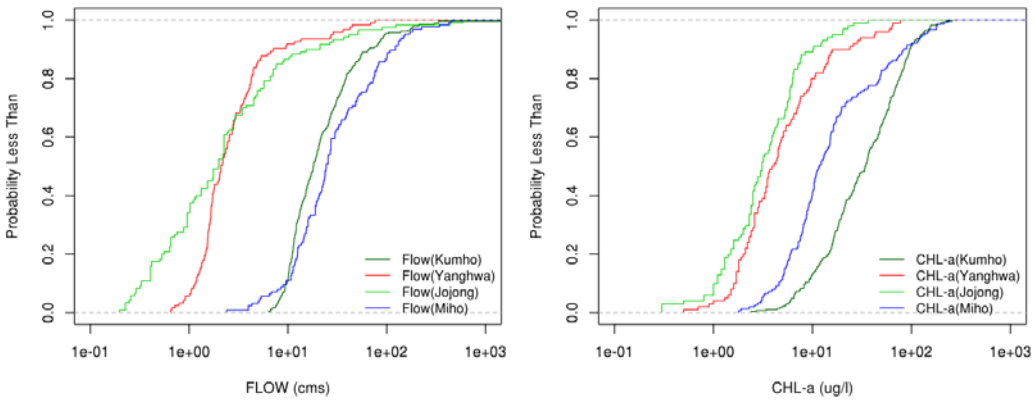

Figure 6-8 Empirical cumulative distribution functions of streamflow (left) and CHL-a (right) for the 4 study catchments.

For DA to be effective, the model has to be reasonably skillful. If the model cannot simulate the biophysiochemical processes that occur in the catchment, one may not expect DA to add skill. There are multiple aspects to consider in evaluating the quality of base model simulations for application of DA. The model may be better at simulating

certain processes and variables than others. The model may represent all observations well individually, but may not be able to simulate co-variability among them. The model may capture co-variability well, but may have phase, or timing, errors in some variables. The HSPF model used in this work was calibrated by the water quality modelers at NIER. Calibration, however, is an ongoing effort which is expected to continue and improve over time. In this work, all aspects listed above are considered in selection of the study catchments. To illustrate how the quality of base model simulations was assessed, the lag-0 correlation between the base simulation and the verifying observation for all observed variables are shown in Figure 6-9 for all four catchments. As may be seen in this figure, the Kumho Catchment generally has the highest correlations between the base simulations and the verifying observations for most of the variables, and the Miho Catchment has the poorest, especially for PO_4. Cross correlation among the variables also showed significant variability among catchments. The above observations suggest that one may expect significant variations in the performance of DA among different catchments and variables.

Below, the DA results for analysis and prediction are presented. Because MLEF-HSPF produces ensembles, it is possible to verify ensemble analysis and prediction using, e.g., the Ensemble Verification system (EVS, Brown et al. 2010). It was learned, however, that the raw ensembles from HSPF are severely underspread due to lack of degrees of freedom in HSPF (Seo et al. 2013); the initial spread quickly collapses as the model is forward-integrated in time. Because the officially-supported HSPF is available only as an executable, it is not possible to add error terms explicitly to the model dynamics. In this subsection, all results presented are limited only for ensemble mean for both analysis and prediction. Analysis results reflect how closely the model-simulated observations match the actual observations based on the updated control vector.

Accordingly, the analysis results reflect the performance of DA as an optimizer. In the hindcasting experiment for the four catchments, predictions were made out to 7 days into the future in each daily assimilation cycle for 2012 for the Kumho and Jojong Catchments and for 2013 for the Miho and Yanghwa Catchments. The ensemble size used was 9 for all four catchments. Initially, all available observations that are valid within the assimilation window were assimilated regardless of the specific variables observed or the number of observations available for a given variable. Evaluation of the results indicated, however, that such a practice does not compare well with assimilating only a single set of observations of all 11 observed variables. This is because changes in the available observations from one assimilation cycle to the next may significantly change the inverse problem in ensemble subspace and hence the DA solution tends to lose temporal consistency. It was also found that assimilating multiple sets of observations within a single assimilation window does not work as well as assimilating only a single, the most recent set of observations. This is because multiple sets of observations may lead to DA solutions that are in conflict from one iteration to the next in the optimization process due to imperfect model and uncertainty modeling. Similar observations were made in assimilating streamflow, MAP and MAPE into hydrologic models (Seo et al. 2003, 2009).

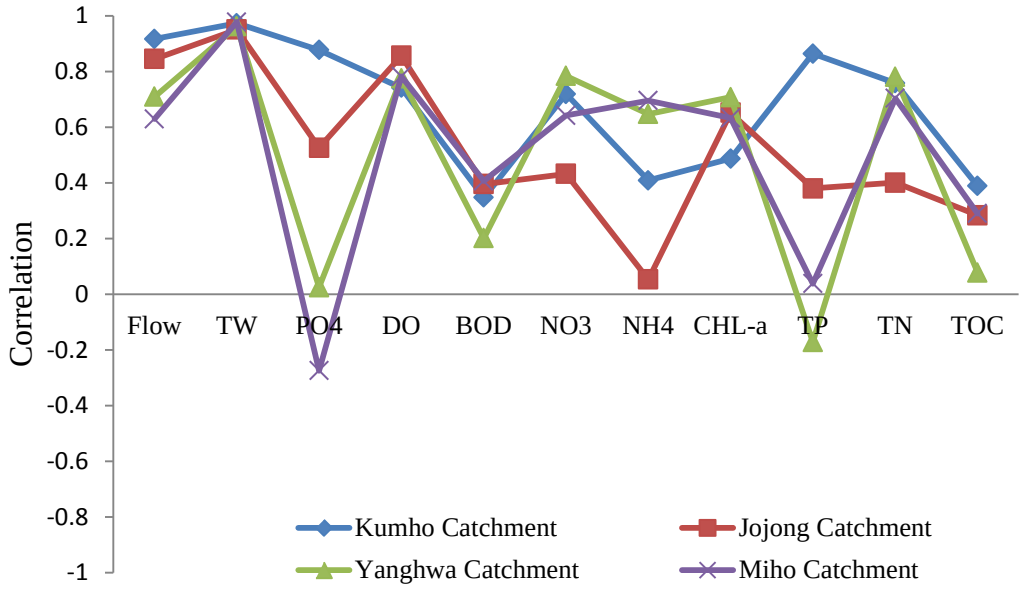

Figure 6-9 Correlation between observed and simulated variables at the outlet of the catchments. The period of record is 2008-2012 for Kumho and 2011-2013 for all others.

Figure 6-10 shows the time series of the Base, BC-Base and BC-DA analysis for streamflow, CHL-a, DO and TW against the verifying observations for the Kumho Catchment for 2012. Note in the figure that, as in the dependent validation analysis results, there are multiple DA analysis results for a single verifying observation due to the fact that DA is performed every day over an assimilation window of 7 days, resulting in as many as 7 analysis results (see Figure 3-1). The analysis results differ depending on the age of the observations. Note in Figure 3-1 that, the newer/older the observations are, the more/less closely they reflect the state of the system at the prediction time. Accordingly, one may expect the DA analysis based on newer observations to contribute larger predictive skill than that based on older observations. Indeed, it was found that assimilation of 7 day-old observations does not produce skillful solutions and hence were not used in evaluation. The quality of analysis based on assimilating 6 day-old

observations (orange circles in Figure 6-10), on the other hand, is acceptable most of the times, but there are occasions when the quality is very poor. This is because, depending on the dynamical state of the model, 6 day-old observations may lack information content to result in a skillful solution. The use of the information content measures such as the degrees of freedom for signal to determine the dynamic state of the system (Kim et al. 2014, Zupanski et al. 2007), however, is not easy because such measures assume perfect modeling of the uncertainties, a tall order in reality. Given the above, a simple screening criterion for accepting or rejecting the DA solution from assimilating 6 day-old observations was employed; if the relative percent error of the analysis solution exceeds a preset threshold, the DA results for that particular assimilation cycle were not used. All results presented below are based on the above screening. Note in Figure 6-10 that the DA analysis tracks the verifying observations much more closely than Base or BC-Base. Figure 6-11 through Figure 6-14 show the RMSE of Base (left bars), BC-Base (middle bars) and BC-DA (right bars) results for analysis of streamflow, CHL-a, DO and TW, respectively, at the outlet locations of the four catchments. Note again that the DA analysis results differ depending on the age of the observations, and that BC-DA consistently reduces RMSE, an indication that the DA algorithm is successful in optimization. The only exception is the streamflow analysis for the Yanghwa Catchment for which DA was not able to reduce RMSE compared to Base. Further investigation showed that for one week (from 2013/06/06 to 2013/06/11) the adjustment factors for MAP and MAPE reached the preset bounds, due probably to very large errors in HSPF and/or the forcings. Note also that BC-Base is not always successful in reducing RMSE over Base. This is due to the interannual variability of the water quality variables and the sampling uncertainty in the bias correction parameters arising from the relatively small number of data points used in their estimation. It is important to note that, even though it

may not consistently reduce errors by itself, BC is necessary to reconcile any possibly large discrepancies between the model space and the real-world space. Figure 6-15 through Figure 6-18 show the RMSE of Base (left bars), BC-Base (middle bars) and BC-DA (right bars) results for Day-1 through -3 predictions for the outlets of the four catchments for streamflow, CHL-a, DO and TW, respectively. Note that, except for Day-1 prediction of DO for Miho, Day-1 prediction of TW for Jojong and Day-1 through -3 predictions of flow for Jojong, BC-DA consistently reduces RMSE, often very significantly to substantially, over Base or BC-Base for Day-1 through -3 predictions for all variables. As may be seen in Figure 6-8, the magnitude of flow in the Jojong Catchment is the smallest among the four catchments. The minimum value of flow to calculate the relative percent error for the screening procedure described above was 10 cms. In 2012, however, more than 70% of the observed flow fell below 10 cms. As such, it is possible that a number of very poor DA results were included in the evaluation statistics for Jojong. Figure 6-19 through Figure 6-22 show the MSE skill score of BC-Base and BC-DA relative to Base for analysis and predictions of streamflow, CHL-a, DO and TW, respectively. A skill score of unity indicates perfect analysis or prediction whereas a skill score of zero indicates that DA does not add any skill to the base simulation or prediction. Note that BC-DA consistently adds skill whereas BC alone does not.

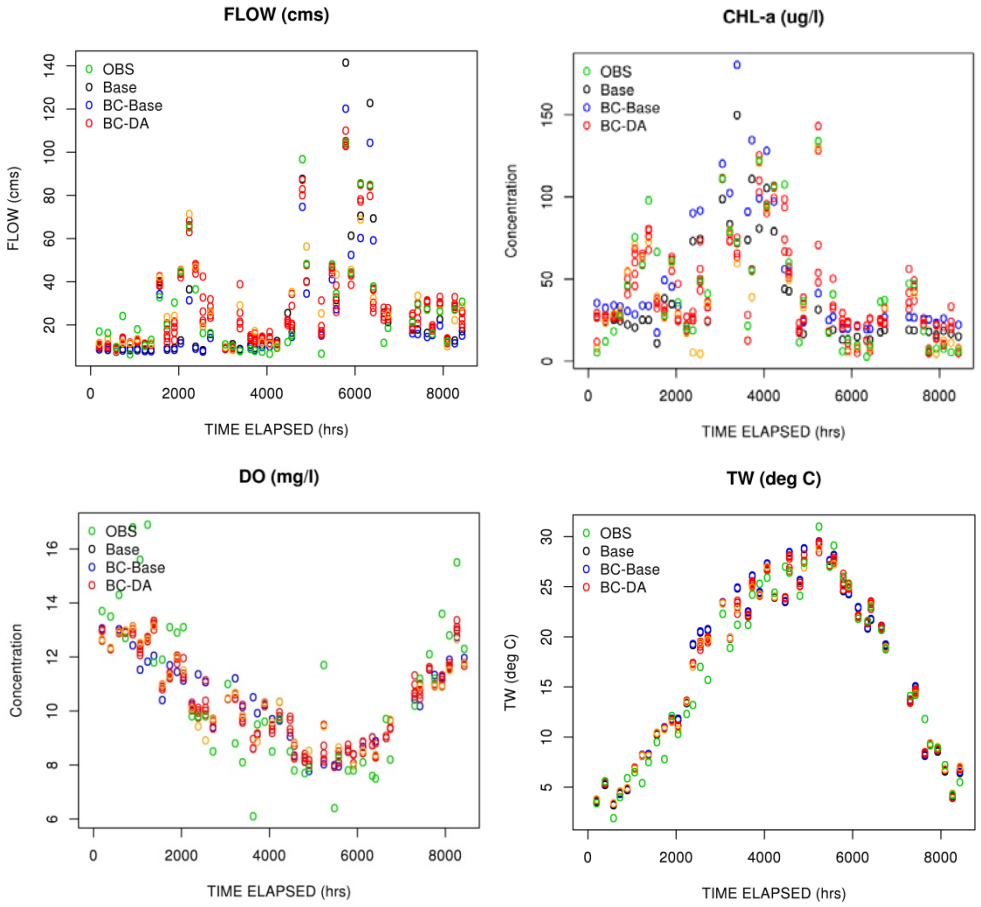

Figure 6-10 Time series of the observed (OBS), base (Base), bias-corrected (BC-Base), and bias-corrected and DA-aided (BC-DA) simulations of flow, CHL-a, DO and TW at the outlet of the Kumho Catchment.

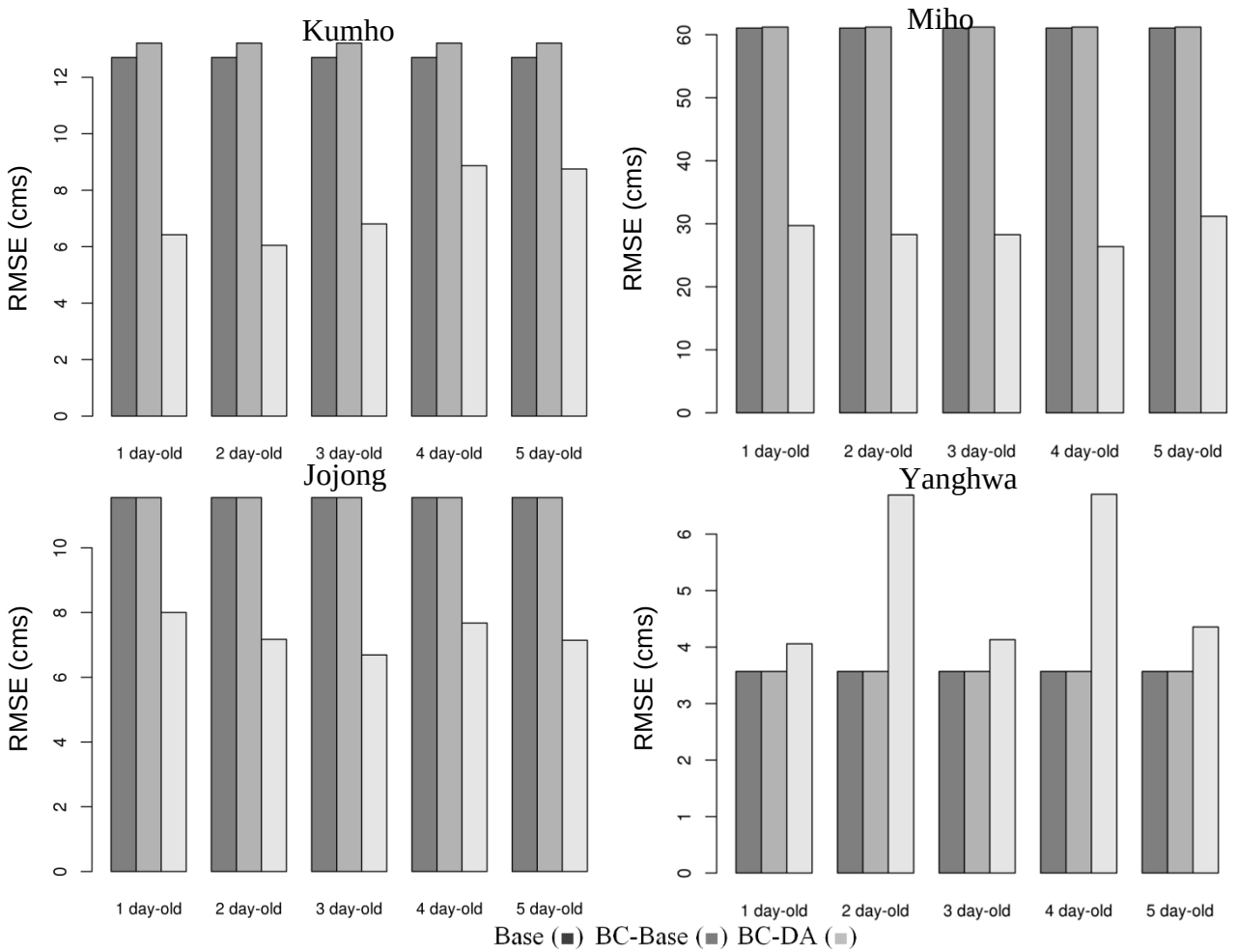

Figure 6-11 RMSE of flow analysis based on 1 day- to 5 day-old observations for the 4 study catchments.

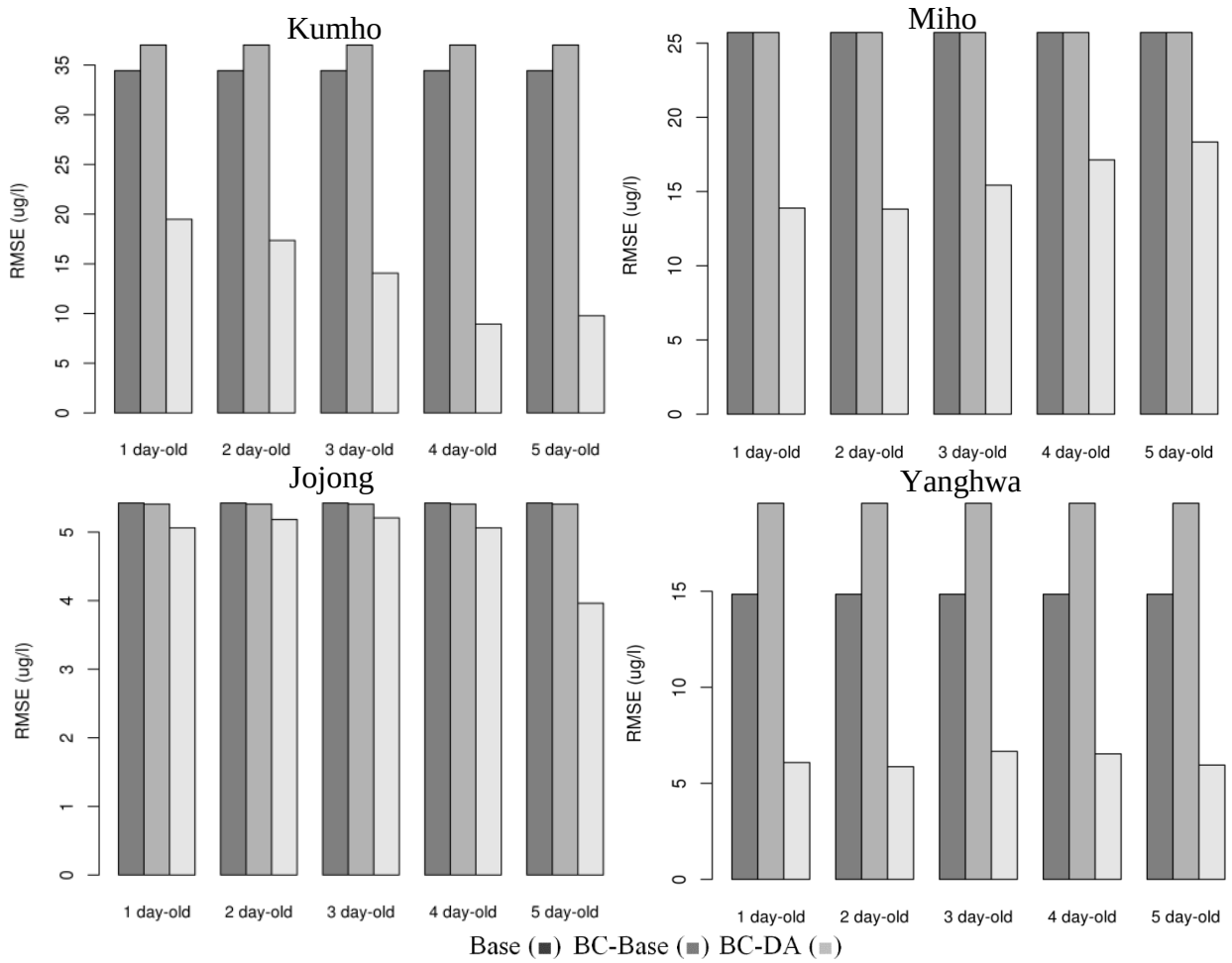

Figure 6-12 RMSE of CHL-a analysis based on 1 day- to 5 day-old observations for the 4 study catchments.

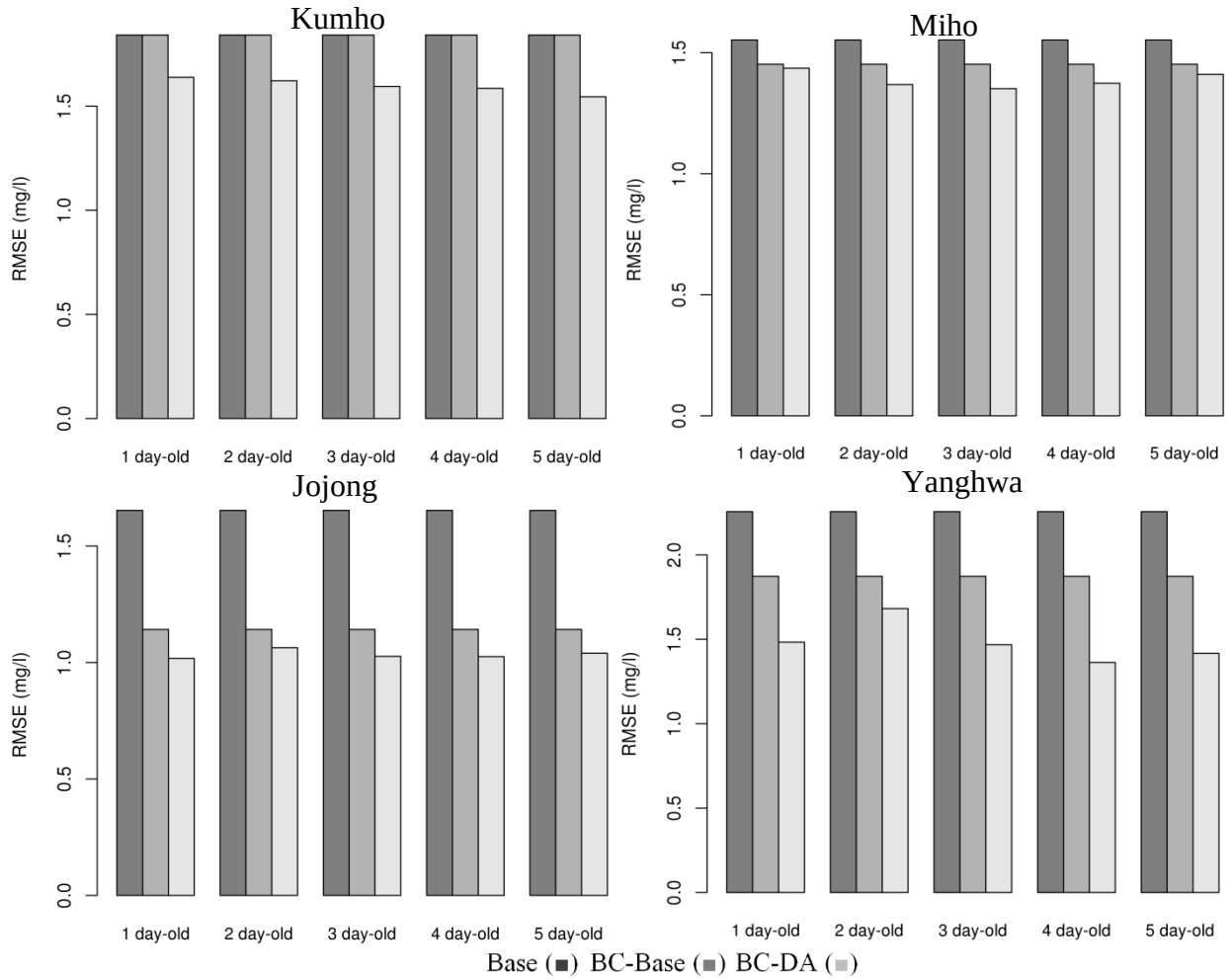

Figure 6-13 RMSE of DO analysis based on 1 day- to 5 day-old observations for the 4 study catchments.

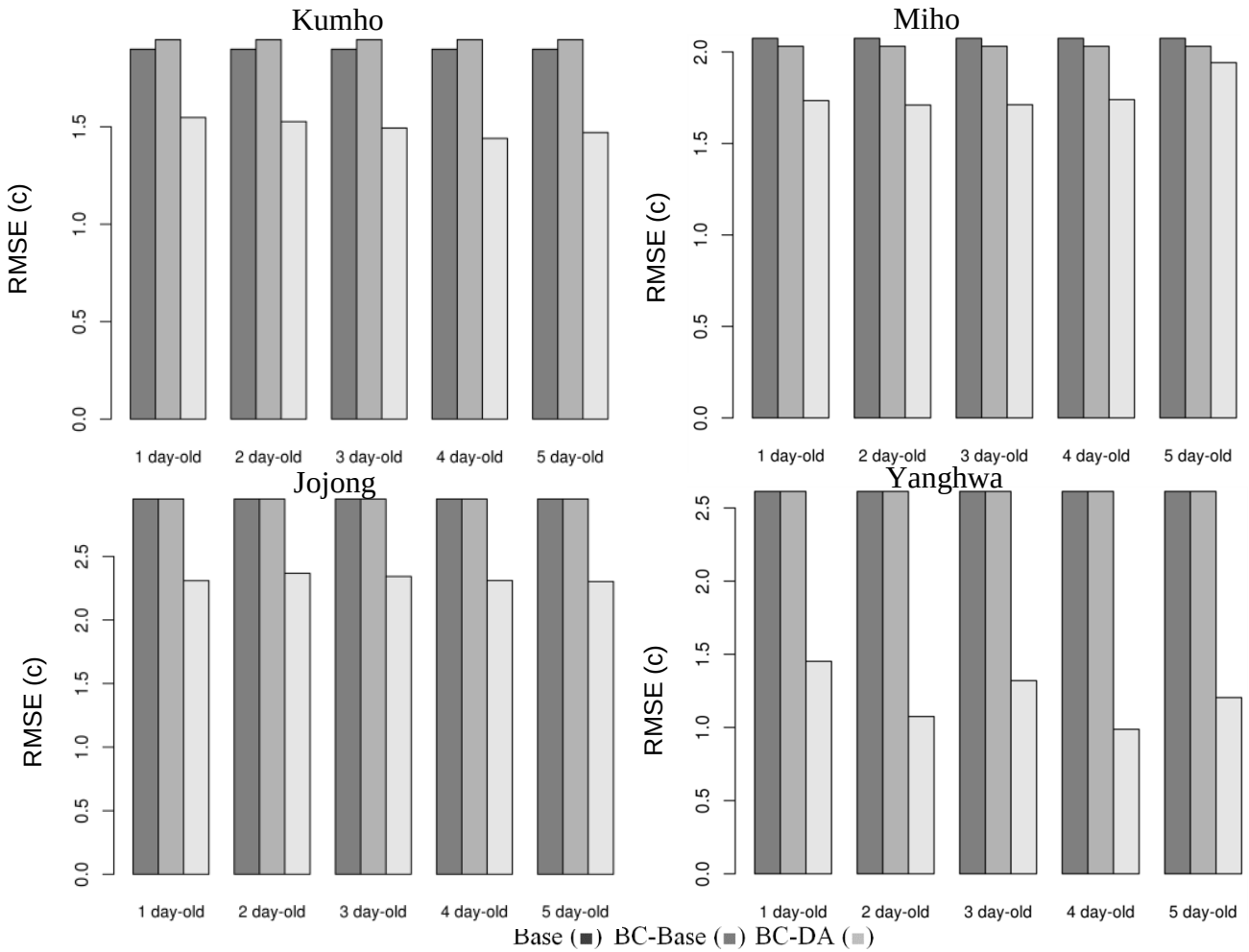

Figure 6-14 RMSE of TW analysis based on 1 day- to 5 day-old observations for the 4 study catchments.

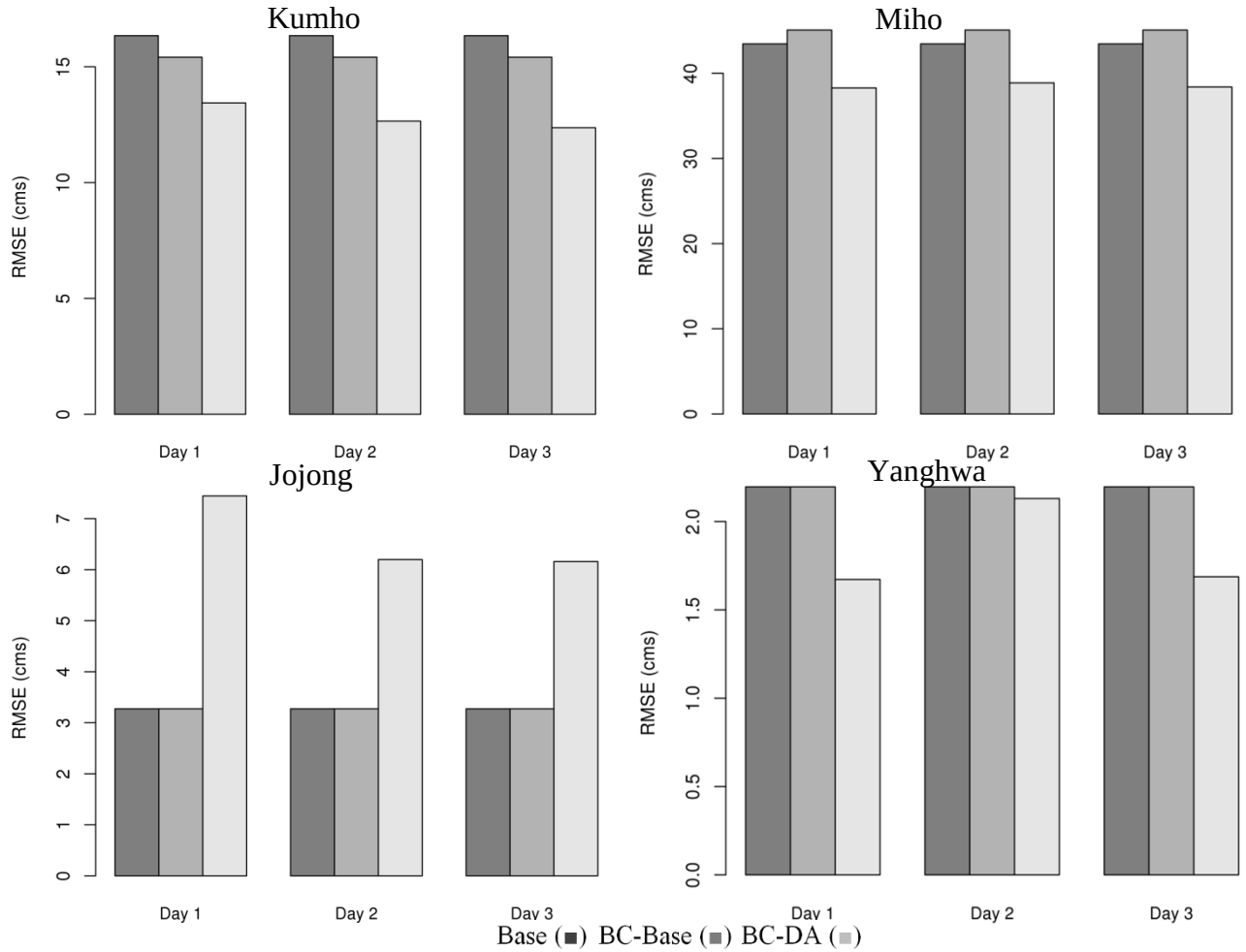

Figure 6-15 RMSE of Day-1 through -3 predictions of flow by Base, BC-Base and BC-DA for the 4 study catchments.

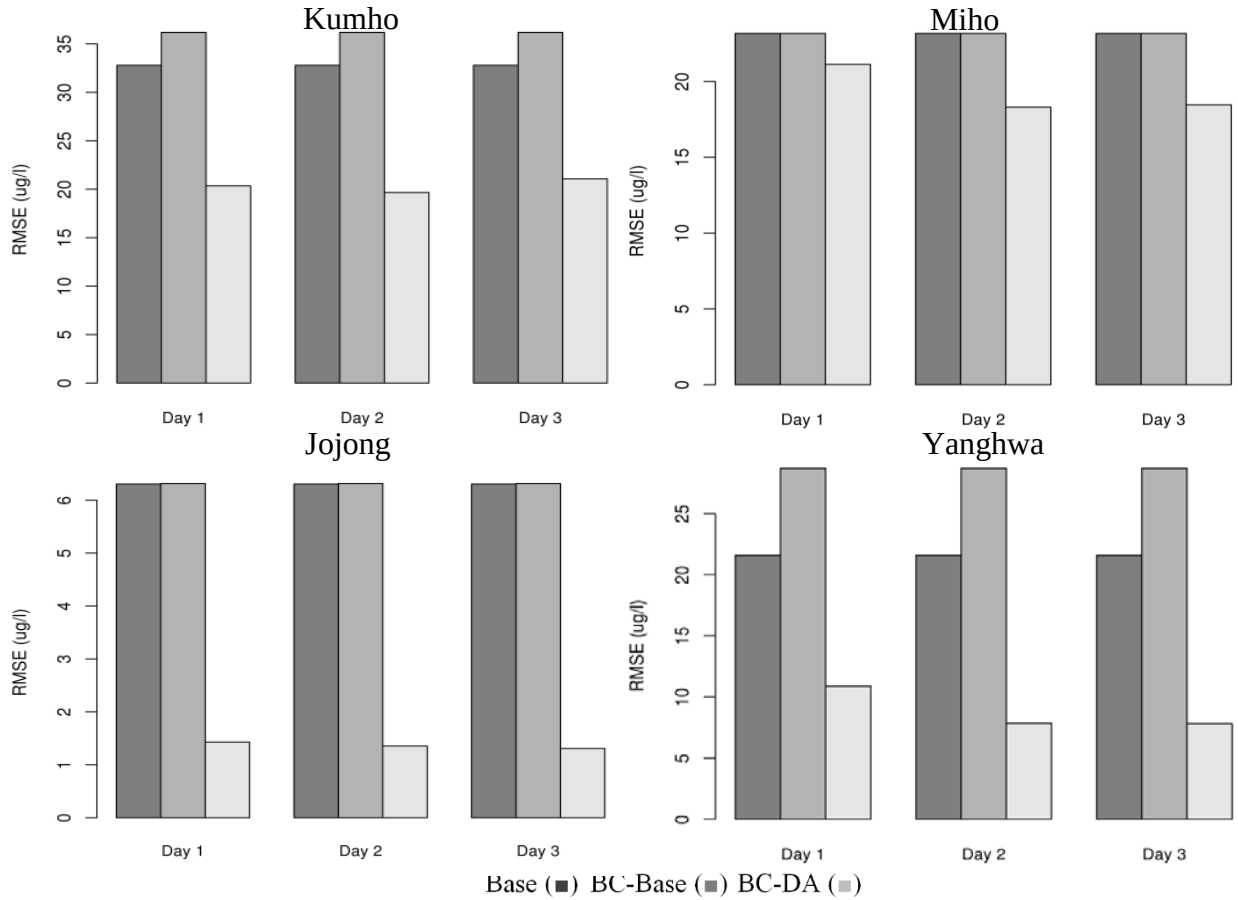

Figure 6-16 RMSE of Day-1 through -3 predictions of CHL-a by Base, BC-Base and BC-DA for the 4 study catchments.

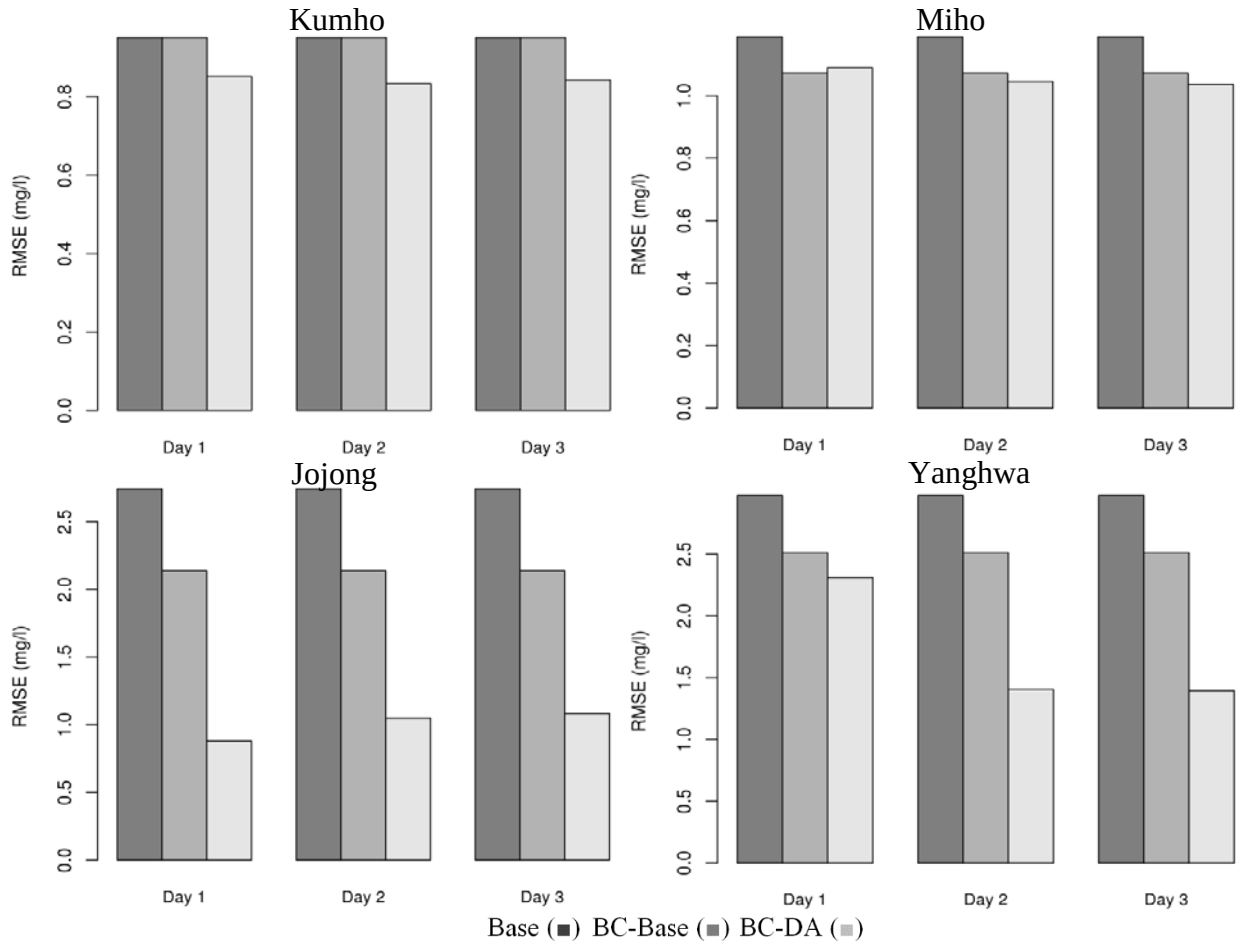

Figure 6-17 RMSE of Day-1 through -3 predictions of DO by Base, BC-Base and BC-DA for the 4 study catchments.

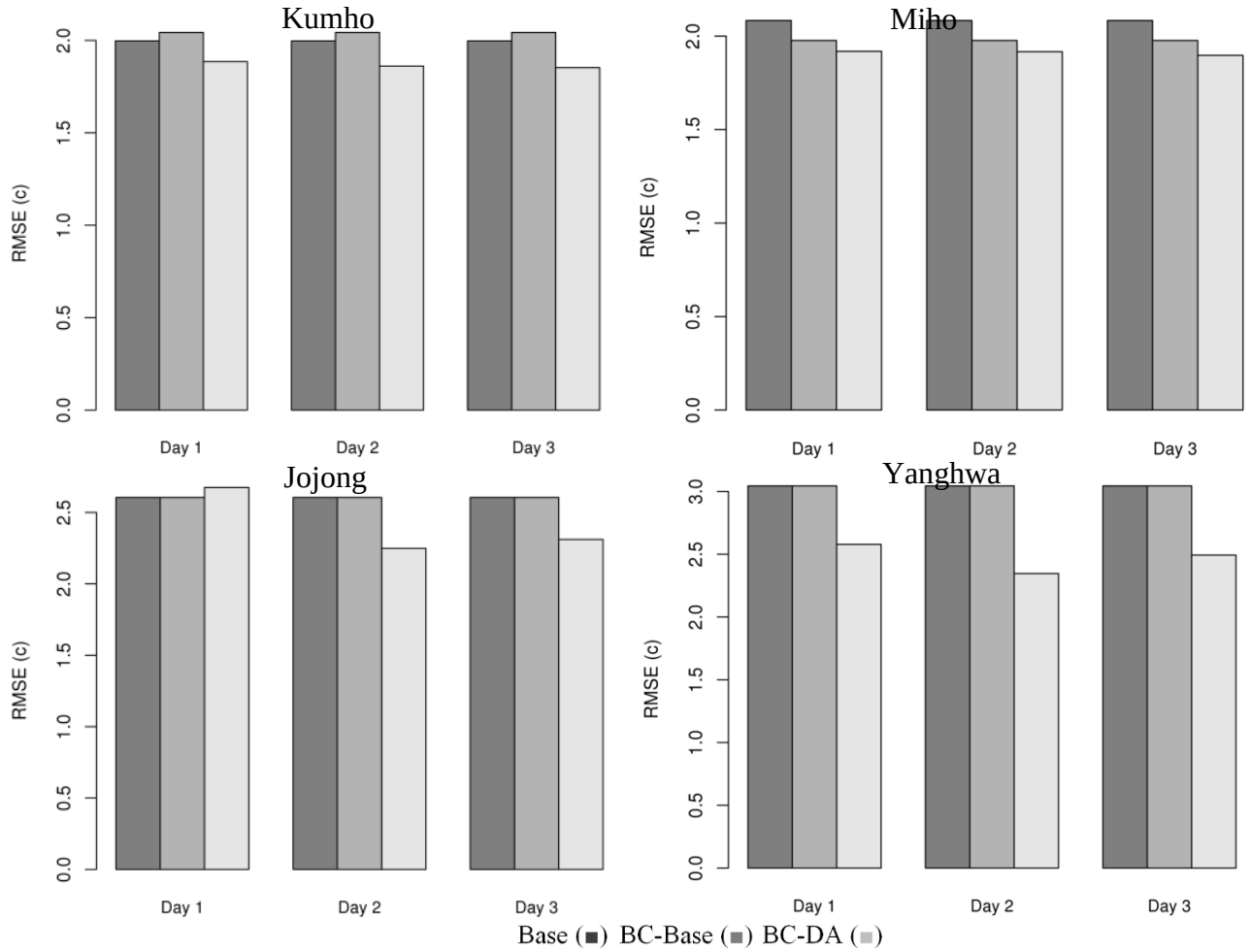

Figure 6-18 RMSE of Day-1 through -3 predictions of TW by Base, BC-Base and BC-DA for the 4 study catchments.

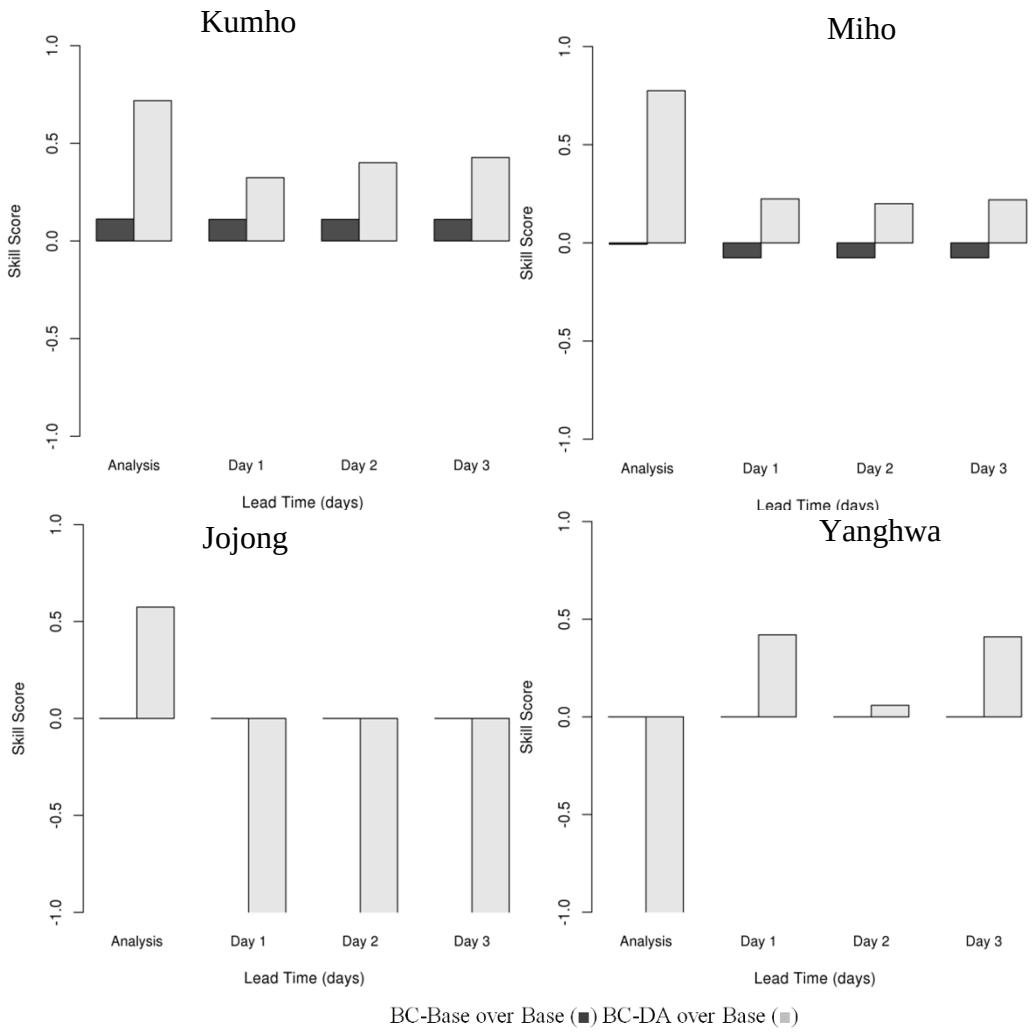

Figure 6-19 MSE skill score of BC-Base and BC-DA over Base (see text for explanations) for analysis and Day-1 through -3 predictions of flow for the 4 study catchments.

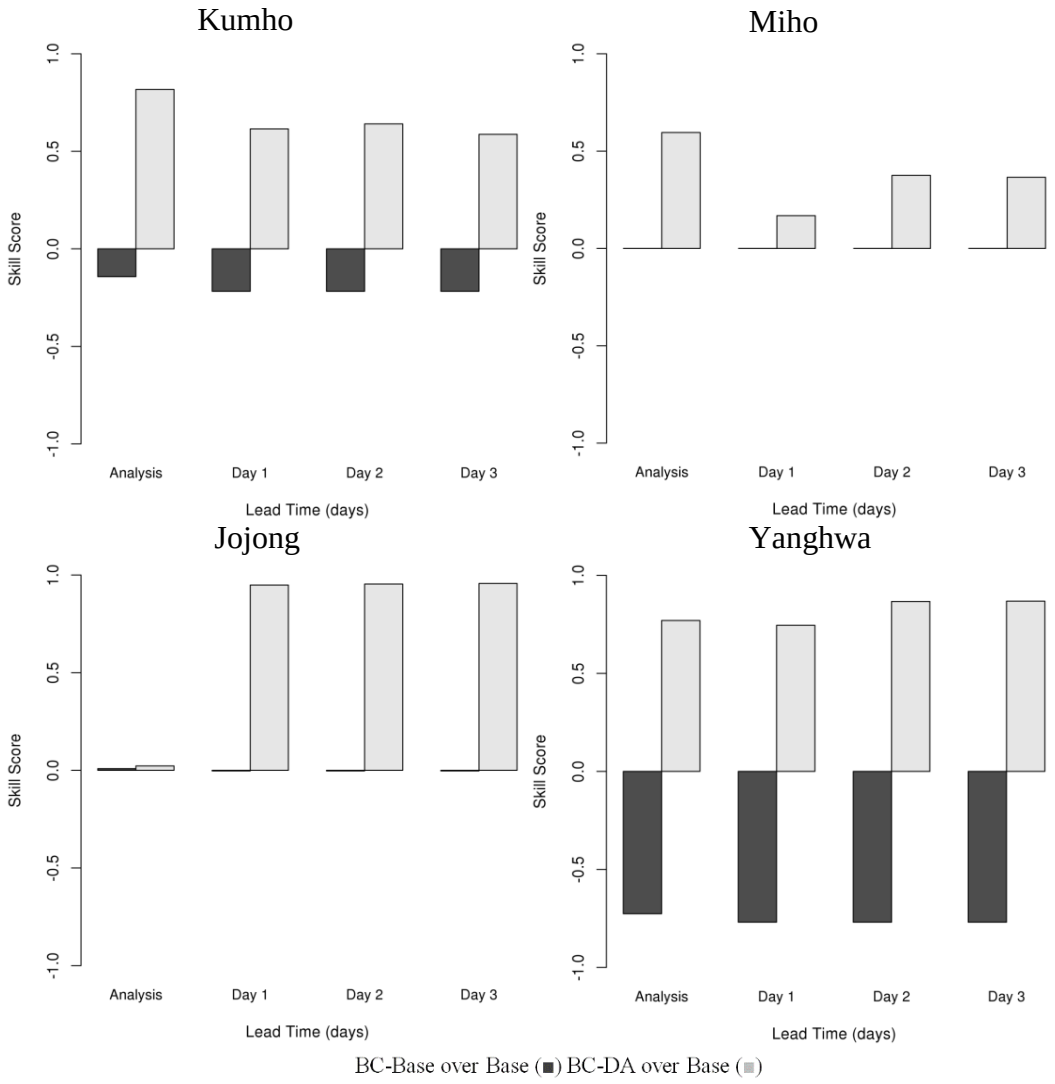

Figure 6-20 MSE skill score of BC-Base and BC-DA over Base (see text for explanations) for analysis and Day-1 through -3 predictions of CHL-a for the 4 study catchments.

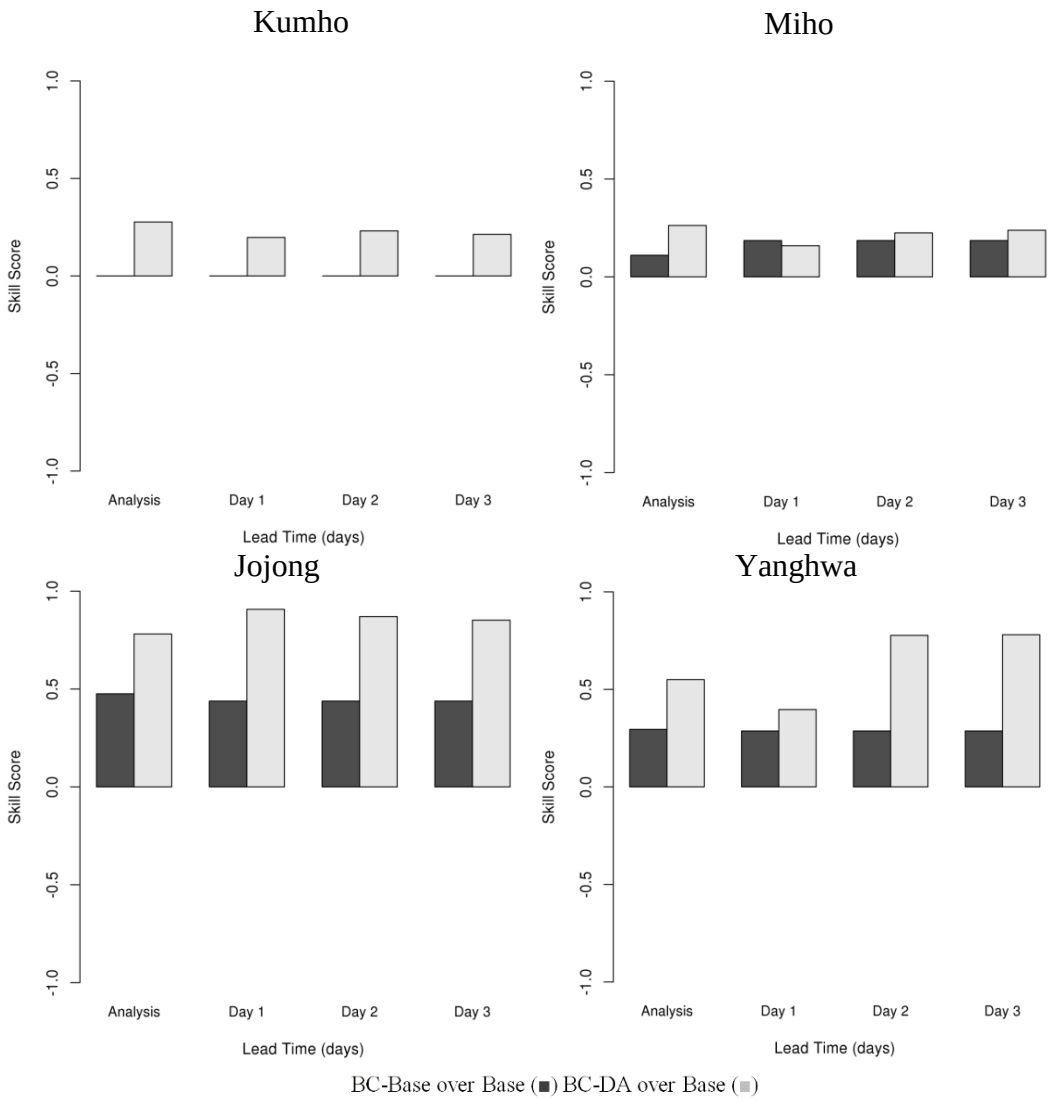

Figure 6-21 MSE skill score of BC-Base and BC-DA over Base (see text for explanations) for analysis and Day-1 through -3 predictions of DO for the 4 study catchments.

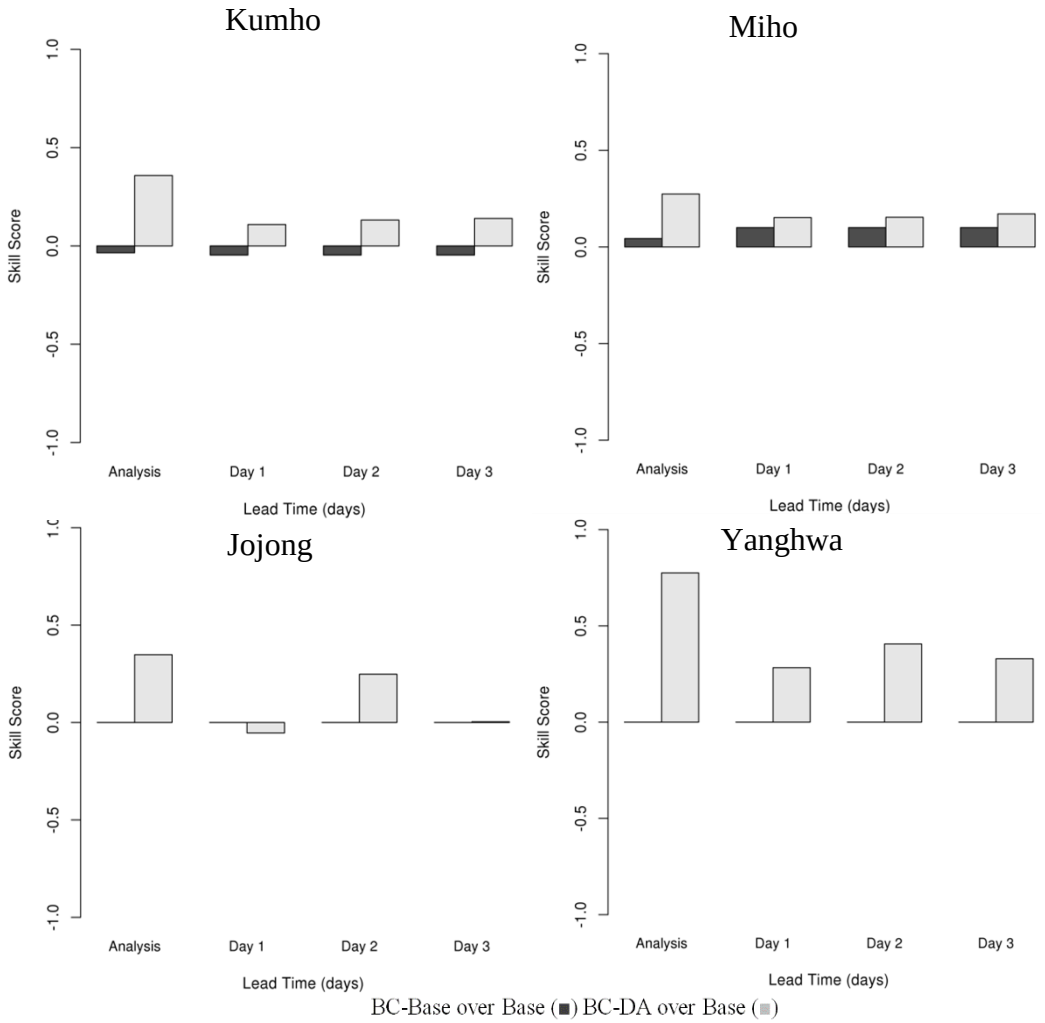

Figure 6-22 MSE skill score of BC-Base and BC-DA over Base (see text for explanations) for analysis and Day-1 through -3 predictions of TW for the 4 study catchments.

The above results show the performance of DA for analysis and prediction only at the catchment outlet. To provide EFDC with more accurate BCs at all locations within the river system, it is necessary for DA to produce skillful predictions at interior locations as well. To illustrate, Figure 6-23 shows two examples of the DA-updated and base-simulated ICs at all reaches in the Kumho Catchment; the top and bottom panels show

the CHL-a and DO results, respectively. Note that the direction of adjustment by DA is in agreement with the adjustment necessary to approach the observations at the outlet location for both variables. It is seen that the DA-updated DO is very reasonable compared to the base simulation states at all the reaches, but that the DA-updated CHL-a states may not be very realistic at some reaches. Addition research is necessary to assimilate observations at both the outlet and interior locations so that the underdeterminedness of the inverse problem may be reduced for improved analysis and prediction at all locations within the catchment.

Figure 6-25 illustrates how the MLEF-HSPF module may operate as part of WQFS-NIER. The WQFS-NIER general adapter retrieves the meteorological, precipitation, water quality, point source and streamflow (mean daily or instantaneous) data from the local database (see Figure 6-24) and converts them into an xml format. The HSPF adapter for WQFS-NIER converts the xml format to the WDM format for ingest by HSPF as part of the MLEF-HSPF operation. Once the MLEF-HSPF run is complete, the results may be presented in WQFS-NIER as shown in Figure 6-25. In the figure, the markers and dotted lines in the upper panel and the solid lines in the lower panel represent the weekly observations, all other solid lines showing diurnal cycles represent model simulations for which different colors represent different catchments. The output from MLEF-HSPF is then exported to LocalDataStore in WQFS-NIER to provide EFDC with the forecast BCs of flow and water quality variables along the main stem and major tributaries.

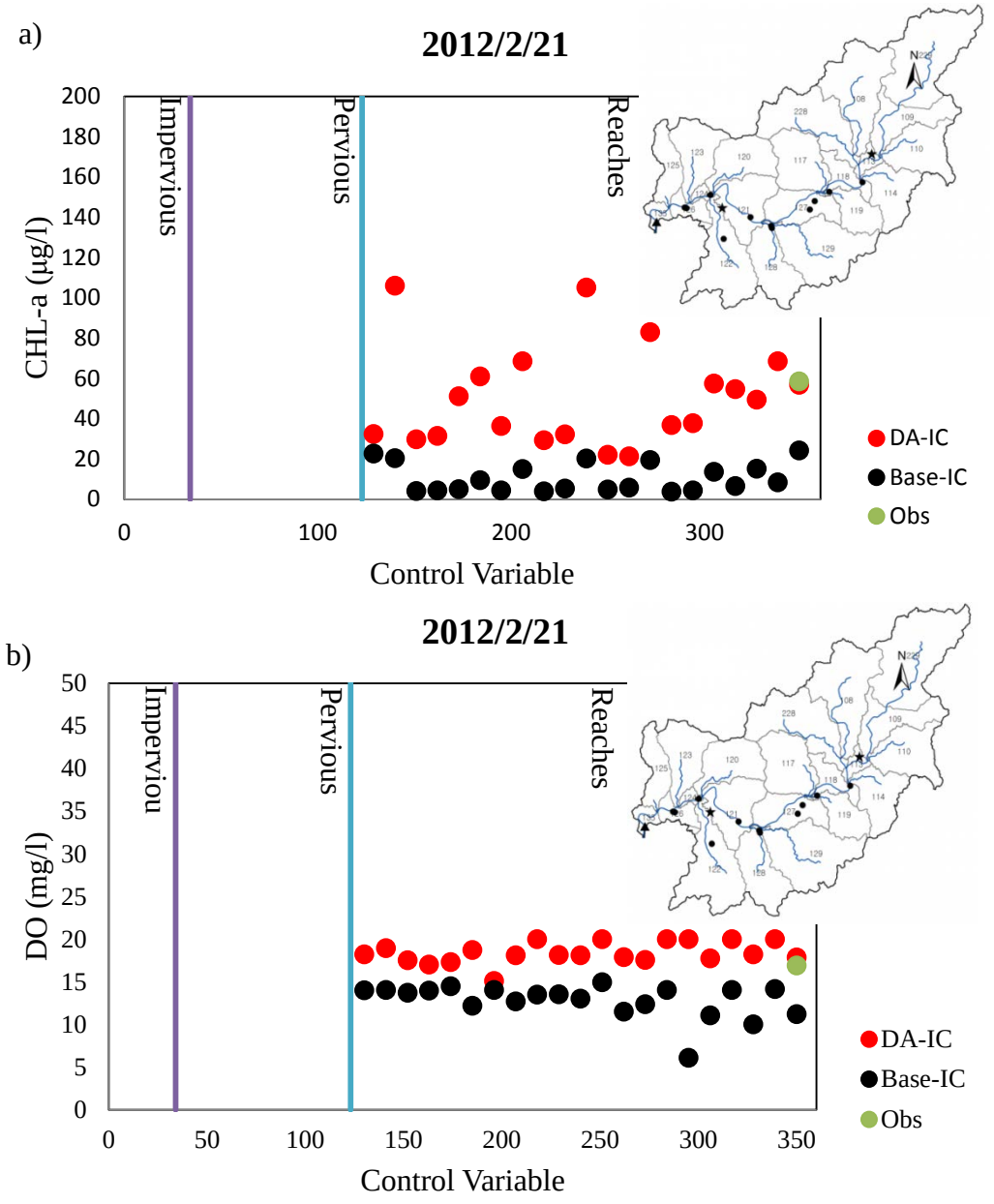

Figure 6-23 Example comparisons of DA-updated model states with the base-simulated at all reaches in the Kumho Catchment for (a) CHL-a and (b) DO. The black, red and green dots denote the base simulated, DA-updated and observed states, respectively. The smaller the control variable number is, the more upstream the reach is.

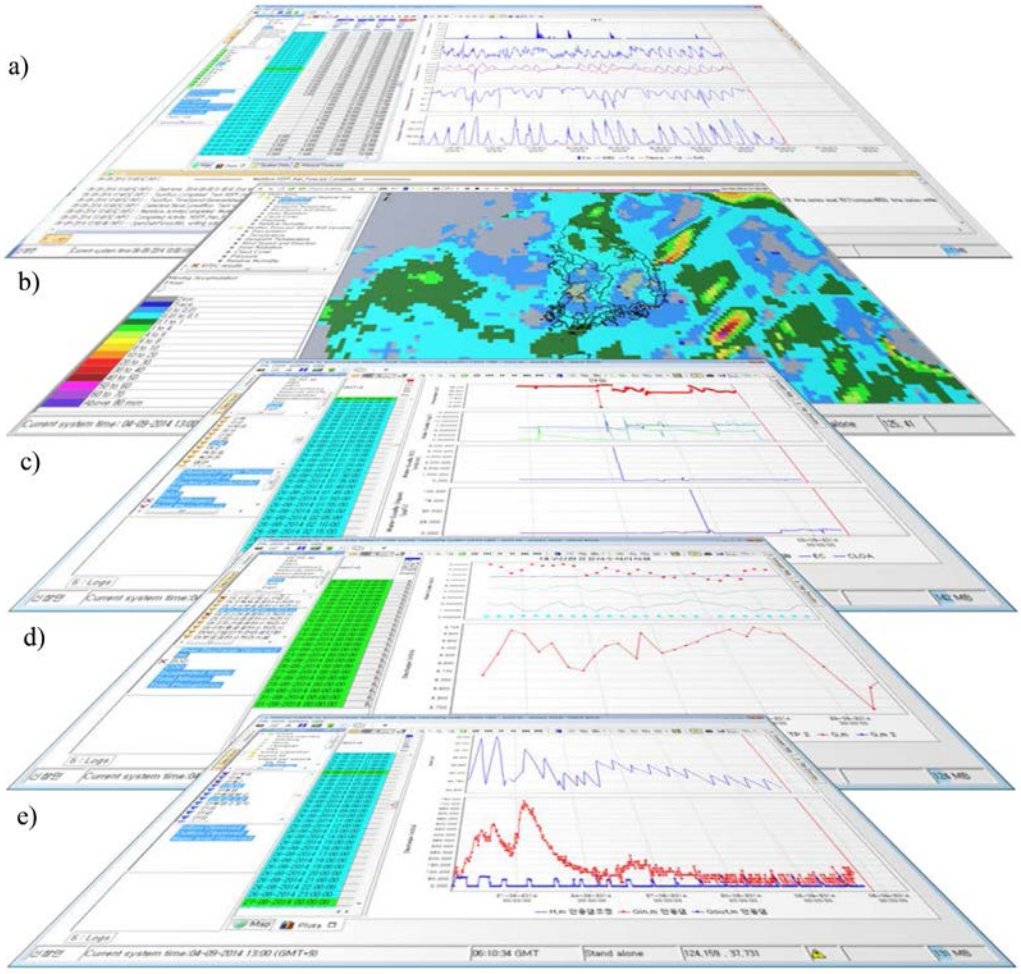

Figure 6-24 An example set of (a) meteorological forcing, (b) precipitation, (c) water quality, (d) point source and (e) streamflow (mean daily or instantaneous) data retrieved daily from the local database of WQFS-NIER.

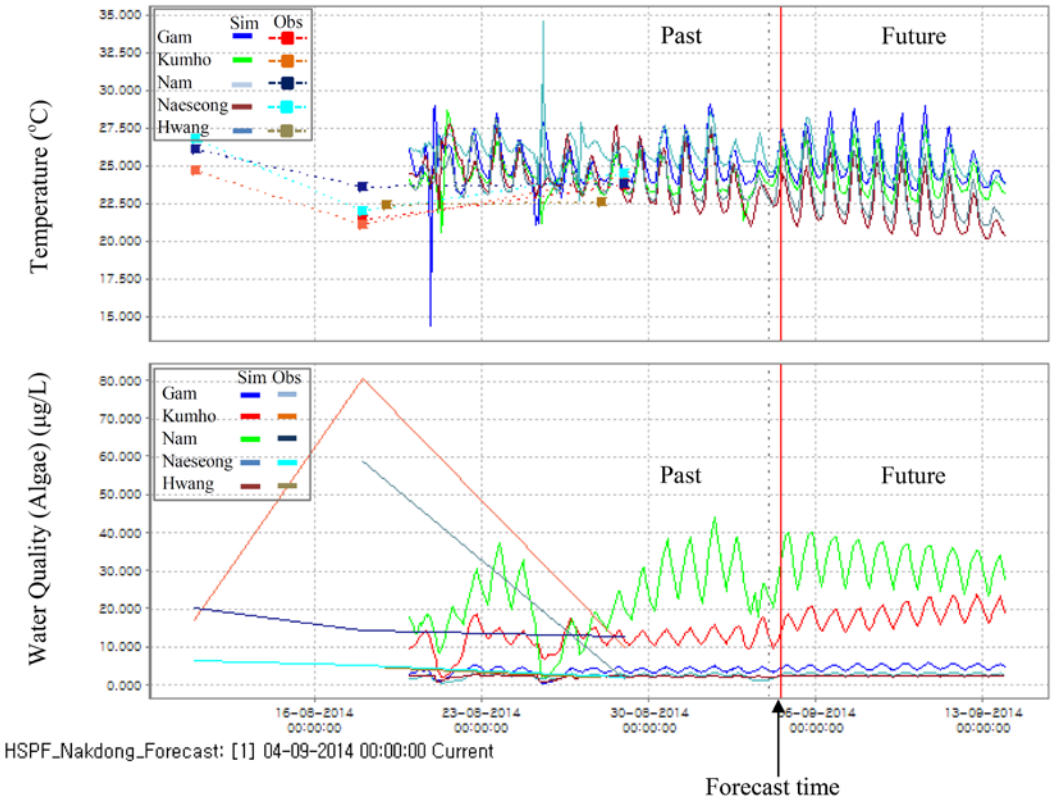

Figure 6-25 An example display of DA-aided analysis and forecast in WQFS-NIER (solid lines with diurnal cycles). Also shown are the observations in markers and dotted lines (top) and solid straight lines (bottom).

6.5. Ensemble verification of DA-aided predictions

The evaluations carried out above pertain only to the quality of ensemble mean. In this subsection, we examine the quality of ensemble results to better understand the HSPF dynamics in the context of ensemble forecasting. It must be acknowledged, however, that the ensemble results are from using MLEF-HSPF solely as a reduced-rank minimizer and no consideration was given for ensemble performance. As such, they are only exploratory in nature. For ensemble verification, the Ensemble Verification System (EVS, Brown et al. 2010) developed by the US National Weather Service Office of Hydrologic Development was used. EVS is a software tool for verification of ensemble forecasts of hydrologic and hydrometeorological variables such as precipitation and streamflow. EVS includes a large number of metrics to assess the quality of both single-valued and ensemble forecasts. In this subsection, only a few of the metrics are presented. The hindcasting experiment for verification of DA-updated state variables was performed for the Kumho Catchment for a two-year period of 2008-2009. The observed variables were predicted out to three days into the future in each assimilation cycle. Figure 6-26 shows the modified box-and-whisker plot of the forecasting error (ensemble member – observed value) for Day-1 through -3 of DA-aided ensemble predictions. The figure shows that the ensemble predictions are severely underspread. Investigations into the response of HSPF to varying levels of ensemble perturbations in the ICs indicate that HSPF collapses even the very large perturbations into tightly bundled ensemble traces rather quickly, suggesting that the model dynamics may lack realism to produce realistic spread. Figure 6-27 shows the Relative Operating Characteristic (ROC) for different thresholds for the three lead times for CHL-a forecast. ROC measures the ability of an ensemble forecast to discriminate between two possible outcomes (i.e., occurrence vs. non-occurrence of an event). ROC plots the Probability of Detection (POD) on the y-axis

vs. the Probability of False Detection (POFD) on the x-axis for a given threshold. The diagonal line represents the climatological forecast or ‘zero skill’ line. Ensemble forecast with perfect discriminatory skill connects (0,0), (0,1) and (1,1). The figure shows that the DA-aided ensemble forecasts have positive discriminatory skill, that the skill decreases as lead time increases, that the skills are higher for moderate to high thresholds than at a low threshold, but that the ensembles are severely underspread as shown by the triangular ROC areas. Figure 6-28 shows the reliability diagram of the CHL-a forecast exceeding 21.7, 47.0 and 82. 5 µg/l of observed CHL-a at lead times of one, two and three days. Perfectly reliable ensemble forecast would place the reliability diagram on the diagonal line, i.e., the forecast probability is unbiased against the frequency at which the observations verify in the mean sense (i.e., over a long period of time). The figure shows that the ensembles are not reliable due to the severe underspreadness observed above.

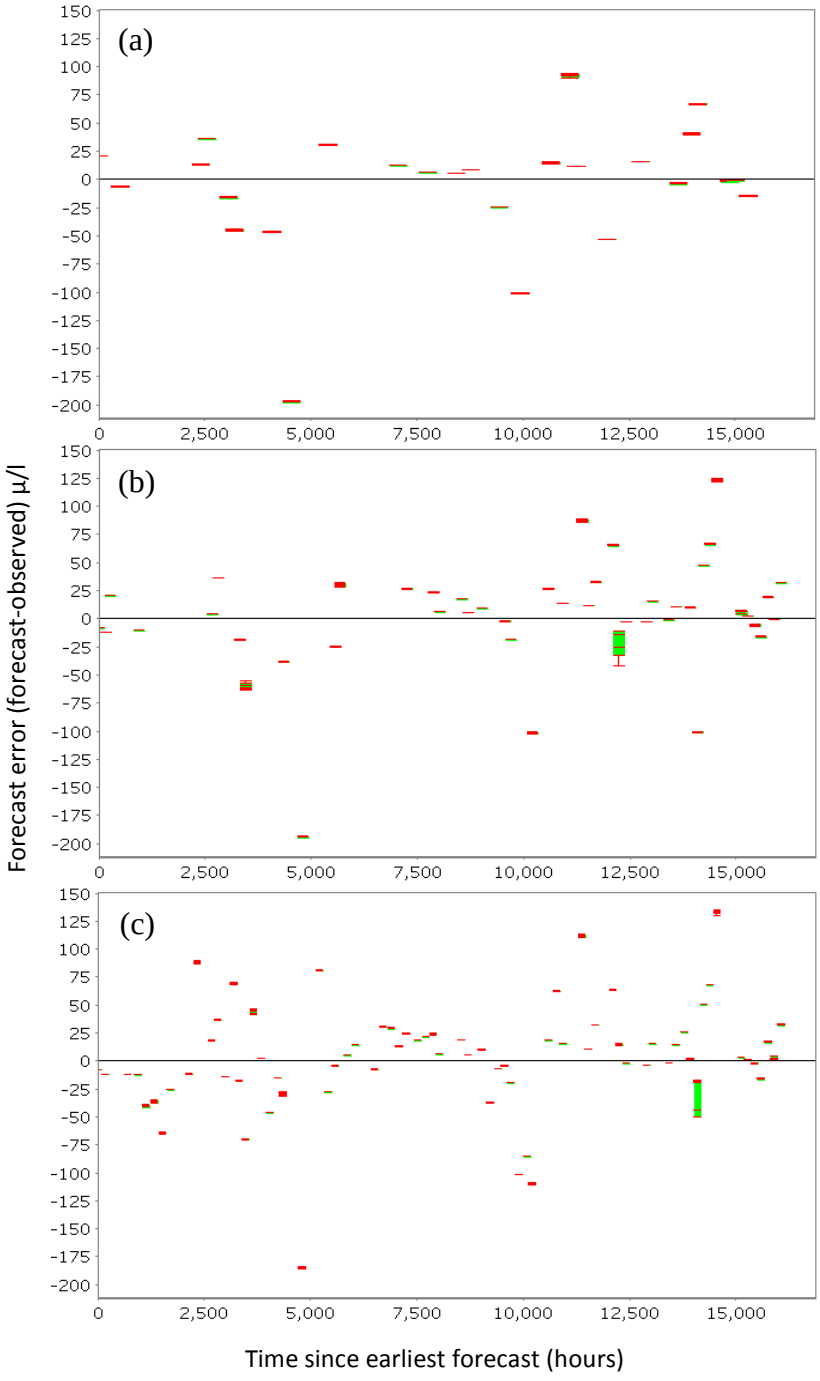

Figure 6-26 The modified box plot of the ensemble forecast errors against forecast time for three lead times ((a) Day-1, (b) Day-2 and (c) Day-3) during 2008-2009 for CHL-a.

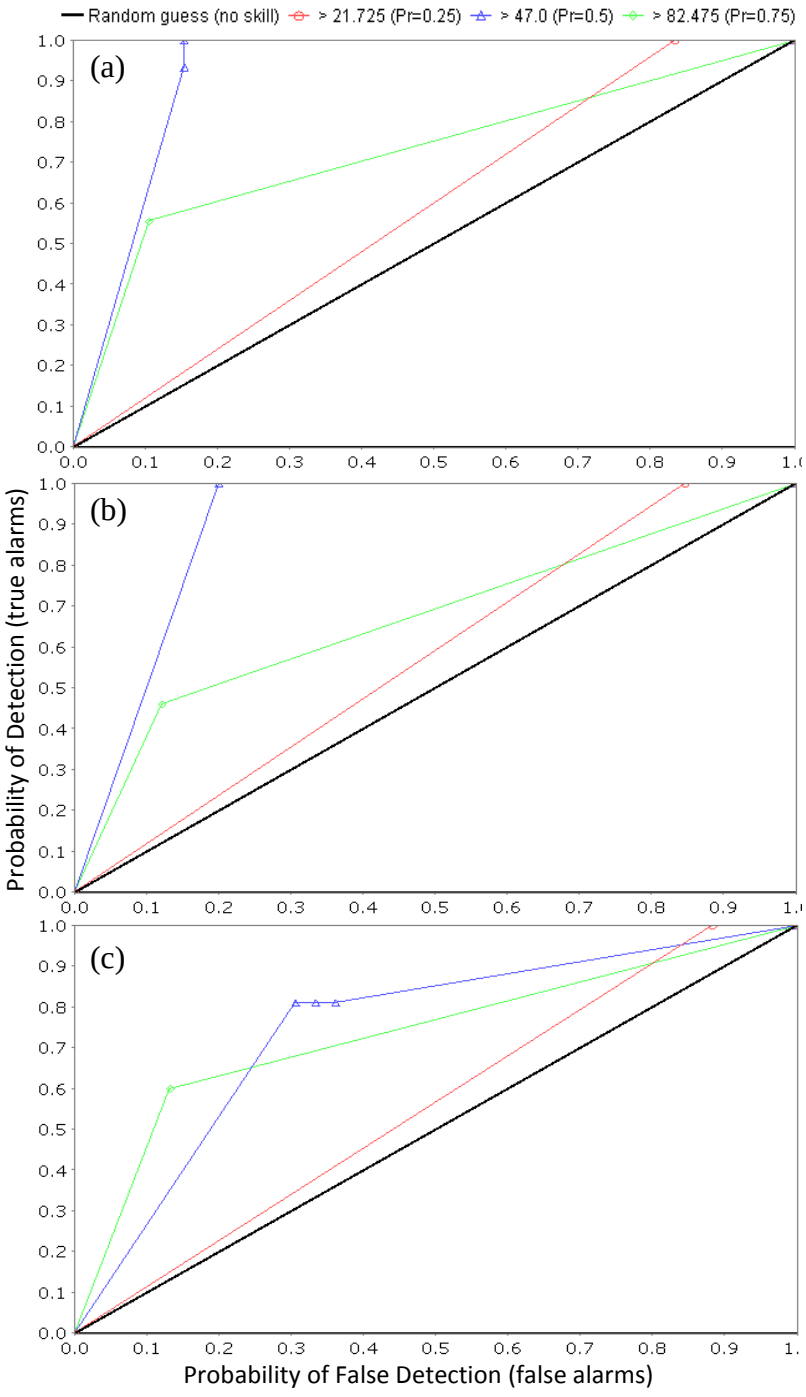

Figure 6-27 Relative Operating Characteristic (ROC) for different probability thresholds for three lead times ((a) Day-1, (b) Day-2 and (c) Day-3) during 2008-2009 for CHL-a.

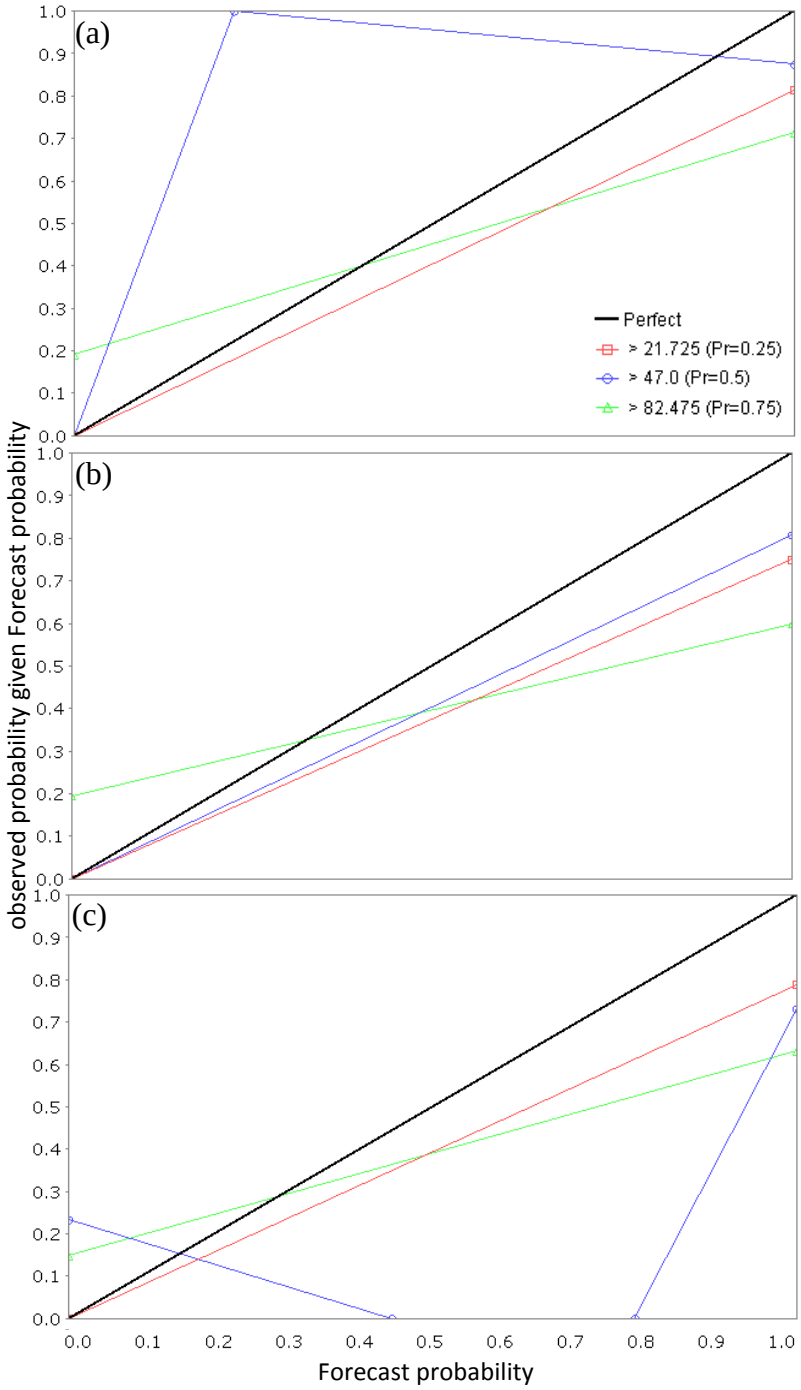

Figure 6-28 Reliability diagram for various event thresholds for three lead times ((a) Day-1, (b) Day-2 and (c) Day-3) during 2008-2009 for CHL-a.

6.6. Time series modeling and prediction

The calibration period of HSPF for the four major River Basins is 2008 to 2010. To allow head-to-head comparisons with Base and BC-DA, the same period of record was used for time series modeling for selected catchments. Figure 6-29a and Figure 6-29b show the time series and auto correlation function (ACF) of the observed DO at the outlet of the Nam Catchment for 2008 to 2010, respectively. Figure 6-30a shows the histogram of the observed DO, which indicates mild positive skewness. To reduce skewness, log transformation was applied. Figure 6-30b shows the histogram of the log-transformed DO. Figure 6-31 shows the time series and ACF of the log-transformed DO. To remove seasonality seen in Figure 6-31, seasonal differencing of the log-transformed DO at a period of 48 weeks was applied. It was found that the resulting series has seasonal nonstationarity for which first-order differencing was applied. Figure 6-32 shows the resulting residual time series, ACF and PACF for the best-fit model, ARIMA(0,0,0)$(0,1,0)_{48}$, for observed DO at the outlet of the Nam Catchment. The same procedure was performed to select the best-fit model for each water quality variable in the six selected catchments. The results are summarized in Table 6-2.

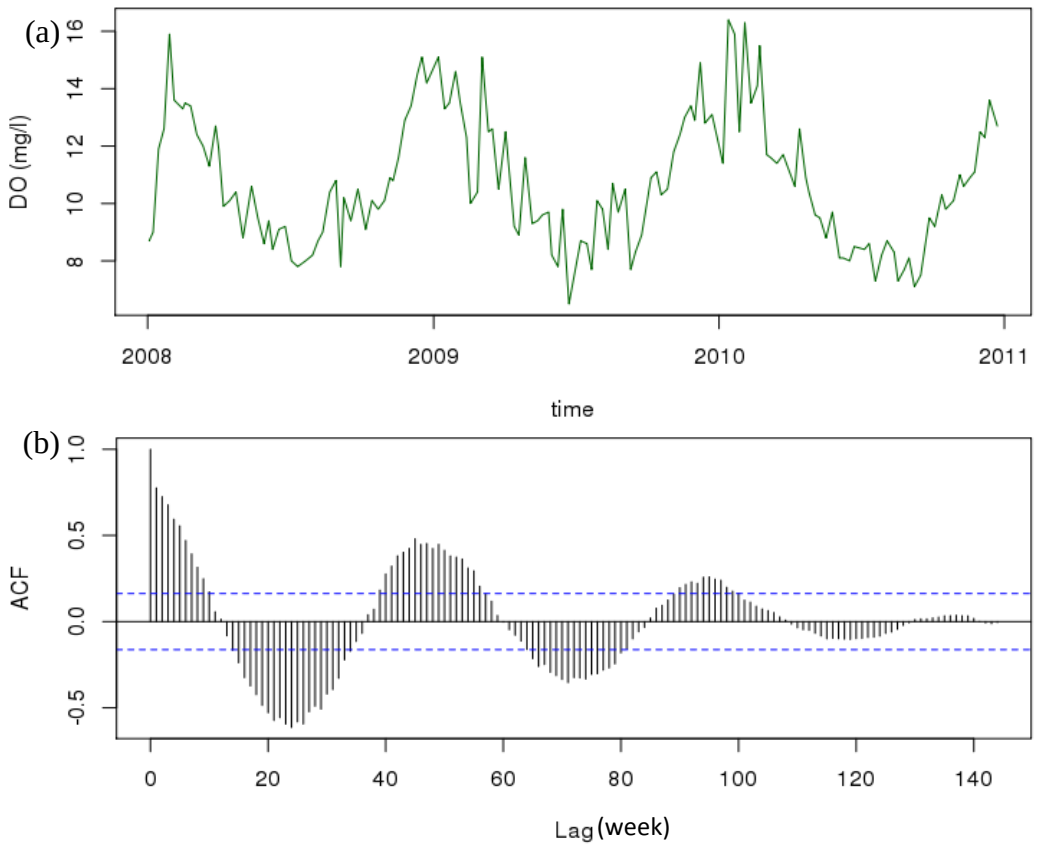

Figure 6-29 Time series plot and ACF of observed DO in the Nam Catchment.

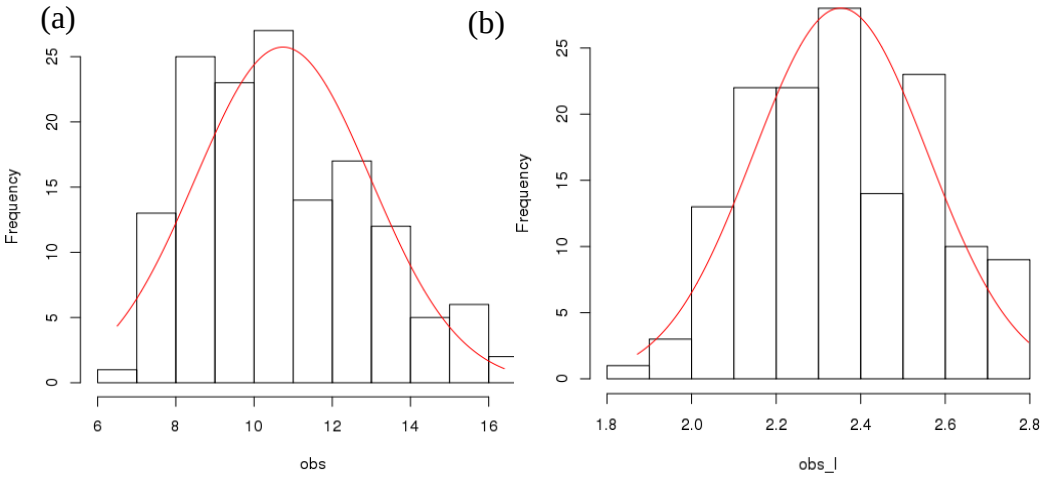

Figure 6-30 Histogram of the observed DO in the Nam Catchment (a) without any transformation, (b) log transformed observation.

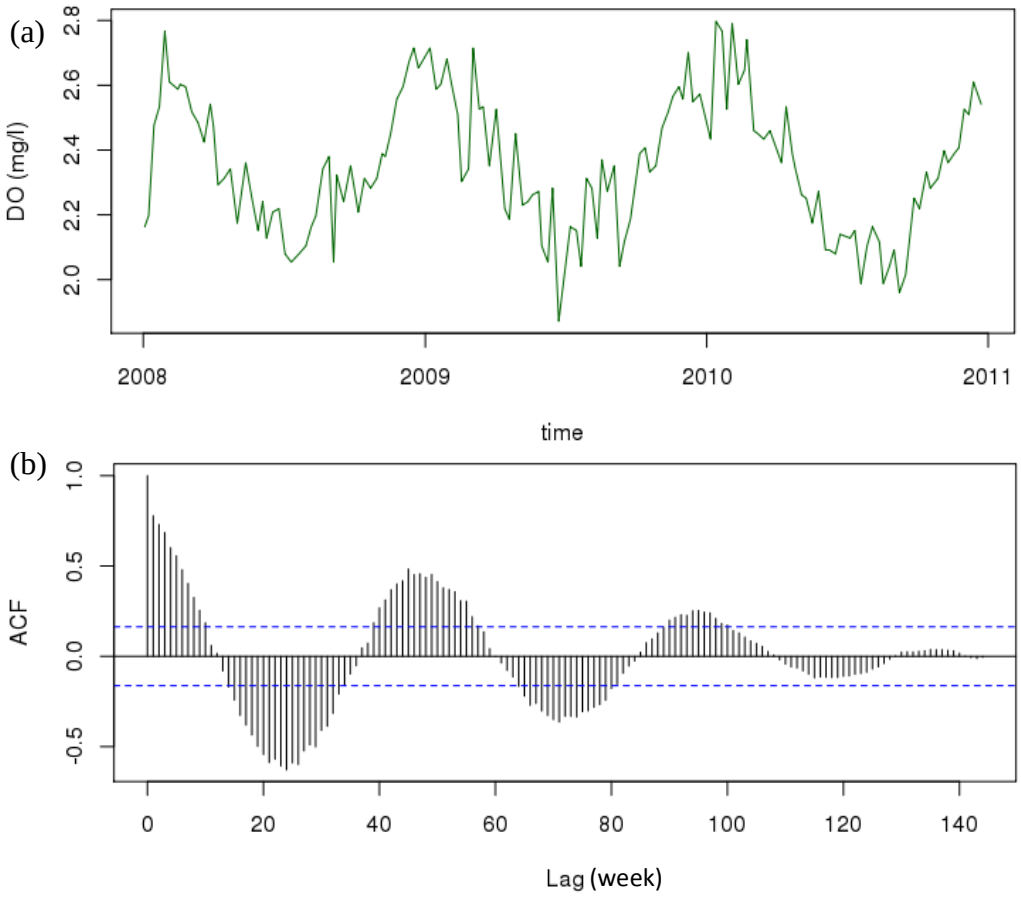

Figure 6-31 Time series plot and ACF of log transformed DO in the Nam Catchment.

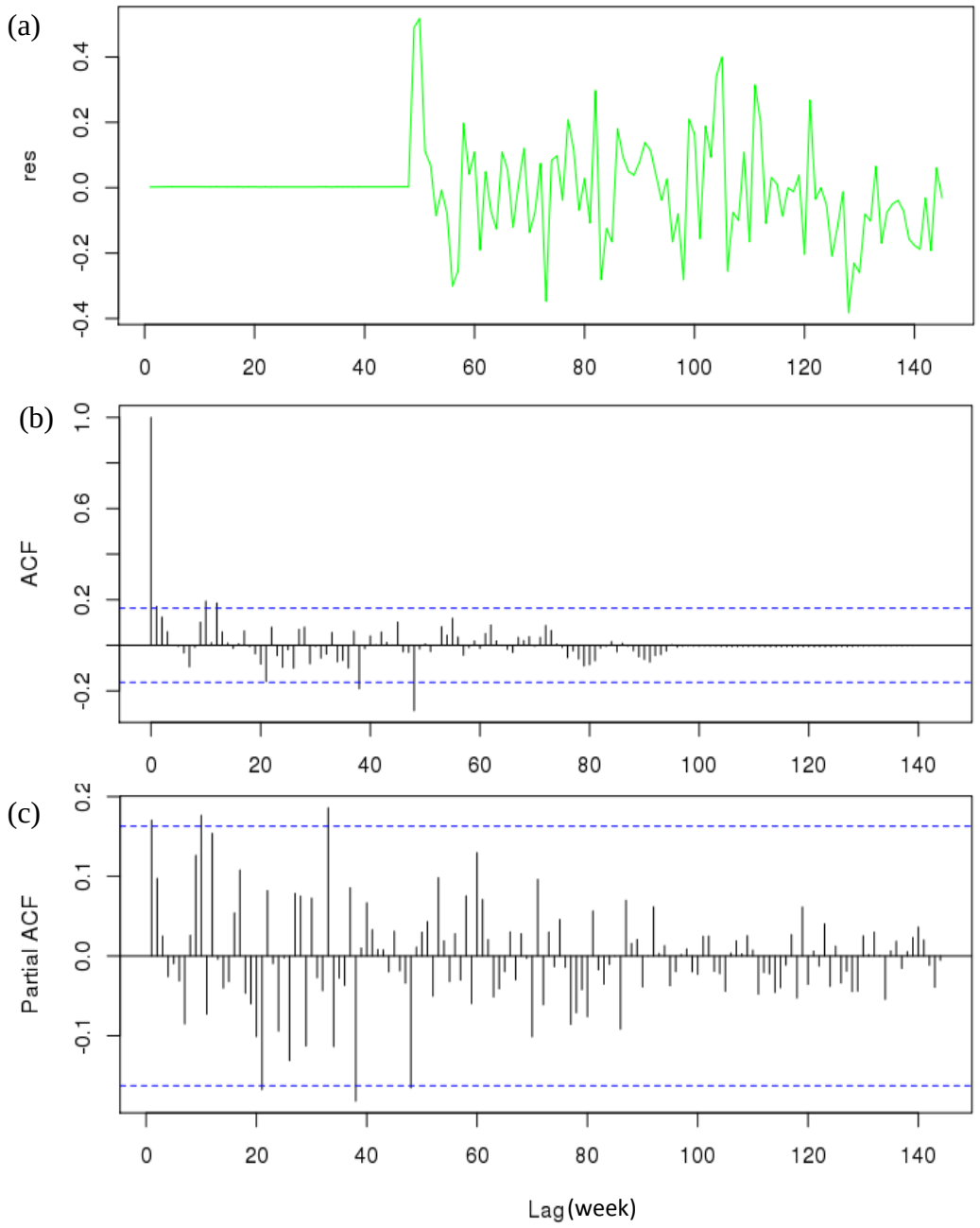

Figure 6-32 (a) residual time series, (b) the corresponding ACF and (c) PACF for log transformed DO for 2008 to 2010 for the most downstream monitoring station of the Nam Catchment.

Table 6-2 Best fitting models for water quality observations for the selected catchments for period of 2008 to 2010.

Variable	Catchment		
	Kumho	**Banbyeon**	**Naeseong**
TW	ARIMA(0,0,0)(0,1,0)$_{48}$	ARIMA(1,0,0)(0,1,1)$_{48}$	ARIMA(0,0,0)(0,1,0)$_{48}$
PO_4	ARIMA(0,1,1)(0,0,1)$_{48}$	ARIMA(1,0,0)(0,0,0)$_{48}$	ARIMA(1,0,0)(0,1,0)$_{48}$
CHL-a	ARIMA(1,0,0)(0,1,0)$_{48}$	ARIMA(1,0,0)(0,1,0)$_{48}$	ARIMA(0,0,0)(0,1,0)$_{48}$
BOD	ARIMA(1,0,0)(0,1,0)$_{48}$	ARIMA(1,0,0)(0,1,0)$_{48}$	ARIMA(0,0,0)(0,1,0)$_{48}$
DO	ARIMA(0,0,0)(1,1,0)$_{48}$	ARIMA(0,0,0)(1,1,0)$_{48}$	ARIMA(0,0,0)(1,1,0)$_{48}$
NH_4	ARIMA(0,0,0)(1,1,0)$_{48}$	ARIMA(1,0,0)(0,1,0)$_{48}$	ARIMA(1,0,0)(1,1,0)$_{48}$
NO_3	ARIMA(1,0,1)(0,1,0)$_{48}$	ARIMA(1,0,0)(0,0,0)$_{48}$	ARIMA(1,0,0)(0,1,0)$_{48}$
TN	ARIMA(1,0,1)(0,1,0)$_{48}$	ARIMA(1,0,0)(0,0,0)$_{48}$	ARIMA(1,0,0)(0,1,0)$_{48}$
TP	ARIMA(1,0,0)(0,1,0)$_{48}$	ARIMA(1,0,0)(0,1,1)$_{48}$	ARIMA(1,0,0)(1,0,0)$_{48}$
TOC	ARIMA(1,0,0)(0,0,0)$_{48}$	ARIMA(1,0,0)(0,0,0)$_{48}$	ARIMA(0,1,1)(0,0,0)$_{48}$
Variable	**Catchment**		
	Nam	**Seom**	**Uchi**
TW	ARIMA(1,0,0)(0,1,0)$_{48}$	ARIMA(0,1,1)(0,1,1)$_{50}$	ARIMA(1,0,0)(0,1,0)$_{50}$
PO_4	ARIMA(1,0,0)(0,0,0)$_{48}$	ARIMA(1,0,1)(0,0,0)$_{50}$	ARIMA(0,1,1)(0,0,0)$_{50}$
CHL-a	ARIMA(1,0,0)(0,0,0)$_{48}$	ARIMA(1,0,0)(0,1,1)$_{50}$	ARIMA(1,0,1)(0,0,0)$_{50}$
BOD	ARIMA(1,0,0)(0,0,0)$_{48}$	ARIMA(0,1,1)(0,0,0)$_{50}$	ARIMA(1,0,1)(0,0,0)$_{50}$
DO	ARIMA(0,0,0)(0,1,0)$_{48}$	ARIMA(1,0,0)(0,1,0)$_{50}$	ARIMA(1,0,0)(0,1,1)$_{50}$
NH_4	ARIMA(1,0,0)(1,1,0)$_{48}$	ARIMA(1,0,0)(0,1,0)$_{50}$	ARIMA(0,0,0)(1,1,0)$_{50}$
NO_3	ARIMA(1,0,0)(0,1,1)$_{48}$	ARIMA(1,0,0)(0,1,0)$_{50}$	ARIMA(0,1,1)(0,0,0)$_{50}$
TN	ARIMA(1,0,1)(0,1,0)$_{48}$	ARIMA(1,0,0)(0,1,0)$_{50}$	ARIMA(1,0,0)(0,0,0)$_{50}$
TP	ARIMA(0,1,1)(0,0,0)$_{48}$	ARIMA(1,0,1)(0,0,0)$_{50}$	ARIMA(1,0,1)(0,1,0)$_{50}$
TOC	ARIMA(0,1,1)(0,0,0)$_{48}$	ARIMA(1,0,1)(0,0,0)$_{50}$	ARIMA(1,0,1)(0,0,0)$_{50}$

☐ No transformation

Box-Cox transformed data

Log transformed data

To compare the time series results with Base and BC-DA, two types of predictions were made using the time series modeling results. To compare with Base, the best-fit time series model was used to make a prediction for the next three years; this result is referred to as TS-Base. For this purpose, the R package 'forecast' was used. If any form of transformation such as log or Box-Cox (Box and Cox 1964) was used, the resulting time series was appropriately back-transformed. Figure 6-33 shows TS-Base for DO at the outlet of Nam:

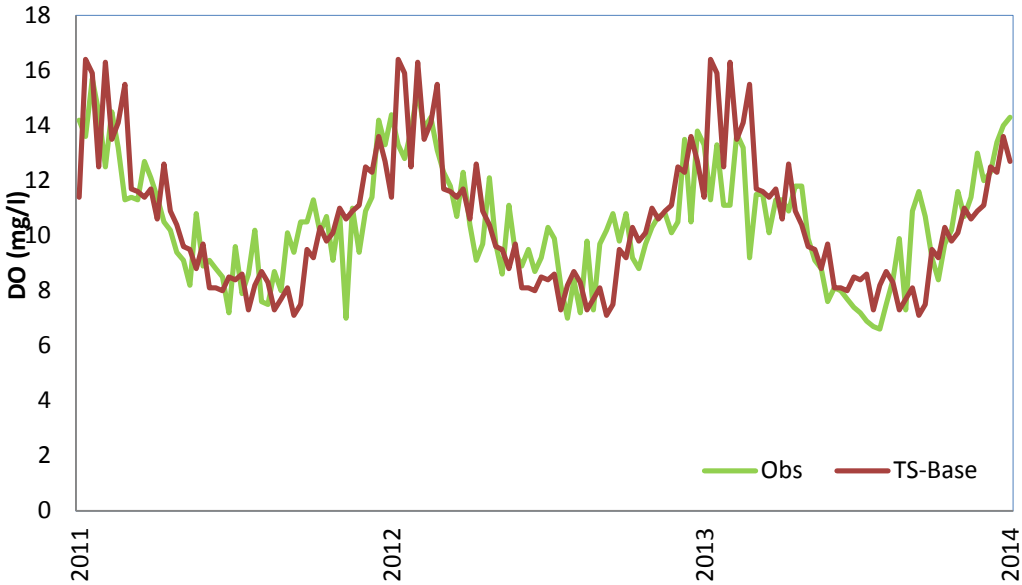

Figure 6-33 TS-Base forecast for DO for the Nam Catchment from the beginning of 2011 to the end of 2013.

To compare with BC-DA, a one week-ahead conditional mean prediction was made every week using the best-fit time series model and the past observations that are necessary for the conditioning. This result is referred to as TS-Pred. Figure 6-34 shows the TS-Pred results for DO at the outlet of Nam Catchment.

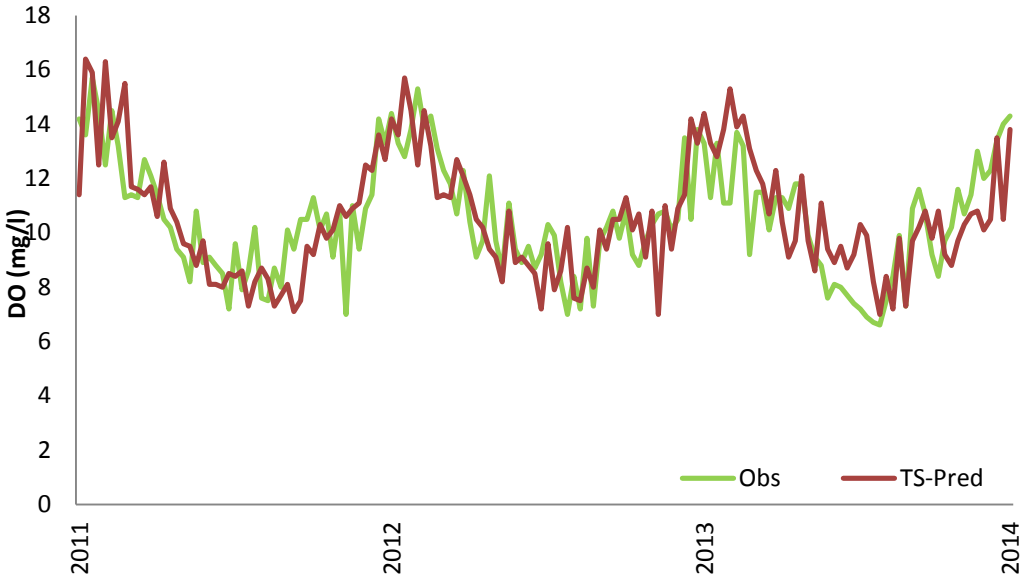

Figure 6-34 TS-Pred for DO for the Nam Catchment from the beginning of 2011 to the end of 2013.

The same procedure was used to produce the TS-Base and TS-Pred results for all water quality variables at the outlets of the selected catchments.

6.7. Comparison between HSPF and DA vs. time series modeling and prediction

To compare Base and BC-DA with TS-Base and TS-Pred, respectively, correlation and NSE were calculated for the period of 2011 to 2013. Figure 6-35 through Figure 6-38 show the correlation coefficient between the observed and simulated and NSE for the simulated for DO and TW for the six selected catchments. The figures show that, as expected, BC-DA improves over Base and TS-Pred improves over TS-Base. The figures also show that, generally speaking, BC-DA improves over TS-Pred and Base improves over TS-Base, respectively, but with departures. For the Banbyeon and Uchi Catchments, the NSEs for both DO and TW are smaller for TS-Pred than TS-Base. It

suggests that the time series modeling for these catchments may not be adequate, there may exist large interannual variability to produce significantly different realizations between the calibration and validation periods or there may be nonstationary changes taking place to render the time series modeling results for the calibration period no longer applicable. It is interesting to note that, while BC-DA improves over Base consistently for both catchments, for the Uchi Catchment, the NSE results for BC-DA and Base are significantly inferior to those for TS-Pred and TS-Base, respectively. The above observation suggests that significant differences in statistical properties of the water quality variables may exist between the calibration and validation periods that may render the HSPF calibration results rather poor for the validation period. That BC-DA is able to improve NSEs very significantly over BASE for both DO and TW for the Uchi Catchment, on the other hand, is an indication that DA is nonetheless effective in improving the ICs of potentially ill-calibrated HSPF. The figures show that the margin of improvement by BC-DA over TS-Pred and by Base over TS-Base is often significant to substantial though there are departures. That Base generally improves over TS-Base affirms the value of water quality modeling using HSPF. That BC-DA generally improves over TS-Pred and Base demonstrates the value of MLEF-HSPF. In addition to the above-mentioned results for the Banbyeon and Uchi Catchments, the NSE result for BC-DA for the Nam Catchment needs further investigation. Finally, it must be noted that the findings above are limited only to 7-day predictions due to lack of sub-weekly observations. To ascertain performance at shorter lead times, to advance understanding of the biophysiochemical processes being modeled, and to improve predictive skill of water quality forecast, it is critically important that routine high-frequency observation of water quality variables be made albeit on a limited scale.

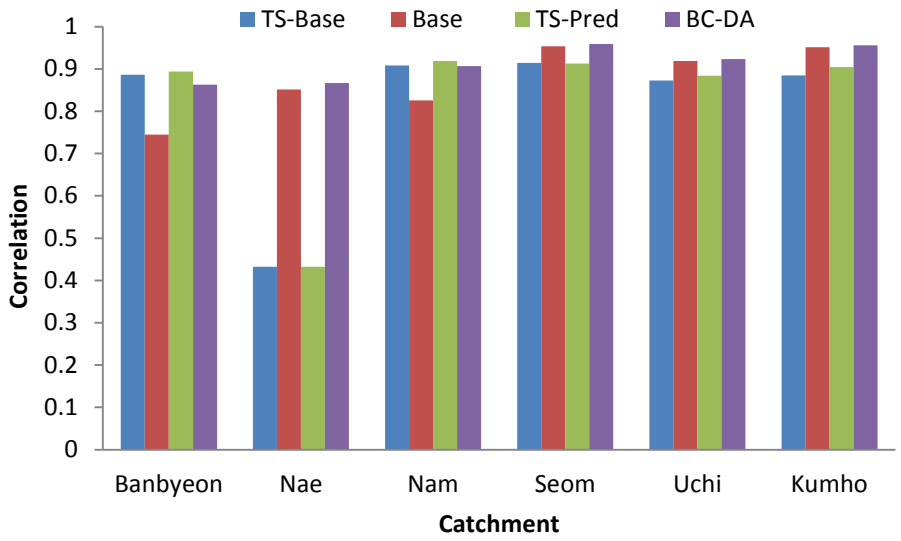

Figure 6-35 Correlation between the observed and predicted DO based on TS-Base (in blue), Base HSPF simulation (in red), TS-Pred (in green) and BC-DA prediction (in purple).

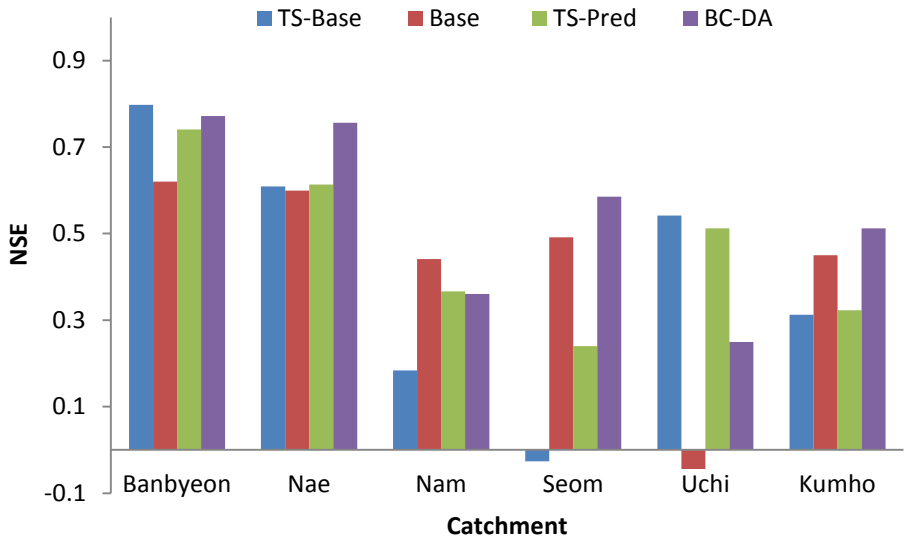

Figure 6-36 NSE between the observed and predicted DO based on TS-Base (in blue), Base HSPF simulation (in red), TS-Pred (in green) and BC-DA prediction (in purple).

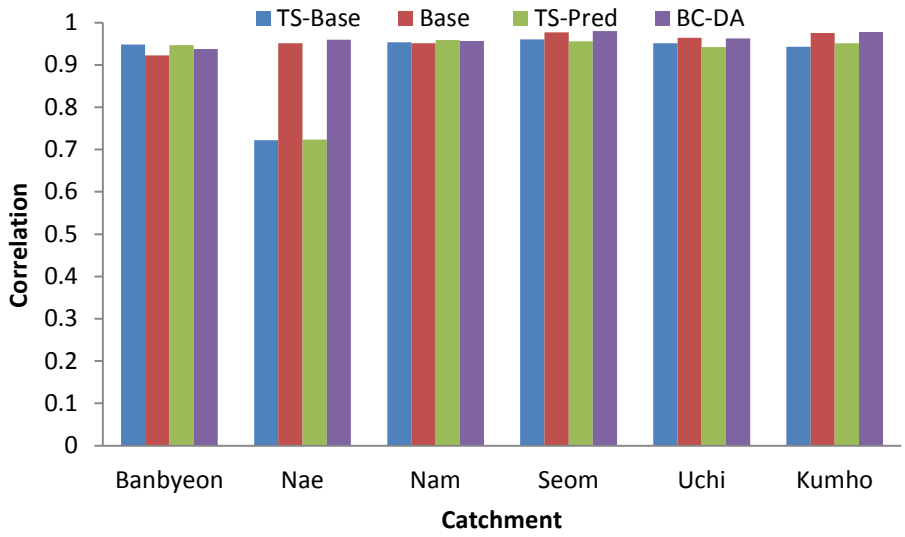

Figure 6-37 Correlation between the observed and predicted TW based on TS-Base (in blue), Base HSPF simulation (in red), TS-Pred (in green) and BC-DA prediction (in purple).

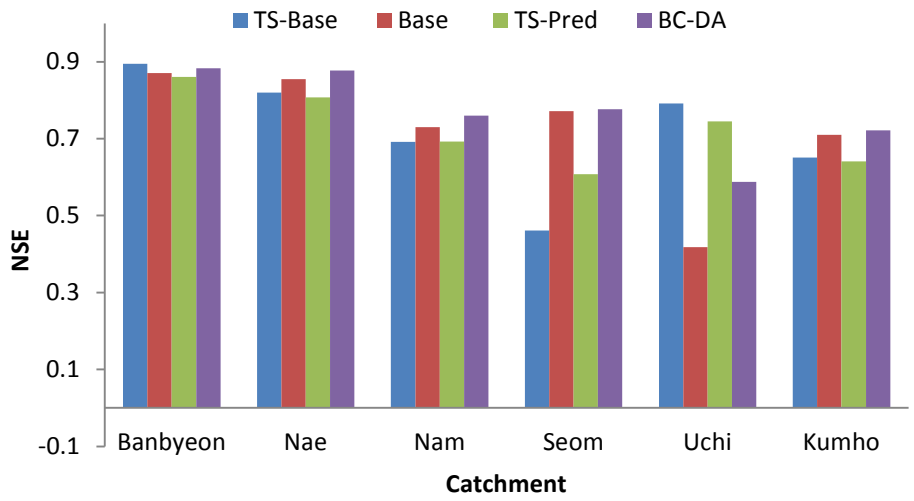

Figure 6-38 NSE between the observed and predicted TW based on TS-Base (in blue), Base HSPF simulation (in red), TS-Pred (in green) and BC-DA prediction (in purple).

Chapter 7

Conclusions and future research recommendations

In watershed water quality modeling, only a very small subset of the model states is actually observed. As such, the model initial conditions (IC) that are necessary for prediction are subject to large uncertainties. If one can reduce these uncertainties by updating the model states based on all available observations that shed light on the state of the system, one may expect significant improvement in short-range water quality forecasting. Toward that end, this research has carried out the design, development, testing and evaluation of a new data assimilation (DA) module for the watershed water quality model, the Hydrologic Simulation Program – Fortran (HSPF, Bicknell et al. 2001). The module enhances maximum likelihood ensemble filter (MLEF, Zupanski 2005) which combines the strengths of variational assimilation (VAR) and ensemble Kalman filter (EnKF). Referred to as MLEF-HSPF, the DA module is capable of handling both nonlinear model dynamics and nonlinear observation equations, does not require adjoint code, and produces ensemble analysis and prediction. MLEF-HSPF is being implemented as a plugin to the Water Quality Forecast System at the National Institute of Environmental Research, or WQFS-NIER. Built on the Flood Early Warning System (FEWS) of Deltares, WQFS-NIER is the main operational water quality forecast system in the Republic of Korea.

Based on extensive experience with hydrologic DA (Lee et al. 2011, 2012, 2015, Rafieeinasab et al. 2014, Seo et al. 2003, 2009), MLEF-HSPF implements a fixed-lag smoother formulation of MLEF, assimilating observations of streamflow, TW, NH4, NO3, PO4, BOD, CHL-a, DO, TP, TN and TOC to update the HSPF state variables in real time. The observations are generally available only about once a week, which constrains the size of the assimilation window to one week in this research. With the 1-week window,

the assimilation cycle is once a day, thereby allowing the control variables to be updated nominally daily. To account for biases in the observed boundary conditions (BC) of mean areal precipitation (MAP) and mean areal potential evapotranspiration (MAPE) valid within the assimilation window, two multiplicative adjustment factors for MAP and MAPE are added to the control vector (Seo et al. 2003, 2009, Lee et al. 2012, 2012).

The original formulation of MLEF (Zupanski 2005) does not account for dynamical model errors. In this research, two approaches were considered to newly account for dynamical model errors in MLEF: direct perturbation and state augmentation. Based on comparative evaluation and computational considerations, the state augmentation approach with dependent model errors was chosen as default.

If significant parametric and/or structural errors exist in the model, DA is not likely to improve predictive skill; it is likely to compensate for the systematic errors, rather than directly addressing the IC uncertainty, in the state updating process. As such, it is necessary to remove or reduce systematic errors as much as possible. For that, a novel parsimonious bias correction procedure (Seo 2013) has been implemented in the observation equation of MLEF-HSPF.

To assess sensitivity of MLEF-HSPF to its various parameters and to optimize their settings, a series of extensive sensitivity analyses was designed and carried out with the following summary results. Examination of the eigenvalue spectra of the information matrix indicates that the choice of 9 ensemble members is reasonable. Sensitivity analysis indicates that a larger ensemble size improves the performance of the DA procedure only marginally, and that the model states updated using different ensemble sizes yield similar spatiotemporal patterns of adjustment.

Sensitivity analysis on the “age” of the observation being assimilated indicates that potency of MLEF-HSPF improves significantly if the observations are less than 6

days old. It suggests that significant improvement in predictive skill may be achieved by increasing the sampling frequency of water quality and hydrologic observations from once a week to once every 5 days or less.

It was seen that bias correction alone does not consistently improve performance, due presumably to sampling uncertainties from interannual variability and/or possible nonstationarities. On the other hand, bias correction is seen to have a larger positive impact on DA by presumably keeping the analysis solution within the feasible model space. If significant parametric and/or structural errors exist in the model, DA is not likely to improve the predictive skills. Through improved calibration, one may expect to reduce parametric uncertainties. The HSPF simulation results suggest that additional calibration of HSPF is necessary for many catchments, which in turn will increase the potency of DA.

It was seen that the quality of the forcing input of MAP and MAPE significantly impacts the quality of the DA solution. It was found that unrealistically large or small multiplicative adjustment factors to MAP and/or MAPE are usually associated with poor analysis solution. The above suggests that estimation of MAP and MAPE in WQFS-NIER needs improvement.

Because MLEF-HSPF is a reduced-rank technique, the analysis solutions may be significantly underdetermined depending on the flow-dependent conditions. Additional research is needed to consistently improve performance by assimilating observations from all available monitoring stations within the catchment thereby reducing underdeterminedness. In this research, hydrologic and water quality states were updated simultaneously. One may consider decomposing the DA problem into first updating the hydrologic states only followed by updating only the water quality states. Such a

decompositional approach is likely to reduce underdeterminedness by reducing dimensionality of the inverse problem.

Evaluation of ensemble DA analysis indicates that HSPF may lack realism to maintain realistic spread among the perturbed model trajectories. Much additional research is needed to improve model physics and stochastic modeling of uncertainty dynamics. To overcome the underspreadness of analysis ensembles in the meantime, one should consider a statistical post-processor that operates on the HSPF output to produce reliable ensembles.

To evaluate the MLEF-HSPF module, hindcast experiments were designed and carried out for four catchments in the Republic of Korea: the Kumho Catchment in the Nakdong River Basin, the Jojong and Yanghwa Catchments in the Han River Basin and the Miho Catchment in the Geum River Basin. The results show that MLEF-HSPF consistently improves analysis and prediction of most of the water quality variables and streamflow. The margin of improvements, however, varies significantly from catchment to catchment and from variable to variable. Improvement was larger for more natural catchments compared to more urbanized catchments. For the Miho Catchment, which has a large fraction of urban areas and lower skill in the base HSPF simulation, DA is seen to add little predictive skill even though significant improvement is seen in DA analysis.

As a “reality check” on HSPF and MLEF-HSPF and to improve understanding of the nature of the biophysiochemical processes modeled and their predictability, time series modeling of the water quality variables was carried out using autoregressive integrated moving-average model (ARIMA). In general, the results affirm the value of water quality modeling using HSPF and demonstrate the value of MLEF-HSPF. Due to lack of sub-weekly observations, however, it was not possible to assess comparative performance at

lead times shorter than 7 days. To ascertain performance for short-range forecasting, to advance understanding of the biophysiochemical processes being modeled, and to improve predictive skill, it is critically important that routine high-frequency observation of water quality variables be made even on a limited scale only.

Finally, due to the computational overhead associated with having to run HSPF in the Windows environment, the computational requirements for MLEF-HSPF can be significant, depending on the number of catchments involved. Hence, for operational implementation of the procedure on a large scale, availability of the necessary computing power is critical.

Appendix A

Sensitivity analysis Results

Sensitivity analyses were performed to assess the sensitivity of MLEF-HSPF performance to the magnitude of its parameters and to address the following questions:

1. How much influence does each of the hydrologic and water quality variables have on DA analysis and prediction?
2. How much impact does updating the hydrologic state variables have on analysis and prediction of the water quality variables
3. Does updating the water quality state variables impact the hydrologic state variables and analysis and prediction of streamflow
4. How sensitive are the analysis and prediction results to the magnitude of the observational error variance
5. What is the sensitivity of DA performance to the prescribed model error
6. What is the optimal ensemble size in terms of performance and computational cost
7. What is the optimal size of the assimilation window in terms of performance and computational cost

A.1. Sensitivity analysis for selection of state variables

To find the optimum selection of active state variables for the Kumho Catchment, the impact of updating one or group of state variable(s) on DA performance has been evaluated. In addition, the impact of using a selection of observations (less obs) or the entire available observations (all obs) was evaluated. Also the effect of not updating the multiplicative adjustment factors for MAP and MAPE (p=0) was assessed. In this section, only analysis and prediction results of six water quality variables and streamflow (BOD, CHL-a, flow, DO, NO_3, PO_4 and TW) are shown. Table 5-2 shows the parameter setting used for these runs. In the Run 1 to Run 28 only one state variable plus multiplicative adjustment factors for MAP and MAPE were active. In the Run 29, the hydrologic state variables and in the Run 30 the water quality state variables were active. In the Run 31,

all the state variables were active and all the observations were available. In the last three runs, the observations of the NH_4, TP, TN and TOC were excluded. In the Run 33, the multiplicative adjustment factor for MAP and MAPE was not updating. In the Run 34, the state variables for NH_4, TP, TN and TOC in the reaches were not updating. Figure A. 1 to Figure A. 7 show the RMSE of BASE, BC-BASE and BC-DA results for analysis and Day-1 through Day-3 predictions of BOD, CHL-a, flow, DO, NO_3, PO_4 and TW where BASE, BC and DA denote the base, bias-corrected base and bias-corrected DA-aided simulations, respectively.

In general, DA improves model performance when a group of state variables is active than when a single state variable is active. When only a single state variable is updated, DA is likely to incorrectly adjust the single active state variable to compensate for biases or errors from other state variables. DA improves model performance further when all state variables are active (Run 31) than when either only the hydrologic (Run 29) or the water quality (Run 30) state variables are active. The RMSE comparison among the last four runs show that the DA procedure is insensitive to the exclusion of the observations of NH_4, TP, TN and TOC. Based on the sensitivity analysis, the recommendation for the Kumho Catchment is either to set all state variables active and use all observations available, or to set all state variables active and use all available observations except for those of NH_4, TP, TN and TOC.

Table A. 1 Active state variables used in each run for the sensitivity analysis.

Variables	Run																																
	1	2	3	4	5	6	7	8	9	10	11	12	13	14	15	16	17	18	19	20	21	22	23	24	25	26	27	28	29	30	31	32	33	34
PE-Precip	√	√	√	√	√	√	√	√	√	√	√	√	√	√	√	√	√	√	√	√	√	√	√	√	√	√	√	√	√	√	√	√		√
CEPS	√																												√		√	√	√	√
SURS		√																											√		√	√	√	√
IFWS			√																										√		√	√	√	√
AGWS				√																									√		√	√	√	√
UZS					√																								√		√	√	√	√
LZS						√																							√		√	√	√	√
GWVS							√																						√		√	√	√	√
RETS								√																					√		√	√	√	√
ISURS									√																				√		√	√	√	√
VOL										√																			√		√	√	√	√
TW											√																		√		√	√	√	√
P-NH_4												√																		√	√	√	√	√
I-NH_4													√																	√	√	√	√	√
RCH-NH_4														√																√	√	√	√	
P-NO_3															√															√	√	√	√	√
I-NO_3																√														√	√	√	√	√
RCH-NO_3																	√													√	√	√	√	√
P-PO_4																		√												√	√	√	√	√
I-PO_4																			√											√	√	√	√	√
RCH-PO_4																				√										√	√	√	√	√
P-BOD																					√									√	√	√	√	√
I-BOD																						√								√	√	√	√	√
RCH-BOD																							√							√	√	√	√	√
CHL-a																								√						√	√	√	√	√
DO																									√					√	√	√	√	√
TP																										√				√	√	√	√	
TN																											√			√	√	√	√	
TOC																												√		√	√	√	√	

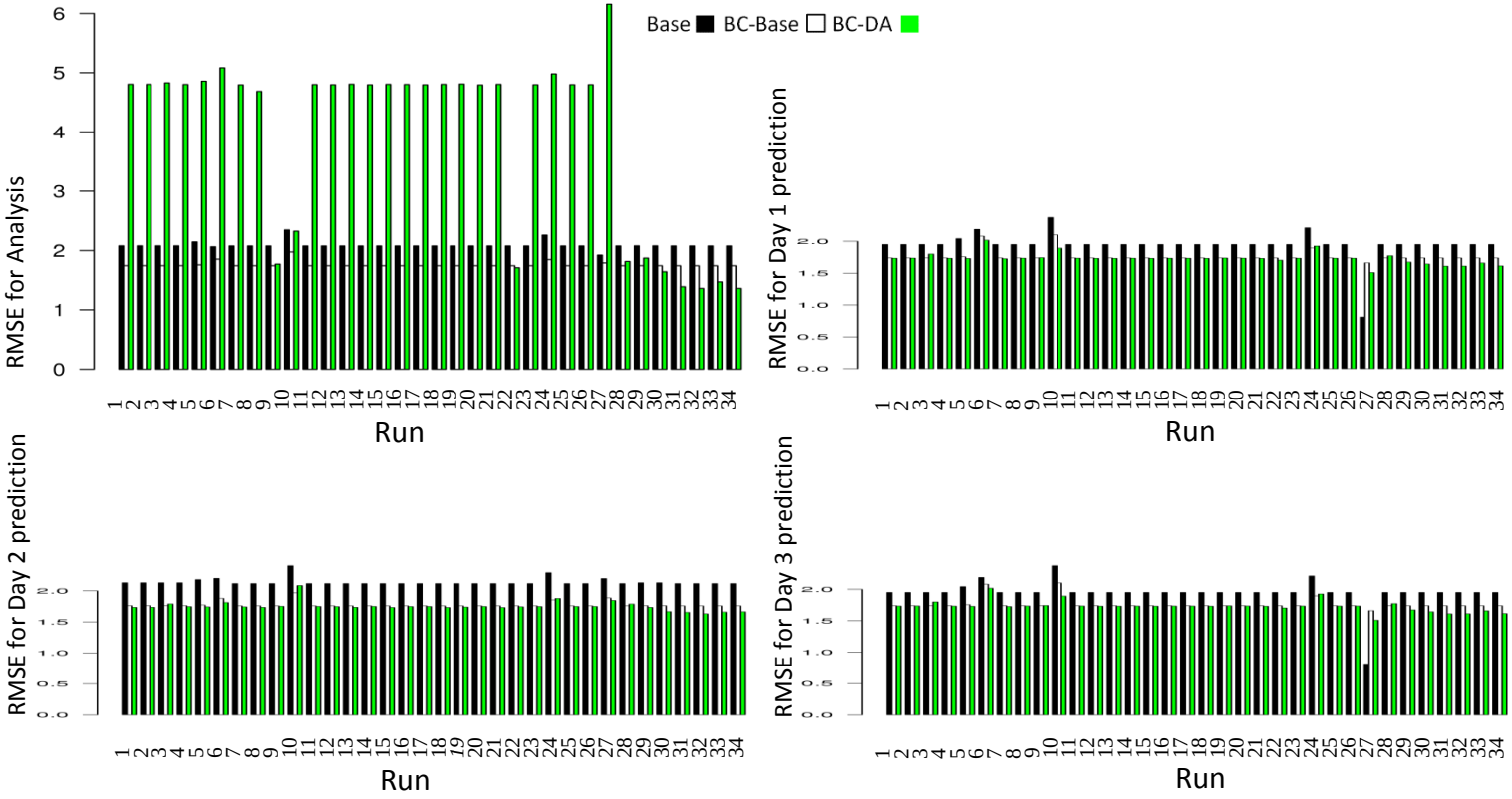

Figure A. 1 RMSE of Base, BC-Base and BC-DA for analysis and Day 1 to Day 3 predictions of BOD.

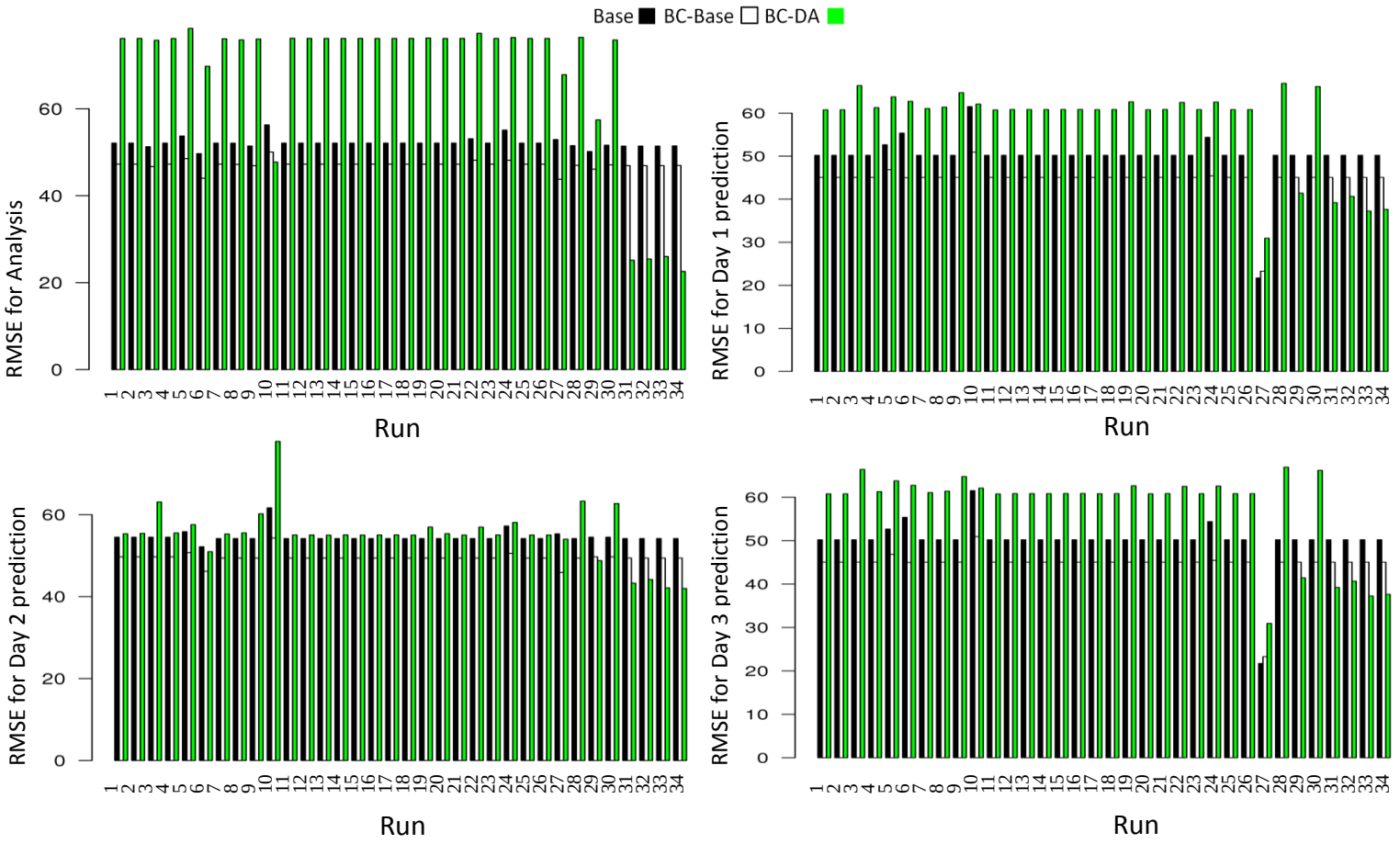

Figure A. 2 RMSE of Base, BC-Base and BC-DA for analysis and Day 1 to Day 3 predictions of CHL-a.

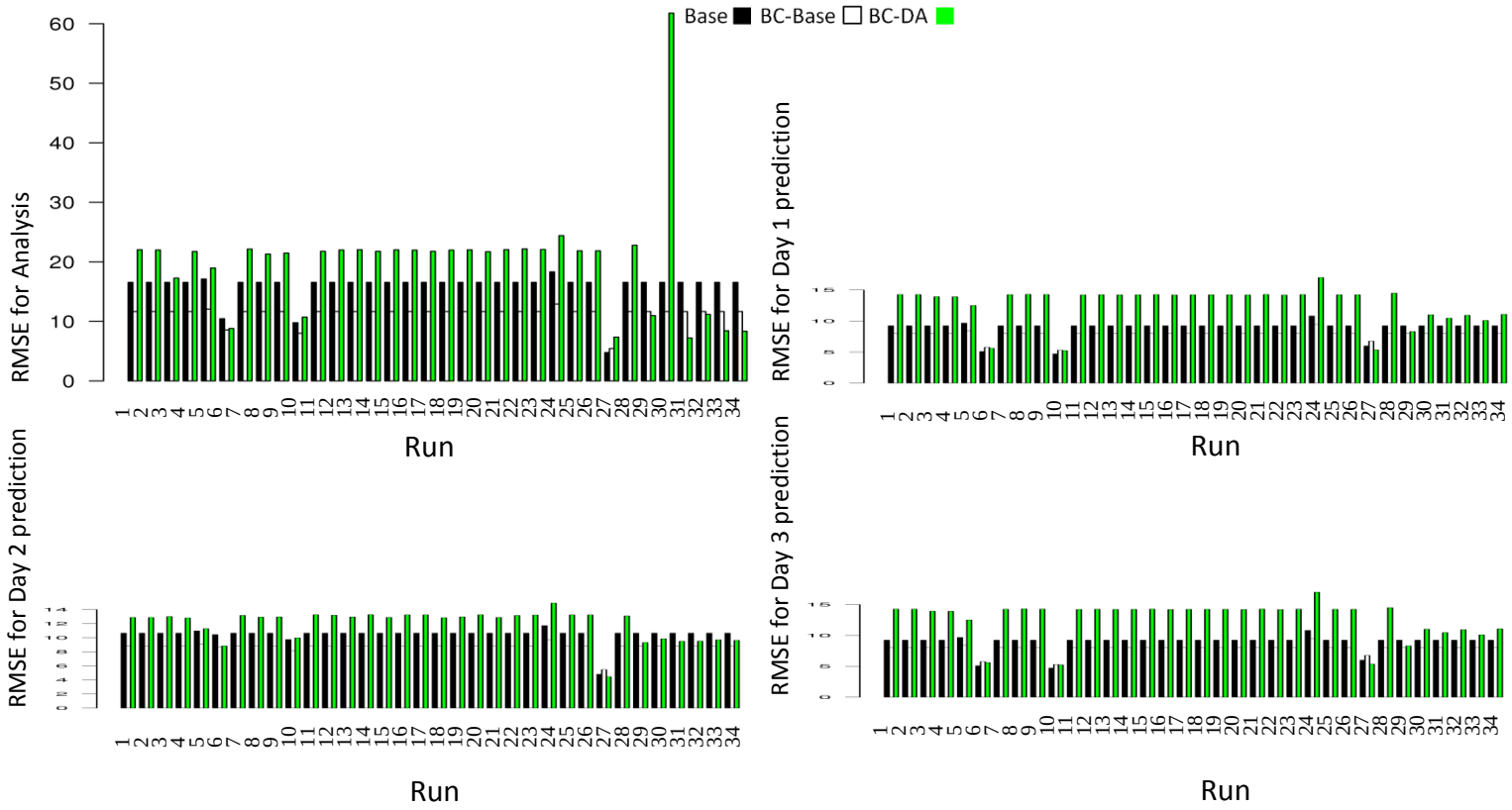

Figure A. 3 RMSE of Base, BC-Base and BC-DA for analysis and Day 1 to Days 3 prediction of Flow.

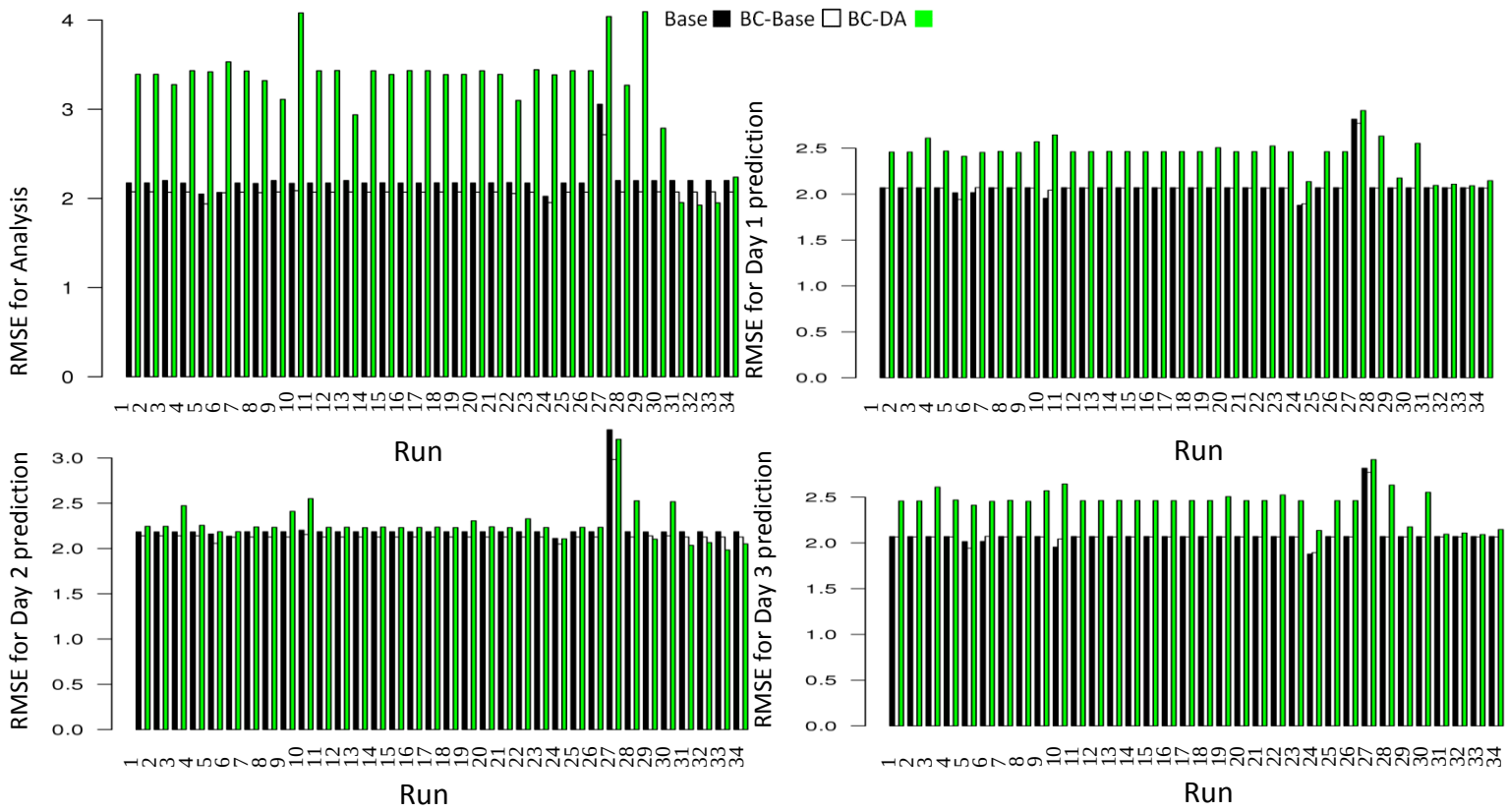

Figure A. 4 RMSE of Base, BC-Base and BC-DA for analysis and Day 1 to Day 3 predictions of DO.

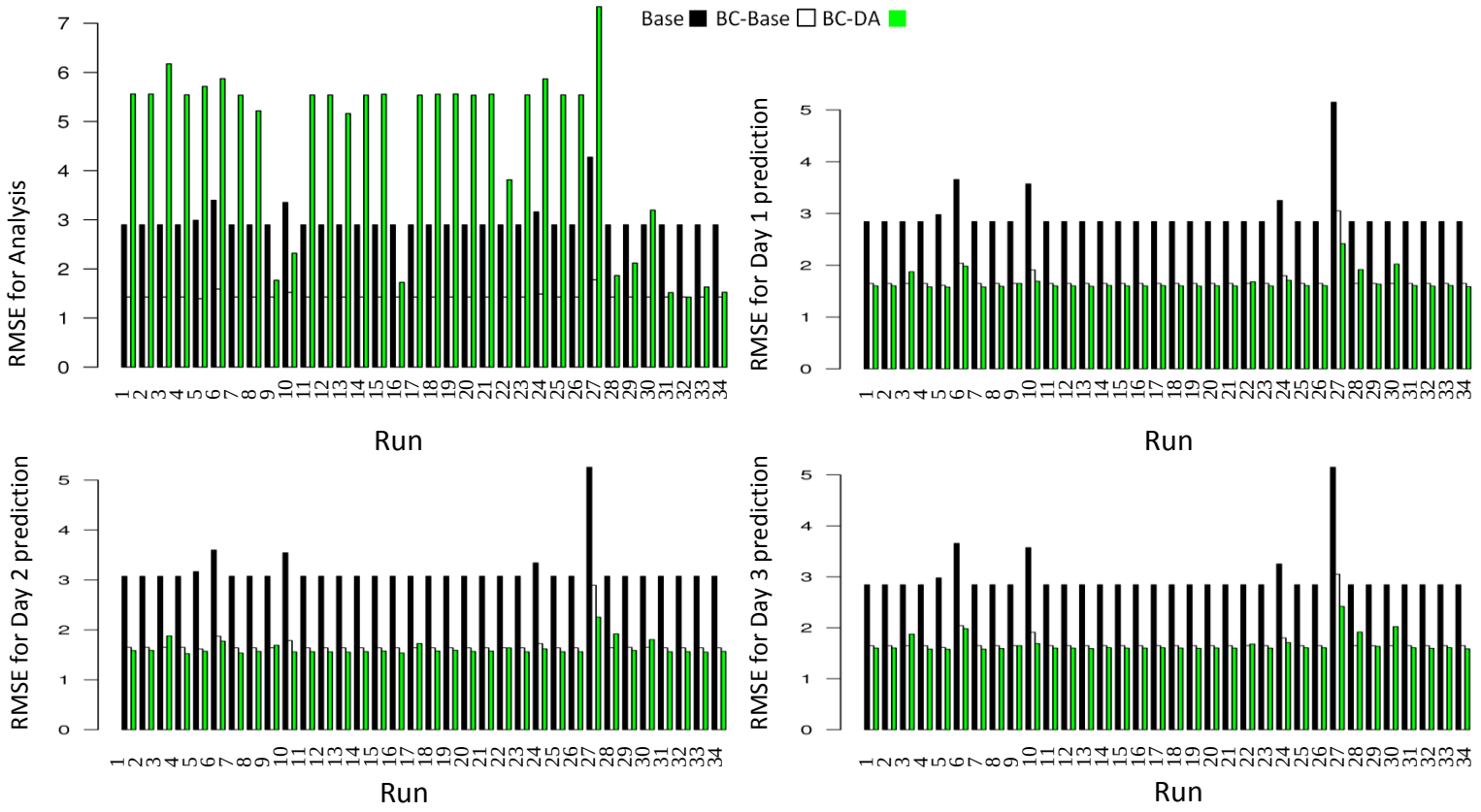

Figure A. 5 RMSE of Base, BC-Base and BC-DA for analysis and Day 1 to Day 3 predictions of NO_3.

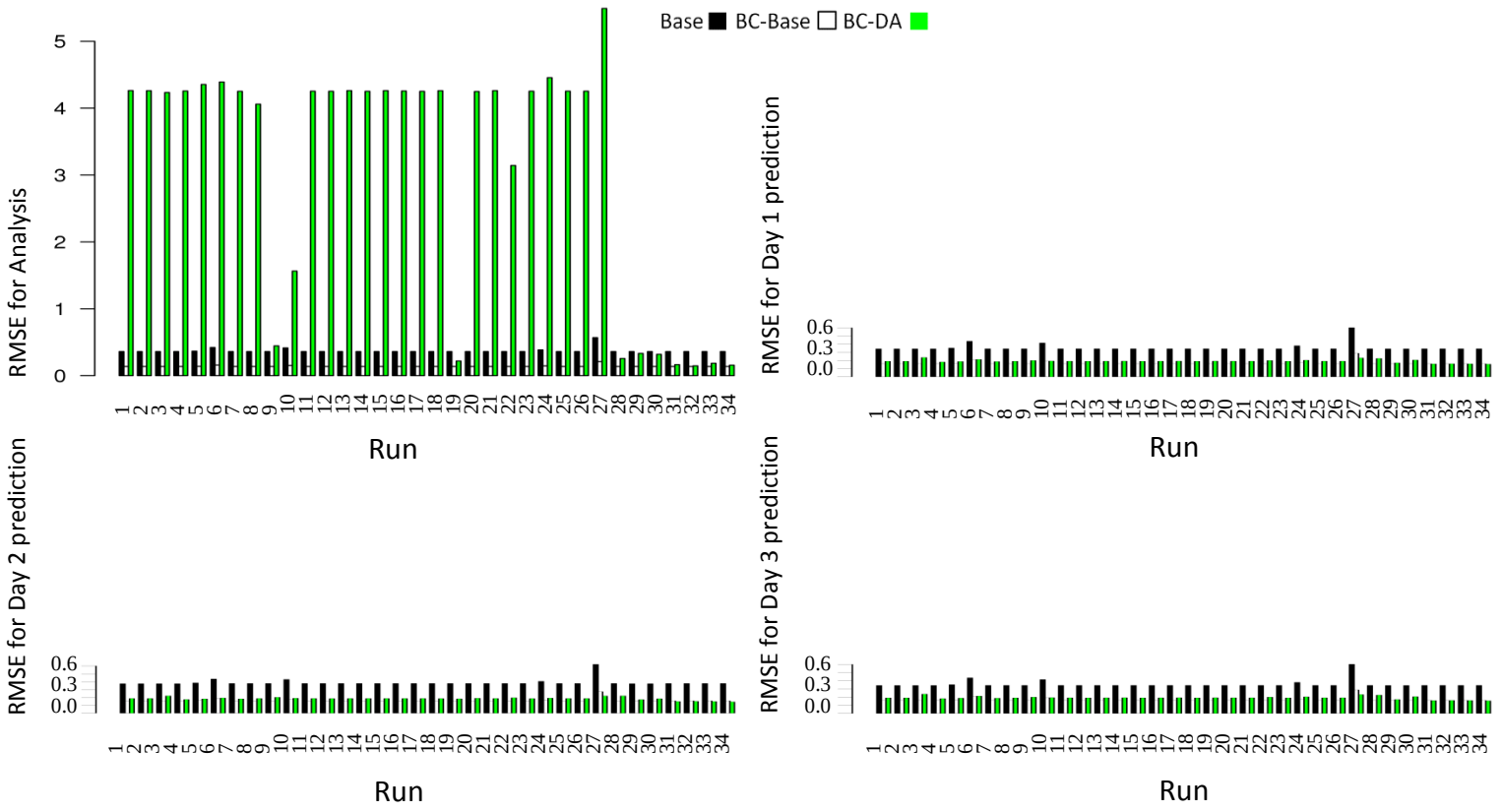

Figure A. 6 RMSE of Base, BC-Base and BC-DA for analysis and Day 1 to Day 3 predictions of PO_4.

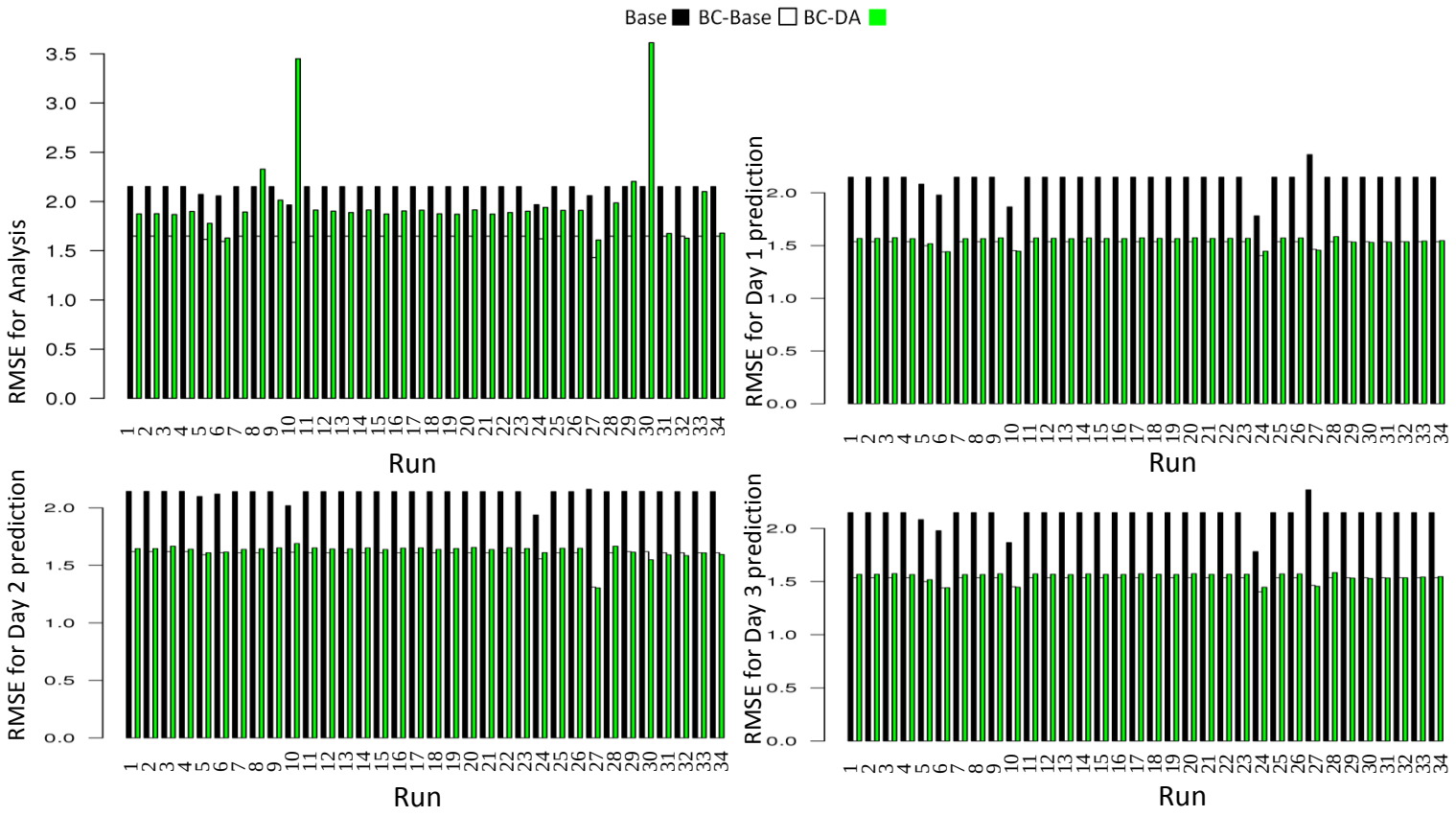

Figure A. 7 RMSE of Base, BC-Base and BC-DA for analysis and Day 1 to Day 3 predictions of TW.

A.2. Sensitivity analysis to the magnitude of model error, initial perturbation and observation error variance

In order to answer the questions 4 and 5, a set of sensitivity analysis was carried out for the Kumho Catchment for a 2-year period of 2008-2009. The perpose was to find sensitivity of DA performance to the prescribed magnitude of the model error (frac_gen), initial perturbation (frac_state) and the observational error variance while the size of assimilation window and the number of ensemble are constant (7 days and 9 ensemble). In this section, only analysis and prediction results of six water quality variables and streamflow (BOD, CHL-a, flow, DO, NO_3, PO_4 and TW) are shown. The model error, initial perturbation and observational error variance were multiplied by 0.1 and 10 and then combinations of these parameters were used to check the sensitivity of DA performance to their magnitudes (see Table A. 2).

The results demonstrate that analysis is more sensitive to the magnitude of these parameters than the predictions (see Figure A. 8 to Figure A. 14). When the initial perturbation was multiplied by 10 (Run 17), the RMSE of analysis and Day-1 to Day-3 predictions of BOD and CHL-a were reduced. However, the RMSE of other water quality variables and streamflow increased. In a case when model error and initial perturbation were multiplied by 10 (Run 6), the RMSE of analysis and Day-1 to Day-3 predictions of flow was reduced however, the RMSE of water quality variables were slightly increased. These observations suggest that, selected magnitudes of these parameters, as it was prescribed in Table 5-2, are optimal for the Kumho Catchment.

Table A. 2 Sensitivity analysis to the magnitude of model error, initial perturbation and observational error variance.

Run	Assimilation Windows	ns	Frac_gen	Frac_state	Observation error variance
1	7	9	0.1	1	1
2	7	9	0.1	0.1	1
3	7	9	0.1	10	1
4	7	9	10	1	1
5	7	9	10	0.1	1
6	7	9	10	10	1
7	7	9	1	1	10
8	7	9	0.1	1	10
9	7	9	0.1	0.1	10
10	7	9	0.1	10	10
11	7	9	10	1	10
12	7	9	10	0.1	10
13	7	9	10	10	10
14	7	9	1	0.1	10
15	7	9	1	10	10
16	7	9	1	0.1	1
17	7	9	1	10	1
18	7	9	1	1	1

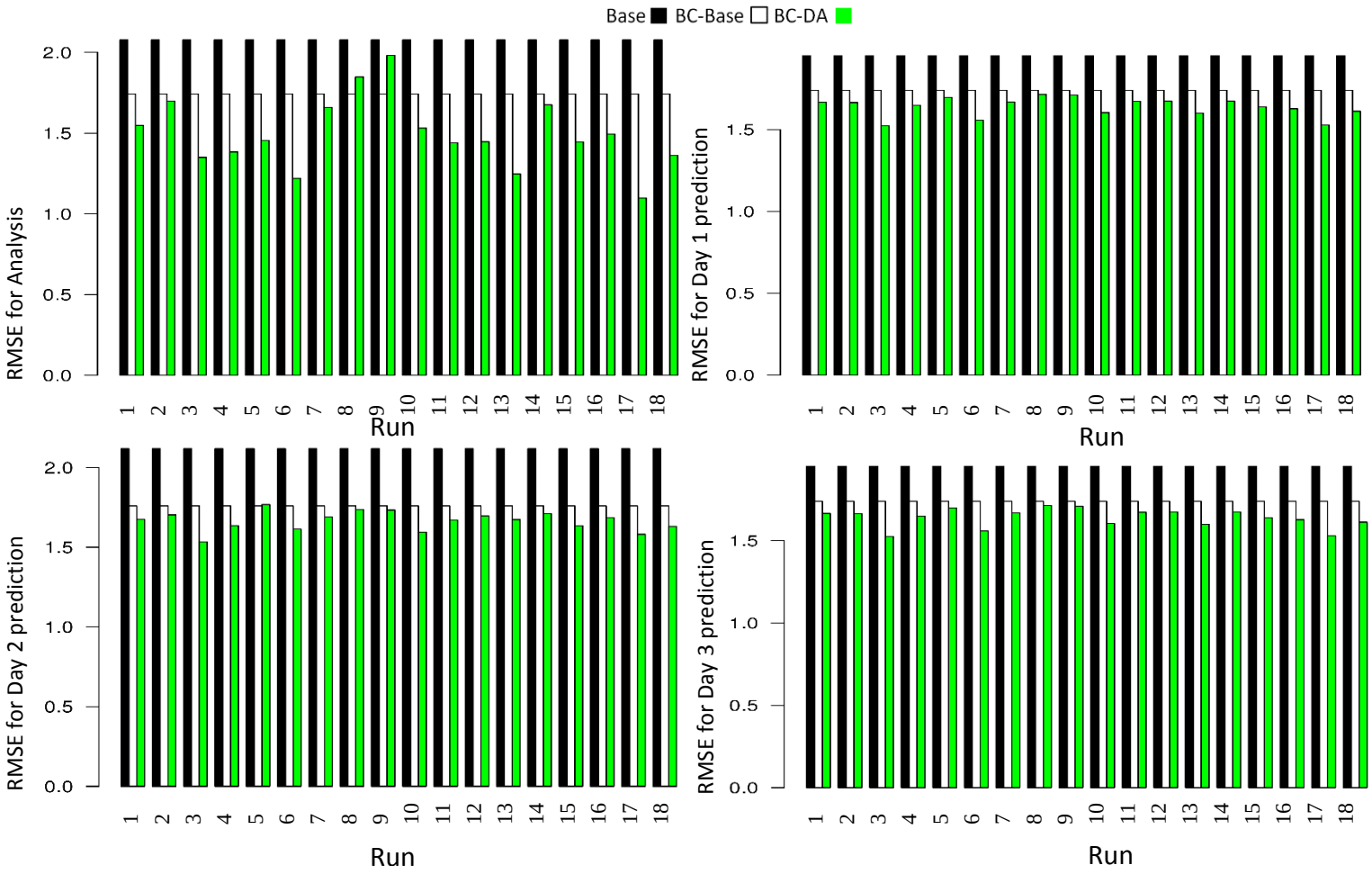

Figure A. 8 Figure 39 RMSE of Base, BC-Base and BC-DA for analysis and Day 1 to Day 3 prediction of BOD.

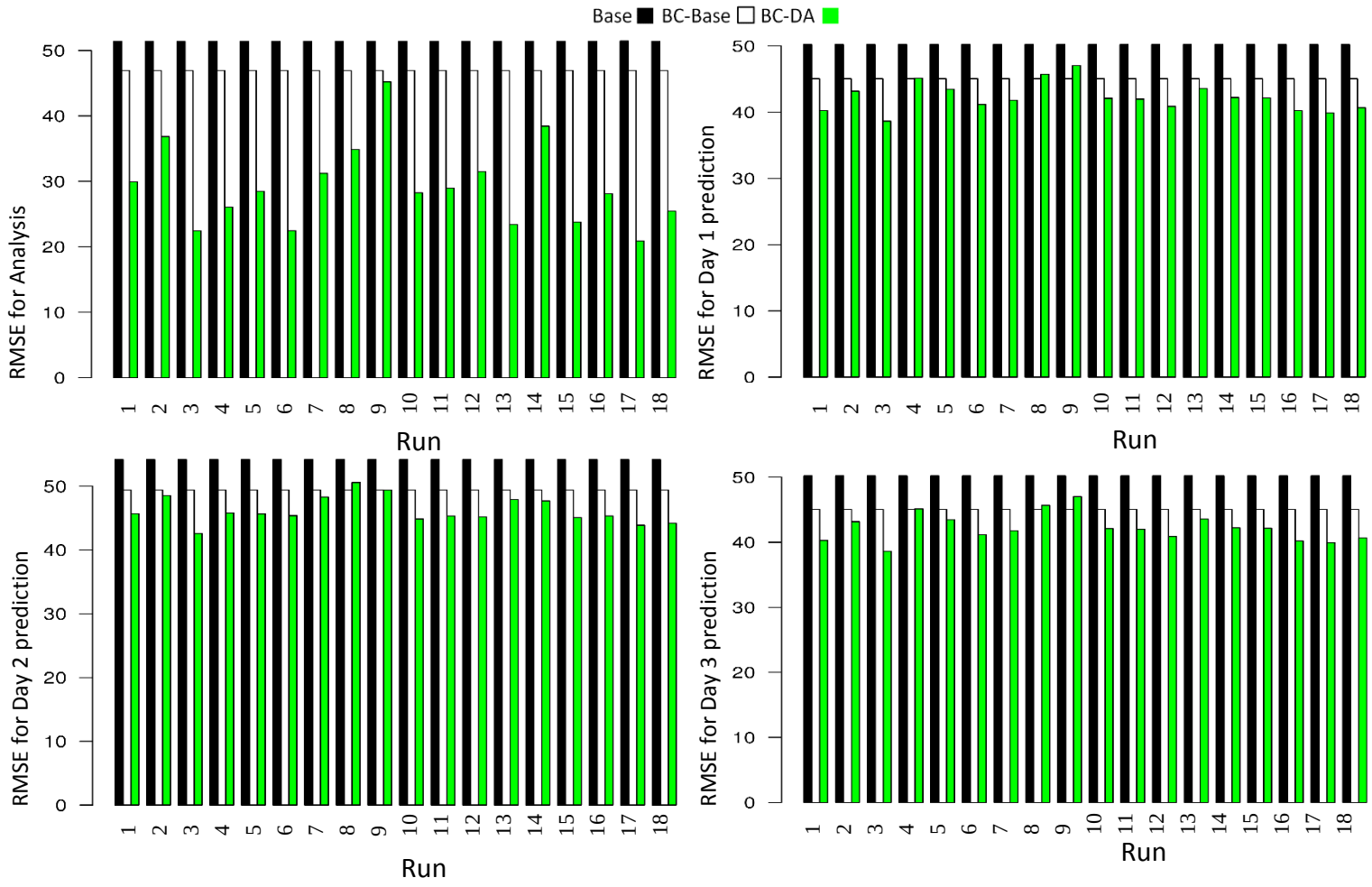

Figure A. 9 RMSE of Base, BC-Base and BC-DA for analysis and Day 1 to Day 3 prediction of CHL-a.

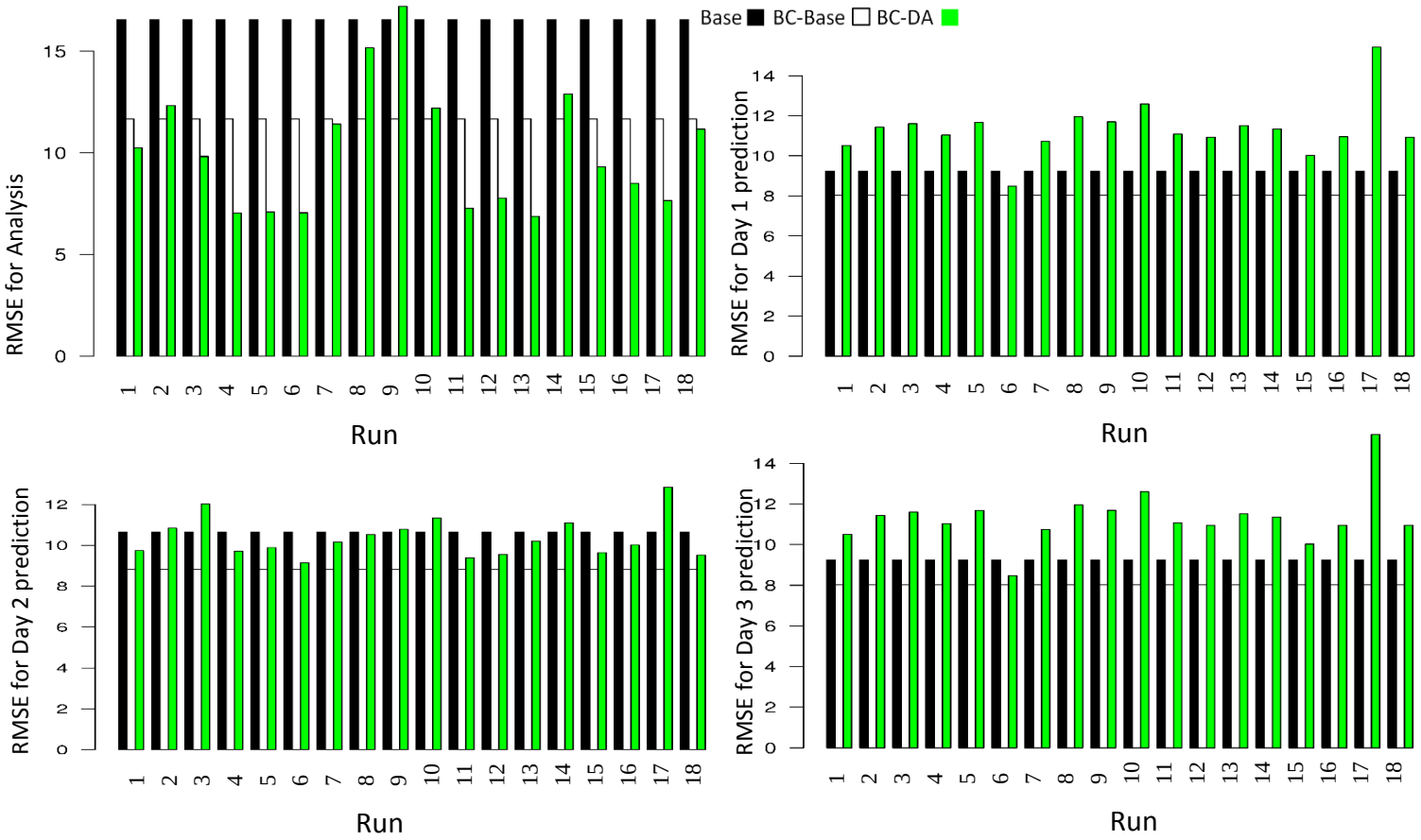

Figure A. 10 RMSE of Base, BC-Base and BC-DA for analysis and Day 1 to Day 3 prediction of Flow.

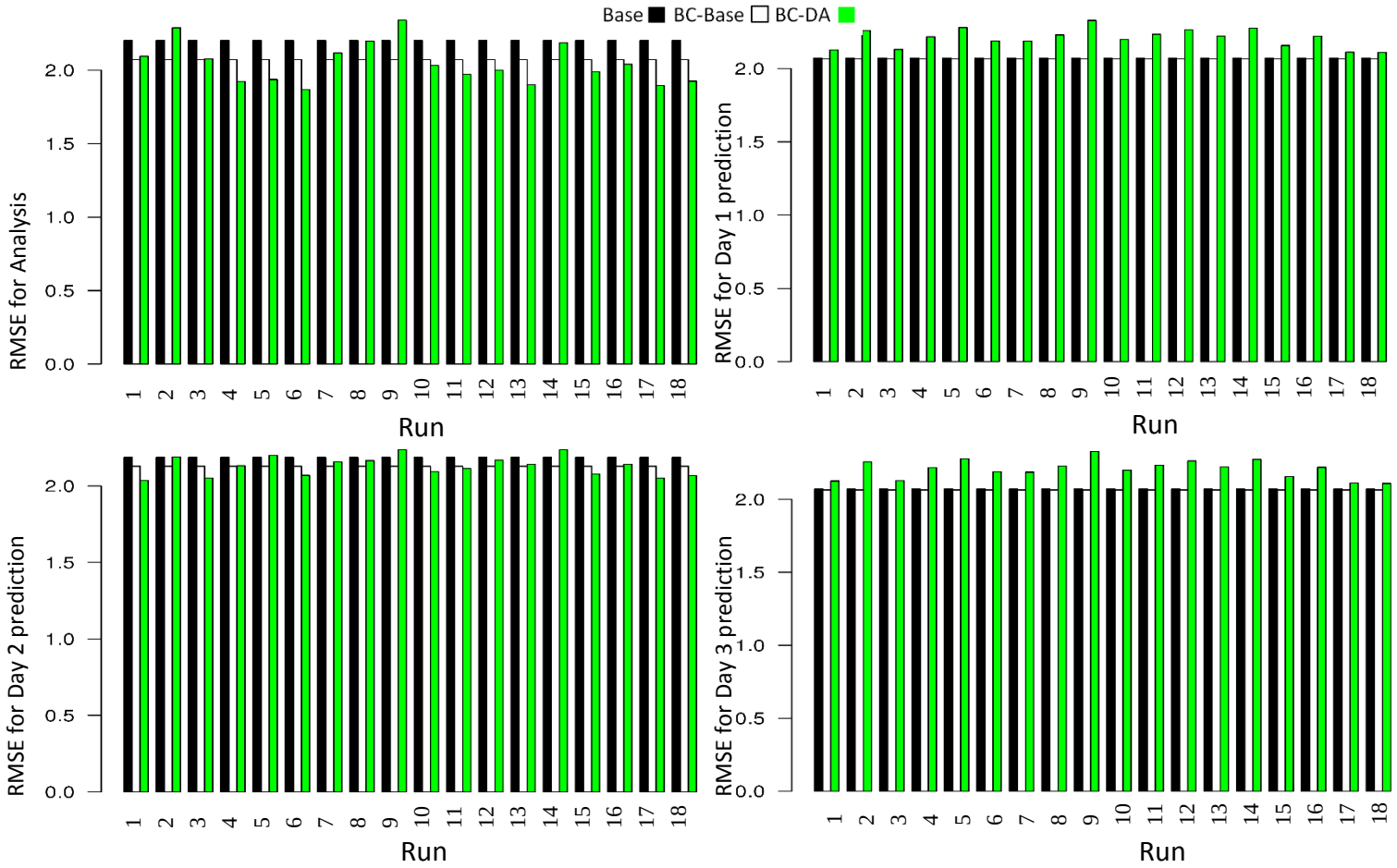

Figure A. 11 RMSE of Base, BC-Base and BC-DA for analysis and Day 1 to Day 3 prediction of DO.

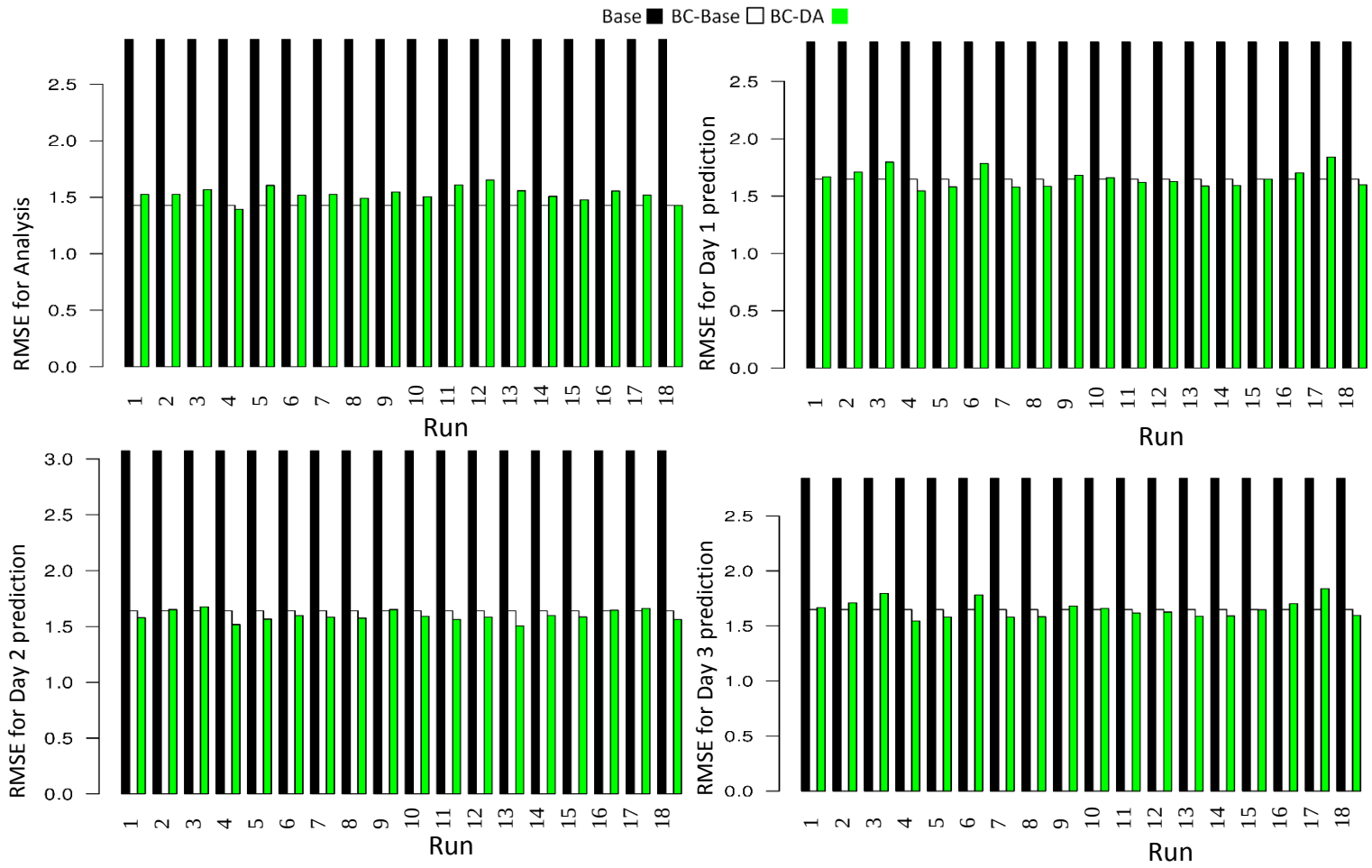

Figure A. 12 RMSE of Base, BC-Base and BC-DA for analysis and Day 1 to Day 3 prediction of NO_3.

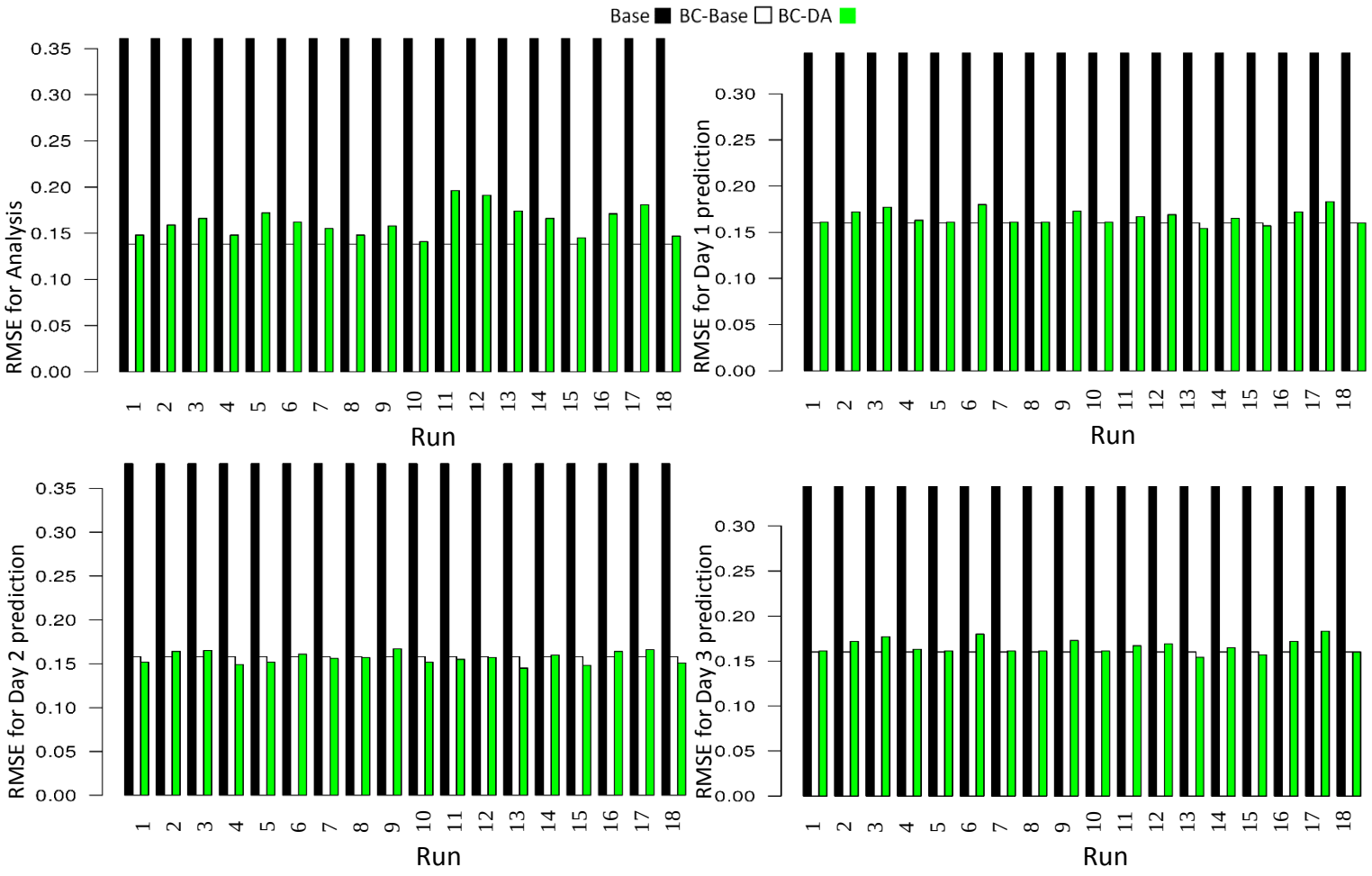

Figure A. 13 RMSE of Base, BC-Base and BC-DA for analysis and Day 1 to Day 3 prediction of PO_4.

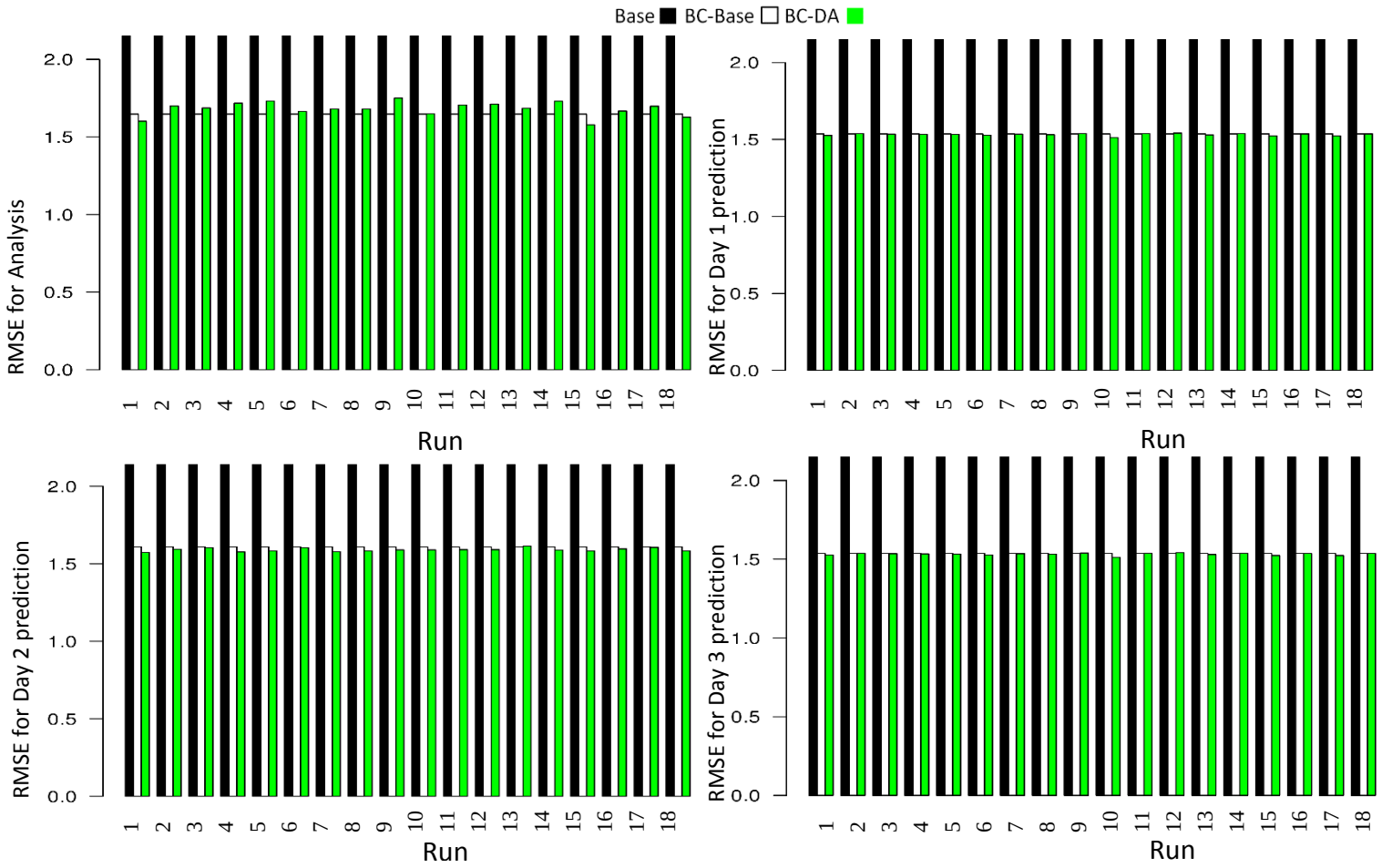

Figure A. 14 RMSE of Base, BC-Base and BC-DA for analysis and Day 1 to Day 3 prediction of TW.

A.3. Sensitivity analysis for selection of ensemble size

Total number of the state variables in the Kumho catchment is 333. Since MLEF is a reduced-rank filter, it will find the optimum solution in the ensemble subspace. One might expect that having a full-rank filter (by increasing the number of the ensembles to the total number of the state variables) or higher rank filter would improve the analysis and prediction results. The aim of this section is to assess the sensitivity of the prediction results to the ensemble size and to answer the question 6. Therefore, a set of systematic sensitivity analysis was carried out for the Kumho Catchment for a 2-year period of 2008-2009 to find the optimum ensemble size with different combination of model error, initial perturbation and observation error variance while the assimilation window was kept constant (see Table A. 3). In this section, only analysis and prediction results of six water quality variables and streamflow (BOD, CHL-a, flow, DO, NO_3, PO_4 and TW) are shown. Ensemble size of 30 was selected in the beginning however if the HSPF terminated prematurely due to computational instability, the run was started with the same settings using ensemble size of 18. Some runs terminated prematurely even with ensemble size of 18. For comparison, those runs are plotted but they were not used for comparison to other runs.

A combination of initial perturbation multiplied by 10 and ensemble size of 30 reduced the RMSE for BOD and CHL-a however, the RMSE of other water quality variables and streamflow increased (Run 17). With the scaling factors of 0.1 and 0.01 for model error and initial perturbation, respectively, DA using an ensemble size of 18 reduces RMSE by 2–8% over DA using an ensemble size of 9 for Day-1 through -3 predictions of BOD and CHL-a. No RMSE changes are observed for DO and TW. The RMSE increases from 2–8% for Day-1 through -3 predictions of NO_3 and PO_4. However,

the computation time would be twice (2 days for 1-year run with ensemble size of 18 compared to 1 day for the same 1-year run with ensemble size of 9).

Thus, based on these results, the ensemble size of 9 was found reasonable in terms of performance and computational cost and it was selected as the optimum size.

Table A. 3 Sensitivity analysis to the ensemble size.

Run	Assimilation Windows	ns	Frac_gen	Frac_state	Observation error variance
1	7	30	0.1	1	1
2	7	30	0.1	0.1	1
3	7	30	0.1	10	1
4	7	18	10	1	1
5	7	30	10	0.1	1
6	7	18	10	10	1
7	7	18	1	1	10
8	7	18	0.1	1	10
9	7	30	0.1	0.1	10
10	7	18	0.1	10	10
11	7	18	10	1	10
12	7	30	10	0.1	10
13	7	18	10	10	10
14	7	18	1	0.1	10
15	7	30	1	10	10
16	7	30	1	0.1	1
17	7	30	1	10	1
18	7	18	1	1	1
19	7	9	1	1	1

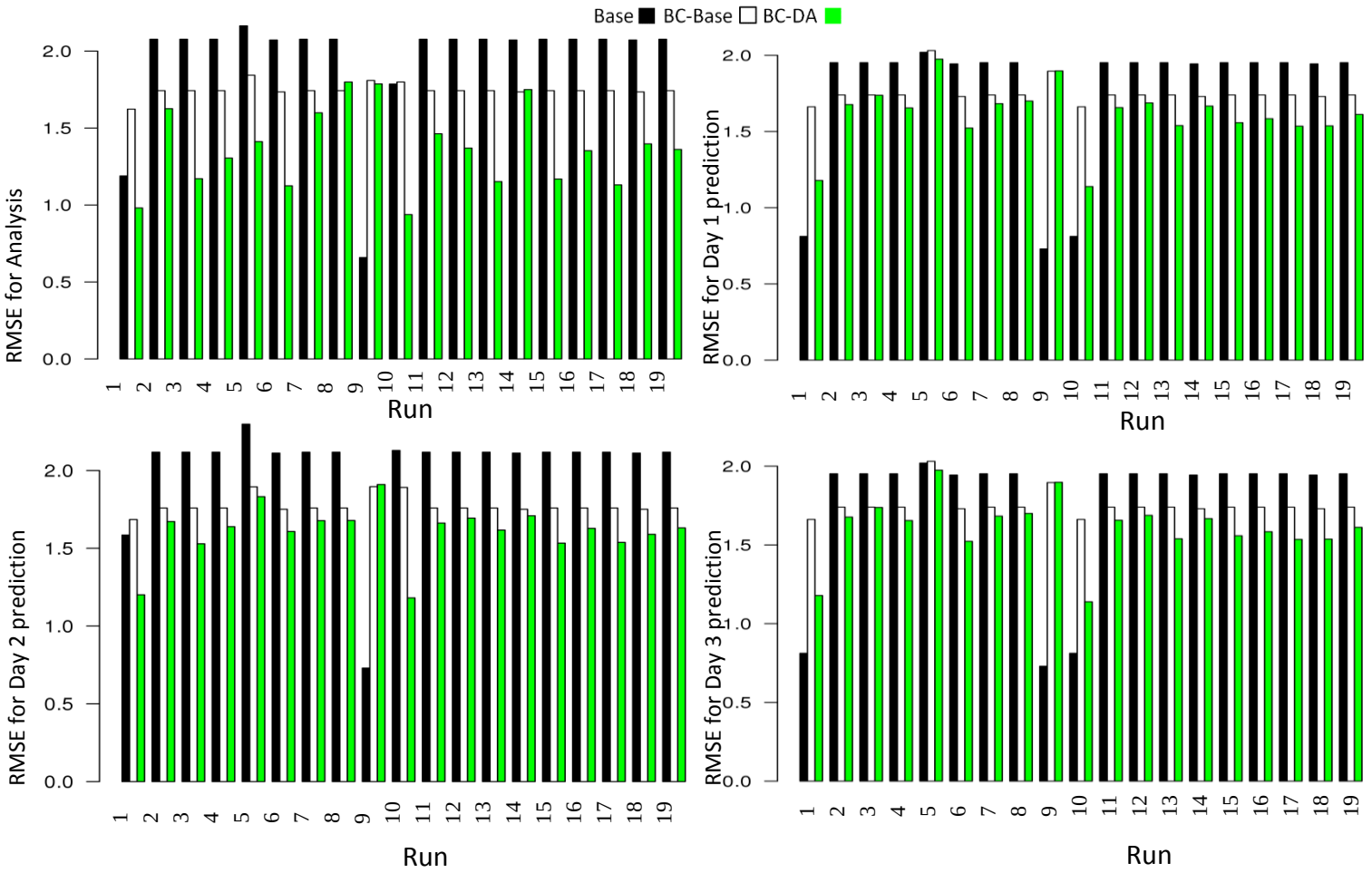

Figure A. 15 RMSE of Base, BC-Base and BC-DA for analysis and Day 1 to Day 3 prediction of BOD.

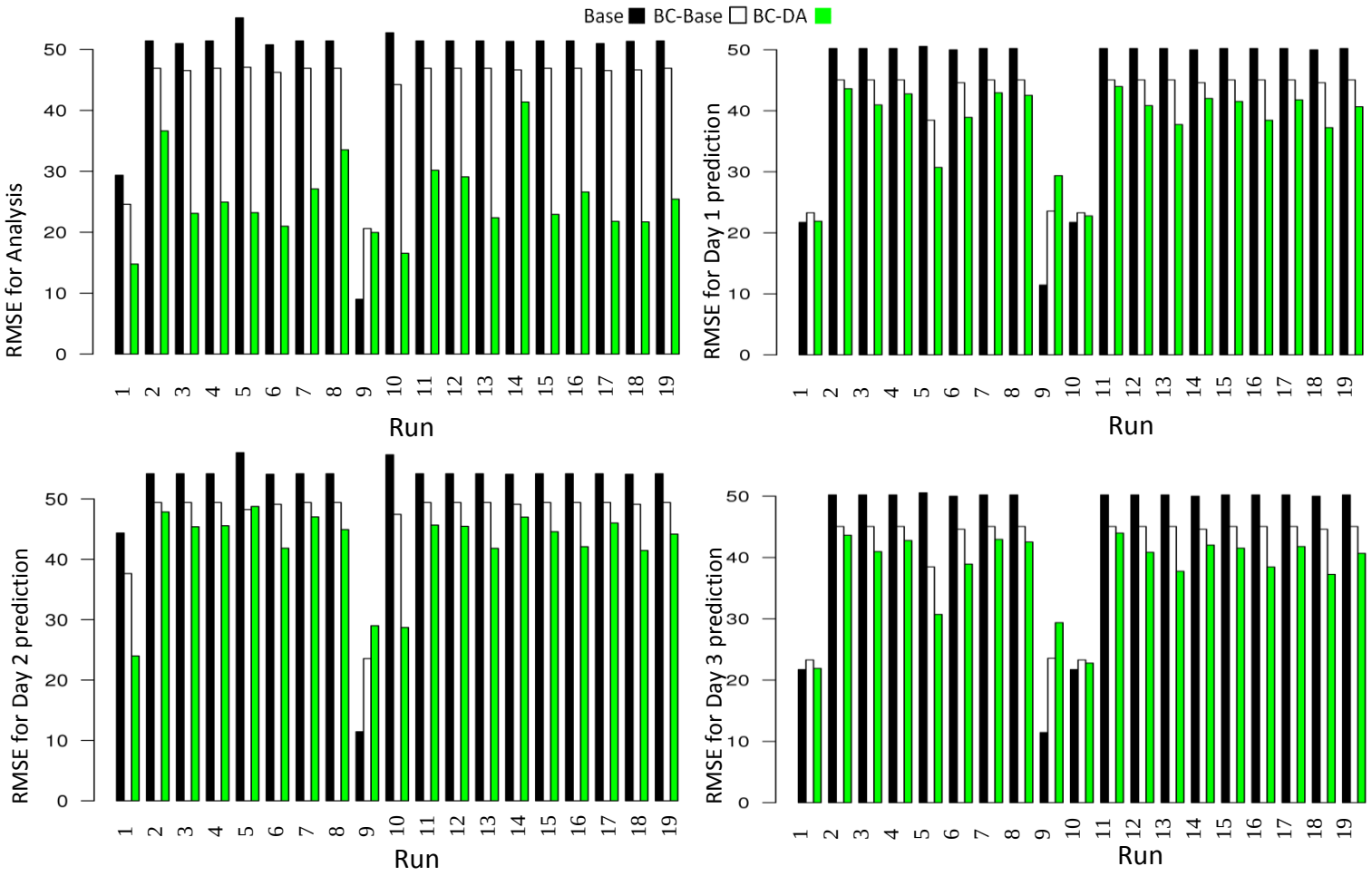

Figure A. 16 RMSE of Base, BC-Base and BC-DA for analysis and Day 1 to Day 3 prediction of CHL-a.

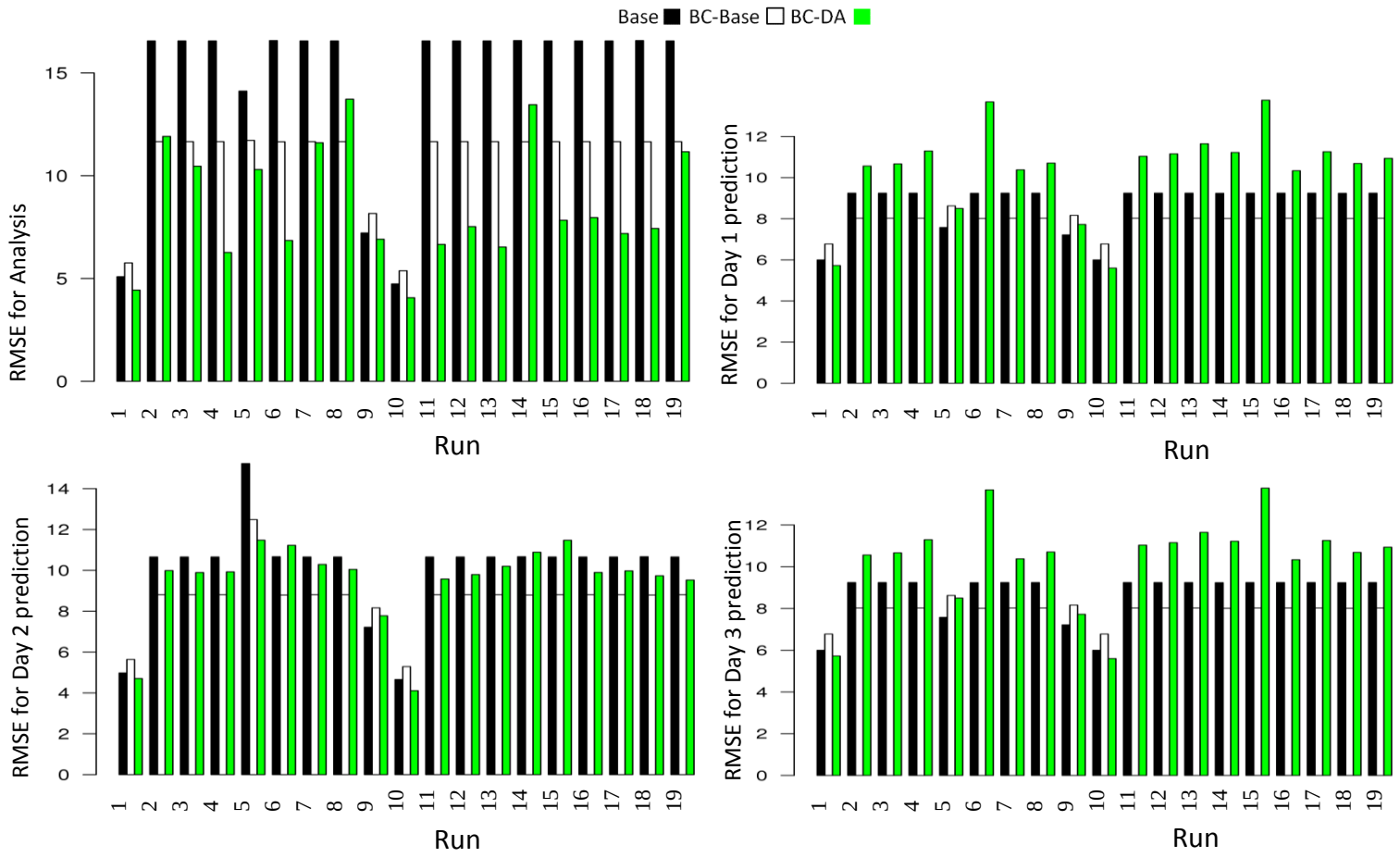

Figure A. 17 RMSE of Base, BC-Base and BC-DA for analysis and Day 1 to Day 3 prediction of Flow.

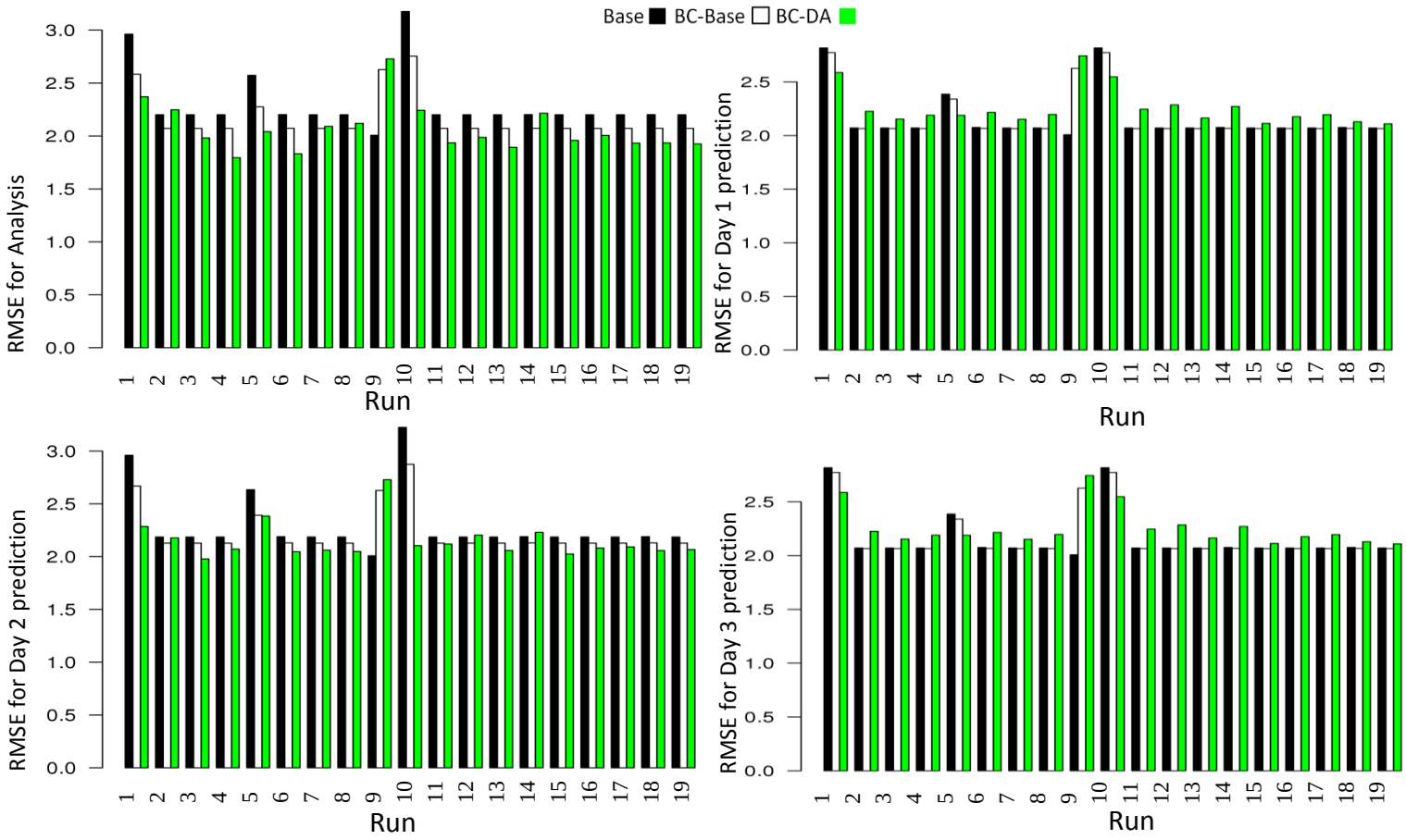

Figure A. 18 RMSE of Base, BC-Base and BC-DA for analysis and Day 1 to Day 3 prediction of DO.

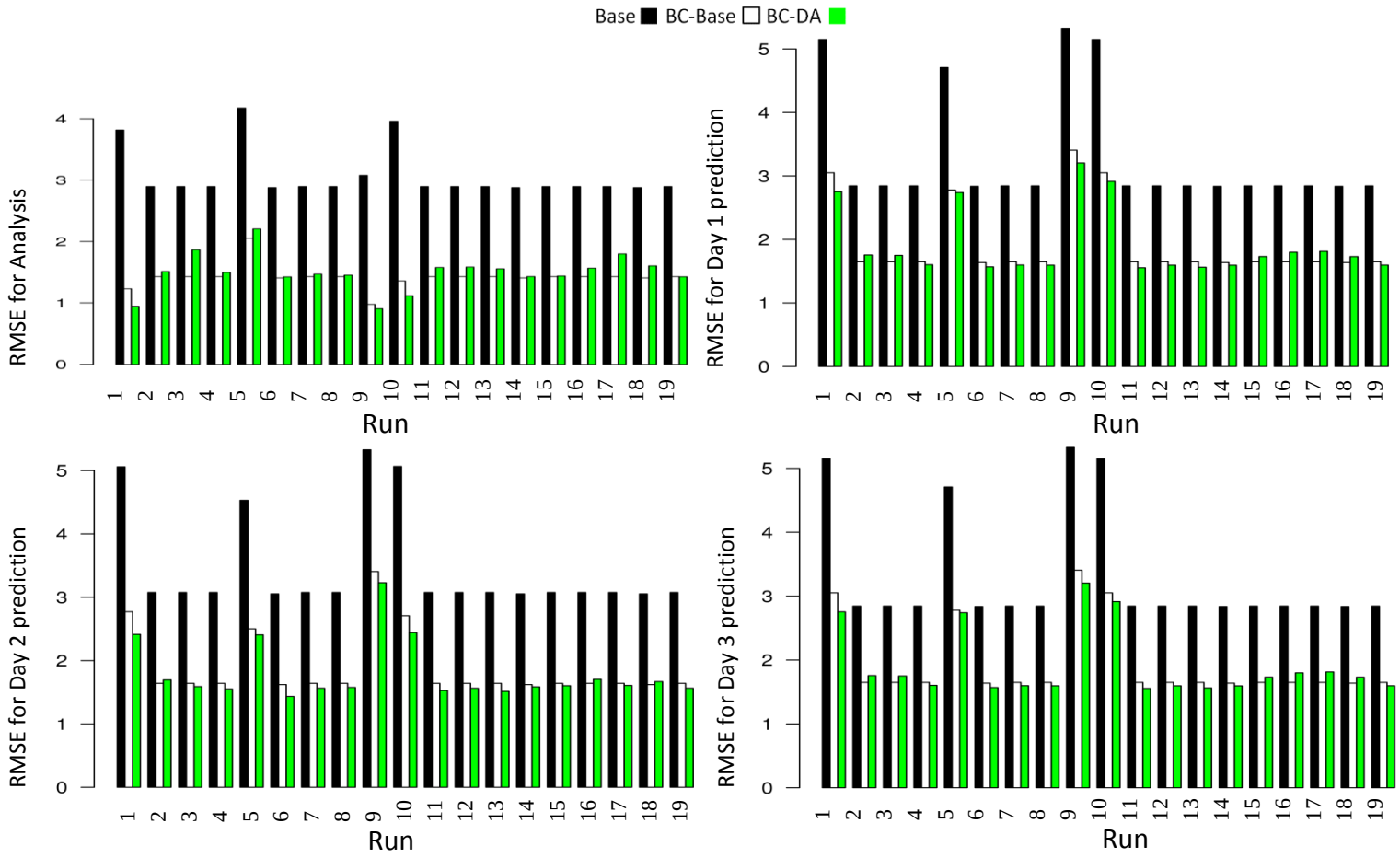

Figure A. 19 RMSE of Base, BC-Base and BC-DA for analysis and Day 1 to Day 3 prediction of NO_3.

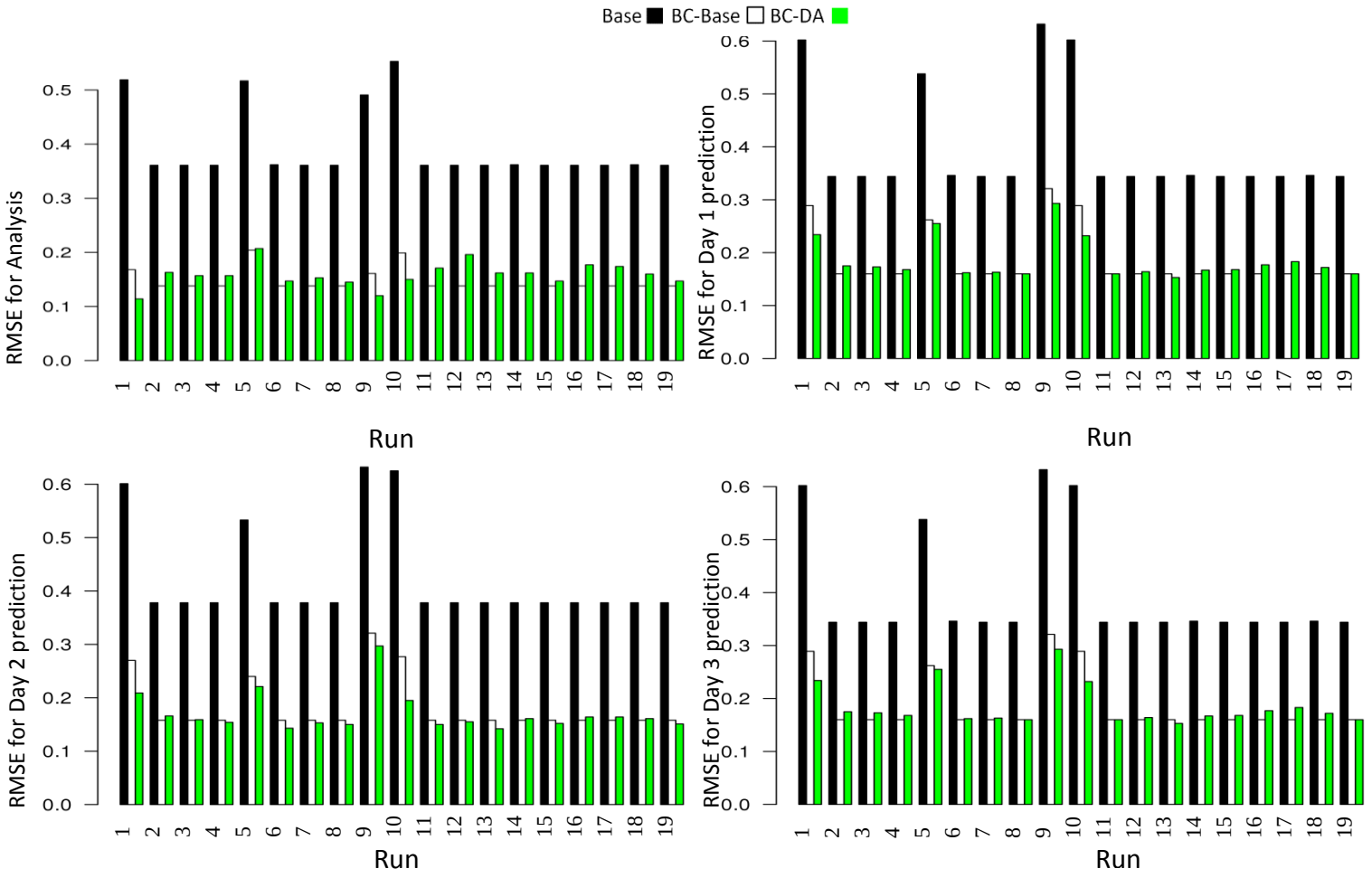

Figure A. 20 RMSE of Base, BC-Base and BC-DA for analysis and Day 1 to Day 3 prediction of PO_4.

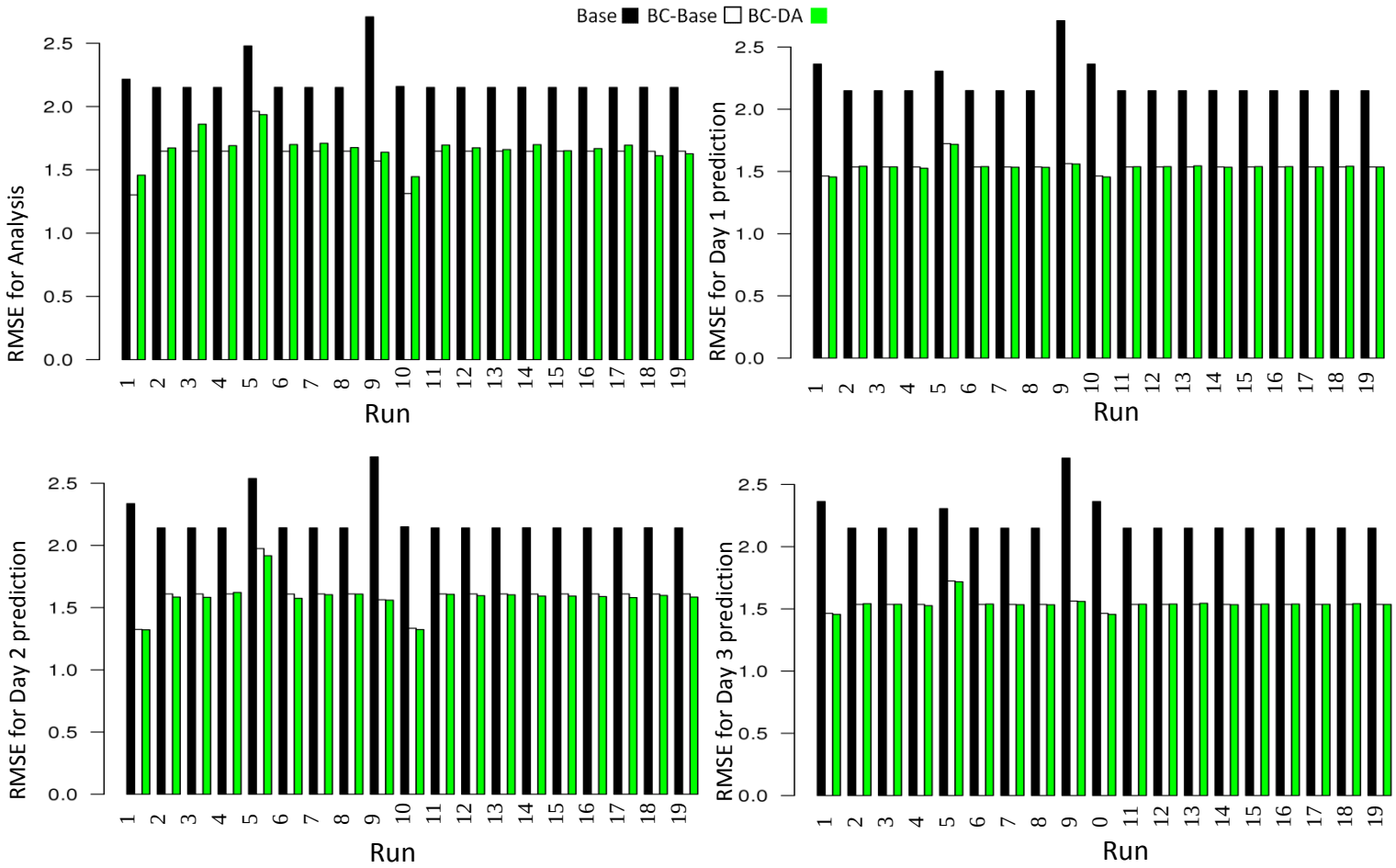

Figure A. 21 RMSE of Base, BC-Base and BC-DA for analysis and Day 1 to Day 3 prediction of TW.

A.4. Sensitivity analysis to the assimilation windows

A set of sensitivity analysis were carried out for the Kumho Catchment for a 2-year period of 2008-2009 to check performance of DA to the size of assimilation window and to answer question 7 (see Table A. 4). In this section, only analysis and prediction results of six water quality variables and streamflow (BOD, CHL-a, flow, DO, NO_3, PO_4 and TW) are shown. For this purpose, the assimilation window was set to 14 days while the magnitude of the model error, initial perturbation and observation error variance were inflated and/or deflated. The ensemble size was kept 9. Due to computational instability, the HSPF terminated prematurely for some runs. For comparison, those runs are plotted however, they were not used for comparison to other runs.

In these sets of runs, all the available observations in the assimilation window were assimilated. Most of the time two sets of observations would be available in each window, therefore it was possible that the older set of observation would not be informative and would not add information to the system in addition to increase the complexity of the inverse problem. Since the sample size between the Run 19 (using assimilation window of 7 days) and other runs in this set (using assimilation window of 14 days) is different, a direct comparison cannot be made. However, as it is shown in Figure A. 22 to Figure A. 28, in all combinations of the model error, initial perturbation and observation error variance and the assimilation window of 14 days the RMSE of the Base simulations for streamflow significantly increased and the RMSE of water quality variables were comparable with assimilation windows of 7 days. A comparison between Run 18 and Run 19 (same parameters setting but with assimilation windows of 14 and 7 days respectively) showed that DA performance was better with assimilation window of 7 days for all the water quality variables and streamflow.

In addition, with the assimilation window of 14 days, the computational burden increased (2 days for 1-year run with assimilation window of 14 days compared to 1 day for the same 1-year run with assimilation window of 7 days).

Table A. 4 Sensitivity analysis to assimilation window of 14 days

Run	Assimilation Windows	ns	Frac_gen	Frac_state	Observation error variance
1	14	9	0.1	1	1
2	14	9	0.1	0.1	1
3	14	9	0.1	10	1
4	14	9	10	1	1
5	14	9	10	0.1	1
6	14	9	10	10	1
7	14	9	1	1	10
8	14	9	0.1	1	10
9	14	9	0.1	0.1	10
10	14	9	0.1	10	10
11	14	9	10	1	10
12	14	9	10	0.1	10
13	14	9	10	10	10
14	14	9	1	0.1	10
15	14	9	1	10	10
16	14	9	1	0.1	1
17	14	9	1	10	1
18	14	9	1	1	1
19	7	9	1	1	1

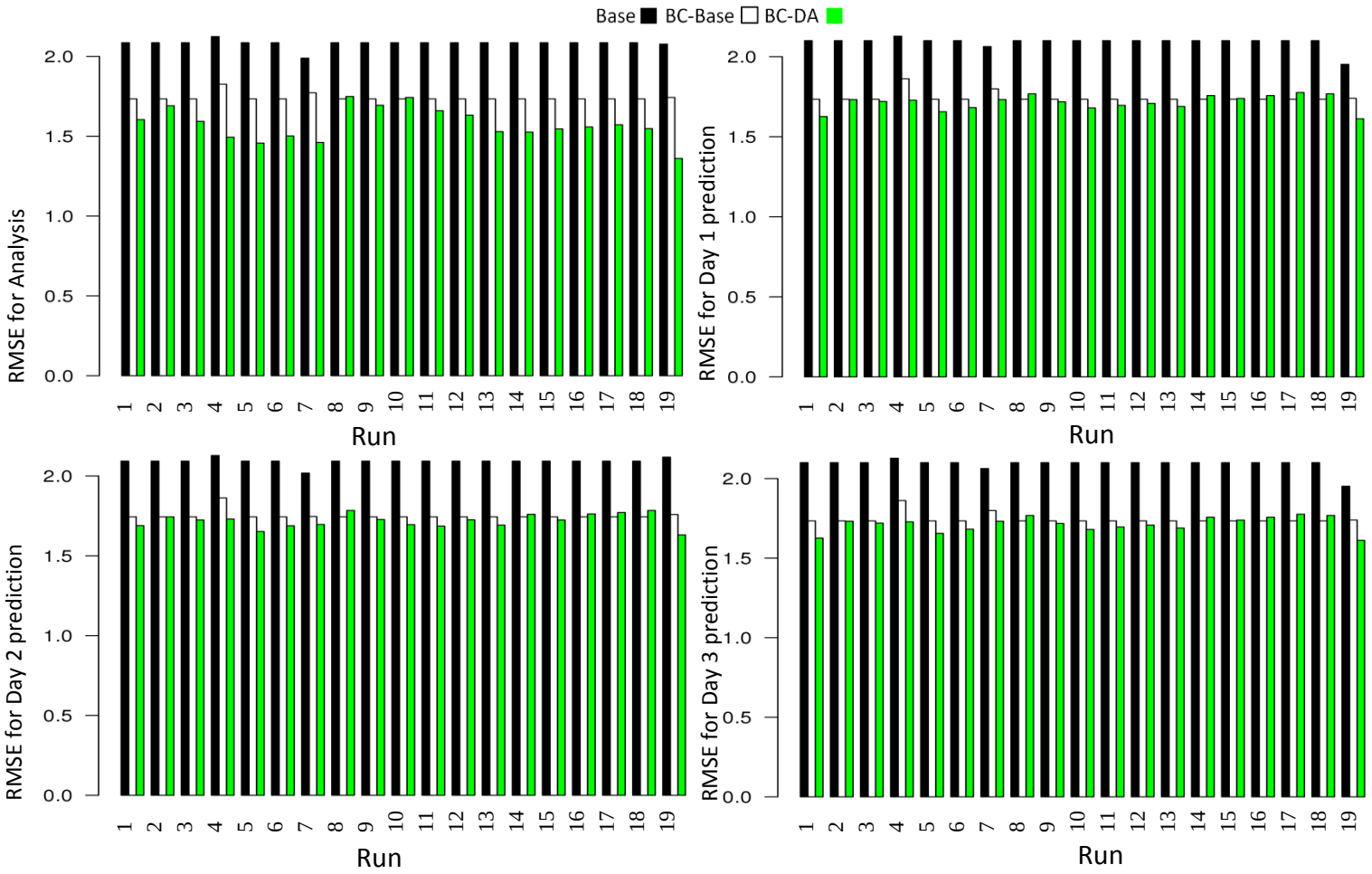

Figure A. 22 RMSE of Base, BC-Base and BC-DA for analysis and Day 1 to Day 3 prediction of BOD.

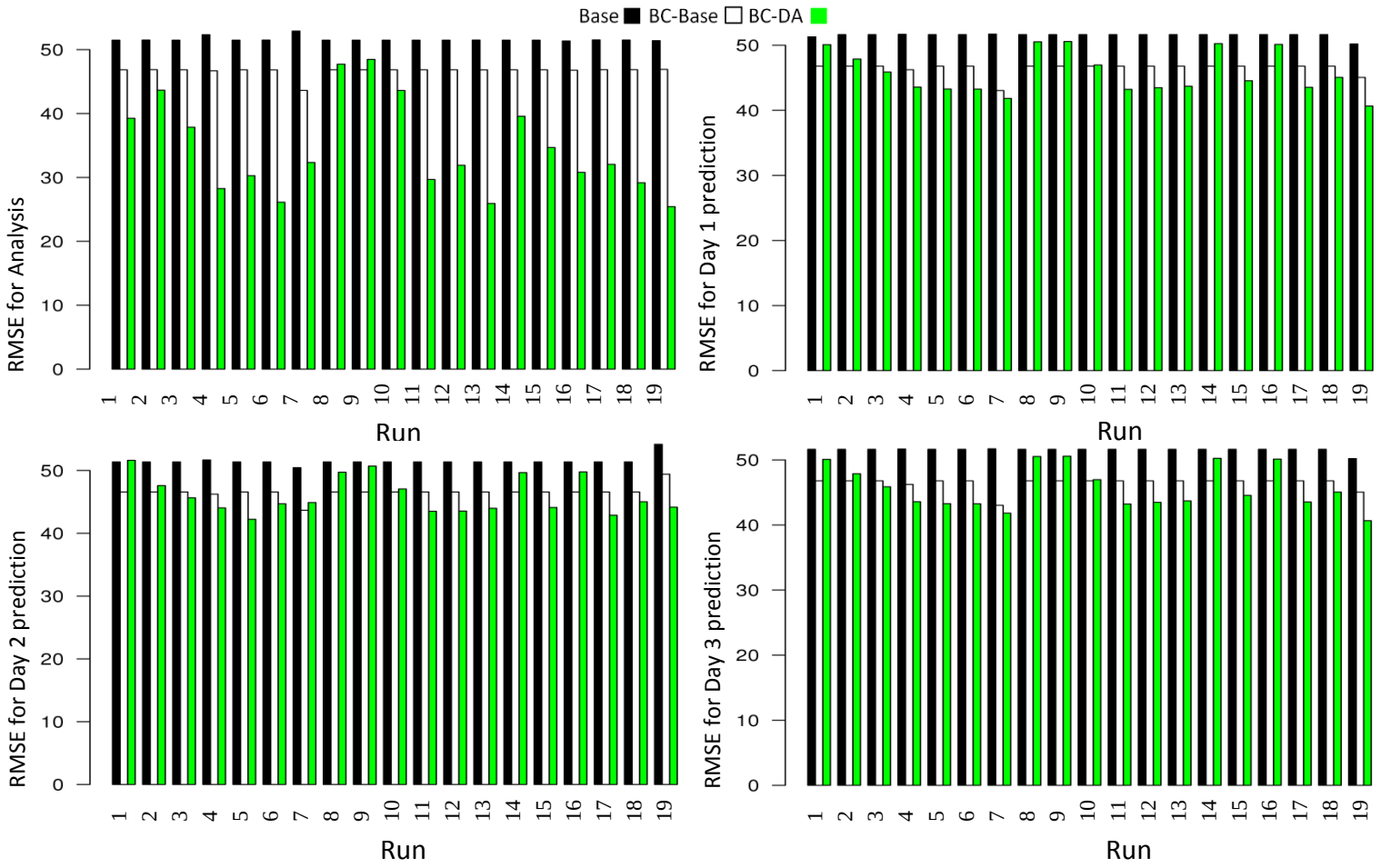

Figure A. 23 RMSE of Base, BC-Base and BC-DA for analysis and Day 1 to Day 3 prediction of CHL-a.

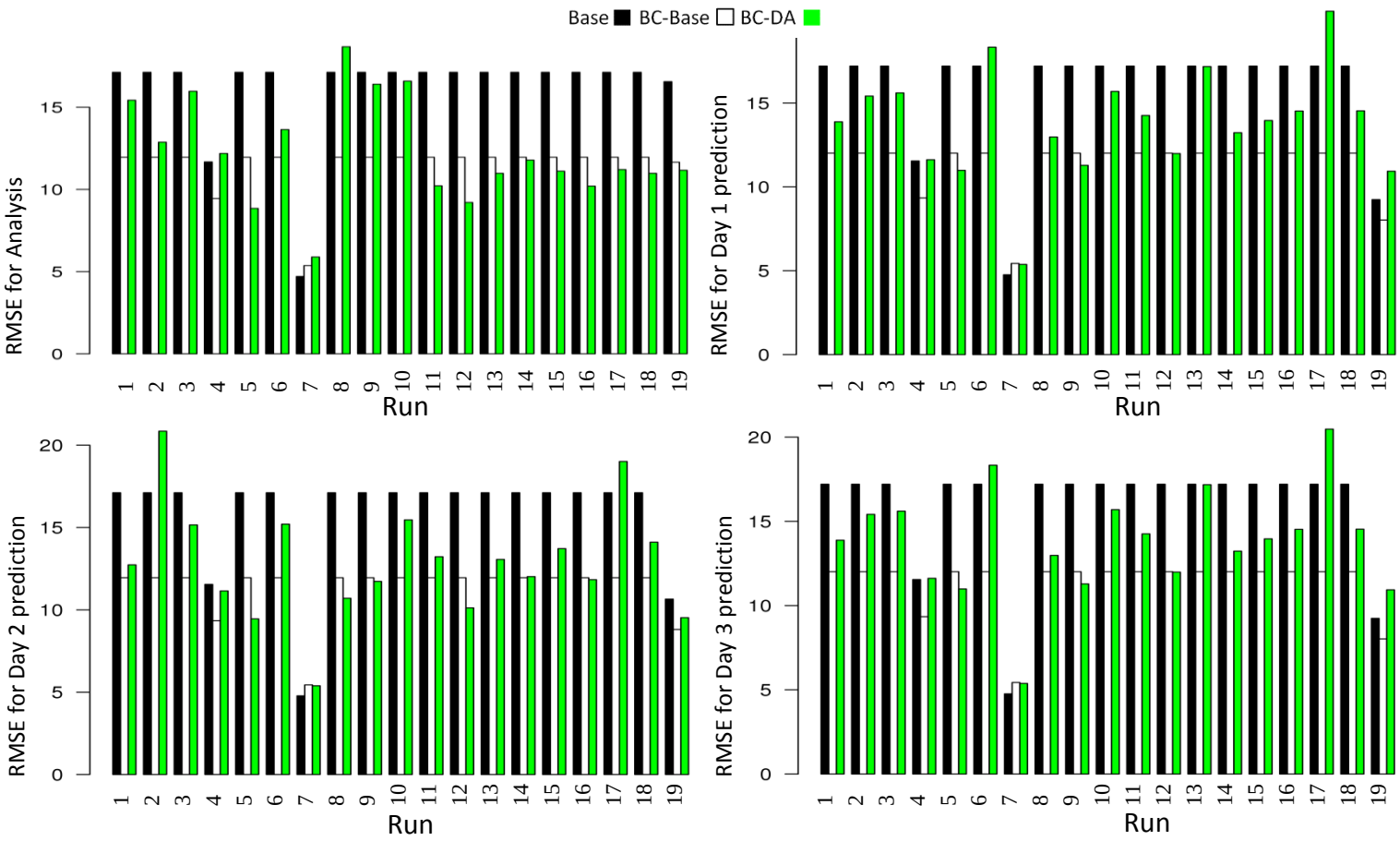

Figure A. 24 RMSE of Base, BC-Base and BC-DA for analysis and Day 1 to Day 3 prediction of Flow.

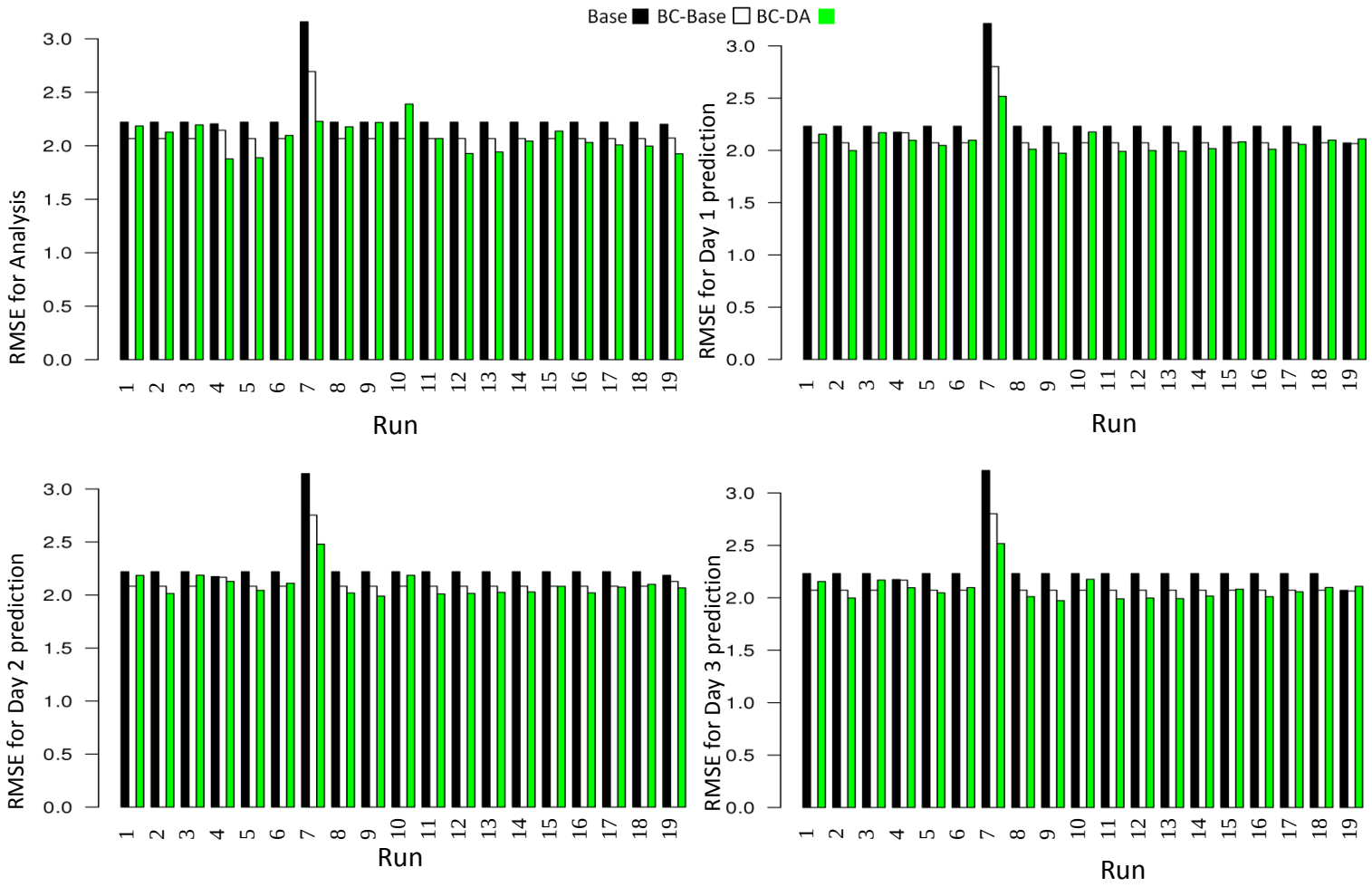

Figure A. 25 RMSE of Base, BC-Base and BC-DA for analysis and Day 1 to Day 3 prediction of DO.

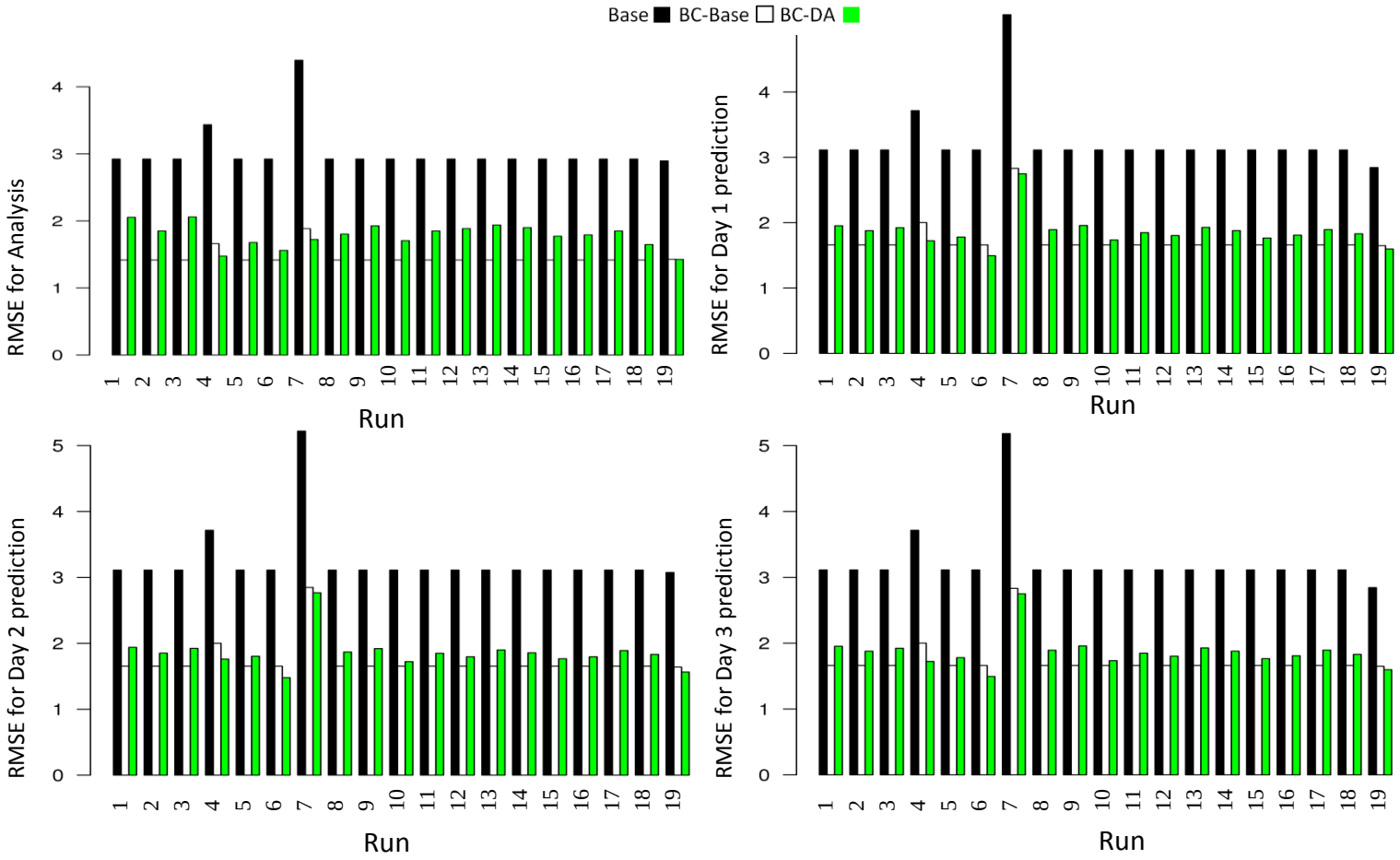

Figure A. 26 RMSE of Base, BC-Base and BC-DA for analysis and Day 1 to Day 3 prediction of NO_3.

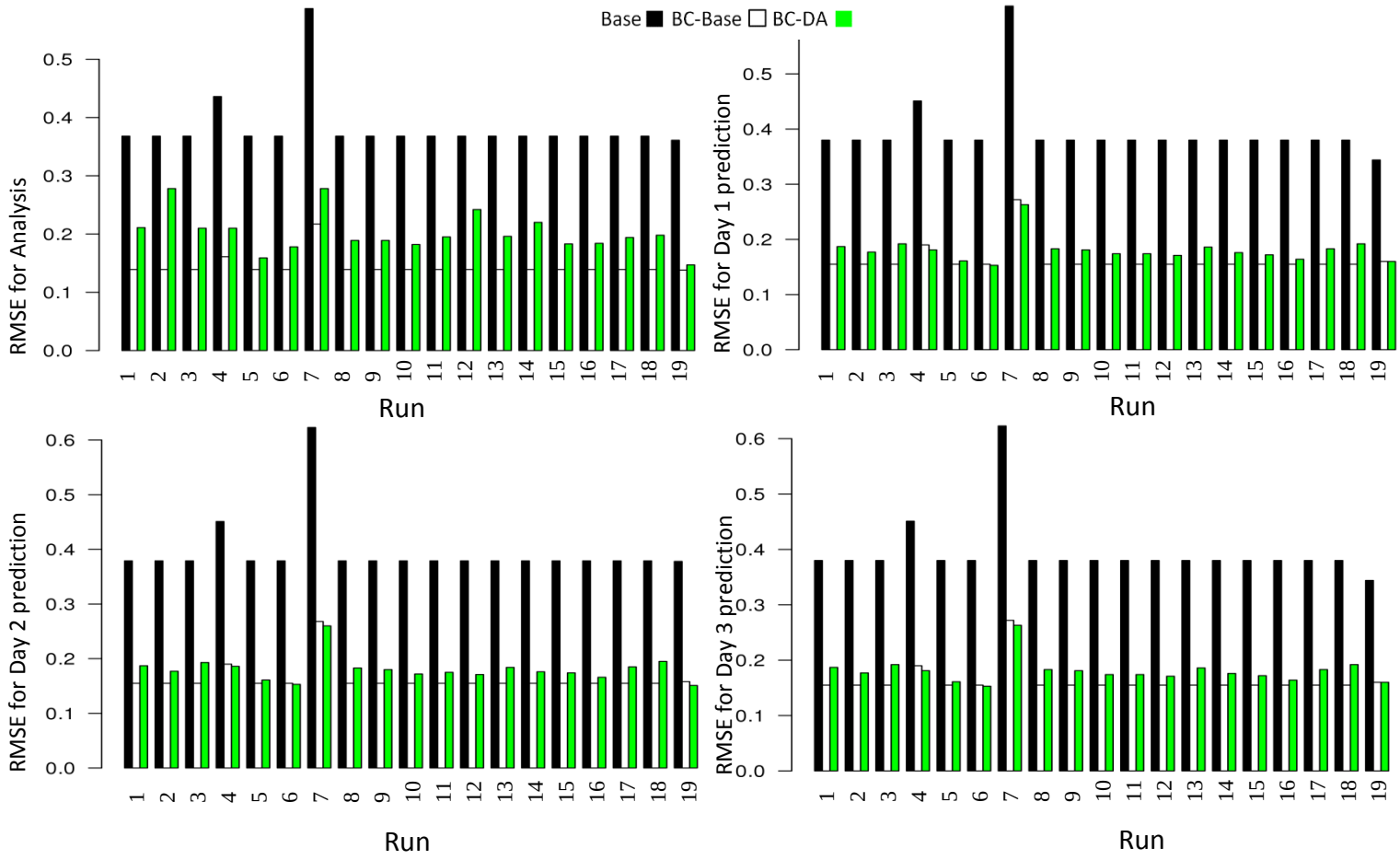

Figure A. 27 RMSE of Base, BC-Base and BC-DA for analysis and Day 1 to Day 3 prediction of PO_4.

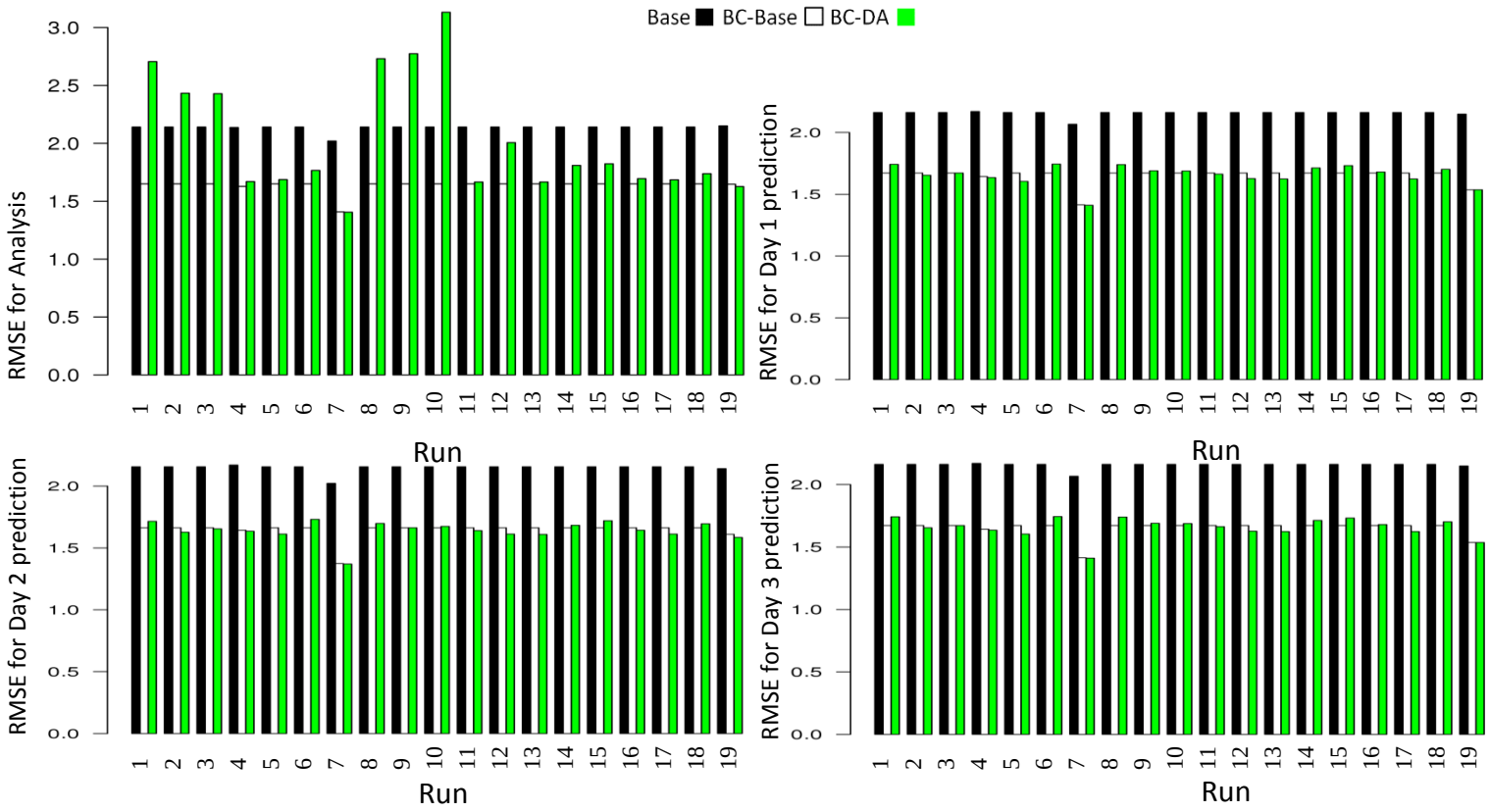

Figure A. 28 RMSE of Base, BC-Base and BC-DA for analysis and Day 1 to Day 3 prediction of TW.

A.5. Sensitivity analysis to the assimilation windows and ensemble size

A set of sensitivity analysis was performed for the Kumho Catchment for a 2-year period of 2008-2009 to check the DA performance to the size of assimilation window and number of the ensembles. In this section, only analysis and prediction results of six water quality variables and streamflow (BOD, CHL-a, flow, DO, NO_3, PO_4 and TW) are shown. Based on the experience, that the HSPF might terminated prematurely due to computational instability with ensemble size of 30, only ensemble size of 18 was used in this set of sensitivity analysis. All the runs were completed for the 2-year period of 2008-2009.

It was observed that the DA performance in analysis and predictions of water quality variables and streamflow with ensemble size of 18 and assimilation window of 14 days were not improved compare to the assimilation window of 7 days and ensemble size of 9. It was concluded that if the selected assimilation window is very large, it is possible that the computational burden would increase due to the increased number of the observations (two and half days for 1-year run compared to 1 day for the same 1-year run). In such a case, even increasing the ensemble size would not improve the DA performance. DA performance is more stable with assimilation window of 7 days. Therefore based on these sets of sensitivity analysis assimilation window of 7 days was selected so that the only one set of water quality observation maybe included in all assimilation cycles.

Table A. 5 Sensitivity analysis to assimilation window of 14 days with ensemble size of 18.

Run	Assimilation Windows	ns	Frac_gen	Frac_state	Observation error variance
1	14	18	0.1	1	1
2	14	18	0.1	0.1	1
3	14	18	0.1	10	1
4	14	18	10	1	1
5	14	18	10	0.1	1
6	14	18	10	10	1
7	14	18	1	1	10
8	14	18	0.1	1	10
9	14	18	0.1	0.1	10
10	14	18	0.1	10	10
11	14	18	10	1	10
12	14	18	10	0.1	10
13	14	18	10	10	10
14	14	18	1	0.1	10
15	14	18	1	10	10
16	14	18	1	0.1	1
17	14	18	1	10	1
18	14	18	1	1	1
19	7	9	1	1	1

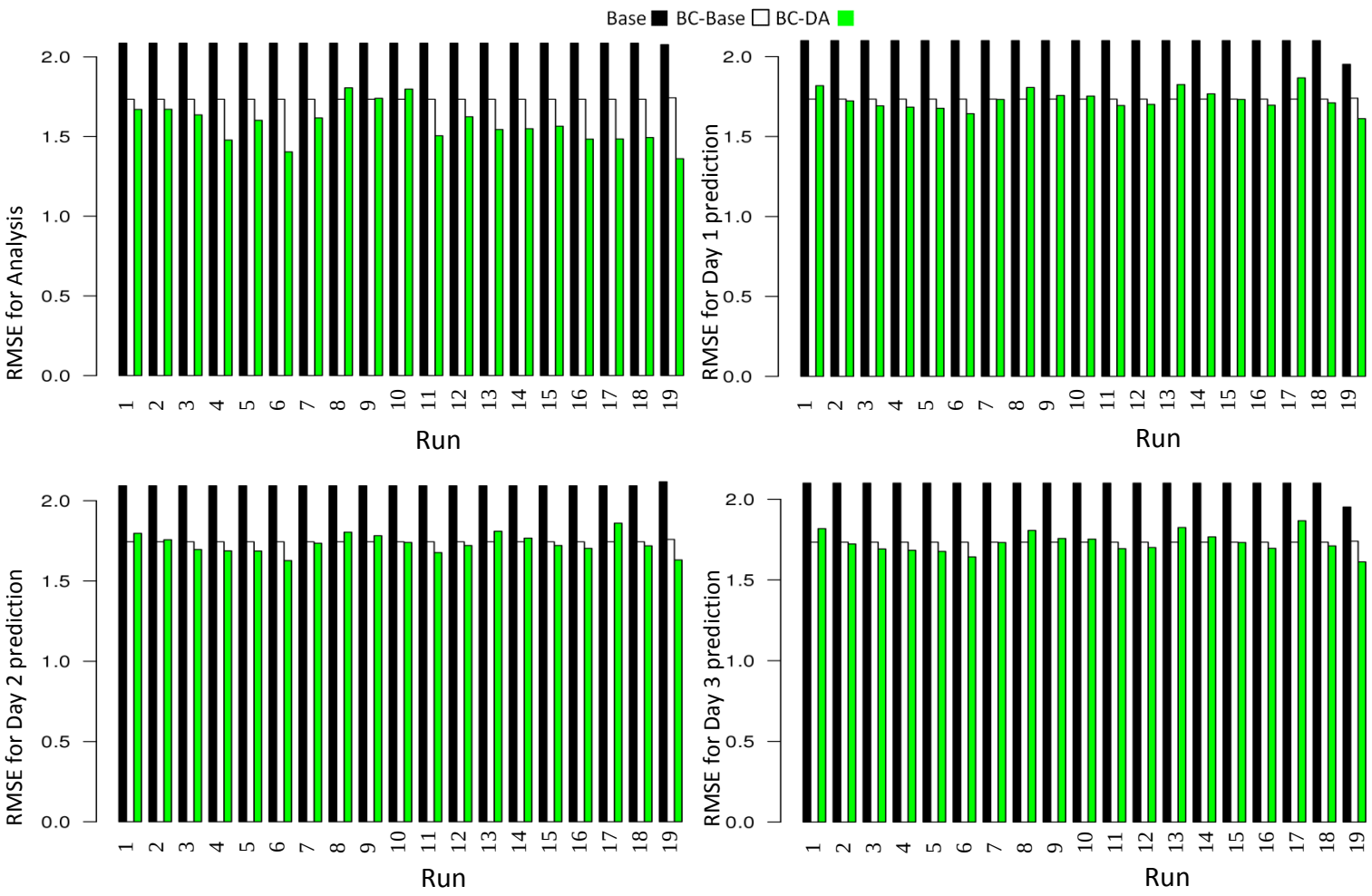

Figure A. 29 RMSE of Base, BC-Base and BC-DA for analysis and Day 1 to Day 3 prediction of BOD.

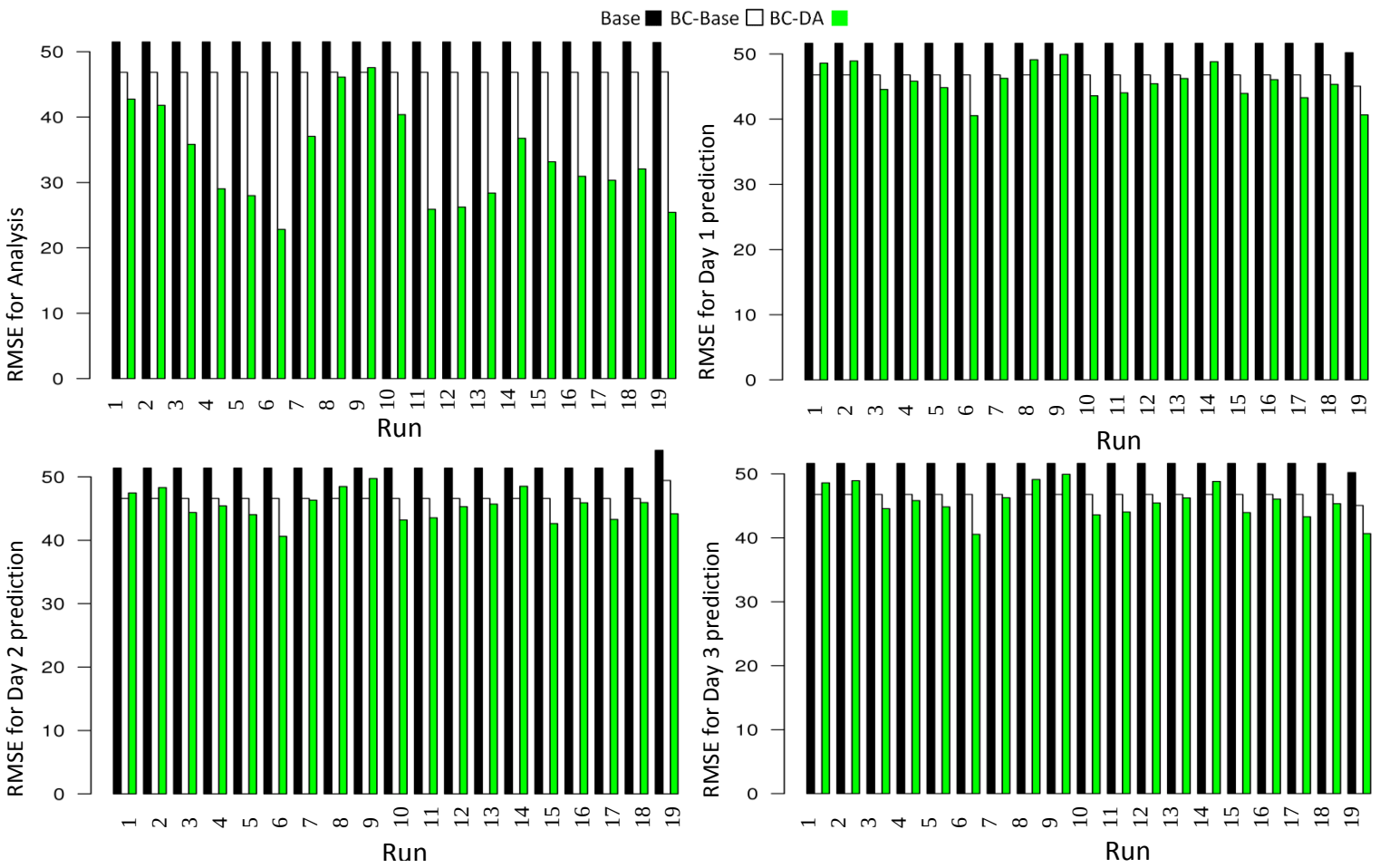

Figure A. 30 RMSE of Base, BC-Base and BC-DA for analysis and Day 1 to Day 3 prediction of CHL-a.

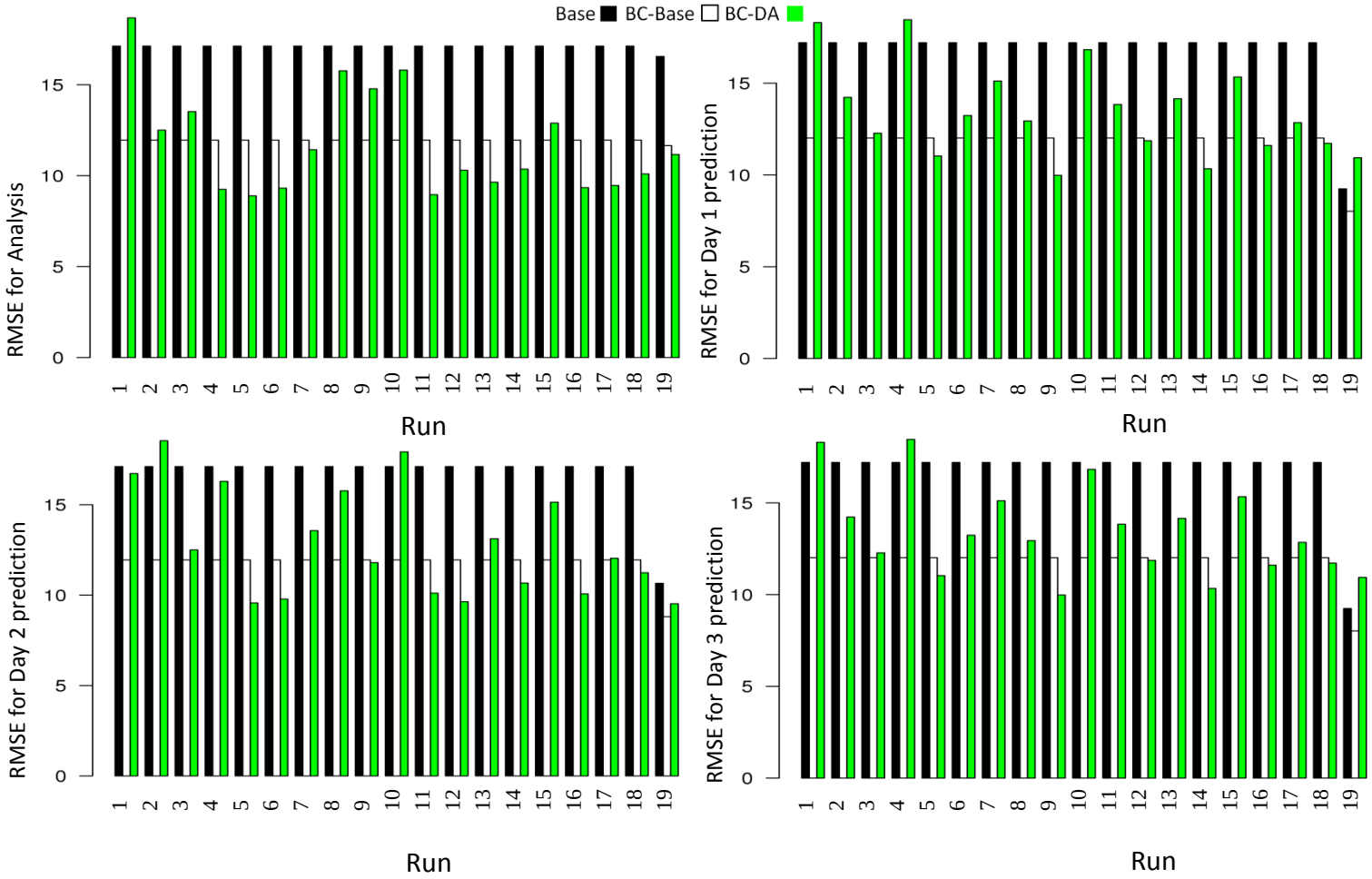

Figure A. 31 RMSE of Base, BC-Base and BC-DA for analysis and Day 1 to Day 3 prediction of Flow.

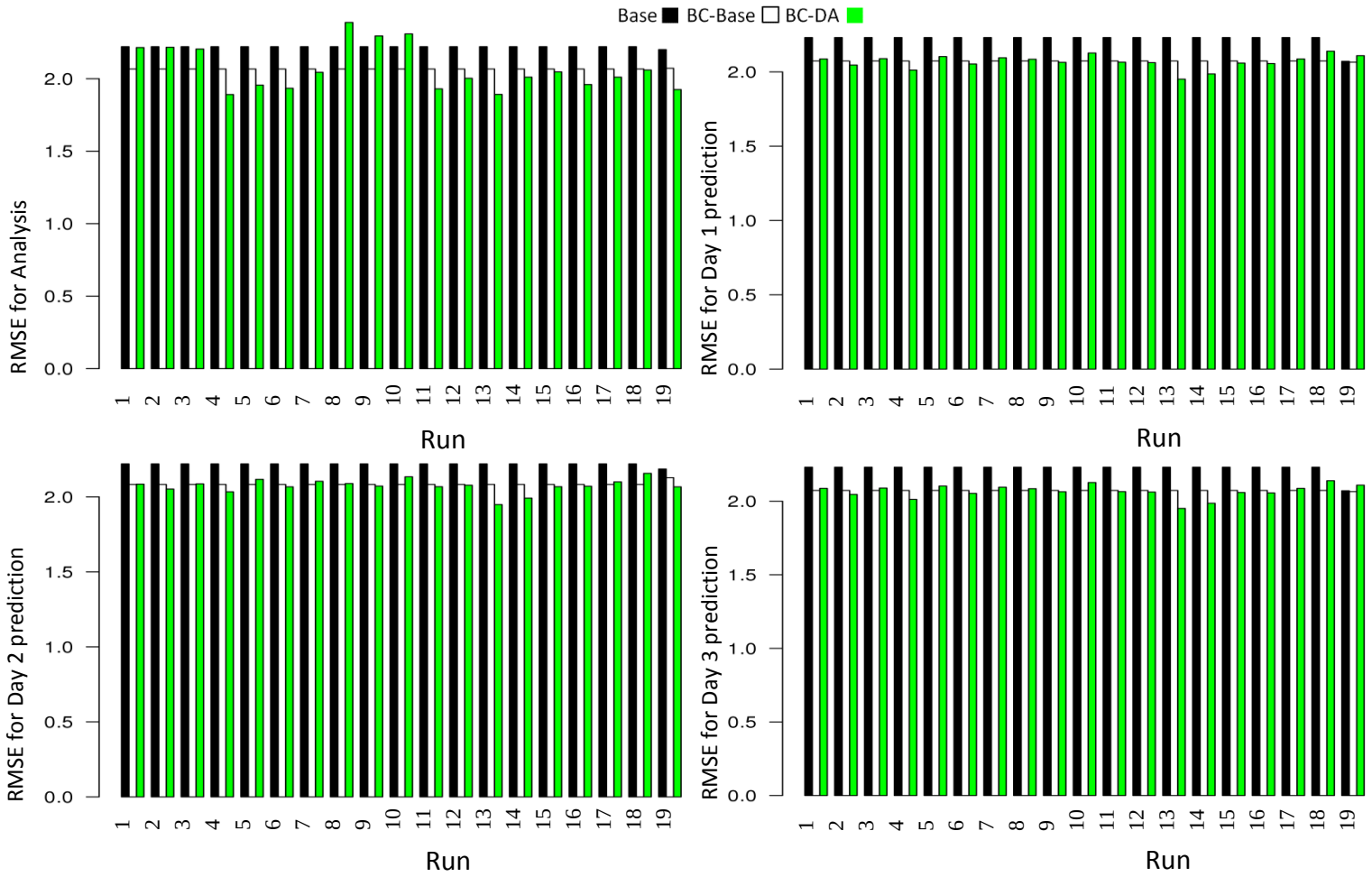

Figure A. 32 RMSE of Base, BC-Base and BC-DA for analysis and Day 1 to Day 3 prediction of DO.

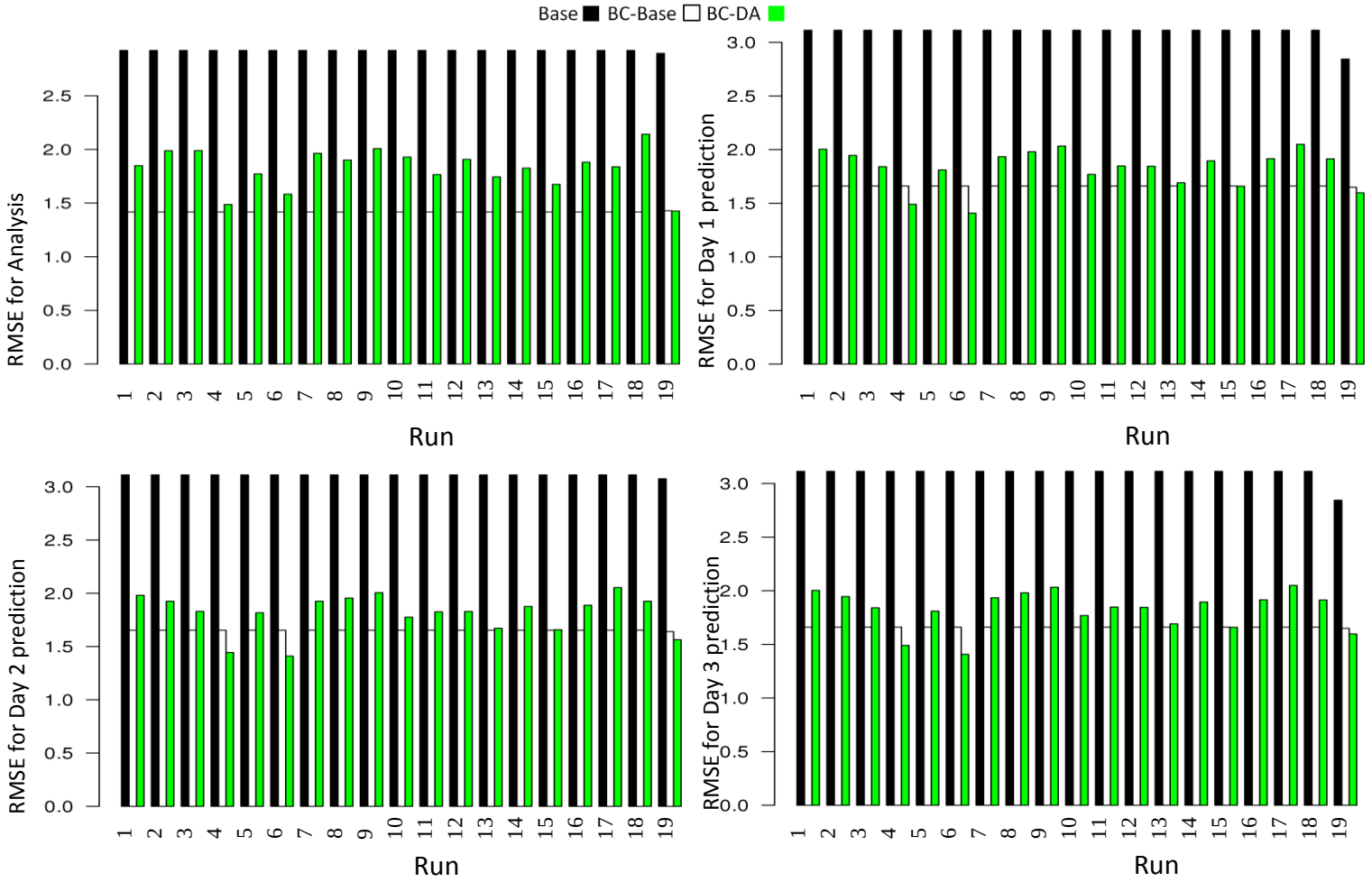

Figure A. 33 RMSE of Base, BC-Base and BC-DA for analysis and Day 1 to Day 3 prediction of NO_3.

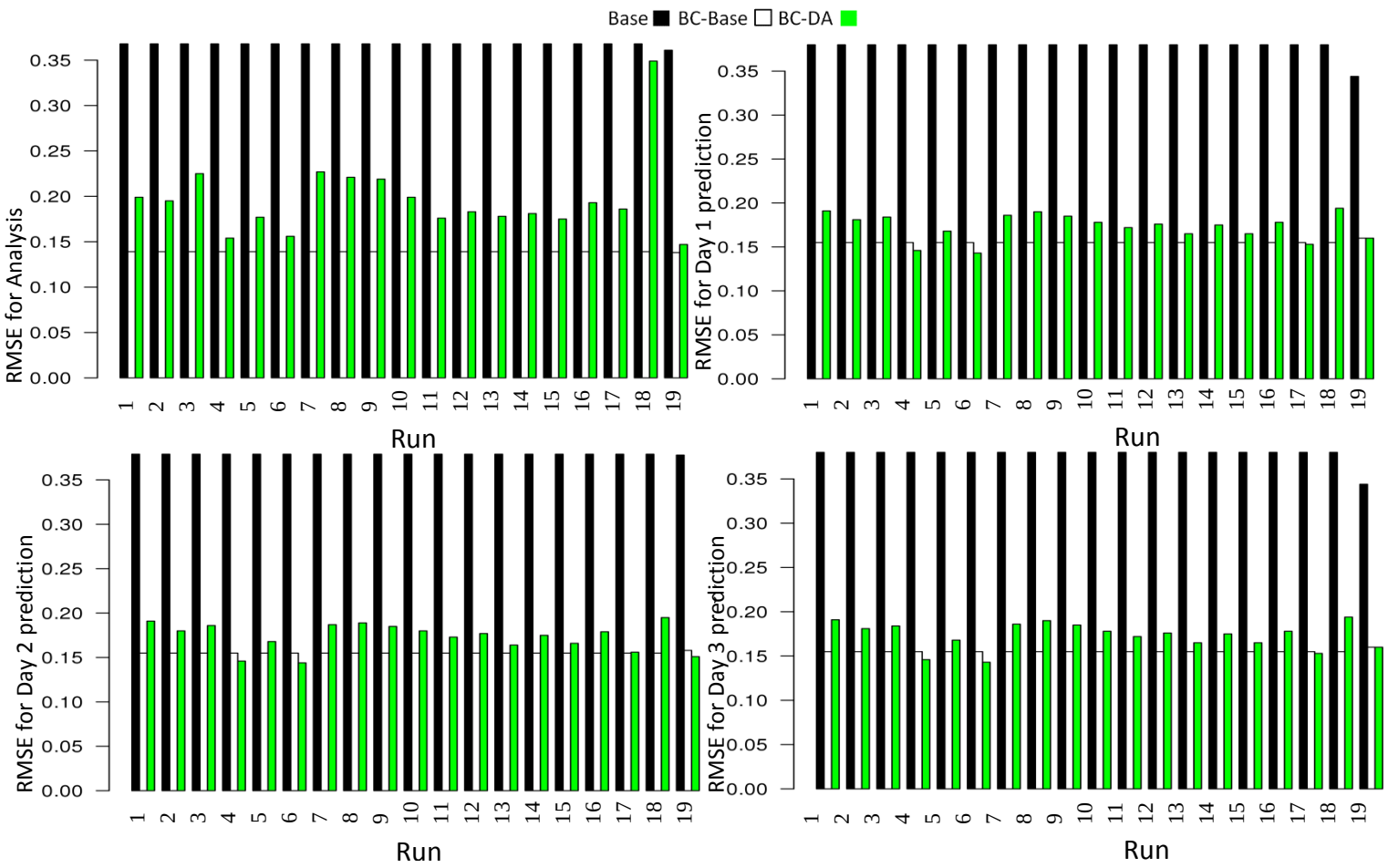

Figure A. 34 RMSE of Base, BC-Base and BC-DA for analysis and Day 1 to Day 3 prediction of PO_4.

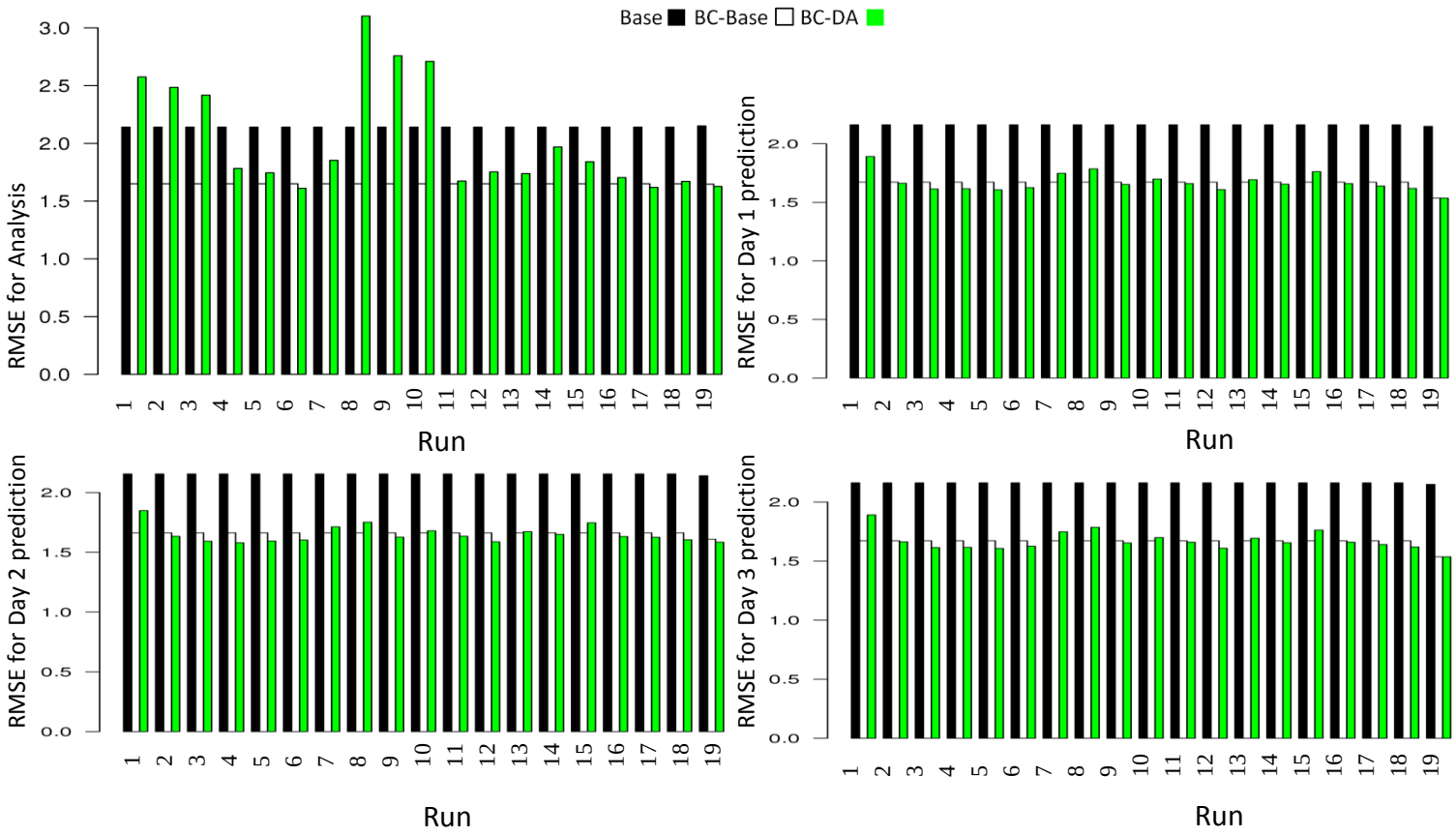

Figure A. 35 RMSE of Base, BC-Base and BC-DA for analysis and Day 1 to Day 3 prediction of TW.

Appendix B

Time Series Modeling

Auto regressive (AR) models can be integrated with a moving average (MA) model to form a general class of time series models called auto regressive integrated moving average (ARIMA) model (Chatfield 2013). The general ARIMA (p,d,q)x(P,D,Q)$_s$ model form is given as:

$$\phi(B)\phi(B^s)\nabla^d\nabla_s^D X_t = \theta(B)\theta(B^s)\varepsilon_t \quad \text{(B-1)}$$

Where X_t is the time series, $\phi(B)$ and $\theta(B)$ are the local AR to the order of *p* and the local MA to the order of *q* respectively, $\phi(B^s)\ and\ \theta(B^s)$ are the seasonal AR to the order of *P* and the seasonal MA to the order of *Q* respectively. The basic seasonal period is s, d is the order of local differentiation, D is the order of seasonal differentiation, ε_t is a residual, ∇ is the backwards difference operator (i.e.$\nabla^1 X_t = X_t - X_{t-1}$) and *B* is the backward shift operator (B$X_t = X_{t-1}$).

To find an appropriate ARIMA model for a time series (best-fit model), an iterative three step approach consisting of model identification, parameter estimation, and diagnostic checking was performed. In each step, the residual plots, auto-correlation function (ACF) and partial auto-correlation function (PACF) were examined. ACF measures the linear relationship between the lagged values of a time series (e.g., ACF at lag 1 is the correlation between X_t and X_{t-1} and ACF at lag 2 is the correlation between X_t and X_{t-2}). The time series that shows no autocorrelation or a very small (close to zero) value of autocorrelation is called white noise. It is expected that when the best-fit model for a variable is determined, ACF should be a white noise series, and in a white noise series, 95% of the spikes in the ACF should lie within $\pm 2(\sqrt{time\ series\ length})^{-1}$. These bounds are generally plotted in the ACF and PACF plots and if more than 5% of the spikes are outside these bounds, then the time series is probably not a white noise. PACF measures the relationship between X_t and X_{t-k}, which is not explained by correlations at all lower order lags. For example, if X_t and X_{t-1} are correlated then X_{t-1} and X_{t-2} should be correlated. Then X_t and X_{t-2} could be correlated as well, which is due to the fact that both are connected to X_{t-1} rather than having to add new information by X_{t-2} to the forecast. Therefore, the PACF is used.

In addition to ACF and PACF, the best-fit model was selected with the smallest Akaike information criterion (AIC) value. AIC is a measure of the ability of the statistical model to quantify the goodness of the fit of the selected model and the parsimony, or simplicity of the model, which is selected. If using a higher order of an MA and/or AR model does not change the AIC significantly, then it is better to use the model with lower orders.

To deal with the skewed data, two forms of transformations were used; logarithmic transformation and Box-Cox transformation. The Box-Cox transformation depends on a parameter called lambda (λ) or transformation parameter. The λ value makes the size of the seasonal variation across the whole series the same. Therefore, it makes it simpler to identify the best-fit model. The logarithmic transformation is a specific form of the Box-Cox transformation in which λ is equal to zero and the natural log base is used. The family of Box-Cox transformations is defined as follows:

$$w_t = \begin{cases} \log(y_t) & if\ \lambda = 0; \\ \frac{y_t^{\lambda}-1}{\lambda} & otherwise. \end{cases} \quad \text{(B-2)}$$

Where y_t denotes the original observations and w_t denotes the transformed observations. If any form of transformation was used in finding the best-fit model, the transformed data will be also used for the forecast. Therefore, it is necessary to reverse the transformation (or back-transform) to obtain forecasts based on the original scale. The reverse Box-Cox transformation is given as follows:

$$y_t = \begin{cases} \exp(w_t) & if\ \lambda = 0; \\ (\lambda w_t + 1)^{1/\lambda} & otherwise. \end{cases} \quad \text{(B-3)}$$

To perform time series modeling, the three-step procedure of model identification, parameter estimation and diagnostics, was performed. In the first step, based on examination of the time series, skewness, and the ACF if necessary, the appropriate form of transformation of the series was performed to achieve normality. Then, seasonality and/or nonstationarity in the observed time series, based on the ACF and PACF, were identified. If the properties of a time

series do not depend on time then it is called a stationary time series. Thus, time series, which show trends or seasonality, are not stationary. Therefore, if necessary, appropriate differencing of the series was performed to achieve stationarity. According to the ACF and PACF of the stationary series, different ARIMA models were identified (see Subsection 6.6). The criterion for the selection of the best-fit model was the model with the smallest AIC value. When the best-fit model is determined, the next step is to use that model and to test and verify if that model is adequate for describing the studied process for each water quality variable. In the section 6.6, an example of the step-by-step procedure to select the best-fit model is explained.

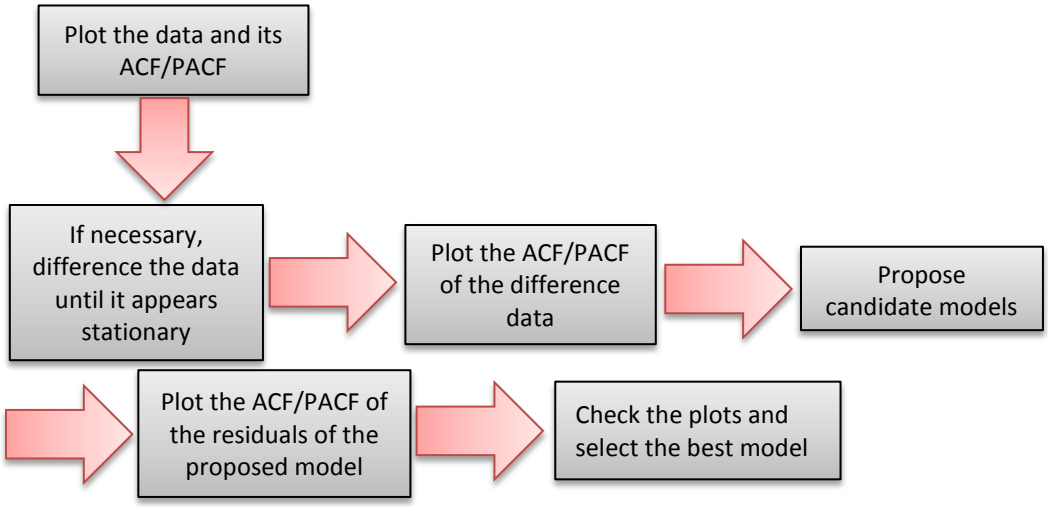

Figure B. 1 Time series procedure to select the best-fit model.

References

Arulampalam, M. S., Maskell, S., Gordon, N., & Clapp, T. (2002). A tutorial on particle filters for online nonlinear/non-Gaussian Bayesian tracking. *Signal Processing, IEEE Transactions on*, *50*(2), 174-188.

Arya, F. K., & Zhang, L. (2015). Time series analysis of water quality parameters at Stillaguamish River using order series method. *Stochastic Environmental Research and Risk Assessment*, *29*(1), 227-239.

Balasuriya, B. L. N., Thanh, N. C., & Phien, H. N. (1982). Time series modeling of water quality. *Environmental Technology*, *3*(12), 563-576.

Batt, R. D., & Carpenter, S. R. (2012). Free-water lake metabolism: addressing noisy time series with a Kalman filter. *Limnology and Oceanography: Methods*,*10*(1), 20-30.

Beck, B., & Young, P. (1976). Systematic identification of DO-BOD model structure. *Journal of the Environmental Engineering Division*, *102*(5), 909-927.

Beck, M. B. (1987). Water quality modeling: a review of the analysis of uncertainty. *Water Resources Research*, *23*(8), 1393-1442.

Bicknell, B. R., Imhoff, J. C., Kittle Jr, J. L., Jobes, T. H., Donigian Jr, A. S., & Johanson, R. C. (2001). Hydrological simulation program-Fortran: HSPF version 12 user's manual. *AQUA TERRA Consultants, Mountain View, California*.

Bode, H., & Nusch, E. A. (1999). Advanced river quality monitoring in the Ruhr basin. *Water science and technology*, *40*(10), 145-152.

Box, G. E., & Cox, D. R. (1964). An analysis of transformations. *Journal of the Royal Statistical Society. Series B (Methodological)*, 211-252.

Box, G. E., Jenkins, G. M., & Reinsel, G. C. (2011). *Time series analysis: forecasting and control* (Vol. 734). John Wiley & Sons.

Bras, R. L., & Rodríguez-Iturbe, I. (1985). *Random functions and hydrology*. Courier Corporation.

Brown, J. D., Demargne, J., Seo, D. J., & Liu, Y. (2010). The Ensemble Verification System (EVS): A software tool for verifying ensemble forecasts of hydrometeorological and hydrologic variables at discrete locations.*Environmental Modelling & Software*, *25*(7), 854-872.

Burgers, G., Jan van Leeuwen, P., & Evensen, G. (1998). Analysis scheme in the ensemble Kalman filter. *Monthly weather review*, *126*(6), 1719-1724.

Burnash, R. J., Ferral, R. L., & McGuire, R. A. (1973). A generalized streamflow simulation system, conceptual modeling for digital computers.

Canale, R. P., DePalma, L. M., & Powers, W. F. (1980). *Sampling strategies for water quality in the Great Lakes*. Environmental Research Laboratory, Office of Research and Development, US Environmental Protection Agency.

Carrassi, A., Vannitsem, S., Zupanski, D., & Zupanski, M. (2009). The maximum likelihood ensemble filter performances in chaotic systems. *Tellus A*,*61*(5), 587-600.

Chen, Q., Guan, T., Yun, L., Li, R., & Recknagel, F. (2015). Online forecasting chlorophyll a concentrations by an auto-regressive integrated moving average model: Feasibilities and potentials. *Harmful Algae*, *43*, 58-65.

Clark, M. P., Rupp, D. E., Woods, R. A., Zheng, X., Ibbitt, R. P., Slater, A. G., Schmidt, J., & Uddstrom, M. J. (2008). Hydrological data assimilation with the ensemble Kalman filter: Use of streamflow observations to update states in a distributed hydrological model. *Advances in water resources*, *31*(10), 1309-1324.

Coad, P., Cathers, B., Ball, J. E., & Kadluczka, R. (2014). Proactive management of estuarine algal blooms using an automated monitoring buoy coupled with an artificial neural network. *Environmental Modelling & Software*,*61*, 393-409.

Cosby, B. J. (1984). Dissolved oxygen dynamics of a stream: model discrimination and estimation of parameter variability using an extended Kalman filter. *Water Science & Technology*, *16*(5-7), 561-569.

Crawford, N. H., & Burges, S. J. (2004). History of the Stanford watershed model. *Water Resource*s Impact, 6(2), 3-5.

DeChant, C. M., & Moradkhani, H. (2012). Examining the effectiveness and robustness of sequential data assimilation methods for quantification of uncertainty in hydrologic forecasting. *Water Resources Research*, *48*(4).

DeChant, C., and Moradkhani, H., (2011a), Radiance data assimilation for operational snow and streamflow forecasting, Adv. Water Resour., 34, 351–364.

Drécourt, J. P., & Rosbjerg, D. (2004). *Data assimilation in hydrological modelling* (Doctoral dissertation, Technical University of Denmark, Department of Hydrodynamics and Water Resocurces).

Eknes, M., & Evensen, G. (2002). An ensemble Kalman filter with a 1-D marine ecosystem model. *Journal of Marine Systems*, *36*(1), 75-100.

Ennola, K., Sarvala, J., & Devai, G. (1998). Modelling zooplankton population dynamics with the extended Kalman filtering technique. *Ecological modelling*,*110*(2), 135-149

Evensen, G. (1992). Using the extended Kalman filter with a multilayer quasi-geostrophic ocean model.

Evensen, G. (1994). Sequential data assimilation with a nonlinear quasi-geostrophic model using Monte Carlo methods to forecast error statistics.

Evensen, G. (2003). The ensemble Kalman filter: Theoretical formulation and practical implementation. *Ocean dynamics*, *53*(4), 343-367.

Evensen, G. (2009). *Data assimilation: the ensemble Kalman filter*. Springer Science & Business Media.

Giustarini, L., Matgen, P., Hostache, R., Montanari, M., Plaza, D., Pauwels, V. R. N., Lannoy G. J. M. De, Keyser R. De, Pfister L., Hoffmann L., Savenije, H. H. G. (2011). Assimilating SAR-derived water level data into a hydraulic model: a case study. *Hydrology and Earth System Sciences*, *15*(7), 2349-2365.

Gordon, N. J., Salmond, D. J., & Smith, A. F. (1993, April). Novel approach to nonlinear/non-Gaussian Bayesian state estimation. In *IEE Proceedings F (Radar and Signal Processing)* (Vol. 140, No. 2, pp. 107-113). IET Digital Library.

Guingla, P., Douglas, A., Keyser, R., Lannoy, G. J., Giustarini, L., Matgen, P., & Pauwels, V. (2013). Improving particle filters in rainfall-runoff models: Application of the resample-move step and the ensemble Gaussian particle filter. *Water Resources Research*, *49*(7), 4005-4021.

Guiot, J., Boucher, E., & Gea-Izquierdo, G. (2014). Process models and model-data fusion in dendroecology. *Frontiers in Ecology and Evolution*, *2*, 52.

Guo, H. C., Liu, L., & Huang, G. H. (2003). A stochastic water quality forecasting system for the Yiluo River. *Journal of Environmental Informatics*,*1*(2), 18-32.

Hamrick, J. M. (2007). The Environmental Fluid Dynamics Code: User Manual.*US EPA, Fairfax, VA, Version*, *1*.

Han, E., Merwade, V., & Heathman, G. C. (2012). Application of data assimilation with the root zone water quality model for soil moisture profile estimation in the upper Cedar Creek, Indiana. *Hydrological Processes*, *26*(11), 1707-1719.

Hoteit, I., Korres, G., & Triantafyllou, G. (2005). Comparison of extended and ensemble based Kalman filters with low and high resolution primitive equation ocean models. *Nonlinear Processes in Geophysics*, *12*(5), 755-765.

Houtekamer, P. L., & Mitchell, H. L. (1998). Data assimilation using an ensemble Kalman filter technique. *Monthly Weather Review*, *126*(3), 796-811.

Huang, J., Gao, J., Liu, J., & Zhang, Y. (2013). State and parameter update of a hydrodynamic-phytoplankton model using ensemble Kalman filter. *Ecological* Modelling, 263, 81-91.

Ide, K., Courtier, P., Ghil, M., & Lorenc, A. C. (1997). Uni ed notation for data assimilation: operational, sequential and variational. Practice, *75*(1B), 181-189

Jazwinski, A. H. (1970). Stochastic Processes and Filtering Theory Academic.New York, 64.

Jian, X., & Yu, Y. S. (1998). A comparative study of linear and nonlinear time series models for water quality. *Journal of the American Water Resources Association*, *34*(3), 651-660.

Kalman, R. E. (1960). A new approach to linear filtering and prediction problems. *Journal of Fluids Engineering*, *82*(1), 35-45.

Kang, D., & Lansey, K. (2009). Real-time demand estimation and confidence limit analysis for water distribution systems. *Journal of Hydraulic Engineering*

Kim, K., Park, M., Min, J. H., Ryu, I., Kang, M. R., & Park, L. J. (2014). Simulation of algal bloom dynamics in a river with the ensemble Kalman filter.*Journal of Hydrology*, *519*, 2810-2821.

Kim, S., Seo, D. J., Riazi, H., & Shin, C. (2014). Improving water quality forecasting via data assimilation–Application of maximum likelihood ensemble filter to HSPF. *Journal of Hydrology*, *519*, 2797-2809.

Komma, J., Blöschl, G., & Reszler, C. (2008). Soil moisture updating by Ensemble Kalman Filtering in real-time flood forecasting. *Journal of Hydrology*,*357*(3), 228-242.

Lee, H., Seo, D. J., & Koren, V. (2011). Assimilation of streamflow and in situ soil moisture data into operational distributed hydrologic models: Effects of uncertainties in the data and initial model soil moisture states. *Advances in Water Resources*, *34*(12), 1597-1615.

Lee, H., Seo, D. J., Liu, Y., Koren, V., McKee, P., & Corby, R. (2012). Variational assimilation of streamflow into operational distributed hydrologic models: effect of spatiotemporal scale of adjustment. *Hydrology and Earth System Sciences*, *16*(7), 2233-2251.

Leisenring, M., & Moradkhani, H. (2012). Analyzing the uncertainty of suspended sediment load prediction using sequential data assimilation. *Journal of hydrology*, *468*, 268-282.

Li, Z., & Navon, I. M. (2001). Optimality of variational data assimilation and its relationship with the Kalman filter and smoother. *Quarterly Journal of the Royal Meteorological Society*, *127*(572), 661-683.

Liu, Y., & Gupta, H. V. (2007). Uncertainty in hydrologic modeling: Toward an integrated data assimilation framework. *Water Resources Research*, *43*(7).

Lorentzen, R. J., & Nævdal, G. (2011). An iterative ensemble Kalman filter.*Automatic Control, IEEE Transactions on*, *56*(8), 1990-1995.

Madsen, H., & Skotner, C. (2005). Adaptive state updating in real-time river flow forecasting—A combined filtering and error forecasting procedure. *Journal of Hydrology*, *308*(1), 302-312.

Mao, J. Q., Lee, J. H., & Choi, K. W. (2009). The extended Kalman filter for forecast of algal bloom dynamics. *Water research*, *43*(17), 4214-4224.

Matgen, P., Montanari, M., Hostache, R., Pfister, L., Hoffmann, L., Plaza, D., Pauwels V. R. N., Lannoy G. J. M. De 2, Keyser R. De & Savenije, H. H. G. (2010). Towards the sequential assimilation of SAR-derived water stages into hydraulic models using the Particle Filter: proof of concept. *Hydrology and Earth System Sciences*, *14*(9), 1773-1785.

McNair, J. N., Gereaux, L. C., Weinke, A. D., Sesselmann, M. R., Kendall, S. T., & Biddanda, B. A. (2013). New methods for estimating components of lake metabolism based on free-water dissolved-oxygen dynamics. *Ecological Modelling*, *263*, 251-263.

Miller, R. N., Ghil, M., & Gauthiez, F. (1994). Advanced data assimilation in strongly nonlinear dynamical systems. *Journal of the atmospheric sciences*,*51*(8), 1037-1056.

Montanari, A., Rosso, R., & Taqqu, M. S. (1997). Fractionally differenced ARIMA models applied to hydrologic time series: Identification, estimation, and simulation. *Water resources research*, *33*(5), 1035-1044.

Moradkhani, H., Hsu, K. L., Gupta, H., & Sorooshian, S. (2005a). Uncertainty assessment of hydrologic model states and parameters: Sequential data assimilation using the particle filter. *Water Resources Research*, *41*(5).

Moradkhani, H., Sorooshian, S., Gupta, H. V., & Houser, P. R. (2005b). Dual state–parameter estimation of hydrological models using ensemble Kalman filter. *Advances in Water Resources*, *28*(2), 135-147.

Murphy, A. H., & Winkler, R. L. (1987). A general framework for forecast verification. *Monthly Weather Review*, *115*(7), 1330-1338.

Nagarajan, K., Judge, J., Graham, W. D., & Monsivais-Huertero, A. (2011). Particle filter-based assimilation algorithms for improved estimation of root-zone soil moisture under dynamic vegetation conditions. *Advances in Water Resources*, *34*(4), 433-447.

Nash, J., & Sutcliffe, J. V. (1970). River flow forecasting through conceptual models part I—A discussion of principles. *Journal of hydrology*, *10*(3), 282-290.

Neal, J. C., Atkinson, P. M., & Hutton, C. W. (2007). Flood inundation model updating using an ensemble Kalman filter and spatially distributed measurements. *Journal of Hydrology*, *336*(3), 401-415.

Nelson, B. R., Seo, D. J., & Kim, D. (2010). Multisensor precipitation reanalysis. *Journal of Hydrometeorology*, *11*(3), 666-682.

Parmar, K. S., & Bhardwaj, R. (2014). Water quality management using statistical analysis and time-series prediction model. *Applied Water Science*,*4*(4), 425-434.

Pastres, R., Ciavatta, S., & Solidoro, C. (2003). The Extended Kalman Filter (EKF) as a tool for the assimilation of high frequency water quality data.*Ecological modelling*, *170*(2), 227-235.

Pham, D. T. (2001). Stochastic methods for sequential data assimilation in strongly nonlinear systems. *Monthly weather review*, *129*(5), 1194-1207.

Press, W. H., Flannery, B. P., & Teukolsky, S. A. (1986). W. T. V etterling, Numerical Recipes in C, The Art of Scientific Computing. *Cambridge U niversity Press*, *1*, 988.

Rafieeinasab, A., Seo, D. J., Lee, H., & Kim, S. (2014). Comparative evaluation of maximum likelihood ensemble filter and ensemble Kalman filter for real-time assimilation of streamflow data into operational hydrologic models.*Journal of Hydrology*, *519*, 2663-2675.

Ragavan, A. J., & Fernandez, G. C. (2006). Modeling water quality trend in long term time series. In *Proceedings of SAS Users Group Meeting (SUGI 31), paper 205* (Vol. 31, pp. 205-31).

Ragnoli, E., Zhuk, S., Donncha, F. O., Suits, F., & Hartnett, M. (2012, October). An optimal interpolation scheme for assimilation of HF radar current data into a numerical ocean model. In *Oceans, 2012* (pp. 1-5). IEEE.

Reichle, R. H., McLaughlin, D. B., & Entekhabi, D. (2001). Variational data assimilation of microwave radiobrightness observations for land surface hydrology applications. *Geoscience and Remote Sensing, IEEE Transactions on*, *39*(8), 1708-1718.

Schilling, W., & Martens, J. (1986). Recursive state and parameter estimation with applications in water resources. *Applied mathematical modelling*, *10*(6), 433-437.

Schweppe, F. C. (1973). Uncertain dynamic systems. Prentice Hall.

Sebens-Babbar, M., Li, L., Song, K., & Xie, S. (2013). On the Use of Landsat-5 TM Satellite for Assimilating Water Temperature Observations in 3D Hydrodynamic Model of Small Inland Reservoir in Midwestern US.

Seo, D. J. (2013). Conditional bias-penalized kriging (CBPK). *Stochastic Environmental Research and Risk Assessment*, *27*(1), 43-58.

Seo, D. J., Cajina, L., Corby, R., & Howieson, T. (2009). Automatic state updating for operational streamflow forecasting via variational data assimilation.*Journal of Hydrology*, *367*(3), 255-275.

Seo, D. J., Kim S., Rafieeinasab A., Riazi H., and Shin C. (2012). Development of real-time data assimilation and initialization modules for HSPF for improved water quality prediction and monitoring, Yr-1 final report to the National Institute of

Environmental Research, Dept. of Civil Eng., The University of Texas at Arlington, Arlington, TX.

Seo, D. J., Koren, V., & Cajina, N. (2003). Real-time variational assimilation of hydrologic and hydrometeorological data into operational hydrologic forecasting.*Journal of Hydrometeorology*, *4*(3), 627-641.

Seo, D. J., Siddique, R., Zhang, Y., & Kim, D. (2014). Improving real-time estimation of heavy-to-extreme precipitation using rain gauge data via conditional bias-penalized optimal estimation. *Journal of Hydrology*, *519*, 1824-1835.

Seo, D.-J., J. Demargne, L. Wu, Y. Liu, J. D. Brown, S. Regonda, and H. Lee (2010). Hydrologic Ensemble Prediction for Risk-Based Water Resources Management and Hazard Mitigation, 4th Federal Interagency Hydrologic Modeling Conference, June 27-July 1, 2010, Las Vegas, NV.

Shin C, 2013. United States Environmental Protection Agency Region 6 Water Quality Modeling Conference and Workshop.

Shirinian-Orlando, A. A., & Uchrin, C. G. (2007). Modeling the Hydrology and water quality using BASINS/HSPF for the upper Maurice River watershed, New Jersey. *Journal of Environmental Science and Health Part A*, *42*(3), 289-303.

Singh, J., Knapp, H. V., Arnold, J. G., & Demissie, M. (2005). Hydrological modeling of the Iroquois River watershed using HSPF and SWAT. *Journal of the American Water Resources Association*, *41*(2), 343-360.

Sloan, W. T., Jenkins, A., & Eatherall, A. (1994). A simple model of stream nitrate concentrations in forested and deforested catchments in Mid-Wales.Journal of hydrology, 158(1), 61-78.

Twigt, D., Tyrrell, D., Rego Lima, J., & Troost, T. (2011, May). Water Quality Forecasting Systems: Advanced Warning of Harmful Events and Dissemination of Public

Alerts. In *Proceedings of the 8th International ISCRAM Conference–Lisbon, Portugal*.

Van Leeuwen, P. J. (2009). Particle filtering in geophysical systems. *Monthly Weather Review*, *137*(12), 4089-4114.

Verwey, A., Heynert, K., Werner, M., Reggiani, P., Kappel, B. V., & Brinkman, J. (2006). The Potential of the Delft-FEWS Flood Forecasting Platform for Application in the Mekong Basin. In *4 th Annual Mekong Flood Forum, Siem Reap, Cambodia*.

Voutilainen, A., Pyhälahti, T., Kallio, K. Y., Pulliainen, J., Haario, H., & Kaipio, J. P. (2007). A filtering approach for estimating lake water quality from remote sensing data. International journal of applied earth observation and geoinformation, 9(1), 50-64.

Vrugt, J. A., & Robinson, B. A. (2007). Treatment of uncertainty using ensemble methods: Comparison of sequential data assimilation and Bayesian model averaging. *Water Resources Research*, *43*(1).

Weerts, A. H., and El Serafy G. Y. H. (2006), Particle filtering and ensemble Kalman filtering for state updating with hydrological conceptual rainfall-runoff models, Water Resour. Res., 42(9), W09403,

Werner, M. G. F., van Dijk, M. A. R. C., & Schellekens, J. A. A. P. (2004, June). DELFT-FEWS: an open shell flood forecasting system. In *Proceedings of the 6th International Conference on Hydroinformatics* (pp. 1205-1212). World Scientific.

Whitaker, J. S., & Hamill, T. M. (2002). Ensemble data assimilation without perturbed observations. *Monthly Weather Review*, *130*(7), 1913-1924.

Whitehead, P. G., & Hornberger, G. M. (1984). Modelling algal behaviour in the River Thames. Water research, 18(8), 945-953.

Worrall, F., & Burt, T. P. (1999). A univariate model of river water nitrate time series. *Journal of Hydrology*, *214*(1), 74-90.

Xie, S. (2012). Remote Sensing Data Assimilation In Water Quality Numerical Models For Simulation Of Water Column Temperature (Doctoral dissertation).

Xie, X., & Zhang, D. (2010). Data assimilation for distributed hydrological catchment modeling via ensemble Kalman filter. *Advances in Water Resources*, *33*(6), 678-690.

Xue, P., Chen, C., & Beardsley, R. C. (2012). Observing system simulation experiments of dissolved oxygen monitoring in Massachusetts Bay. *Journal of Geophysical Research: Oceans (1978–2012)*, *117*(C5).

Yan, H., DeChant, C. M., & Moradkhani, H. (2015). Improving Soil Moisture Profile Prediction With the Particle Filter-Markov Chain Monte Carlo Method

Zhang, H., & Pu, Z. (2010). Beating the uncertainties: ensemble forecasting and ensemble-based data assimilation in modern numerical weather prediction.*Advances in Meteorology*, *2010*.

Zhang, S. Q., Zupanski, M., Hou, A. Y., Lin, X., & Cheung, S. H. (2013). Assimilation of precipitation-affected radiances in a cloud-resolving WRF ensemble data assimilation system. *Monthly Weather Review*, *141*(2), 754-772

Zingone, A., & Enevoldsen, H. O. (2000). The diversity of harmful algal blooms: a challenge for science and management. *Ocean & Coastal Management*,*43*(8), 725-748.

Zupanski, D., & Zupanski, M. (2006). Model error estimation employing an ensemble data assimilation approach. *Monthly Weather Review*, *134*(5), 1337-1354.

Zupanski, D., Denning, A. S., Uliasz, M., Zupanski, M., Schuh, A. E., Rayner, P. J., Peters W. & Corbin, K. D. (2007). Carbon flux bias estimation employing

maximum likelihood ensemble filter (MLEF). *Journal of Geophysical Research: Atmospheres (1984–2012)*, *112*(D17).

Zupanski, D., Hou, A. Y., Zhang, S. Q., Zupanski, M., Kummerow, C. D., & Cheung, S. H. (2007). Applications of information theory in ensemble data assimilation. *Quarterly Journal of the Royal Meteorological Society*, *133*(627), 1533-1545.

Zupanski, D., Zhang, S. Q., Zupanski, M., Hou, A. Y., & Cheung, S. H. (2011). A prototype WRF-based ensemble data assimilation system for dynamically downscaling satellite precipitation observations. *Journal of Hydrometeorology*,*12*(1), 118-134.

Zupanski, M. (2005). Maximum likelihood ensemble filter: Theoretical aspects.*Monthly Weather Review*, *133*(6), 1710-1726.

Biographical Information

Hamideh Riazi was born March 23, 1983 in Tehran, Iran. She received the Bachelor of Science and the Master of Science in Agriculture Engineering (Irrigation and drainage) from Tehran University in 2006 and 2009, respectively. She began doctoral studies in water recourses engineering in University of Texas at Arlington in 2012 .She was awarded the Outstanding Graduate student in the Department of Civil Engineering at the University of Texas at Arlington in 2014. She has served as a Graduate Research assistant and Graduate Teaching assistant in the Department of Civil Engineering at the University of Texas at Arlington.